UPWARD FLAME SPREAD ON VERTICAL SURFACES

by

KUANG-CHUNG TSAI

DOCTOR OF PHILOSOPHY

UNIVERSITY OF EDINBURGH

2001

DECLARATION

It is declared that this thesis and the results therein contained are the work of the author, himself, and have been produced under the supervision of Professor D. D. Drysdale.

Abstract

Previous studies have demonstrated upward flame spread on vertical surfaces to be one of the most serious fire scenarios due to the concurrent direction of flame propagation and air flow. The unburned zone of the wall ahead of the pyrolysis zone consequently receives heat directly from the flame, causing the temperature of the unburned wall to rise quickly and the flame to spread more rapidly. In order to avoid the occurrence of hazardous wall fires, there is a need to select materials which satisfy performance-based regulations. This approach needs information from reliable fire models which simulate accurately the fire behaviour of materials in their end-use configuration. However, none of the existing models are used in this way. This is because of the limitations of the models themselves, in particular the assumptions involved and uncertainties in the empirical correlations used in the models.

This study focuses on the early stages of the upward flame spread. An existing model which uses data directly from the Cone Calorimeter test was examined. A non-standard test procedure was developed which gives results capable of giving better predictions from the model. The flame height and heat feedback to the unburned wall were also examined and more information obtained. The flame height was measured from steady burning vertical fuels and from a gas-fuelled panel to examine the commonly accepted relation that the flame height is proportional to the 2/3rds power of the heat release rate per unit width of the wall fire $\dot{Q}'$. In the former experiment, the flame height and $\dot{Q}'$ were measured directly in the same experiments, providing data for the early stages of fire spread. In addition, the effect of different geometric configurations was examined. The latter experiment revealed a width effect, questioning the validity of $\dot{Q}'$ being the only parameter determining the flame height. Experiments were also carried out to measure the heat transfer to the unburnt material above the pyrolysing zone. A lower value was found to be more representative than the ones used previously.

With these modifications, the model was found to give good agreement with experimental measurements of vertical spread on sheets of PMMA. Two additional

cases were studied: wall fires influenced by an inert parallel wall and by the proximity of a corner. The measurement of flame height and heat feedback provides data for further investigation and modelling work.

Acknowledgements

The author gratefully acknowledges the help and support from the following people during the course of this research:

Prof. Dougal Drysdale for his supervision, advice, understanding, encouragement and also "English correction". After his supervision, doing research became one of my career choices.

Jo Sherratt, Neil Wood, Kevin Anderson, Chris Burnside and Kevin Broughton for their technical support and help.

Prof. Jenn-Chuan Chern, Mr. Sam Chou and Dr. Min-Yung Lei for bringing me into this challenging field, suggestions before I came to Edinburgh and encouragement during these three years.

All my brothers and sisters in Kindly Light Baptist Church in Taiwan, in Edinburgh Mandarin Fellowship and in International Fellowship (Charlotte Chapel) for their prayers throughout these three years.

My friends in Taiwan and Edinburgh for their friendship and care.

My parents, grandparents, sister and brothers for their support. Being their family is one of the most enjoyable things in my life!

Finally, I would like to thank **God** for leading me to Edinburgh, experiencing His love and faithfulness.

Table of Contents

Chapter 3: Experimental Work and Results

Chapter 4: Computer Modelling

Chapter 5: Discussion

List of Figures

Nomenclature

a	constant (-) or separation between two parallel walls (m)
A	area (m^2)
A_h	horizontal pyrolysis area on the wall (m^2)
A_o	initial area (m^2)
A_p	pyrolysis area (m^2)
A_w	pyrolysis area on the wall (m^2)
b	constant (-)
c or C_p	specific heat capacity (J/kg K)
C_o	constant (-)
D	linear dimension of a fire e.g. length of line burner (m)
g	gravitional acceleration (m/s^2)
h_i	heat transfer coefficient (-)
H	height of fuel (m)
k	thermal conductivity (W/m K)
K	constant (-)
K_f	constant (-)
l	heating length (m)
L	latent heat (kJ/g)
L_o	sample thickness (m)
m	mass (g or kg)
$\dot{m}'$	mass loss rate per unit width (g/s m)
$\dot{m}''$	mass loss rate per unit area (g/s m^2)
n	constant (-) or molecular number (mole)
p	pressure (atm)
$\dot{q}'$	heat flux per unit width (kW/m)
$\dot{q}''$	heat flux per unit area (kW/m^2)
$\dot{q}''_{imp}$	imposed heat flux (per unit area) (kW/m^2)
$\dot{q}''_{net}$	net heat flux (kW/m^2)
$\dot{q}''_r$	irradiance in the Cone Calorimeter (kW/m^2)
$\dot{q}''_w$	heat flux from flame to unburned wall (kW/m^2)
$\dot{q}''_{wo}$	maximum heat flux from flame to unburned wall (kW/m^2)
$\dot{q}''_{wc}$	convective heat flux from flame to unburned wall (kW/m^2)
$\dot{q}''_{wr}$	radiative heat flux from flame to unburned wall (kW/m^2)
Q	volumetric flow rate of gaseous fuel (m^3/s)
$\dot{Q}$	heat release rate (kW)
$\dot{Q}_l$	heat release rate per unit length of line burner (kW)
$\dot{Q}'$	heat release rate per unit width (kW/m)
$\dot{Q}_{tot}$	total heat release rate (kW)

$\dot{Q}_b'$	heat release rate per unit width of burner (kW/m)
$\dot{Q}''$	heat release rate per unit area (kW/m^2)
$\dot{Q}''_{max}$	maximum heat release rate per unit area (kW/m^2)
$\dot{Q}''_{max,50}$	peak heat release rate at 50 kW/m^2 (kW/m^2)
$\dot{Q}_l'^*$	a dimensionless RHR parameter $\dot{Q}_l'^* = \dot{Q}'/\rho \quad C_p T_o g^{1/2} D^{3/2}$ (-)
t	time (s)
t'	dummy integral variable (-)
t_b	time to burnout (s)
t_{bo}	burning duration (s)
t_i *or* t_{ig}	time to ignition (s)
t_f	the time as the flame tips reach a specific position (s)
$t_{flashover}$	time to flashover
t_p	dummy variable (-)
$t_p(X)$	the time to pyrolysis (s)
T	temperature (°C or K)
T_f	adiabatic flame temperature
T_o	initial temperature (°C or K)
T_{ig}	ignition temperature (°C or K)
T_s	surface temperature (°C or K)
u_∞	free stream gas velocity (m/s)
V	flame spread rate (m/s or mm/s)
V_p	rate of spread of the pyrolysis front (m/s or mm/s)
V_{pp}	rate of spread of the peak pyrolysis front (m/s, cm/s or mm/s)
w	width (m)
X	height (m)
X'	height on the opposing parallel wall (m)
X_b	height of burnout (m)
X_f	flame height (m)
X_{fo}	initial flame height (m)
X_o	initial height (m)
X_p	height of pyrolysis front (m)
X_{po}	initial height of pyrolysis front (m)
X_{pp}	height of peak pyrolysis front (m or cm)
Y	horizontal distance (m)
Y_b	width of burnout region (m)
Y_o	initial width (m)
Y_p	width of pyrolysis area (m)
Y_{pb}	width of pyrolysis zone at bottom of walls (m or cm)
Z	depth (m)

Greek Symbols and Abbreviations

α	thermal diffusivity ($=k/\rho c$) (m^2/s) or constant (-)
β	constant (-)
δ	thickness or thermal depth (m)
δ_{cr}	critical thickness for flame spread (m)
δ_p	the depth of pyrolysed material (m)
ΔA^i	area increment at the i th time step (m^2)
Δh	change in enthalpy (kJ/kg)
ΔH_c	heat of combustion (kJ/kg)
$\Delta H_c'$	heat of combustion per unit width (kJ/kgm)
ΔH_g	effective heat of gasification (kJ/kg)
Δt	time increment (s)
ΔT	temperature difference (°C or K)
$\Delta \rho$	density difference (kg/m^3)
ε	emissivity (-)
ε_p	Location of pyrolysis front at time τ (m)
ϕ	forward heat transfer parameter (-)
$\phi(\tau)$	impulse response of surface temperature to heat (-)
$\phi_{crit.}$	critical forward heat transfer parameter (-)
Φ	flame spread parameter (-)
γ	constant (-)
ρ	density of material (kg/m^3)
ρ_o	density of air (kg/m^3)
σ	Stefan-Boltzmann constant (5.668×10^{-11} $kW/m^2\text{-}K^4$)
τ	time to ignition (s)
φ	Uniform net heating flux (kW/m^2)
κ	flame absorption coefficient (-)
λ	decay coefficient (-) or the expression of $ln(X_p/X_{po})$ (-)
ξ	the height above the pyrolysis front (m)
FTP	parameter: flux-time product
RHR	heat release rate
SPF	self propagating flux

Chapter 1

Introduction and Objectives

1.1 Introduction

These is an old Chinese saying describing the functions of water: Water can lift ships and also turn ships over. Fire also has positive and negative functions for human beings. On one hand, fire provides heat, light, warmth and power. On the other hand, unwanted fire can cause loss of life and property. In the UK alone, 110,700 accidental and 88,300 malicious fires were reported in the year 1998 (Watson and Gamble, 1999); and in the year 1995, £ 863 M loss was estimated from the Association of British Insurers (FPA, 1998).

From an analysis of the 1998 figures (Watson and Gamble, 1999), more than three-quarters of all casualties occur in dwellings and other buildings. Unfortunately, there is a risk of fire in every building that is designed. In order to prevent unwanted fires in buildings, reports of fire investigation and fire statistics become useful but sorrowful lessons for further improvement in building design.

1.2 The Hazard of Upward Flame Spread

Experience of analysing unwanted fires has shown that most fires in buildings start in furnishings. Combustible wall linings can make the situation much worse because plenty of heat from the fire can be absorbed for pyrolysing the unburned leading edge ahead the burning area. This can lead rapidly to flashover. Thus, upward flame spread on vertical surfaces becomes an important driving force for fire growth. A recent investigation on a multi-story fire in a high-rise apartment building discovered an extremely rapid upward fire spread (20-30 seconds for the fire to proceed upward by one 3-m floor) through balconies in the building (Hokugo *et al.*, 2000). In addition, warehouse fires are also significant examples of upward flame spread where large areas of vertical

combustible surfaces can exist in high storage bays. The configurations in warehouses may lead to even more rapid fire growth than would be supposed because the storage arrays provide a vertical channels between two stacks which increase the heat transfer to neighbouring combustible materials.

1.3 Fire Tests Relevant to Upward Flame Spread on Vertical Surfaces

In order to avoid the occurrence of upward flame spread in a building, wall-lining materials, products or assemblies have to be selected on the basis of their performance in fire tests. The threat to life and health of people in building fires depend on the fire size (i.e. heat release), the amount of smoke evolved and the toxicity of the combustion products so that these three should be considered as the dominant hazard parameters in fires. From an economic point of view, small-scale fire tests are preferred. However, the performance of a material in a small-scale test may not represent its end use or cover all possible fire scenarios. Thus the result should be examined carefully before being adopted and might only be regarded as information about the potential of a material to generate heat, smoke and toxic gases in a rather simplistic way. The Cone Calorimeter is the most popular small-scale fire test apparatus, which can provide important fire parameters relevant to these three dominant hazards.

1.3.1 The Cone Calorimeter

The Cone Calorimeter is a small-scale apparatus which is capable of measuring the rate of heat release (RHR), the effective heat of combustion, mass loss rate, ignitability, smoke/soot and toxic gases (Babrauskas, 1995). A 10×10 cm specimen is set up horizontally or vertically, facing a conical heater which allows a radiant heat flux from 10 to 100 kW/m^2 to be produced at the surface of the specimen (see Fig. 1.1). A spark ignitor is used to ignite the fuel vapours under a chosen irradiance and the time dependent RHR under the given conditions can be calculated by using the principle of oxygen consumption (Thornton, 1917, Huggett, 1980). These two parameters, the time to ignition and RHR are analysed in this thesis as they have direct effects on fire growth on vertical surfaces.

1.3.2 The Room/Corner Test

Room/corner test (ISO/DIS 9705) is a full-scale fire test for wall lining materials and was designed to simulate the real fire behaviour of materials in their end use. The test comprises a room (2.4×2.4×3.6m) with a normal sized doorway (0.8×2m) and the test specimen is mounted on the walls and on the ceiling (see Fig. 1.2). The ignition source, a sand bed burner, is located in a corner to simulate the worse case (to be discussed in Sec. 2.4). Its output is 100kW during the first 10 minutes and 300kW for the next 10 minutes. RHR is obtained by oxygen consumption calorimetry (ISO, 1993).

1.3.3 The SBI Test

The ISO/DIS 9705 room/corner test is in the very final stages of becoming an ISO Standard (Sundstrom, 1991). However, a disadvantage of the room/corner test is its high cost. Recently, another intermediate-scale test apparatus, the Single Burning Item test (SBI), has been developed to achieve the benefits of more accurate reflection to the fire conditions of real fires than small-scale tests and more cost effective than full-scale tests. The design of the SBI test was directed to have better methods for estimation of fire critical effects such as ease of ignition and growth of fire to an uncontrolled state.

Test specimens are mounted on a trolley to form two walls joined vertically at right angles (see Fig. 2.3). Both walls are 1.5 m high but their widths are 1.0 m for the long wall and 0.5 m for the short. A 250 mm-sided triangular sandbox through which propane is fuelled acts as the SBI ignition source and is positioned at the base of the corner to simulate the thermal attack of a waste-paper basket in a corner of a room. The RHR, smoke and toxicity production are still the primary parameters measured.

1.4 The Risk Assessment of Upward Flame Spread and the Concept of Performance-Based Design

Fire safety engineers are responsible for ensuring that buildings will be safe in the event of fires. Practically they have to assess the risk associated with a fire hazard involving particular burning materials, products or assemblies in special fire scenarios. The traditional way adopted is by using fire tests which measure particular fire properties (discussed in Sec.1.3). The results have then been used to rank materials based on a single fire property. Unfortunately, fire performance of a material or a component in a small-scale fire test cannot represent its end use. Adopting a large-scale test to assess the fire risk of a specific configuration always consumes time and money. Even adopting an intermediate-scale test apparatus, from the viewpoint of a designer, this kind of prescriptive approach will not always meet the needs or expectations of building owners. In addition, this kind of approach may not cover all fire scenarios (Custer and Meacham, 1997), and does not give quantitative data for use in "engineering design".

A new concept has been accepted: the fire protection consideration for a specific design situation should depend on the final integrated performance of each sub-system, e.g. fire suppression facility, the fire resistance of each component. This is so called "**performance-based approach**". On the contrary, a "**prescriptive-based approach**" checks all sub-systems individually. The performance-based approach is more scientific and is likely to be more cost-effective. In the UK, a framework called DD 240 (BSI, 1997) has been provided, which is reviewed by the public and will become a British Standard after modification. DD 240 takes into account many factors, including building construction, means of escape, human factors, smoke control, fire detection, alarm systems and suppression, and their contribution to the achievement of fire safety objectives. Flexibility is allowed when equivalence can be shown. Another example is a building fire safety risk assessment system developed by Victoria University of Technology and the National Research Council of Canada. They considered the concepts of design fires, modelling the physical phenomena of fire growth and spread, predicting the times of occurrence of those events relevant to life safety, with the inclusion of fire brigade performance (Beck, 1994).

It has now become clear that there needs to be better predictive and integrated ways to make fire safety decisions. However, a prerequisite is the accurate prediction of all the sub-systems. Unfortunately, for example, the prediction of fire growth associated with a specific fire scenario is still not reliable enough. The development of fire models for accurate predictions is still needed.

1.5 Objectives of this Thesis

Therefore, attention should still be drawn to the development of fire models which are capable of reliably predicting the rate of fire growth in a specific fire scenario. The better understanding of a fire phenomenon is always the prerequisite. Thus, in this thesis, experiments were designed to analyse the mechanisms and characteristics involved in upward flame spread such as flame heights and heat transfer from flames. Extensions were given to two worst cases: upward flame spread in a corner and between two vertical walls.

Computer modelling of a fire phenomenon is of importance as it connects the understanding of the fire phenomenon with its risk assessment and practical performance-based design. Adopting data from small-scale fire test apparatuses as input of fire models is preferred because it is cost-effective. An upward flame spread model developed at Edinburgh University, which uses data from the Cone Calorimeter, was reviewed and modified. Such progress may prove to be a suitable basis by which the data from the Cone Calorimeter could be used for the purpose of material selection and for carrying out risk assessment.

Fig.1.1 - Schematic view of the Cone Calorimeter.

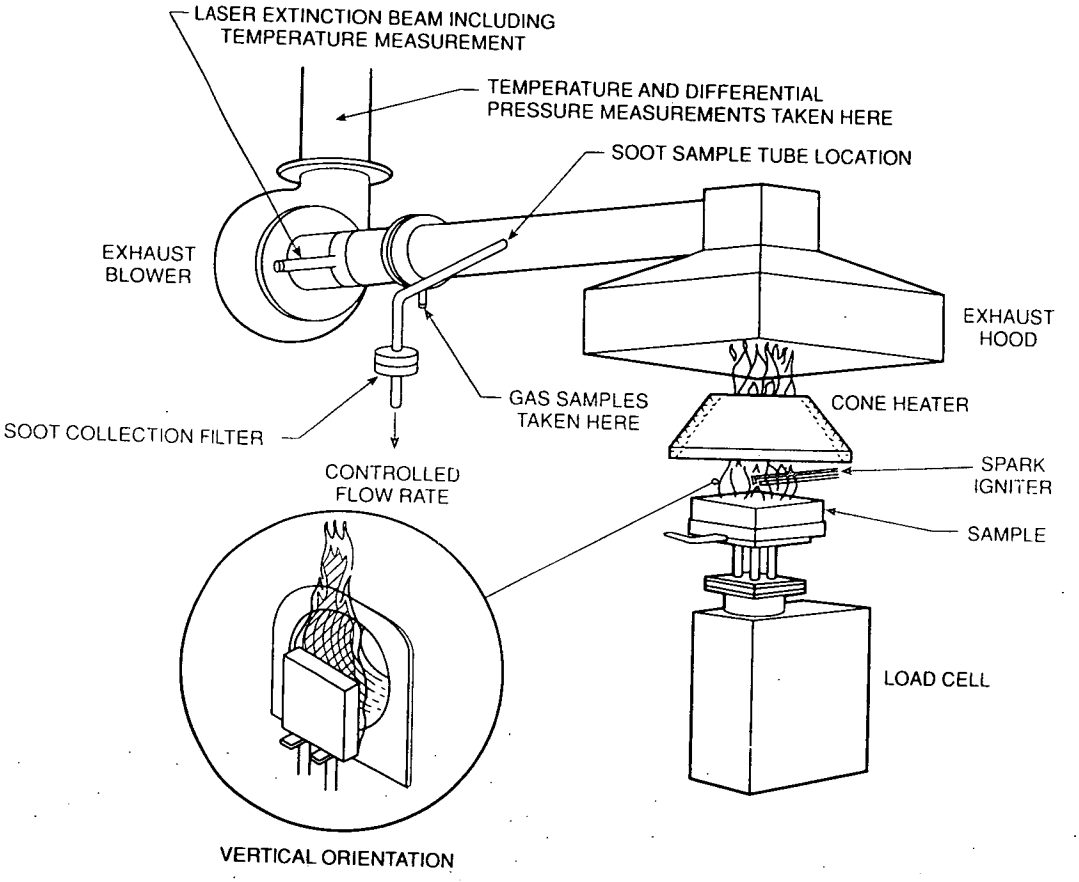

Fig.1.2 - The schematic diagram of ISO 9705 room/corner test.

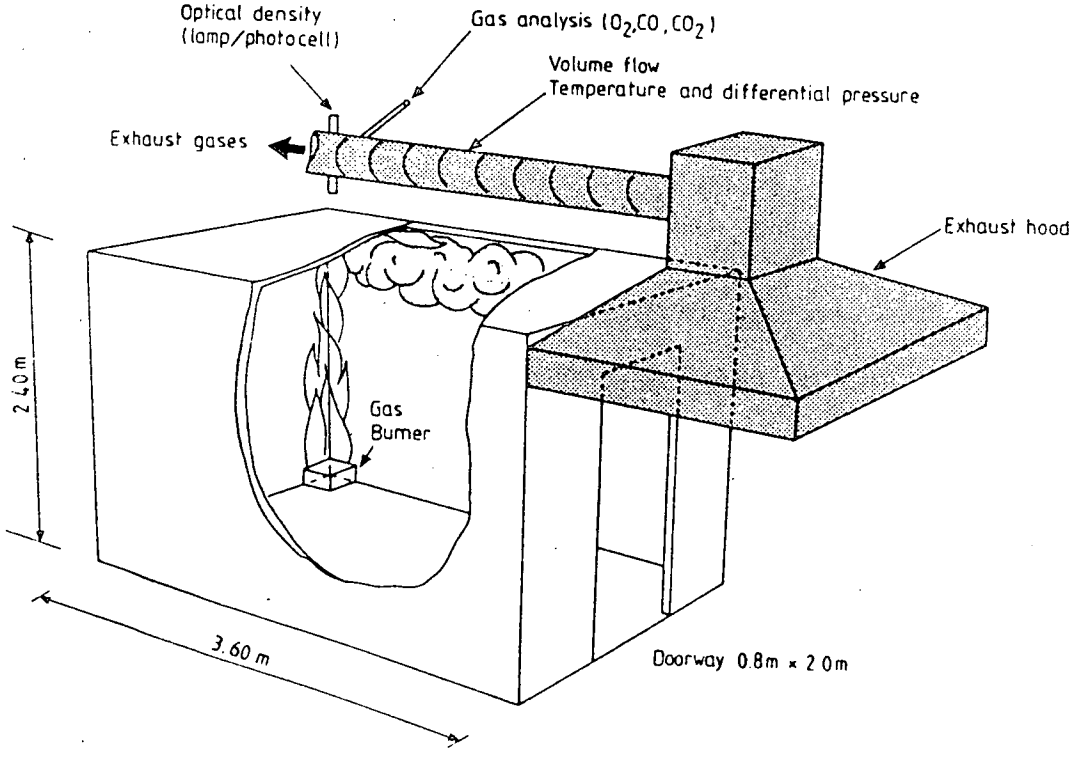

Fig.1.3 - The schematic diagram of SBI (Single Burning Item) test rig.

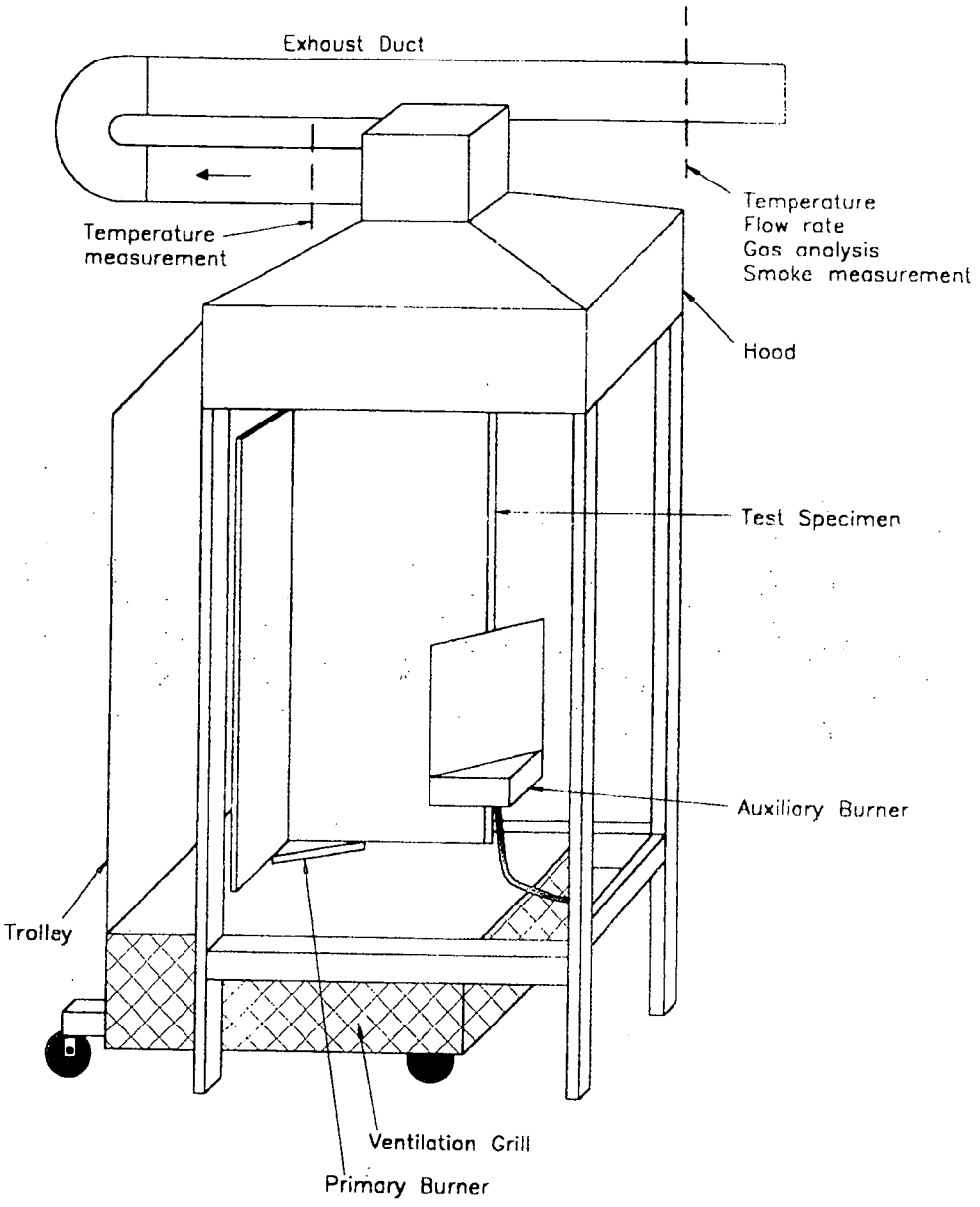

Chapter 2

Literature Review: Upward Flame Spread

2.1 Introduction

In order to prevent unwanted wall fires, one must have an understanding of the physical processes involved. In this chapter, some fundamentals of fire related to flame spread are reviewed first. Afterwards, previous research involving experimental, theoretical and modelling approaches to upward flame spread on flat surfaces are discussed. Then an investigation of two extended cases of wall fires, in a corner and between two parallel walls, is presented.

2.2 Ignition and Flame Spread

Ignition may be regarded as one of the most important stages involved in a fire because it describes the initiation of a combustion phenomenon. "Ignition may be defined as that process by which a rapid, exothermic reaction is initiated, which then propagates and causes the material involved to undergo change, producing temperatures greatly in excess of ambient." (Drysdale, 1998). Depending upon whether the fuel is ignited with or without the aid of an external ignition source, the result is accordingly classified as piloted or spontaneous. Piloted ignition is of importance because it occurs at lower temperatures and most fires involve an ignition source.

In practice, ignition can be noted by the appearance of a flame in flaming combustion in which wall fires are classified. Flame is the visible portion of the volume within which combustion is occurring, and is well known as a gas phase phenomenon (Lewis and von Elbe, 1987). This statement infers that all the solid fuels (and liquid fuels), which are so called condensed-phase fuels, have to change to the gaseous phase before burning. In

solid combustion, the main mechanism applied to yield volatile vapours from the fuel surface and enter the flame is chemical decomposition, or pyrolysis (Drysdale, 1998).

Conclusively, Kanury (1988) described three sets of conditions which have to be fulfilled to ignite a condensed-phase material.

(1) sufficient quantities of combustible vapours have to be released as a result of preheating the solid or liquid;
(2) these vapours have to be mixed with the oxidant in the gas phase;
(3) this mixture has to be either at a high enough temperature to induce self-accelerating oxidation (i.e., spontaneous or autoignition) or to be provided with a pilot source to induce local self-accelerating oxidation.

2.2.1 Flashpoint, Firepoint & Flammability Limits of Liquid Fuels

The research on wall fires should deal with the ignition of "solid" fuels. However, it is easier and more general to describe the ignition of liquid fuels first. For liquid fuels, the first condition noted above describes a proper situation in which the fuel vapours produced must be more or less enough to start a flame. Limits of flammability of liquids are thus defined by experimentally determined fuel concentrations at a specified temperature and pressure, bounded by lower and upper **flammability limits** (Zabetakis, 1965). The former denotes the fuel percentage of a limit mixture when oxidant is in excess, and the latter denotes when fuel is in excess. In addition, for those flames in which fuel vapours ("volatiles") and oxidiser (oxygen in air) are intimately mixed before combustion is initiated, **premixed flames** are defined, and **diffusion flames** describe those flames in which fuel vapours and air are initially separate, reacting as they mix.

Flashpoint is defined as the lowest temperature at which the vapour-air mixture is flammable at the surface; that is, the vapour pressure corresponds to the lower flammability limit. At the flashpoint, only a short duration flame or a "flash" will be produced if an ignition source is introduced. If a sustained burning of flammable liquid is required, a further temperature increase is needed to generate a continuous, i.e. sustained,

flame. The minimum temperature for continuous flaming is defined as **firepoint**.

2.2.2 Piloted Ignition of Solid Fuels

Unlike liquid fuels, the flashpoint and firepoint of solids can not be measured easily. A corresponding concept of rate of pyrolysis or mass flux is established. Sufficient volatile flow can be described as a critical mass flux of fuel vapours and the firepoint of solid can be defined in term of surface temperature, i.e. the ignition temperature (Drysdale, 1998).

2.2.3 The Relationship between Ignition and Flame Spread

After the initiation of flaming combustion, the combustible material starts to burn and release heat. Some of the heat produced continues to raise the temperature of its neighbouring unburned zone, producing flammable fuel vapours which are ignited by an ignition source played by the leading flame itself and then forcing this zone to become involved. This results in the propagation of flame. As a result, flame spread can be considered as an advancing ignition front in which the leading edge of the flame acts both as the source of heat (to raise the fuel ahead of the flame front to its ignition temperature) and the source of pilot ignition (Drysdale, 1998). The flame spread may then result in the increase of flame size and burning rate, and consequently causes larger fires, e.g. compartment fires.

2.2.4 Flame Spread Rate over Solids

For a flame to spread, sufficient heat energy must be transferred from the flame with or without external heat flux to the unburned zone ahead of the flame to pyrolyse the solid. There fuel vapours escape from the surface, mix with air to produce a flammable mixture ahead of the leading edge of the flame and are then ignited by the flame itself. Therefore, the rate of flame spread is determined by the ability of the flame to transfer necessary heat to pyrolyse the solid and to ignite the flammable mixture ahead of it.

2.3 The Factors Influencing Flame Spread Rate over Solids

Williams (1977) presented a fundamental equation of flame spread by postulating that the rate of heat transfer across the "surface of fire inception" determines the rate of flame spread.

$$\rho V \Delta h = \dot{q}'' \tag{2.1}$$

where V is the flame spread rate, $\dot{q}''$ is the net heat flux, ρ is the fuel density and Δh is the change in enthalpy as unit mass of fuel is raised from its initial temperature T_o to ignition temperature T_{ig}. By substituting Δh in terms of the specific heat c, T_o and T_{ig}, the V can be expressed in the following form.

$$V = \frac{\dot{q}''}{\rho c (T_{ig} - T_o)} \tag{2.2}$$

This "fundamental equation of flame spread" views flame spread over combustibles as a process of continuous ignition of the successive upstream materials. It is a simple energy conservation equation and only for steady conditions. However, this equation identifies the factors affecting the rate of flame spread. From Equation 2.2, it is shown that the net heat flux absorbed by the "successive upstream material", the density, specific heat and the difference between initial and ignition temperature of the fuel determine the velocity of flame spread.

2.3.1 The Net Heat Flux

From Equation 2.2, one can see that the flame spread rate increases as the net heat flux increases. Several physical, chemical and environmental factors have effects on the net heat flux.

2.3.1.1 Surface Orientation and Direction of Flame Spread

The surface of a solid can be at any orientation. After the solid is ignited, a flame becomes established. The density difference ($\Delta\rho/\rho = \Delta T/T$) between the flame and surrounding air creates air entrainment. The buoyancy always drives the air to move upwards. Along the burning solid, the presence of inclined surface orientation results in an "imbalance" of the air flow into the opposite sides of the flame, which determining the length of the flame and the angle between the flame and the combustible surface (Smith, 1992). The interactions at different angles of inclination are shown in Figure 2.1.

In Fig. 2.1 (a)-(c), it can be seen that the buoyancy-induced flow of air is entrained opposite to the direction of the flame spread. 'Counter-current spread' is so defined (Fernandez-Pello and Hirano, 1983). 'Co-current spread' describes those situations when the flow of air and flame spread are in the same direction, e.g. Fig. 2.1 (d) and (e). A critical inclined angle between 15^0 to 25^0 was found by Drysdale and Macmillan (1992) with 6mm thick PMMA slabs with sidewalls (150 mm long, 30 to 60 mm wide), which suggested a transition from counter-current flame spread mode to co-current one. Smith (1992) observed a similar transition at a critical inclined angle of 27^0 for a 0.3m square fire source mounted in the base of a trench. Wu and Drysdale examined two different cross-section trenches, 0.276 m and 0.09 m square, both 2 m long. They found a critical angle of 20^0 for the larger trench, which increased to 27^0 for the small one. Both Smith (1992) and Wu and Drysdale (1994) observed the critical angle to be independent of the heat release rate. In addition to the experimental approaches, Woodburn and Drysdale (1998) used CFD simulations to study the dynamics of fires in inclined trenches. The critical angle obtained was closed to that measured experimentally (Smith, 1992; Wu and Drysdale, 1994). They further found the critical angle to be dependent on the burner geometry and on the geometry of the trench through their CFD simulations.

Fig. 2.2 demonstrates the significant difference of heat transfer patterns in counter- and co-current flame spread by exemplifying horizontal and vertical upward flame spread. Focus is on the unburned leading edge of these flames because the heat transfer in this

region significantly affects the fire growth thereafter. For the vertical upward flame spread, the induced airflow makes the flame closer to the unburned combustible material and also lengthens the heating region. Therefore, the unburned zone in the upward flame spread can receive considerable radiation from the flame and convection through gas phase in addition to conduction through solid phase. On the contrary, in the horizontal and downward flame spread, the primary heat transfer mode is through conduction (at least for thick fuels). Conclusively, for the upward flame spread, the stronger and greatly-extended heating both help increase the heat absorbed in the unburned leading edge for ignition, consequently exponentially accelerating the flame spread.

Fig 2.1 – The interaction between a spreading flame and the surface of a (thick) combustible solid for different angles of inclination: (a) -90^0 (b) -45^0(c) 0^0(d) $+45^0$(e) $+90^0$. (← the direction of flame spread). (after Drysdale, 1998)

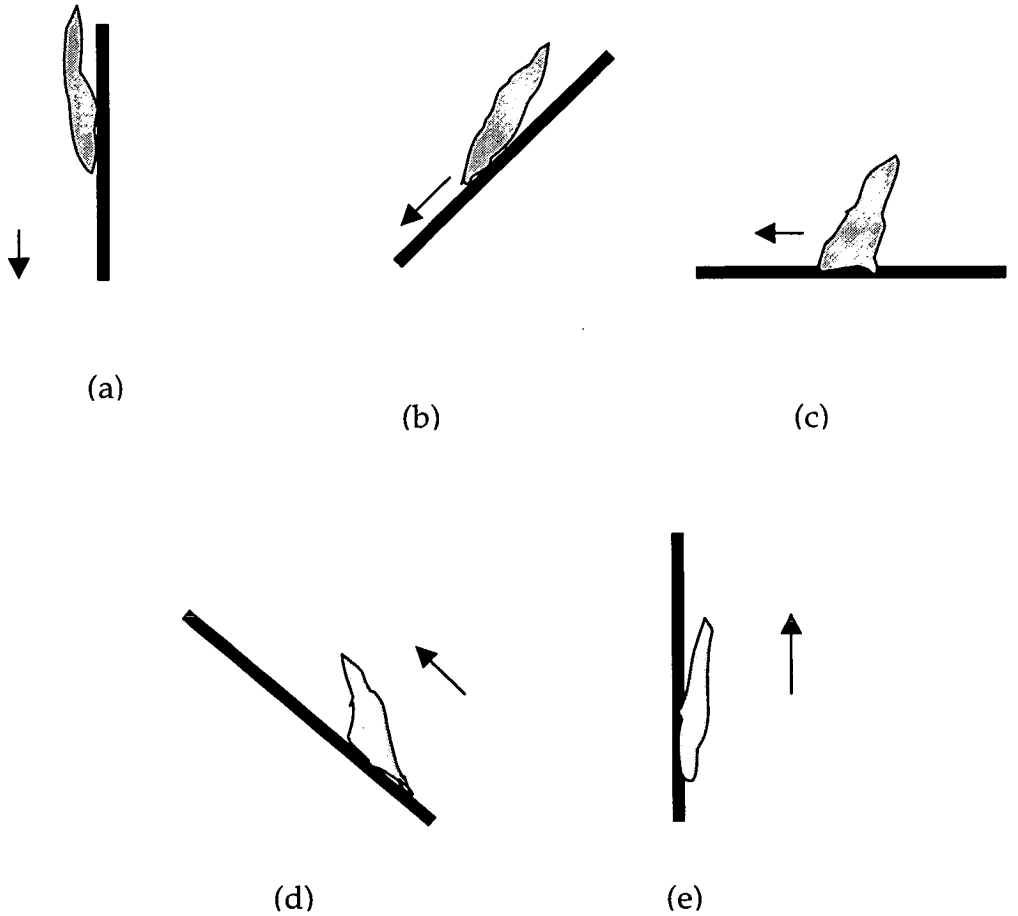

Fig 2.2 – Heat transfer mechanisms in (a) horizontal and (b) upward flame spread.

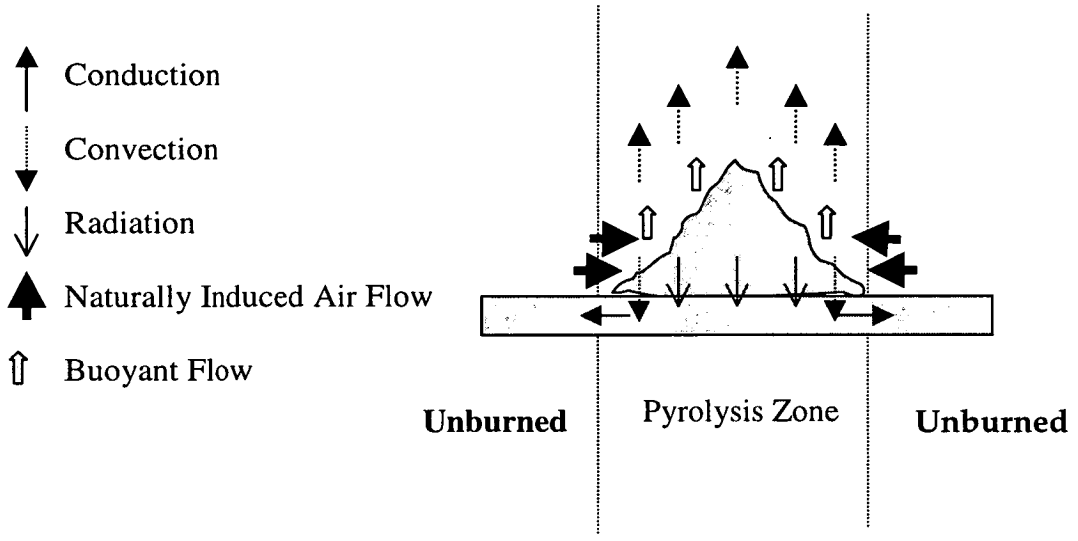

(a) Horizontal Flame Spread

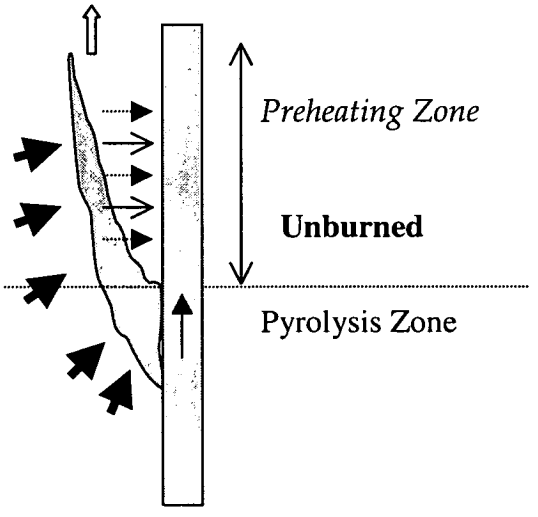

(b) Upward Flame Spread

Experimental evidence of flame spread rate measurements on different materials at different ranges of inclined angles has also been carried out. The flame spread rate on PMMA was reported by Drysdale and Macmillan (1992) to be from c.0.08 mm/s to c. 0.6mm/s (with sidewalls) at the inclined angles from 0^0 to 60^0. With physically thin fuels, burning can occur simultaneously on both sides. Their data on computer cards also showed an increase of flame spread rate from c.1.8 to 14 mm/s at the angle from 0^0 (horizontal) to 30^0. The measurement of Hirano *et al.* (1974) on computer cards also showed an increase of flame spread rate from c. 1.2 mm/s to 2.5 mm/s at the angle from -90^0 (vertically downwards) to -10^0

2.3.1.2 External Radiant Heat Flux & Preheating Effect

The external radiant heat has an effect on both the pyrolysis zone and the unburned zone of the combustible solid, therefore, helping the flame spread in two ways. In the pyrolysis zone, the extra heat transfer increases the rate of the vaporisation of fuel, and consequently produces a stronger flame. Simultaneously, in the unburned zone, the heat flux preheats the fuel ahead of the flame front, which causes the temperature of the fuel to rise more rapidly. Hasemi *et al.* (1991) analysed the effect on an upward flame spread on a vertical wall, and indicated that the external radiation directly enhances the temperature of the unburned surface. In addition, the external heat flux increases the pyrolysis rate which leads to an increase of the incident heat flux from the flame to the unburned surface. The increased pyrolysis rate enhances the flame height, which plays an important role in the acceleration of the flame spread, but this only affects upward flame spread (details will be discussed in Sec.2.4.3).

2.3.1.3 Thickness, Conductivity and Width of Fuel

In Sec. 2.3, the "Fundamental equation of flame spread" describes flame spread as a process of continuous ignition. For an advancing flame front, the exposure time for the unburned fuel is l/V. where V is the rate of spread and l is the "heating length", i.e. the length of sample perpendicular to the advancing flame over which the temperature raises

from T_o (ambient) to the ignition temperature T_{ig}. For thermally thin materials, the time to achieve the ignition temperature t_i under a given heat flux is directly proportional to the product of $\rho c \delta$, where ρ is density, c is specific heat capacity and δ is thickness of the material (Simms, 1963). Thus, the flame spread rate, which is inversely proportional to t_i, is also inversely proportional to δ. However, for thermally thick materials, the thickness should be replaced by the "depth of heating" which can be given approximately by $(\alpha t)^{1/2}$ (Drysdale, 1998), where α is the thermal diffusivity ($k/\rho c$) and t is the time in seconds during which the surface of the solid is exposed to a heat flux. After rearrangement, the flame spread rate becomes independent on the thickness of the material. Experimental evidence has been demonstrated for thermally thin materials by Magee and McAlevy (1971) and Suzuki *et al.* (1994), showing that as thickness increases, the downward flame spread rate of thin cellulosic specimen (thickness from 0.2 to 2.0mm) and filter paper (thickness from c. 0.25 to 5mm) decreases. In addition, Suzuki *et al.* (1994) showed the flame spread rate of filter paper was independent of thickness as which is over c. 5 mm and the flame even not spread as the material is too thick (for thickness > 8.4 mm).

It is reasonably expected that the higher conductivity, the lower rate of flame spread. This is also because more heat is transferred into the solid by conduction.

While the width of fuel increases, the burning zone expands. Experiments by Kashiwagi (1974) and Ray *et al.* (1980) on the horizontal flame spread on carpet and PMMA have shown that the size of flames can determine the heat transfer mechanism, which means radiation may play a more important role with the increase of fire size (Ray *et al.*, 1980, Drysdale, 1998). For upward flame spread (in which convective heat transfer from the flame to the unburned zone is also important) the increased radiant heat transfer from the flame (to the unburned zone) will consequently accelerate the spreading. However, for downward flame spread, radiant heat transfer influences the heating on the ahead unburned region very slightly, and consequently has little effect on it.

2.3.1.4 Atmosphere Composition, Gravity and Atmospheric Pressure

When oxygen concentration is increased, combustion efficiency is enhanced. The flame is hotter, so heat is transferred more rapidly. In addition, gravity has influence on buoyant effect, consequently affecting the induced flow velocity in the leading edge of flame. As gravity increases, the buoyant flow is greater and then increases the flow rate (Fernandez-Pello, 1995). For counter-current flame spread, e.g. horizontal or downward flame spread, the acceleration of induced flow rate ahead of the flame front takes away some heat used for igniting the unburned zone. The spread of the flame thus slows. This gravity effect was proved experimentally (from 1g to 4g) by Altenkirch *et al.* (1980) on downward flame spread on thermally thin fuels. In addition, more rapid upward flame spread can be postulated as gravity increases because the stronger induced gas flow helps the flame spread.

Flame spread under microgravity conditions has drawn some attention because of increasing activity in space. The absence of gravity eliminates the effect of buoyancy, therefore, changing the flame shape, etc. This microgravity research also helps combustion researchers understand other mechanisms involved more easily.

Atmospheric pressure also affects flame spread rate. Experimental results from McAlery and Magee (1969) and Bhattacharjee *et al.* (1991) for horizontal flame spread and Altenkirch *et al.* (1980) for downward flame spread derive that flame spread accelerates when pressure increases. This is partly due to the effective oxygen enrichment which enhances flame stability at the surface (Drysdale, 1998). In addition, Bhattacharjee *et al.* (1991) stated from experimental observations that increased gas-phase radiation causes an increase in the optical depth of the flame and heat transfer back to the fuel surface, which may increase flame spread rate with increasing pressure.

2.3.2 Density and Specific Heat

Foamed plastics and low-density combustible materials can develop fire and spread flame very easily because the surface temperature rises very quickly when exposed to heat. In addition, the larger the specific heat of a material is, the harder the material to be heated to its ignition temperature, because the specific heat is defined as the quantity of heat required to raise the temperature of a unit mass by one degree. The density ρ and specific heat c are often considered together with the conductivity of a material k (Section 2.3.1.3), giving the expression of "thermal inertia" ($k\rho c$) because these three material properties are the ones directly relevant to the response of the surface to heating.

2.3.3 The Difference of Initial and Ignition Temperature

It is reasonable to expect that the closer initial and ignition temperature are, the less energy is needed to raise the unaffected fuel to its ignition temperature ahead of the flame. Therefore, the less the difference of initial and ignition temperature is, the less heat is needed to achieve the ignition temperature and the faster the flame will spread.

2.4 Upward Flame Spread on Vertical Flat Surfaces

2.4.1 The Phenomenon

As discussed in Sec. 2.3.1.1, the " imbalance" of air flow entrained from the "two sides" of the incline of a burning surface influences the formation of combustion boundary layers. Experimental observations from Drysdale and Macmillan (1992) and Smith (1992) demonstrated a critical angle existing by which the development of a flame is distinguished as concurrent or counter-current. Upward flame spread is a typical concurrent flame spread. The hot, still reacting or post combustion gases generated at the burning region of the material form a buoyancy-induced flow ahead of the pyrolysis front close to the unburned combustible surface. The fuel vapours generated downstream of the pyrolysis front that are not consumed immediately by the upstream diffusion flame are driven ahead of the pyrolysis front where they keep reacting with the oxidiser, thus extending the diffusion flame downstream from the pyrolysis front (Fernandez-Pello and Hirano, 1983).

The process of upward flame spread can be further illustrated in Fig.2.3. The "wall" is undergoing pyrolysis (burning) in the region (X_p-X_b) and the surface ahead of the burning zone is exposed to flame over the height (X_f-X_p). X_b, X_p and X_f represent the heights of burnout front, pyrolysis front and flame tip from the bottom edge of the "wall".

Fig.2.3 - The schematic of upward flame spread.

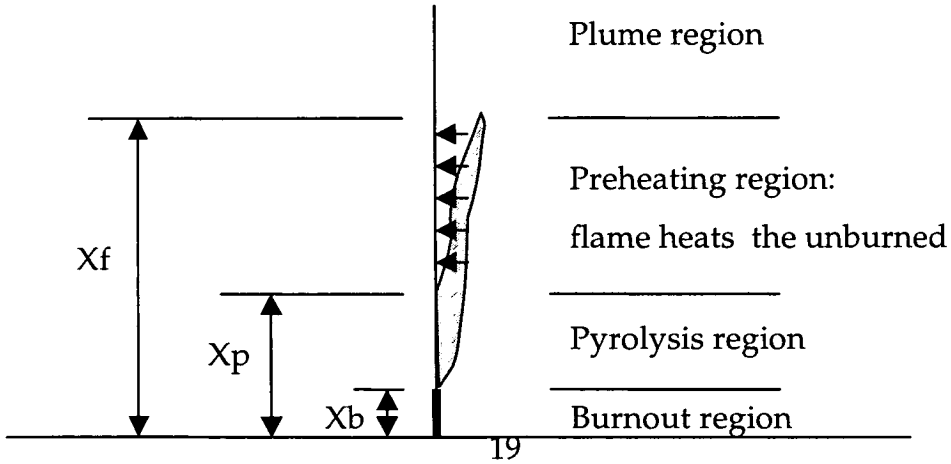

2.4.2 The Controlling Mechanisms of Upward Flame Spread

Upward flame spread attracted combustion scientists relatively early (before the 1970s), and attention has been drawn to establish its mathematical formulation. Friedman (1968) described the status of the scientific understanding of the flame spread phenomenon in the late 1960s after he examining results of some idealised experiments. The effects analysed were roughness, exposed edges, air velocity, sample orientation, material substance, width/fire size, pressure, nitrogen dilution and equimolar substitution of helium for nitrogen. He concluded combustion science was still not able to specify mathematically the laws governing a flame spread process and there was uncertainty as to which variables exert dominant effects. Although combustion scientists had produced some experimental data, no firmly established flame-spread theory in terms of known parameters existed even for the simplest imaginable geometry (Friedman, 1968). Afterwards, a large number of researchers had focused on finding out the controlling mechanisms of flame spread (e.g. Friedman, 1968; de Ris, 1968; Hirano *et al.*, 1974; Fernandez-Pello and Hirano, 1983; Wichman, 1992; Fernandez-Pello, 1995; Thomas, 1995) and upward flame spread is one special case. It can be imagined that the flame spread research, both theoretical and experimental, started with simple materials, laminar flow conditions and idealised configurations. These studies provide insights for further investigations on upward flame spread.

For a flame to spread, sufficient combustible vapours must be present to react with the oxidiser under suitable conditions. It implies that, as Fernandez-Pello described (1984), the flame spread phenomenon results from an interaction of transport processes in the gas and condensed phases, the vaporisation of the fuel and the chemical reaction of the fuel vapours with the gaseous oxidiser. Thus, the heat transfer and gas phase chemical kinetics aspects of a flame spread process are the two key reactions to establish a flame spread theory.

2.4.2.1 The Analysis on Laminar Flames on Vertical Fuel Surfaces

A useful starting point for the discussion of flame spread research is the theoretical model presented by de Ris (1968), which assumed primary importance of the "heating mechanism" in the vicinity of the pyrolysis front for modelling approach of flame spread on horizontal surfaces and ignored reaction kinetics. This "thermal modelling" approach described ignition and flame spread as a result of inert heating of the solid to an ignition temperature, including the considerations of the effects of stoichiometry, heat of combustion, gas-phase conductive heat transfer, radiation from the flame, mass transfer, fuel vaporisation and fuel-bed thermal properties. Applying this concept, a mathematical model of laminar horizontal flame spread over a combustible solid was conducted, showing reasonably good agreement with available experimental data of flame spread rate (Huggett *et al.*, 1965). The output from the model additionally demonstrated that the flame spread rate is strongly influenced by the adiabatic stoichiometric flame temperature and the fuel bed thermal properties, although the fuel bed conductivity parallel to the propagation direction was not found to be a strong influence on flame spread rate.

Although the legitimacy of ignoring reaction kinetics was still worth arguing, several theoretical treatments for laminar burning on vertical fuels have been derived by using the same assumption, and have also showed good agreement with experimental measurements. Kim *et al.* (1971) applied steady-state laminar diffusion flame equations of continuity, momentum and energy to a boundary layer equation, showing that laminar burning rates are governed by both geometric (or fluid mechanical) and chemical effects. Kung (1974) coupled both the gas-phase laminar diffusion flame processes and in-depth wood pyrolysis in the solid phase to predict the burning rate of vertical wooden slabs. Moreover, by making use of a boundary layer approximation to describe the flow and of an ignition temperature to define the rate of flame spread (Fernandez-Pello, 1978), the time-dependent heights of pyrolysis front and flame front of upward laminar flame propagation were predicted. In these theoretical studies, the rate of flame spread was singly determined by the rate at which the surface temperature of the combustible is

raised to a prescribed value, i.e. ignition temperature, through heat transfer from the flame.

The experimental methods for studying flame spread mechanisms and examining parameters relating to spread rate were reviewed by Fernandez-Pello and Williams (1976). The techniques surveyed included motion-picture and still photography, thermocouples used for measuring gas-phase and solid-phase temperatures, interferometic temperature measurements, radiometer measurements, gas sampling and analysis by gas-phase chromatography, particle track photography and pulsed-wire velocity measurement. In addition, the difficulty of measuring upward flame spread rate was noted.

Significantly, these theoretical models were somehow capable of predicting the rate of laminar upward flame spread carried out experimentally with assistance of the experimental methods summarised above. However, real fires are usually turbulent. Experimental observation on vertical burning PMMA slabs by Orloff *et al.* (1974) found laminar burning extends to a height of about 10 cm and fully turbulent burning is established for those with pyrolysis heights greater than 18 cm. Another investigation on upward fire spread over textiles also showed a very short initial laminar period (Markstein and de Ris, 1973).

2.4.2.2 Experimental Observations on Laminar and Turbulent Flames on Vertical Fuel Surfaces

Before 1980, the research primarily focused on laminar flames only because they are steadier. When more complex situations (e.g. turbulent buoyant diffusion flame with radiation loss) were considered, the analytical solution of these theoretical models became much more difficult. Within the steadier combustion reacting region, the flammable fuel vapours can mix better with the oxidiser, and the completeness of combustion is expected to be high. Therefore, even for carbon-rich materials, not much soot is produced as the flame is laminar. Thus there is not much radiation present.

However, when the flame grows upwards, more turbulence is observed. The subsequent lower degree of completeness of turbulent combustion thus results in more radiation (Drysdale, 1998).

Large-scale experiments performed with 4.5 cm thick, 41cm wide and 157cm high PMMA sheets (Orloff *et al.* 1974) have shown that the ratio of radiant heat release to the sum of radiation and convection is 69.2% at height of 38.1cm and increases to 80.9% at the height of 152.4cm. In addition, their measurement on the spread rate of the pyrolysis front showed that once the flow becomes turbulent, the spread rate is almost linearly dependent on the pyrolysis height, thereby implying a spread rate increasing exponentially with time. The turbulent flame height X_f was found to correlate with the pyrolysis height X_p.

$$X_f \propto X_p^{0.781} \tag{2.3}$$

Another series of experiments conducted by Orloff *et al.* (1976), focusing on burning rates per unit area in a large-scale vertical PMMA wall fire, also observed that radiative heat transfer accounts for from 75 to 87 % of the total feedback to the burning surface with height from 0.51 to 3.56m. They found the burning rate per unit area increases nearly linearly with height along the 3.56m high slab. The higher burning rate on higher portion of the slab can be explained because the flame was thicker. de Ris and Orloff's study (1974) using a gas-supplied burner also observed a strong increase of the ratio of radiant to total heat transfer to fuel when the flame is growing, suggesting the dominance of radiation in upward turbulent burning of most practical fuels.

For non carbon-rich materials, however, experiments by Ahmad and Faeth (1978) on 51-305 mm high wicks soaked with methanol, ethanol and 1-propanol demonstrated a different heat transfer behaviour. Only 10-20% of the heat flux to the surface is through radiation. This investigation confirmed that for non carbon-rich materials, convection is always the dominant heat transfer mode to the fuel no matter whether the flame is laminar and turbulent. This is a result of low soot content of the flames.

2.4.2.3 Early Theoretical Analysis of Turbulent Flames on Vertical Fuel Surfaces

The transport processes controlling the upward flame spread was simulated by Markstein and de Ris (1973) by utilising the measurement of mass- and heat-transfer rates obtained from a steady-state gas burner. Five assumptions were made to simplify the complexity of the upward flame problem: 1) two-dimensionality of flow, 2) neglect of gas-phase chemical kinetic phenomena, which are not rate-controlling for moderate and rapid upward spread, 3) neglect of details of pyrolysis, 4) neglect of edge-spread phenomena, and 5) neglect of detailed effects of fuel construction. Finally, a power law relationship between pyrolysis spread rate V_p and pyrolysis length X_p was found (Equation 2.4), reporting an accelerating flame-spreading process and an asymptotic value of terminal spread rate.

$$V_p \propto X_p^{0.5} \tag{2.4}$$

After the paper of Sibulkin *et al.* (1975) noticed that the flame spreading problem can be conceptually divided into two parts, the determination of the flame spreading velocity for a specified surface heat flux distribution and that of heat flux for a given burning configuration, Sibulkin and Kim (1977) presented solutions for flame spread rate for upward burning of finite slabs and rods and for a semi-finite fuel bed given distributions of surface heat flux. It became necessary to specify values of heat flux distribution and heating extent on the unburned region ahead of the pyrolysis area, however, there was no theory or sufficient data to determine these two parameters from the fuel geometry and properties. A "forward heat transfer parameter" ϕ, the ratio of the forward heat transfer (per unit width) $\dot{q}'$ to the RHR by combustion (per unit width) $\Delta H_c^{'}$, was consequently proposed to achieve the expression of flame spread rate.

$$\phi \equiv \frac{\dot{q}'}{\Delta H_c^{'}} \tag{2.5}$$

ϕ=0.13 was measured for PMMA and it is implied that there is a critical value of ϕ, $\phi_{crit.}$, given by the specific heat, heat of combustion and difference of the ambient to its pyrolysis temperature of fuel, over which the flame accelerates as it propagates upwards and below which a steady solution exists.

An accurate treatment of the radiative processes remained the condition for achieving success of modelling turbulent wall fires. Two flame radiation models developed by Tamanini (1978) were input in a modified k-ε-g model of turbulence to calculate the rate of burning of large-scale vertical walls. The k-ε-g procedure was generated by the introduction of algebraic formulae for the stresses and the mass/energy turbulent fluxes, and by the use of wall correction factors. The two models were produced by adopting one of these two scenarios: 1) the radiated power is a constant fraction of the energy liberated per unit time by chemical reaction; and 2) radiation is emitted by a thin, constant-temperature layer of soot particles at the flame fronts in addition to assuming a constant temperature soot and the most radiation emission by soot near the flame front. The prediction of the k-ε-g model of turbulence demonstrated fairly good agreement compared with the experimental data of PMMA (Orloff *et al.*, 1976) especially as adopting the latter radiation model. In addition, calculated values for amount of unburned fuel, entrainment coefficient, contribution by radiation to total wall flux and fuel mass fraction at the wall were also reported as a function of height along the wall. During the past twenty years, great progress has been made to better calculate the radiation in a fire, which is reviewed by Cox (1995) and Cox and Kumar (2000).

A study published by Delichatsios (1982) of turbulent convective flows and burning on vertical walls provided a great contribution towards understanding turbulent wall flows although it was not a flame spread model. He focused on a burning wall without appreciable radiation and noted that a model for turbulent wall flows dominated by buoyancy forces (e.g. natural convective flows, wall burning and flows with constant buoyancy flux) was not yet available. In contrast to turbulent free flows in which self-similar flow is maintained (Delichatsios, 1981), the presence of the wall precludes the self-similar flow, causing various coefficients in integral models with the variation of the

downstream distance and with the thermal boundary conditions on the wall. He proposed a two-turbulent-layer model which incorporates explicitly the wall effects by dividing the flow into two parts: an inner turbulent flow close to the wall, and the outer turbulent flow which is similar to a free flow. His prediction was in excellent agreement with Ahmed and Faeth's (1979) and Tamanini and Ahmad's (1979) measurements of wall fires fuelled by methanol, ethanol and ethane. But the author criticised Ahmad and Faeth's model (1979) for failing to include the distinct effects of buoyancy on the flow close to the wall.

Loh and Fernandez-Pello's study (1983) examined de Ris' assumption (de Ris, 1968) of ignoring chemical reaction kinetics as they studied the dependence of the spread rate of the pyrolysis front on the velocity and oxygen concentration of a concurrent forced flow. Their measurements obtained for flames spreading over thick PMMA sheets in a flat plate flow configuration showed that the spread rate of pyrolysis front on different environmental conditions can be correlated in terms of a non-dimensional parameter (Equation 2.6) equal to a constant.

$$\frac{V_p(T_{ig}-T_o)^2}{u_\infty(T_f-T_{ig})^2}=const. \qquad (2.6)$$

where V_p is the rate of spread of the pyrolysis front, u_∞ is the free stream gas velocity, T_f is the adiabatic flame temperature, T_{ig} and T_o are the pyrolysis and initial temperatures of PMMA. This correlation shows that the flame spread process is primarily controlled by heat transfer mechanism, since no finite rate kinetic terms appear in the correlation. In addition, the comparison of model predictions and experimental results seemed to accept the validity of ignoring chemical reaction kinetics in concurrent flame spread mode.

Review papers published by Fernandez-Pello and co-workers (1983, 1984) summarised the state of the understanding of flame spread in the early 1980s. Based on the advances in the experimental study of the mechanisms controlling flame spread over the surface of combustible solids, Fernandez-Pello and Hirano (1983) noted the heat transfer and gas phase chemical kinetic aspects are the two important mechanisms of the flame spread

process. Focusing on flame spread in oxidising flows that oppose or concur with the direction of propagation, the authors concluded that concurrent flame spread is primarily controlled by the rate of heat transfer by radiation and convection from the downstream flame to the unburned fuel. Thus the rate of concurrent flame spread depends on how quickly the surface temperature of unburned fuel can be raised to its pyrolysis temperature, which depends on the length of the flame and the heat flux from the flame to the unburned surface.

Fernandez-Pello (1984) presented a summary of the modelling status in the early 1980s of the phenomena of the spread of flames over the surface of solid combustibles. Concurrent flame spread is a special case. He described " At present there is a good understanding of what are the controlling mechanisms and what is a necessary formation to develop a rigorous analysis. The problem is very complicated and difficult to solve mathematically if an analytical solution is sought. The formation of a rigorous mathematical model of the flame spread process would consist of the conservation equations through the appropriate boundary conditions. This would require the solution of a system of coupled, two-dimensional, elliptic, non-linear partial differential equations that would include variable material properties, appropriated gas phase chemical kinetics and solid phase pyrolysis mechanisms." These difficulties have been examined in more detail in recent years (Fernandez-Pello, 1995).

Due to the difficulties of seeking a solution, different levels of simplifications were applied. Most of these models assumed the rate of the chemical reaction is infinite. These models can be classified as heat transfer models since they did not address chemical kinetic effects. The assumption is very reasonable especially as applied in concurrent flame spread modelling because the rate of chemical kinetics is very fast compared with the heat transfer processes.

The mathematical problem describing the heat transfer mode of concurrent flame spread basically consists in the solution of solid and gas phase energy equations. In the solid phase, the normal temperature gradients are much larger than the longitudinal ones, and

the one dimensional, transient form of the energy equations is sufficient to describe the solid phase process. An exception is the charring of materials because the char and the virgin material have different densities and the interface between the char and the virgin material varies with time, which results in great difficulty in solving equations. In the gas phase, an analysis would provide the heat flux at the solid-gas interface, a boundary condition that is essential for the accurate determination of the rate of flame spread. However, the gas phase problem is not always solved rigorously to deduce the boundary conditions for the solid phase analysis. Experimental information or expressions from steady burning surface analyses were used for these boundary conditions (Sibulkin and Kim, 1977, Markstein and de Ris, 1973, Orloff *et al.*, 1974, Annamalai and Sibulkin, 1979).

The author concluded that in realistic conditions, material properties, finite rate of kinetics, turbulence and radiation effects influence the spreading process and rigorous solutions were still difficult to achieve. However, the feedback from experimental information or engineering analyses can improve the modelling work. Fernandez-Pello and Quintiere (1982) provided a good example depending on material testing data to determine unknown or semi-empirical parameters to predict the behaviour of concurrent flame spread.

2.4.2.4 Concluding Remarks

In the early 1980s, the heat transfer behaviour has been demonstrated to be the only important mechanism for upward flame spread, a typical concurrent flame spread. Therefore, integrating and developing formations of the intensity and extent of the heat transfer effect, i.e. the heat flux and flame height in upward flame spread modelling, became important. Several models, e.g. Karlsson, 1993; Grant and Drysdale, 1995 (details in Sec. 2.4.5.1) have been developed, applying the correlations of these two parameters. A reliable expression is needed for the modelling work. In addition, models need the properties of combustible materials as input. Several small-scale tests have been developed to provide information.

In the following sections, the flame height and heat flux will be reviewed first because of their usage in the new approach of modelling work which will be introduced afterwards.

2.4.3 Flame Height

Flame is the luminous portion of the volume within which combustion is occurring. Thus flame height could be inferred as the vertical visible extent of the gas phase burning process. Because the flame height determines the extent of heating above the burning area, determination of flame height has become an important issue of fire safety engineering.

Thomas *et al.* (1961) attempted to explore the relationship between flame height from a given fire and the fuel characteristics and dimensions of the fire. They measured the height of the external flames from burning wood cribs on a square horizontal base, inside a cubical, open-sided enclosure and also flame heights on strips of hanging fabric. They noted that for a freely burning fuel, buoyancy plays an important role in determining flame height. Their results showed that a functional relationship (Equation 2.7) exists for the first case: burning cribs of wood on a square horizontal base although weaker relations were proposed for the other two scenarios.

$$\frac{X_f}{D} = f\left(\frac{\dot{Q}^2}{gD^5}\right) \tag{2.7}$$

where X_f is flame height, D is the dimension of a fire, $\dot{Q}$ is the RHR of the fire. This is different from the previous finding that X_f/D is a constant for turbulent, high momentum fuel jets (Hottel and Hawthorne, 1949), demonstrating a limiting case of the ($\dot{Q}^2/D^5$) relation.

2.4.3.1 Previous Theoretical and Experimental Investigations

Several theoretical analyses for the flame height of wall fires have been conducted and have led to correlations (Delichatsios, 1984; Quintiere *et al.*, 1986; Eklund, 1986). Delichatsios (1984) extended his postulate (Delichatsios, 1983) to the cases of free turbulent line plumes and two-dimensional turbulent wall fires that flame heights in buoyant diffusion flames (laminar or turbulent) are essential independent of the stoichiometry and only dependent on total heat release rate. Following the physical arguments of the effect of buoyancy and the mass flow rate at flame tips where the convective heat release rate is enough to enhance the temperature of the mixture of fuel vapours and oxidiser from ambient to their characteristic flame temperature, a correlation was derived.

$$X_f \propto \frac{\dot{Q}'^2}{\rho_o^2 C_p^{\,2} T_0^{\,2} g}^{1/3} \tag{2.8}$$

where X_f is the flame height, $\dot{Q}'$ is the RHR per unit width of the material.

The flame height expression was supported by experimental results (Steward, 1964; Orloff *et al.*, 1977).

In addition, the author presented an integral model for predicting flame heights in vertical wall fires. He assumed that, above the flame tip, burning is complete so heat is transferred only by convection. For sooty flames, the convective heat flux is an order of magnitude less than the radiant heat flux so the heating of the wall surface above the flame tip was neglected. Moreover, conceptually, flame height was determined as the vertical position where the fuel concentration is zero. Introducing radiation empirically as an external input to the model, the pyrolysis rates in PMMA fires, the flow in an ethane wall fire dominated by radiation and the flame height in PMMA fires and in small turbulent convective fires can be predicted fairly well.

Quintiere *et al.* (1986) also derived an expression for flame height by assuming that a flame extends until the fuel is completely consumed. That is, the entrainment rate of air primarily controls the flame height. They demonstrated that flame heights of wall fires are proportional to the energy release rate per unit width in a 2/3 power law (n =2/3 in Equation 2.9).

$$X_f = K\dot{Q}'^n \tag{2.9}$$

Aeklund (1986) discussed the flame height phenomenon from another viewpoint addressing flame as a region of intense vorticity generation. He considered the flame tip occurs when enough oxygen has been brought into the flame to combust the burning wall volatiles at a stoichiometric ratio and the oxygen induced into the flame is related to the vortex strength of the flame. Although this assumption is far too simplistic (much more air is entrained than is needed to burn the volatiles), he established a two-dimensional vortex model which was able to predict the flame height.

$$X_f = 5.0 \left(\frac{\dot{Q}'}{\rho_o C_p T_o g^{1/2}} \right)^{2/3} \tag{2.10}$$

where $\dot{Q}'$ is the RHR per unit width of the material

All of these studies concluded that the flame height is proportional to the rate of heat release per unit width in a two-thirds power law (n=2/3 in Equation 2.9).

Several experimental investigations (Orloff *et al.*, 1974, Hasemi, 1984, Saito *et al.*, 1985, Quintiere *et al.*, 1986, Sugawa, 1991, Tu and Quintiere, 1991, Coutin *et al.*, 1999) using different experimental rigs have also been carried out to analyse the flame height phenomenon. A comparison of these experiments is given in Table 2.1, showing the type of fire (linear burner or wall fire; whether steady or spreading fires, laminar or turbulent), the geometric configuration and whether or not sidewalls were present. These experiments can be classified into three types: (1) linear fires produced by line burners

against a wall, and (2) wall fires produced by vertical gas burners, and (3) vertical burning fuels in which the rate of mass loss was measured or estimated and the heat of combustion assumed to be constant.

(1) Linear fires produced by line burners against a wall

Porous line burners against isothermal and thermally thin walls were used in studies by Hasemi (1984) and Sugawa *et al.* (1991) to simulate the wall fires. In Hasemi's study (1984), the burner dimensions (width (D) × length (L)) were 0.0375m × 0.27m, 0.82m × 0.27m, and 0.0075m × 0.92m, where D was taken as the characteristic dimension) were used and sidewalls were present in his isothermal wall case to help maintain a two-dimensional flow but not in the thin wall case to help maintain two-dimensional flow. Sidewalls are not mentioned in Sugawa's study (1991). By changing the rate of supply of gaseous fuel, different rates of heat release were simulated. The corresponding heights of the flame tips were determined from video recordings. The rate of heat release (RHR) per unit width was calculated from Equation 2.11.

$$\dot{Q}' = \dot{m}' \Delta H_c \tag{2.11}$$

where $\dot{m}'$ is the rate of supply of fuel (per unit width of burner) (kg/m.s) and ΔH_c is its heat of combustion (kJ/kg).

A dimensionless RHR parameter $\dot{Q}_l^{'*} = \dfrac{\dot{Q}'}{\rho\ C_p T_o g^{1/2} D^{3/2}}$ was found to determine the flame height as follows:

$$X_f / D = \gamma \dot{Q}_l^{'*n} \tag{2.12}$$

where X_f is the flame height, D is a characteristic length and γ is a constant. In Hasemi's study (1984), for $\dot{Q}_l^{*} > 1$, n= 2/3 and γ= 6.0. For $\dot{Q}_l^{*} < 1$, n= 0.8. In Sugawa's study (1991), n was confirmed experimentally to be 2/3 in the range $5 < \dot{Q}_l^{*} < 20$.

Table 2.1 Flame situations (line or wall fires; steady or spreading flames; laminar or turbulent), geometric configuration and sidewall effects of previous experimental set-ups on flame height correlations.

	Line or wall fire	Geometric configuration	Laminar or turbulent	Spreading or steady flame	Sidewall	Method used to obtain $\dot{Q}'$ (**)
Hasemi (1985)	line fires	without floor but with a line burner below burning slabs	-	steady	yes	ΔHc(E) $\dot{m}'$ (C) (Eqn.2.6)
Sugawa *et al.* (1991)	line fires	with floor	-	steady	no	ΔHc(E) $\dot{m}'$ (C) (Eqn.2.6)
Coutin *et al.* (1999)	wall fires	without floor	turbulent	steady	entirely, partially confined and unconfined	ΔHc(E) $\dot{m}'$ (C) (Eqn.2.6)
Quintiere *et al.* (1986)	wall fires	without floor but with a line burner below burning slabs	turbulent	spreading (*)	yes	$\dot{Q}''$ (E) (Eqn.2.9)
Tu and Quintiere (1991)	wall fires	without floor but with a line burner below burning slabs	turbulent	spreading	yes	ΔHc(E) $\dot{m}''$ (M) (Eqn.2.10)
SQW (1985)	wall fires	with floor	turbulent	spreading	no	ΔHc(E) $\dot{m}''$ (E) (Eqn.2.10)
Orloff *et al.* (1974)	wall fires	with floor	from laminar to turbulent	spreading	yes	-

(*) The flame produced was spreading but measurements were carried out as it became steady.

(**) (E), estimated; (C), controlled (gas flow); (M) ,measured

Hasemi's data (1984) with natural gas and other gaseous fuels were interpreted by Tu and Quintiere (1991): the results are plotted in Figure 2.4 and show the following correlation:

$$X_f = 0.032\dot{Q}'^{0.76} \tag{2.13}$$

The r^2 value is 0.89. The value of n is appreciably greater than the expected value of 2/3 derived from theoretical analyses.

Fig.2.4 Previous flame height correlations carried out with gas burner line fires by Hasemi (1985), SQW (1985) and Kulkarni (SQW and Kulkarni's data were interpreted from Tu and Quintiere's study (1991)).

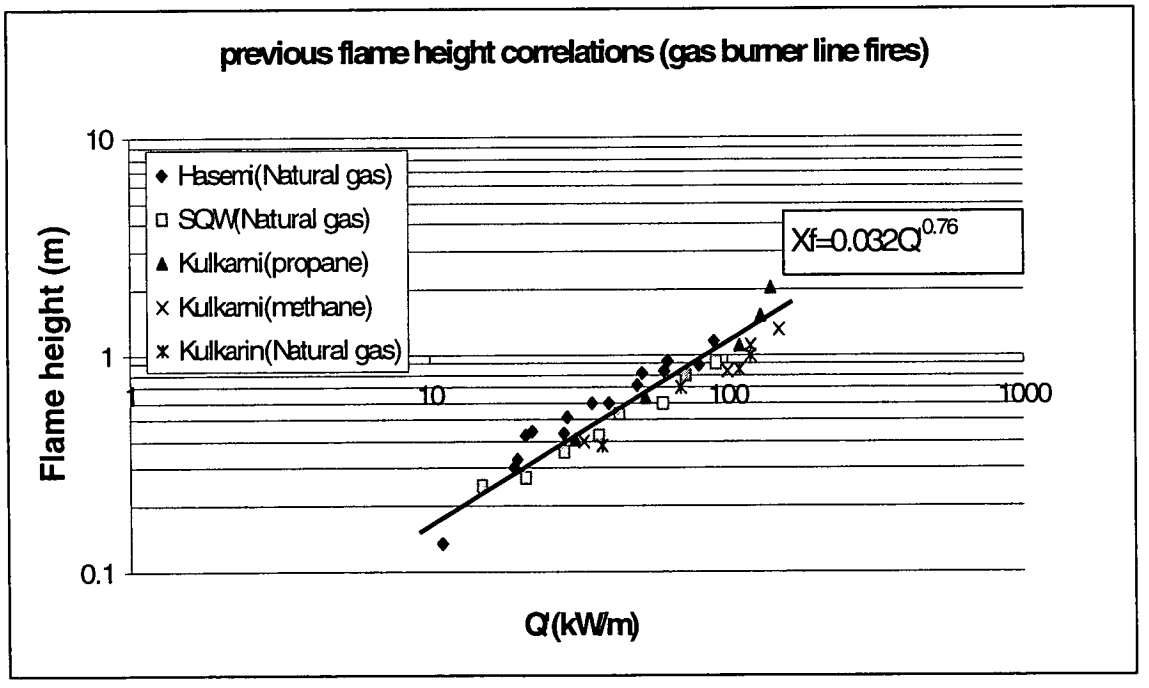

In the study of Sugawa *et al.* (1991), four methods to determine the visible flame heights were discussed, i.e. (1) infrared images, (2) judgement by eye, (3) normal photographs and (4) video tape recordings. The results according to these four methods were compared with one another. The flame heights depend strongly on the definition and the observation or record methods. To use an infrared camera, a minimum temperature of flame has to be determined first and the highest position of the temperature contour line was defined as the flame tip. In their study, this was 250^0C. An agreement was showed between the results carried out by these four methods. However, personal difference in eye-averaged flame heights seemed to be unavoidable.

(2) Wall fires produced by vertical gas burners

Wall fires were simulated by vertical gas burners in the form of flat panels by Coutin *et al.* (1999). The burner width was fixed at 0.4 m and the burner height was set at 0.25, 0.5 and 1 m. Three configurations were studied with their measurement: (a) The burning wall was entirely confined by two sidewalls, (b) The burner was partially confined over its lower part and (c) Unconfined. The $\dot{Q}'$ was calculated using Equation 2.11. A new and objective methodology using a CCD camera was applied to map flame luminosity.

They observed that the flame height is sensitive to the geometric configuration. Pyrolysis height and burner width seemed to affect the flame height correlation. However, no systematic measurements were made and no clear conclusions were drawn.

(3) Vertical burning fuels, assuming a constant heat of combustion

Flame height measurements on 28.4 cm square samples of burning materials in a vertical orientation were made by Quintiere *et al.* (1986). A pilot ignition flame was placed at the base and sidewalls were provided to prevent lateral air entrainment. By exposing the samples to different levels of external radiation, various solid fuel burning rates could be simulated. Once steady burning had been achieved, the flame height was measured.

Assuming a constant heat of combustion, RHR per unit width was calculated by following Equation 2.14.

$$\dot{Q}' = \dot{Q}'' X_p \tag{2.14}$$

where $\dot{Q}''$ is the RHR per unit surface area. Their data followed the 2/3 power law (see Equation 2.9) although there was considerable scatter. Tu and Quintiere (1991) modified the experimental rig to allow the measurement of transient mass loss rate and the corresponding flame height for both charring and non-charring materials (PMMA and wood; 28.5 cm wide and 29.5 cm high). Using Equation 2.15,and then Equation 2.14,

$$\dot{Q}'' = \dot{m}'' \Delta H_c \tag{2.15}$$

the flame height correlation was found to obey the 2/3 power law, but the value of K (flame height constant in Equation 2.9) was higher than for the results obtained from line fires against a wall (Hasemi, 1984). Figure 2.4 compares the data of Quintiere *et al.* (1986) and Tu and Quintiere (1991). The best fit still follows Equation 2.9 with a correlation coefficient of 0.79, but with $n = 0.58$.

$$X_f = 0.09 \dot{Q}'^{0.58} \tag{2.16}$$

Orloff *et al.* (1974) and Saito *et al.* (SQW) (1985) also measured flame heights but used PMMA sheets up to 150 cm in height. In both of these studies, line burners were adopted to ignite the lowest edge of samples, but sidewalls were only used by Orloff *et al.* (1974). One significant difference from the earlier work was the presence of a floor which would have altered the mode of air entrainment at the base of the "wall". The flame height of the spreading flame was correlated in SQW's study (1985) by calculating the RHR per unit width from the estimated fuel supply rate and heat of combustion (Equation 2.15 and then 2.14). The flame height correlation obeyed Equation 2.9, but with a higher value of n than that obtained from steady burning experiments (Quintiere *et al.*, 1986). This can

been seen in Figure 2.5 which compares all of the above correlations. The higher power may be a result of the higher pyrolysis rates achieved in the upper part of the pyrolysing fuel during the spreading process (Saito *et al.*, 1985, Orloff *et al.*, 1974). It was also noted that the presence of sidewalls increased the length of the flames because two-dimensional flow patterns were maintained (Saito *et al.*, 1985).

Fig.2.5 - Previous flame height correlations carried out with burning solid fuels by Tu and Quintiere (1991), Quintiere et al (QHH) (1986) and Harkleroad (interpreted from (Tu and Quintiere,1991)).

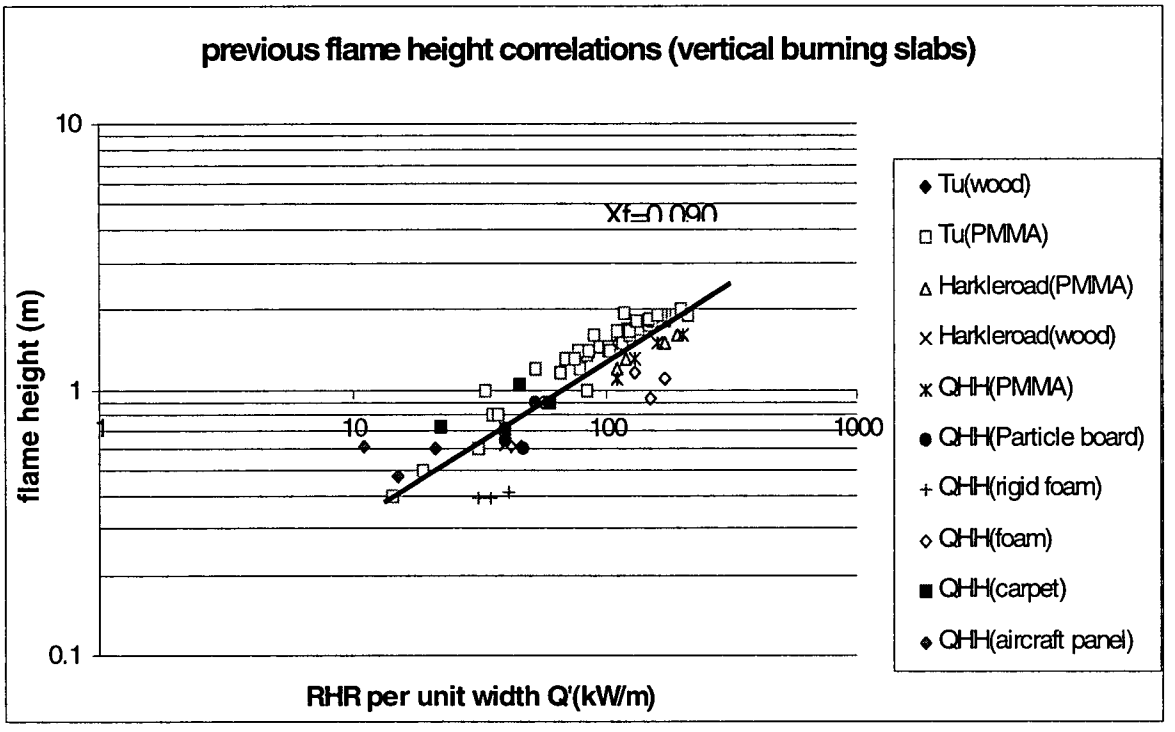

2.4.4 Heat Transfer from Flame to Unburned Surfaces

The wall flame heat flux distribution was measured by Hasemi (1984, 1985) by using porous, methane line burners (30cm long, 3.7 or 8.2cm wide) against an isothermal wall and methane line burner (92 cm long and 7.5cm wide) against thermally thin walls. The isothermal wall case adopted sidewalls but without a floor present. On the contrary, the

thin wall case was conducted with a floor present but without using sidewalls. Using line burners, he noted that the behaviour of flames near the burners may be different from that of vertical fuels. However, after comparing his data with others (Ahmad and Faeth, 1978, Liburdy and Faeth, 1978), very consistent correlations were made lying in four distinct regions by utilising the same parameter characterising the visible flame heights of gas burner line fires, $\dot{Q}_l^{'*} = \dot{Q}'/\rho_0 C_p T_o g^{1/2} D^{3/2}$.

(1) $X/\dot{Q}_l^{'*\,2/3}\mathrm{D} \leq 1$ (lower part of the solid flame)

$\dot{q}_w''$ tends to increase with height.

(2) $1 \leq X/\dot{Q}_l^{'*\,2/3}\mathrm{D} \leq 2.8$ (upper part of the solid flame)

$\dot{q}_w''$ is apparently constant, and it appears to be a weakly increasing function of $\dot{Q}_l^{'*}$. The flame thickness is almost constant with height.

(3) $2.8 \leq X/\dot{Q}_l^{'*\,2/3}\mathrm{D} \leq 10$ (transition region)

The slope is the steepest among the four regions with all the data points falling onto

$$\dot{q}_w'' \approx 45(X/\dot{Q}_l^{'*\,2/3}\,\mathrm{D})^{-5/2} \tag{2.17}$$

(4) $10 \leq X/\dot{Q}_l^{'*\,2/3}\mathrm{D}$ (buoyant plume region)

The heat flux here can be correlated by

$$\dot{q}_w'' \approx 2.5(X/\dot{Q}_l^{'*\,2/3}\,\mathrm{D})^{-1.3} \tag{2.18}$$

Quintiere *et al.* (1986) also took heat flux measurement along with their flame height work with 28.5× 28.5cm burning surfaces (PMMA, rigid form, carpet, flexible form, aircraft panel and particle board). Heat flux meters were flush mounted on the centreline of a contiguous water-cooled plate which was located above the samples. Cooled side-plates were also included to form a channel and restrict side flow into the flames and preserve two-dimensionality of the boundary layer flow over the plate. Their results were

plotted in terms of X/X_f and were very consistent with Hasemi's correlations plotted in the same format (1985).

Quintiere and Cleary (1994) used dimensional analysis to examine heat transfer from flame to vertical surfaces. Configurations included a line fire against a wall, a square burner flame against a wall and in a corner, and window flames impinging on a wall. Their discussion began with the expression of total heat flux $\dot{q}_w''$ combined by two heat transfer modes, convective $\dot{q}_{wc}''$ and radiative $\dot{q}_{wr}''$. After employing several other correlations, dimensional or dimensionless, the heat flux can be expressed as a function of X/X_f, Y/X_f, X_f /D and κD where X, Y are vertical and horizontal distances, X_f is flame length, D is burner dimension and κ is the flame absorption coefficient.

Their analysis suggested that the heat flux distribution is similar with distance from the source normalised with flame length (X/X_f) after examining previous data of methane line burner fire (Hasemi, 1985), liquid saturated wall fires (Ahmad and Faeth, 1979) and burning wall materials (Quintiere *et al.*, 1986). In addition, they found the maximum flame heat flux (occurring at $X/X_f \approx 0.2$-0.3) is about 30 kW/m^2 for flame as high as 2 m.

Brehob *et al.* (2001) suggested another dimensionless format expressing the heat flux distribution using the data of Quintiere *et al.* (1986) and Kim (1991)

$$\frac{\dot{q}_w''}{\dot{q}_{wo}''} = \exp\left[-C_o\left(\frac{X - X_p}{X_f - X_p}\right)\right] \tag{2.19}$$

where $\dot{q}_{wo}''$ is the maximum heat feedback from flames to surface and the decay factor C_o was determined to be 1.37. The correlation allows determination of $\dot{q}_w''$ based on a single value of $\dot{q}_{wo}''$ which they suggested may be treated as a "fire property" of the wall material.

2.4.4.1 The Averaged Heat Flux from Flame to Unburned Surfaces

Recent modelling work for upward flame spread on flat surfaces will be reviewed in the next section. Most of the models considered the heat flux correlation but to simplify the problem assumed the $\dot{q}_w''$ to be constant over the preheating region and then zero above (Saito *et al.,* 1985; Mowrer and Williamson, 1991; Delichatsios *et al.*, 1991; Delichatsios and Delichatsios, 1991; Delichatsios and Chen, 1995; Grant and Drysdale, 1995; Anderson *et al.*, 1996; Kokkala *et al.*, 1997; Qian and Saito, 1997; Quintiere and Lee, 1998). Saito *et al.* (1985) used 25 kW/m^2 as the constant heat flux exposed from which mass loss rate was deduced for their steady-state model. Good consistency has been shown with their PMMA flame spread rate measurement. Mowrer and Williamson (1991) chose 30 kW/m^2 as the irradiance of the Cone Calorimeter under which material flammability properties were carried out. In addition, they chose 50 kW/m^2 to obtain the data of burning duration time. Delichatsios and co-workers (1991) also adopted 30 kW/m^2 to be the fixed total flame heat flux of burning walls with flame heights shorter than 1.5 m in their Upward Fire Spread and Growth (UFSG) code, and considered radiative and convective heat transfer separately for flames higher than 1.5 m. However, 25 kW/m^2 was used in their projects concerning PE/PVC cables (1995) and charring materials (1995). In addition, Grant and Drysdale (1995) took the average of the heat flux measured with their tests on cardboard, and suggested 20 kW/m^2 to represent the heating scenario. Applying the Grant and Drysdale model, Anderson *et al.* (1996) used 35 kW/m^2 as the constant heat flux for hardboard, plywood and wallpaper covered wood surfaces. But 25 kW/m^2 was chosen again in the modelling work of Kokkala *et al.* (1997), which focused on wood surface products, Qian and Saito (1997) which analysed the difference of the heat feedback over vertical flat and corner walls, and Quintiere and Lee (1998) which assessed ignitor and thickness effects on upward flame spread. Table 2.2 summarises the representative heat flux chosen by these models.

Table 2.2- The summary of the representative heat flux in preheating zone (Fig. 2.3) chosen by upward flame spread models

Modelling work	Heat flux chosen (kW/m^2)	
Saito *et al.* (1985)	25	
Mowrer and Williamson (1991)	30	50 for obtaining burning duration time data
Delichatsios *et al.*(1991)	30	
Delichatsios and Delichatsios (1995)	25	
Delichatsios and Chen (1995)	25	
Grant and Drysdale (1995)	20	Averaged value during the whole burning process
Anderson *et al.* (1996)	35	
Kokkala *et al.* (1997)	25	
Qian and Saito (1997)	25	
Quintiere and Lee (1998)	25	

2.4.5 New Approaches for Upward Flame Spread Modelling

In Sec. 2.4.2.4, a review of the state of art of modelling upward flame spread in the early 1980s identified two major points. First, the heat transfer behaviour has been demonstrated to be the dominant mechanism of upward flame spread. The intensity and extent of the heat transfer effect, i.e. the heat flux and flame height, are two important parameters. Second, it was difficult to quantify material properties, finite rate of kinetics, turbulence and radiation effects influencing the spreading process in realistic conditions and to achieve rigorous solutions. Experimental data became the alternative input to provide unknown or semi-empirical parameters. Fernandez-Pello and Quintiere (1982) demonstrated a good example depending on material testing to predict the

behaviour of concurrent flame spread. In addition, several small-scale tests have been developed to provide information for the modelling work and for practical selection of materials. Models based on the thermal theory of Saito *et al.* (1985) are discussed first (Sec.2.4.5.1), then alternative approaches are considered (Sec.2.4.5.2- 2.4.5.5).

2.4.5.1 Modelling Work Initiated by the Thermal Theory of Saito *et al.* (1985)

SQW's approach

A thermal theory of steady-state upward flame spread discussed by Saito *et al.* (SQW) provided a conceptually new approach to the modelling work. Several assumptions were made in their thermal theory:

1. The material is homogeneous and its thermal properties are constant with temperature.
2. The responsible energy flux for spread, both radiative and convective, occurs to be approximately 25 kW/m^2 for $(X_p < X < X_f)$, which was observed by Quintiere *et al.* (1986) and X_p is the height of the pyrolysis front, and 0 kW/m^2 for $X>X_f$ where X_f is the height of flame tips,
3. $(X_f - X_p)$ remains approximately constant during spread, and the upward flame spread rate is

$$V_p = 4\dot{q}''^2 (X_f - X_p)/[\pi k\rho c(T_{ig} - T_o)^2] \tag{2.20}$$

where k, ρ and c are the thermal conductivity, density and heat capacity, respectively, of the fuel and T_o and T_{ig} are the ambient and ignition (or pyrolysis) temperatures of the fuel. Equ.2.20 can be rewritten as

$$V_p = (X_f - X_p)/\tau \tag{2.21}$$

where τ is the time to ignition.

$$\tau = \frac{\pi k \rho c (T_{ig} - T_o)^2}{4\dot{q}''^2} \tag{2.22}$$

4. As a simplification for describing time dependent spread, this expression continues to apply with $(X_f - X_p)$ variable and that remains an approximately constant time characteristic of upward spread.

Equ. 2.21 needs expressions of the time to ignition τ, flame height and pyrolysis height. τ depends on fuel properties, the ambient temperature and the level of the heat flux to the fuel from the flame. X_p and X_f can be expressed as:

$$X_p = X_{po} + \int V_p(t_p) dt_p \tag{2.23}$$

where X_{po} is the value of X_p at an initial time t=0 and t_p is the dummy variable of integration, and

$$X_f = K[\dot{Q}_b' + \Delta H_c \int \dot{m}'' dx]^n \tag{2.24}$$

where $\dot{Q}_b'$ is the RHR per unit width of the burner used, ΔH_c is the heat release per unit mass of fuel consumed, $\dot{m}''$ is the mass loss rate per unit area of the fuel, n and K are constants.

For non-charring materials, $\dot{m}''$ is approximately independent of X in the range $0<X<Xp$. Thus,

$$V_p = \frac{dX_p}{dt} = [K(\dot{Q}_b' + \dot{Q}'' X_p)^n - X_p]/\tau \tag{2.25}$$

where τ, n, K and $\dot{Q}''(=\Delta H_c \dot{m}'')$ are taken as known constants, and $\dot{Q}_b'$ is a known, "adjustable" function of time. Solving the integral equation Equation 2.25, the position

of X_p can be predicted. However, for charring materials, more expressions have to be involved because of the variation of $\dot{m}''$.

Kulkarni and Fischer's model

Kulkarni and Fischer (1989) extended SQW's theory to accept an arbitrarily specified local mass loss rate as a function of time and allowed the power n of the flame height correlation (Equation 2.24) not equal to unity, unlike previous model in which n was set equal to unity to simplify analysis.

Their mass loss rate data was obtained by a load cell continuously recording the weight of the sample. Other inputs to the model were $k$pc , ignition temperature T_{ig} and heat of combustion ΔH_c, which was determined using a Cone Calorimeter.

Thomas's Analysis

Thomas (1994) further discussed SQW's theory focusing on the flame height correlation. A difference appears of the power n of the correlation (Equ. 2.9) used in upward flame spread modelling: between 2/3 and unity. From the theories and experimental data (Section. 2.4.3), 2/3 is the power which should be used. However, for any real positive $\dot{Q}_b'$, $\dot{Q}''(=\Delta H_c \dot{m}'')$ and $K_{2/3}$, there is a value of X_p at which $(dX_p)/(dt)$ becomes zero (Equ.2.25 with n =2/3). The models based on the 2/3 power law always predict extinction whilst those based on the unity power law permit the possibility of exponential acceleration.

His analysis noticed that the power n plays a critical role as the integral (Equ.2.25) is solved. After introducing wall friction, burnout at the rear and a finite width of burning, the flame continues to spread without extinction.

The progress made by Mowrer and Williamson (1991)

Mowrer and Williamson (1991) developed another model following SQW's thermal theory by including the consideration of burnout. Once burnout commences, the rate of fuel burnout can be expressed as:

$$V_b = (X_p - X_b) / t_{bo} \tag{2.26}$$

where X_b is the position of burnout front and t_{bo} is the burning duration. A linearised flame length approximation was used following Quintiere et al. (1986), SQW (1985) and Cleary and Quintiere (1991). Before burnout commences

$$\frac{X_f}{X_p} = K_f \dot{Q}'' \tag{2.27}$$

where K_f is a constant and $\dot{Q}''$ is the RHR per unit area of fuel. After burnout begins, the dimensionless flame length is expressed as:

$$\frac{X_f - X_b}{X_p - X_b} = K_f \dot{Q}'' \tag{2.28}$$

Finally, before burnout commences,

$$X_p = X_{po} \exp[(K_f \dot{Q}'' - 1)t / \tau] \tag{2.29}$$

where τ is time to ignition. The flame spread rate will be acceleratory if $X_f > X_p$ and deceleratory if $X_f < X_p$, i.e., if $K_f \dot{Q}'' < 1$.

After burnout begins,

$$X_p - X_b = (X_{fo} - X_{po}) \exp[(K_f \dot{Q}'' - \frac{\tau}{t_{bo}} - 1)(t - t_b) / \tau] \tag{2.30}$$

Where X_{fo} is the flame height at t=0 and t_b is the time to burnout. If the parameter $(K_f\dot{Q}''-\frac{\tau}{t_{bo}})>1$, acceleratory spread is predicted.

The Cone Calorimeter was used, however, only for determining flammability parameters $\dot{Q}''$, t_f, t_b and t_{bo}. The irradiance level of the cone heater was determined to be 30 kW/m^2 for the flame spread on flat vertical surfaces and 50 kW/m^2 for larger scale room/corner tests.

Karlsson's model

Karlsson (1993) combined the thermal theory of concurrent flame spread developed by Saito, Quintiere and Williams (SQW) (1985) with empirical flame height correlations and pioneered the use of RHR data from the Cone Calorimeter to produce an approximate method for predicting fire growth in a corner configuration. Full details will be shown in Sec. 2.5 discussing upward flame spread in a corner, but the assumptions were as follows:

(1) The material is thermally thick, homogeneous and its thermal properties are constant with temperature.
(2) Chemical kinetics is excluded.
(3) The flame length, X_f, depends on a power of $\dot{Q}'$, the total heat release rate per unit width.
(4) Heat flux from the flame is constant only within the region $X_p < X < X_f$.

He obtained the following expression for the upward flame velocity (an integral equation of the Volterra type (second kind)):

$$V(t)=\frac{1}{\tau}[K\{X_{po}\dot{Q}''(t)+\int_0^t \dot{Q}''(t-t_p)V(t_p)dt_p\}^n-(X_{po}+\int_0^t V(t_p)dt_p)] \qquad (2.31)$$

where $V(t)$ is the flame spread rate, τ is the ignition delay time, X_{po} is the initial burning region, K and n are constants, t is time, t_p is the dummy variable of integration and $\dot{Q}''(t)$ is the rate of heat release (RHR) from the burning material expressed mathematically as

$$\dot{Q}''(t) = \dot{Q}''_{max} e^{-\lambda t} \tag{2.32}$$

where $\dot{Q}''_{max}$ is the maximum value of the RHR from the Cone Calorimeter at 30 kW/m^2, and λ is the decay coefficient, determined empirically from the RHR data (Fig.2.6). By solving Equation 2.31 analytically, the rate of flame spread can be predicted.

Fig.2.6- Mathematical representation of the material RHR.

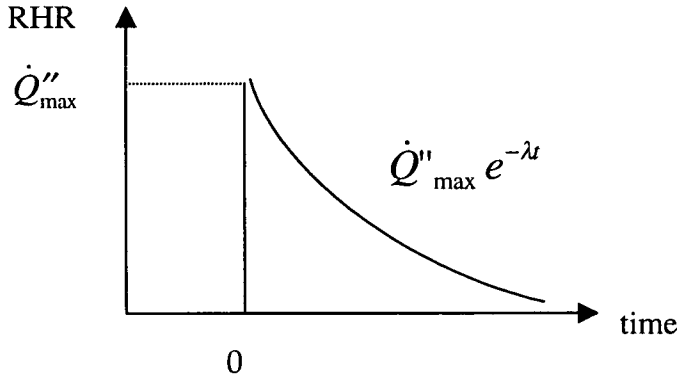

Grant and Drysdale's Model

In the Karlsson model, burnout is not considered. Grant and Drysdale (1995) developed the model further not only to include burnout, but also to allow the heat release rate data from the Cone Calorimeter to be used directly as input, without using the approximate form as given in Equation 2.32. This resolves the problem which arises if the RHR data cannot be approximated by this equation which assumed that the RHR reaches its maximum value as soon as the sample is ignited, then decreases with a decay coefficient λ.

Before burnout occurs, the expression for the flame spread rate is given by Equation (2.31), but after burnout occurs, the velocity becomes,

$$V(t) = \frac{1}{\tau}[K\{\int_{t-t_b}^{t} \dot{Q}''(t-t_p)V(t_p)dt_p\}^n - (\int_{t-t_b}^{t} V(t_p)dt_p)] \qquad (2.33)$$

where t_b is the burnout time. The integral equations (Equations 2.31 and 2.33) (Volterra type, second kind) were solved numerically.

The Cone Calorimeter tests were carried out at an irradiance of 20 kW/m^2, the average of measured heat flux from flame to unburned surface of 7.5 mm thick cardboard. (This model will be used in this study to predict the flame spread rate of a wall fire and details of this model will be discussed again in Chapter 4.)

The Examination of Grant and Drysdale's model with other materials by Anderson *et al.*

Anderson *et al.* (1996) used hardboard, plywood and wallpaper covered wood surfaces to examine Grant and Drysdale's model (1995). The irradiance of the cone heater was set up to be 35 kW/m^2, which is higher than those determined by other researchers (Table 2.2). In their study, very good agreement of flame spread rate predicted by Grant and Drysdale's model (1995) was found with experimental data, but the steady-state flame spread rate was not supported by measurement.

Model Performance for Wood Products

Kokkala *et al.* (1997) developed a model solving Equation 2.21 directly and examined this model with wood products. They showed in their large scale tests that the upward flame spread in a charring material proceeds in two phases. (1) After ignition the flame spreads first but it stops after a few minutes. Then the rate of heat release begins to decrease. (2) Once the heat wave reaches the rear surface, the insulation causes the

interior temperatures to increase and the rate of heat release per unit area increases again making the flame spread further up the wall. In addition, the substrate behind the wall material had an effect on the heat release rate.

2.4.5.2 Hasemi's Model

Based on a concept of ignition and flame spread as a result of inert heating of the solid to an ignition temperature, Hasemi (1985) presented an engineering model of the upward turbulent flame spread on a vertical combustible surface. If the formation of char at the fuel surface is negligible, the surface temperature at X can be represented as

$$T_s(X,t) - T_o = \int_0^t \dot{q}_w''(X, t-\tau)\phi(\tau)d\tau \tag{2.34}$$

where $T_s(X,t)$ is the surface temperature at X, T_o is the initial temperature, $\dot{q}_w''(X, t-\tau)$ is the heat flux applied to the surface at $(t-\tau)$ after ignition, $\phi(\tau)$ is an impulse response of the surface temperature to heat application and its functional form is dependent on wall conditions. The location of the pyrolysis front can be given as a function of time by solving Equation 2.35.

$$T_{ig} - T_o = \int_0^t \dot{q}_w''(X, t-\tau)\phi(\tau)d\tau \tag{2.35}$$

After ignoring surface reradiation for simplicity, expressing $\phi(\tau) = (\pi k\rho c\tau)^{-1/2}$ for a semi-infinitely thick combustible wall and replacing τ with X_p by $\tau = X_p/V_p$, the upward flame spread rate V_p can be solved as

$$V_p = \{\int_0^{\infty} (\dot{q}_w''(\xi + X_p)/\sqrt{\xi})d\xi\}^2 / \pi k\rho c(T_{ig} - T_o)^2 \tag{2.36}$$

where ξ is the height above the pyrolysis front.

For thermally thin materials, $\phi(\tau)$ was taken as $\exp(-h_i t/c\delta)$ where h_i is the heat transfer coefficient and δ is the thickness of the material. The flame spread rate becomes

$$V_p = \frac{1}{\rho c \delta (T_{ig} - T_o)} \int_0^{\infty} \dot{q}_w''(\xi + X_p) \exp(-h_i \xi / \rho c \delta V_p) d\xi \qquad (2.37)$$

To solve the flame spread rate equations Equation 2.36 and 2.37, it appears that the value of $\dot{q}_w''$ has to be estimated whist k, ρ, c, and T_{ig} are material properties. The expression of $\dot{q}_w''$ was carried out by experiments and has been introduced in Section 2.4.4 described by Equations 2.17 and 2.18. The prediction by this model was found to be slightly higher than experimental data. The author's explanation was that a steady state flame spread rate was conducted which gives the upper limit of V_p for growing wall flames.

Hasemi and coworkers (1991) further worked on unsteady-state upward flame spread, noticing the steady state flame spread is somehow unusual since the nature of upward flame spread in unwanted fires is essentially transient.

Because the distribution of the heat flux from flame to unburned surfaces can be related to flame height (Section 2.4.4, (Hasemi, 1985)) and V_p and the distance of $(X_f - X_p)$ are constant in steady state flame spread, the heat flux consequently can be expressed as a function of location within the preheating region. On the contrary, in unsteady state flame spread, the heat flux from the flame to the unburned surface should be expressed as a function of the ratio of the location and flame height. Therefore, different from Equation 2.35 for steady state burning, the location of pyrolysis front can be given by

$$T_{ig} - T_o = \int_0^t \dot{q}_w''(X_p / Q_l^{*2/3} \varepsilon) \phi(\tau) d\tau \qquad (2.38)$$

where $Q_l{}^*$ is the parameter characterising flame height (Section 2.4.3.1) and ε_p is the location of pyrolysis front at the time τ, ($(Q_l{}^{*2/3}\ \varepsilon_p)$ is a quantity proportional to flame height). The authors found that the only function satisfying Equation 2.31 is an exponential function, thus

$$X_p = X_{po} \exp(\alpha t) \tag{2.39}$$

and

$$V_p = dX_p / dt = \alpha X_p \tag{2.40}$$

Equation 2.40 shows that the flame spread rate is not a constant and is related to X_p. This was demonstrated experimentally by Orloff *et al.* (1974) giving the V_p for PMMA

$$V_p \propto X_p{}^{0.964} \tag{2.41}$$

Finally, the flame spread rate becomes

$$V_p = \frac{X_p}{\pi \kappa \rho c (T_{ig} - T_o)^2} [\int_0^\infty \dot{q}_w{}'' \{\exp(\lambda) / Q_l{}^{*2/3}\} / \sqrt{\lambda} d\lambda]^2 \tag{2.42}$$

where $\lambda = ln(X_p/X_{po})$. The steady state flame spread rate can be written in a form comparable to Equation 2.42.

$$V_p = \frac{X_p}{\pi \kappa \rho c (T_{ig} - T_o)^2} [\int_0^\infty (Q_l{}^{*1/3}\ \dot{q}_w{}''(\lambda + 1/Q_l{}^{*2/3}\} / \sqrt{\lambda}) d\lambda]^2 \tag{2.43}$$

The form of these two equations (Equations 2.42 and 2.43) is similar.

2.4.5.3 Mitler's Model

Mitler (1990) started his model also with the concept of ignition and flame spread as a result of heating of an inert solid to an ignition temperature. The surface temperature of a semi-infinite slab was given by the same algorithm as Equation 2.35 in another form

$$T_s - T_o = \frac{1}{\sqrt{\pi k\rho c}} \int_0^t \frac{\varphi(t')dt'}{\sqrt{t-t'}} \tag{2.44}$$

where φ(t)is the uniform net heating flux, t is time and t' is the dummy integral variable. $k\rho c$ was found from the LIFT apparatus (Quintiere and Harkleroad, 1985).

Mitler (1990) described that the equation is the basis for most analytic approaches, and there are drawbacks in the approaches: a number of simplifying assumptions or transformations must be made. Some of these have been: linearised radiation loss, a constant heat flux in the preheating region up to the flame tip height and zero thereafter, temperature-independent $k\rho c$.

In Mitler's model (1990), the heating flux φ(t) was expressed by the assumed linear superposition of the fluxes from the burner and from the wall fire. In addition, as in Hasemi's model (1985, 1991), flame height correlation as a function of $\dot{Q}'$ was needed to express the heat flux distribution.

Following

$$\dot{Q}' = \frac{\dot{m}\Delta H_c}{w} = \{\int \dot{m}''(X)dX\}\Delta H_c \tag{2.45}$$

where w is the width of the burning slab and $\dot{m}''$ is the mass loss rate. Mass loss rate became the parameter to determine the flame height and then heat flux. Mitler (1990)

provided two options for obtaining this $\dot{m}''$: the first option is to use the quasi-steady-state algorithm described by Mitler (1989), which is based on an energy balance at the surface. However, it requires data which are not always readily available, and it cannot handle heterogeneous, charring or composite materials. Also, transient pyrolysis and in-depth radiation absorption are neglected. The difficulties are largely avoided with the second option: to use experimental mass loss rates from the Cone Calorimeter as input, instead. The second approach automatically included the effects of charring, of transient heating, etc., to a first approximation. The mass loss rate found in this second option is obtained at one fixed irradiance. Mitler (1990) introduced arguments to allow the heating flux from the flame vary from point to point as well as being a function of time. The author reported that, compared with the results of PMMA experiments carried out by Orloff *et al.* (1974), good agreement was demonstrated applying both these two options.

2.4.5.4 Delichatsios' Model

The model of Delichatsios *et al.* (1991) also started with the concept of ignition and flame spread as a result of inert heating of the solid to an ignition temperature. They employed an exponential temperature profile across the wall, giving the temperature T at the depth Z during heat-up:

$$T = T_o + (T_s - T_o)e^{-Z/\delta} \tag{2.46}$$

and during pyrolysis:

$$T = T_o + (T_p - T_o)e^{-(Z-\delta_p)/\delta} \tag{2.47}$$

where δ is the thermal depth and δ_p is the depth of pyrolysed material.

δ and δ_p are determined by the heat flux to the unburned fuel $\dot{q}_w''$ and material properties. The height of pyrolysis front can consequently be predicted by solving 1-D heat conduction equations derived from Equations 2.46 and 2.47. As in the models reviewed before, $\dot{q}_w''$ was expressed in association with flame height X_f. The key flammability

properties of materials, that were required as an input to the upward flame spread model, were discussed by Delichatsios and Saito (1991), summarising the measurement methods and their interpretation. Very good agreement was shown with the experimental data of pyrolysis front history of PMMA wall fires (Orloff *et al.*, 1974).

The $\dot{q}_w''$ is related to the mass loss rate of the pyrolysing material. For steady-state (or quasi-steady) burning,

$$\dot{m}'' = \frac{\dot{q}_w''}{\Delta H_g} = \frac{\dot{q}_w''}{L + c(T_{ig} - T_o)} \tag{2.48}$$

where ΔH_g is the effective heat of gasification for a thermally thick solid, L is the latent heat of pyrolysis. However, if the effect of transient pyrolysis is considered, Delichatsios and Delichatsios (1992) derived a new expression:

$$\dot{m}'' = \frac{\dot{q}_w''}{\Delta H_g} fcn\left[\frac{t - t_p(X)}{t_p(X) - t_f(X)}, \frac{L}{c(T_{ig} - T_o)}\right] \tag{2.49}$$

where t is time, t_p(X) is the time to pyrolysis, (t_p-t_f) is the time interval between the arrival of the flame front at the location X and the time at which the location X starts to pyrolysis. The effect of transient pyrolysis was demonstrated in their study of laminar upward flame spread on non-charring materials (Delichatsios and Delichatsios, 1992) and turbulent one on non-charring materials (Delichatsios *et al.*, 1995). Upward flame spread on charring material and PE/PVC cables in a tray configuration were studied (Delichatsios and Chen, 1995; Delichatsios and Delichatsios, 1995). The upward flame spread rate on these special materials were carried out by means of a methodology determining material properties used in their upward flame spread model.

2.4.5.5 Beyler *et al.*'s Model

In Beyler *et al.*'s model (1997), prior to ignition, the wall surface is assumed to be a semi-infinite one-dimensional slab with a time dependent surface heat flux determined from the wall and external sources. The conduction model used was an approximate solution to the semi-infinite slab problem using an assumed cubic temperature profile. The resulting temperature profile becomes:

$$T_{ig} - T_o = \frac{\dot{q}''_{net}\delta}{3k}[1 - \frac{Z}{\delta}]^3 \tag{2.50}$$

where δ is the thermal penetration depth and Z is the depth into the wall surface. The surface temperature at any time was then given by the following differential equations:

$$2(T_s(X,t) - T_o)\frac{dT_s(X,t)}{dt} - \frac{[T_s(X,t) - T_o]^2}{\dot{q}''_{net}(X,t)}\frac{d\dot{q}''_{net}(X,t)}{dt} = \frac{\dot{q}''_{net}(X,t)}{3k\rho c} \tag{2.51}$$

$$\frac{d\dot{q}''_{net}(X,t)}{dt} = -4T_s(X,t)^3\frac{d\dot{q}''_{net}(X,t)^3}{dt} \tag{2.52}$$

These two equations were solved using a fourth order Runge-Kutta method for each time step. The net heat flux can be calculated from the following equation:

$$\dot{q}''_{net}(X,t) = \dot{q}''_{imp} + \dot{q}''_{w} - \sigma\varepsilon[T_s(X,t) - T_o]^4 \tag{2.53}$$

where $\dot{q}''_{imp}$ is the imposed heat flux (a constant and uniform heat flux used to heat material surface), $\dot{q}''_{w}$ is the heat flux from the flame to surface, σ is the Stefan-Boltzmann constant (5.668×10^{-11} kW/m^2-K^4) and ε is the emissivity. The model needed data of $k\rho c$ and T_{ig}, which were determined from ignition experiments in the Cone Calorimeter. Their RHR prediction was very consistent with experimental measurement of PMMA carried out by Wu *et al.* (1993), plywood by Delichatsios *et al.* (1995) and vinyl ester panel by Ohlemiller and Cleary (1995).

2.5 Upward Flame Spread in a Corner

Upward flame spread in a corner has long been recognised to constitute a great hazard than that on a flat surface. Ohlemiller *et al.* (1998) pointed out two reasons for this. First, the walls (and flame volumes) can exchange radiation; this enhances the local burning rate and, in turn, this accelerates fire spread. Second, the plume of hot gases is diluted less rapidly because the air inflow is partially blocked by the second wall; this allows the plume to transfer more of its heat to the wall surfaces, again enhancing the flame spread process.

The interaction of a wall (or walls) and a fire source was discussed by Zukoski (1995), showing that the presence of a wall (or walls) near the source of a plume can strongly influence the entrainment of air and other properties of the plume. Fig. 2.7 shows a characteristic sketch of three cases in Zukoski's study (1995): a fire source near or flush with walls and corners. He suggested that the interaction of an axisymmetric plume with a vertical wall or a corner formed by two walls could be estimated approximately by using a reflection principle: an axisymmetric plume source placed next to a plane vertical surface or wall would develop as half of a plume which has a source with twice the heat release rate, and the plume placed in a corner, as a quarter plume rising from a source with four times its heat release rate.

Fig. 2.7- Fire sources near walls and corners. (a) circular fire source near a wall. (b) semi-circular fire source against a wall. (c) fire source in a corner.

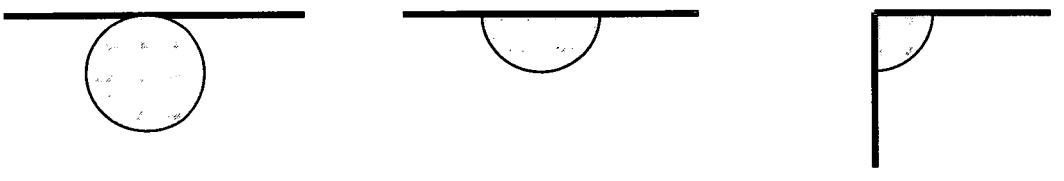

(a) (b) (c)

Experimental work showed that, when a circular burner was placed with one edge tangent to a vertical wall (Fig.2.7(a)), the plume continued to develop as an axisymmetric plume with the wall roughly to one edge tangential. The plume geometry and entrainment rate were not strongly affected by the presence of the wall because entrainment was not blocked by the wall.

However, when a semicircular burner was placed with its straight edge against a wall (Fig.2.7(b)) the plume was attached to the wall and developed as a half plume with flame height and entrainment rate closely approximating those for a full circular burner with twice the fuel flow rate. Similarly, when a quarter segment of a round burner was placed in a corner, the plume attached to both walls and developed as if it were one quarter of the plume rising above a circular burner with four times the fuel-flow rate.

2.5.1 The Corner/ Wall Fire Initiating from a Square Burner

Hasemi and Tokunaga (1984) used square burners (side length: 0.3 and 0.5 m) to examine this conceptual method which assumes the existence of an "imaginary fire source", with the same intensity as the actual fire source, in the other side of the wall. The authors noticed that this method does not take account of wall friction nor heat loss due to conduction through the wall. In addition, the existence of walls near a fire source is thought to suppress the growth of eddy scale in the plume. They measured the temperature and flame height on the plumes. A dimensional parameter was observed to characterise the flame height.

$$\dot{Q}^* \equiv \dot{Q}/\rho_\infty C_p T_o g^{1/2} D^{5/2} \qquad (2.54)$$

where $\dot{Q}$ is heat release rate and D is the characteristic size of fuel (e.g., the side length for square fuels and the diameter for round fuels).

For unconfined plumes, the height of flame tips was correlated

$$X_f/D = 3.5\dot{Q}^{*n} \tag{2.55}$$

where n ≈ 2/3 for $\dot{Q}^*$<1 and n ≈ 2/5 for $\dot{Q}^*$>1.

For fire plumes against a wall, the height of flame tips was expressed

$$X_f/D = 3.5\dot{Q}^{*2/5} \tag{2.56}$$

This coincides generally with that in the unconfined case for $\dot{Q}^*$>1, and for the plumes in a corner,

$$X_f/D = 4.3\dot{Q}^{*2/3} \tag{2.57}$$

The results (Equations 2.48, 2.49 and 2.50) showed a significantly different effect of the presence of a wall and corner-walls.

Compared with the study of Hasemi and Tokunaga (1984) deriving the flame height relation in a corner of walls for $\dot{Q}^* < 4$, Kokkala (1993) made measurements of visible flame height, temperature and heat flux up to $\dot{Q}^* = 23$ in a similar configuration. Three square burners with side length of 0.17, 0.3 and 0.5 m were used. His data for flame height were correlated

for $\dot{Q}^*$<8.6

$$X_f/D = -1.73 + 4.96\dot{Q}^{*2/3} \tag{2.58}$$

or

$$X_f/D = 3.03\dot{Q}^{*0.90} \tag{2.59}$$

both with r^2=0.993.

For $\dot{Q}^*$> 8.6,

$$X_f/D = 15.6 + 0.40\dot{Q}^* \tag{2.60}$$

Reasonably good agreement was shown among the correlations carried out by Hasemi and Tokunaga (1984) and Kokkala (1993) for low $\dot{Q}^*$.

Kokkala (1993) reported his measurement of heat flux carried out at a distance of 20 mm from the corner, showing the heat flux can be expressed as a function of dimensionless height X/X_f. From his data, it can be seen that the heat flux distribution of these three burners differed systematically. The maximum values produced by the three burners all occurred in the range $0.06 < X/X_f < 0.6$, however, the 0.5 m square burner produced the highest among the three ones. The author noticed that this was expected because the radiation depends on the thickness of the flame. The 50 cm burner produced the thickest flame due to its largest burning area.

For the 0.17 m burner the peak heat flux to the wall was between 50-60 kW/m^2 and for the 0.30 m burner between 70-80 kW/m^2. However, in the 0.5 m burner, the heat flux depended strongly on the level of heat output ranging from 20 kW/m^2 at 40 kW to 115 kW/m^2 at 300 kW. This was because of the separation of the flame from the wall with the smallest heat release rate.

Because the corner fire scenario has been recognised to be a challenging configuration, the tests like room/corner (ISO 9705) were developed to represent a real scale fire test (Sec. 1.3.2). Williamson and Dembsey (1990) summarised the history of corner testing, showing the first one was carried out in 1950s. While the room/corner fire test is recognised to be realistic, it is not useful for material development due to its high cost and large material requirements. Further, the results from ISO 9705 tests cannot be used to predict the material's performance in other fire scenarios. As a result, there is an ongoing interest in relating bench scale fire tests to more real scale fire tests like the ISO 9705 test, and in the use of results of bench scale tests in models that can predict material performance over a wide range of fire scenarios of importance (Beyler, 2000).

The first attempt applying a laboratory-scale test for making predictions of room fire growth over interior finish materials was done by Smith and Satija (1983). The criteria they considered for describing when a product will start to burn was not the surface temperature but a parameter "FTP, flux-time product".

$$FTP = \quad [(\dot{q}''-SPF)^n \Delta t] \tag{2.61}$$

where $\dot{q}''$ = average incident flux over time increment Δt

SPF= self propagating flux; that flux at which a flame will just propagate from a point of flame impingement

n= empirical constant; for many materials n=1; for retarded materials, n may be greater than 1

The minimum FTP was determined from the material energy release rate data from a dynamic calorimetry apparatus (1984). Combining the consideration and expressions of the heating of upper layer, venting, wall plume, etc., the rate of involvement of combustible surfaces can be carried out.

Ostman and Nussbaum (1989) developed a relationship for predicting the time to flashover in a full-scale fire test. The relation was based on bench-scale RHR measurements in the Cone Calorimeter.

$$t_{flashover} = a\frac{t_{ig}\sqrt{\rho}}{\dot{Q}''_{\max,50}} + b \tag{2.62}$$

where $t_{flashover}$ is the time to flashover, t_{ig} is the time to ignition in small scale test at 25 kW/m^2, $\dot{Q}''_{\max,50}$ is the peak heat release rate at 50 kW/m^2, ρ is the density of the linings, and a and b are constants. The determination of the irradiance of 25 and 50 kW/m^2 was based on trial and error.

Goransson and Wickstrom (1990) reported a model that predicted the rate of heat release of linings in the room/corner test, based on the Cone Calorimeter test results. The total heat release rate can be expressed as follows.

$$\dot{Q}_{tot}(t) = \dot{Q}_b(t) + \sum_{i=1}^{N} \Delta A^i \dot{Q}'' \tag{2.63}$$

where $\dot{Q}_{tot}(t)$ is the total heat release rate, $\dot{Q}_b(t)$ is the heat release rate from the burner, ΔA^i is the area increment at the i th time step Δt ($N \times \Delta t = t$) and $\dot{Q}''$ is the heat release rate

history of the material involved which is measured under 25 kW/m^2 irradiance in the Cone Calorimeter. The burning area growth is assumed to depend on time as

$$A(t) = A_0 + \beta\left(\frac{t}{t_{ig}}\right)^2 \tag{2.64}$$

where A_o is the area behind the burner at the initial stage, equal to 2 m^2, β is a constant empirically obtained to be 0.05 m^2/s. However, after 10 minutes, when the burner output is raised, the A_o is 5 m^2, β is 0.5 m^2/s. Very good agreements were shown with experiments.

Karlsson *et al.* (1990) presented a model using material properties derived from standarised bench-scale tests as input data to predict the fire growth in the room/corner test and a 1/3 scale test. Before the pyrolysing area propagates to the nearest corner and a strip of material at the top of the wall starts to pyrolyse, the total heat release rate was expressed:

$$\dot{Q}_{tot} = \dot{Q}_b + A_w\dot{Q}''+A_h\dot{Q}'' \tag{2.65}$$

where $\dot{Q}_{tot}(t)$ is the total heat release rate, $\dot{Q}_b(t)$ is the heat release rate (RHR) from the burner, $\dot{Q}''$ is the RHR from the wall material, A_w is the pyrolysing area on the wall and A_h is the horizontal pyrolysing area. In Equation 2.65, the A_w was approximated to be the product of the width of the burner and the distance between the burner to the ceiling. A_h was expressed empirically with material properties $k\rho$ c. The expression of $\dot{Q}''$ needed experimental data. Thus, the ignitability test (ISO 5657) and RHR test (the Ohio State University apparatus, an open configuration NIST test and the Cone Calorimeter) were used to provide data. In addition, downward flame spread rate was available if the surface spread of flame test was carried out for T_{ig} (the ignition temperature) and Φ (flame spread parameter).

Two years later, Karlsson (1993) presented another model for calculating the RHR in the room/corner test, where lining materials were mounted on both walls and ceilings. This has been discussed in Sec.2.4.5.1.

Cleary and Quintiere (1991) also developed a model to predict fire spread over a surface and its resultant energy release. They considered wall, floor and ceiling orientations, but only the flame spread on walls will be discussed here. The total heat release rate can be expressed

$$\dot{Q}_{tot} = \dot{Q}'' A_p \tag{2.66}$$

where $\dot{Q}''$ is the RHR of material and A_p is the pyrolysis area.

For the wall case, Fig. 2.8 illustrates the pyrolysis area. Therefore, before burnout ($t<t_b$),

$$A_p = 2[X_p Y_0 + (Y_p - Y_0)X_0 + \frac{1}{2}(X_p - X_0)(Y_p - Y_0)] \tag{2.67}$$

After burnout,

$$\begin{aligned} A_p = {} & 2[X_p Y_0 + Y_p X_0 + \frac{1}{2}(X_p - X_0)(Y_p - Y_0)] \\ & - 2[X_b Y_0 + Y_b X_0 + \frac{1}{2}(X_b - X_0)(Y_b - Y_0)] \end{aligned} \tag{2.68}$$

Fig. 2.8- The pyrolysis area on one of the corner walls. The area of the initial ignited rectilinear zone is $2X_0Y_0$, and the fronts of extended pyrolysis zone is (X_p, Y_p) and those of burnout is (X_b, Y_b).

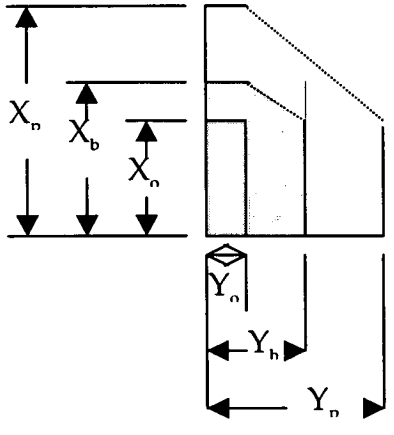

The X_p, X_b can be obtained following SQW's theory (1985) which has been discussed in Sec. 2.4.5.1. The required information was the RHR of material $\dot{Q}''$, burning time t_b and ignition time t_{ig}. The Cone Calorimeter was used to provide these data by interpreting the RHR curve (see Fig. 2.9). The RHR of material $\dot{Q}''$ was taken as the average of the RHR.

Fig. 2.9- The schematic of data from the Cone Calorimeter.

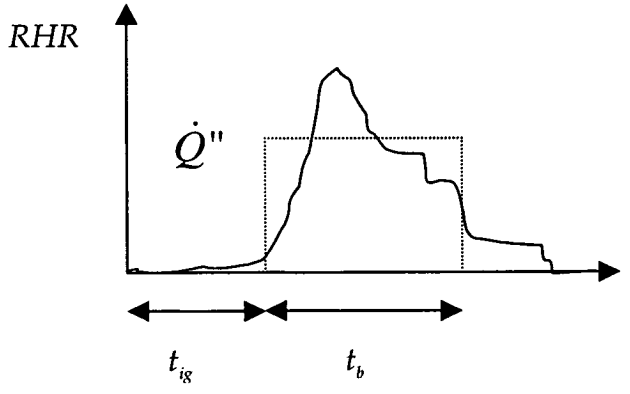

The Y_p, Y_b can be obtained by solving the Equation (2.69).

$$\frac{dY_p}{dt} = \frac{\Phi}{k\rho c(T_{ig} - T_0)^2} \tag{2.69}$$

where Φ is the flame heating parameter in opposed flow spread, which is directly derivable from the LIFT (ISO 5658) standard procedure.

Two years later, Quintiere (1993) presented another model including the consideration of room thermal feedback (e.g. from the upper layer hot gas). However, this will not be discussed.

2.5.2 The Corner/ Wall Fire Initiating from the Bottom of the Corner Walls

Hasemi (1996) measured the flame height and incident heat flux distribution on an open wall corner, simulating wall fires at the corner with fuel injection only from vertical perpendicular surfaces without from a square burner (without a square burner). Two porous burners (width W of 0.225 m and height H of 0.45 and 0.9 m) were used to form a corner (see Fig. 2.10). The flame height was observed to correlate with a dimensionless RHR parameter Q_v^*.

$$Q_v^* = \frac{\dot{Q}}{\rho C_p T_o (gH)^{1/2} (WH)} \tag{2.70}$$

The flame height correlation is---

$$X_f / H = 6.0 Q_v^{*0.60} \tag{2.71}$$

The heat flux was measured and the results showed that the heat flux meters nearest to the corner received the highest heat flux compared with other heat flux meters at the same horizontal level. The heat fluxes at the corresponding heights, i.e. at identical X/H, were relatively close and the maximum was c. 35 kW/m2. In addition, no clear correspondence was seen at greater distances from the corner, suggesting strong dependence of the horizontal heat flux distribution on the width of the burning zone.

Fig. 2.10- The schematic of the L-burners used by Hasemi (1996).

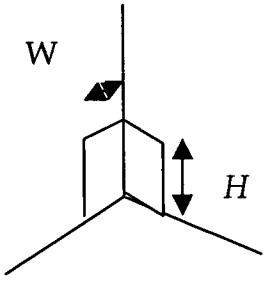

Qian *et al.* (1994) pointed out the difference of upward flame spread modelling work between that on vertical flat surfaces and in a corner: most of the models for flat surfaces treated the flame spread as one-dimensional (Sec.2.4.5), however, transient three-dimensional nature of the fire induced flow has to be considered for corner fires. They used an infrared imaging temperature measurement technique to study flame spread behaviour and the pyrolysis region spread characteristics. Temporal isotherms on large PMMA samples were successfully obtained, from which the progress rate of the pyrolysis front was automatically deduced. It was found from their infrared images that the pyrolysis front shape was always "M-shaped", i.e., little spread in the corner, with the maximum rate of spread within a few centimeters of the corner.

Four sets of experiments were carried out to help identify the mechanisms by which the M-shape is formed. The PMMA slabs were 1.6 m high, 0.3 m wide and 0.02 m thick and were flush-mounted and fixed to large Marinite walls.

1: Effect of ignition mode

Three modes of ignition were tested: first, a uniform line ignition was applied at the bottom of both corner walls; second, a "spot" ignition at the bottom corner; third, only one side wall was ignited on its bottom. For all the three cases, a very similar M-shape pyrolysis front shape was resulted.

2: Effect of solid-phase conduction heat loss

Two different corner configurations (case A and B in Fig.2.11) were designed to test this assumption. In case A, two PMMA samples were glued together to form a solid corner; while in case B, a hollow corner was formed. For case A, a large conduction heat loss was expected through the solid corner wall; while a minimal loss was expected for case B. From the experimental observation, a very similar M-shape was still seen.

Fig.2.11- The schematic of two configurations of PMMA samples in a corner.

3: Fire-induced flow cooling

The two walls were separated by 1 cm to reduce the fire-induced flow along the corner. The 1 cm distance was sufficiently smaller than the distance between the corner and the pyrolysis front peak. The M-shape was still observed.

4: Flame displacement effect

From their tests, they found that the distance between the maximum gas temperature location and the wall corner can change by changing the corner angle. They investigated this by designing experiments for corner angles of 45^0, 90^0, 135^0 and 180^0. They found that if the angle was greater than 135^0, there was no M-shape formation. This can be explained if, for corner angles $<135^0$, the mixing of pyrolysis products and air is poor and fuel rich mixture is found between the corner and the flame. The thickness of this fuel rich layer is great enough to reduce heat transfer to the corner where the temperature does not reach pyrolysis temperature and the M-shape is formed.

In addition, they used different materials (cardboard, particle board and black PMMA) to examine the M-shape mechanisms, suggesting that the material properties were not likely important for the M-shape formation.

The flame spread rate was measured on their 1.6 m high PMMA samples with ignition length on the foot of the wall of a "spot", 10 cm, 20 cm, 30 cm and 40 cm. It was found that with increasing ignition width from a "spot" to 20 cm, the upward flame spread rate of the peak pyrolysis front V_{pp} increased; while for 20 cm $\leq$ ignition length $\leq$ 40 cm, the V_{pp} remained constant. The authors suggested that this is because the fire-induced flow

in the corner may not be enhanced further with the ignition length ≥ 20 cm.

For X_{pp} < 20 cm, the ignition effect was significant and transition from laminar flame spread to turbulent occurred. The best fit for X_{pp} > 20 cm:

$$X_{pp} = 0.003t^{1.84} \tag{2.72}$$

The spread rate V_{pp} (in cm/s) for X_{pp} (in cm) for the flames with ignition length ≥ 20 cm was observed to be proportional to X_{pp}:

$$V_{pp} = 0.0134X_{pp}^{0.944} \tag{2.73}$$

This is three times faster than that for the same scale vertical flat wall carried out by Orloff *et al.* (1975) (Equation 2.74). (Equation 2.73 can be compared with Equation 2.74 for vertical flame spread on a flat surface, where X_p represents the peak location of pyrolysis front of a wall fire on a wide vertical surface.)

$$V_p = 0.00374X_p^{0.964} \tag{2.74}$$

The width of the pyrolysis zone at the bottom of the walls, Y_{pb} (in cm), was also found a function of time

$$Y_{pb} = 0.0113t + Y_0 \tag{2.75}$$

where Y_o is the ignition length in cm.

A similar fit of the geometry of the pyrolysis region (> 20 cm) was found with the X_p and Y_p normalised by X_{pp} in vertical direction and Y_{pb} in horizontal direction.

$$\xi = 32.74\eta^5 - 107.24\eta^4 + 127.87\eta^3 - 67.30\eta^2 + 14.0\eta + 0.02 \tag{2.76}$$

where

$$\xi = \frac{X_p}{X_{pp}} = \frac{X_p}{0.003t^{1.84}} \tag{2.77}$$

and

$$\eta = \frac{Y_p}{Y_{pb}} = \frac{Y_p}{0.0113t + Y_0} \tag{2.78}$$

The heat flux was measured by 5 heat flux meters located at 25, 50, 75, 100 and 125 cm above the bottom of the wall along the locations where peak pyrolysis front occurred. Also recorded were the heat fluxes when the flame tips and pyrolysis fronts reached the heat flux meters. A decreasing heat flux was observed as the height of the burning zone increased. However, no clear trend was observed with the heat flux as the pyrolysis front reached the heat flux meters. Furthermore, a maximum heat flux around 32.5 kW/m^2 was achieved.

Qian and Saito (1997) further applied their experimental observations to develop a model for upward flame spread in a corner. They treated the corner/wall fire as two wall fires on each wall with cross-radiation, etc. from the other wall. Therefore, one-dimension thermal model, which neglects the lateral heat transfer and defines the flame spread as a consequence of heating unignited portion of the fuel to the ignition temperature, was applied (the same as Equation 2.44).

Information needed was the relation of heat flux from flame to unburned surfaces, which can be expressed (associated with the correlation of X_f and t):

$$\dot{q}'' = 8.22 \left(\frac{X}{X_f}\right)^{-2..3} = 8.22 \left(\frac{X}{0.094t^{1..3}}\right)^{-2..3} = 0.00435X^{-2.3}t^3 \tag{2.79}$$

Finally, for PMMA,

$$X_p = 0.0136t^{1.526} \tag{2.80}$$

Compared with experimental data (Equation 2.72, Qian *et al.* 1995), good agreement was only found for the early period (<200 s).

A field model (CFD) developed by Lewis *et al.* (1999) was used to predict the flame spread of a wall fire on a flat vertical surface and in a corner. Controlling mechanisms of buoyancy-driven flow, combustion, soot production, radiation heat transfer and solid pyrolysis were incorporated into a fire-specific CFD code. The predictions carried out were compared with the data of Orloff *et al.* (1974) on PMMA wall fire and of Qian *et al.* (1994) on PMMA fire in a corner. Fairly good agreement was found.

2.6 Upward Flame Spread on Confined Parallel Walls

Upward flame spread has been considered to be the 'worst' orientation for rapid fire development over a combustible wall lining. However, there are other configurations which can lead to even more rapid fire growth. One example is to be found in storage arrays in warehouses where the vertical channels between adjacent stacks offer an ideal pathway for fire growth (Foley and Drysdale, 1995). There is a need to understand fire spread mechanisms involved in the vertical parallel case in more detail to enable better quantification and reduction of risks.

Kim *et al.* (1974) focused on the laminar burning between parallel fuel surfaces, studying the factors influencing the burning rate between two walls. They found that the burning rate (mass loss rate) of inward-facing combustible boards depended on the channel geometry:

$$\dot{m}'' = f\left(\frac{H}{(a/2)^4}\right) \tag{2.81}$$

where H is the height of vertical fuel surfaces and a is the separation between them. For small values of $H/(a/2)^4$ the total burning rate is proportional to $H^{3/4}$ and does not depend on the separation, whilst for large $H/(a/2)^4$ the total burning rate is dependent on the height of the fuel surface but proportional to a^3. Between these two extremes lies a transition region.

Tamanini and Moussa (1980) studied the turbulent burning of vertical parallel walls and also pointed out that the space of the two walls is an important parameter influencing the fire behaviour of the two burning walls. It is anticipated if the two walls are sufficiently far apart, the interaction is minimal and the rate of burning approaches that of the single wall case. As the space between the walls is reduced, the following effects gradually alter the physical picture:

(1) an increasing fraction of the radiation from the flame and from the hot fuel surfaces, otherwise lost to the surroundings, reaches the burning walls.

(2) The scale of the turbulent eddies is reduced by the presence of the additional solid boundary (the other wall); and

(3) The flow of oxygen available for combustion in the gap is reduced.

They observed that while the first and last effects act, respectively, in the direction of increasing and decreasing the rate of fuel production by the wall, the net effect is not very clear.

They designed experiments to study the fire behaviour of vertical burning parallel walls and obtained data for single wall case for comparison. The instrumented walls they used were 0.459 m wide and 0.942 m high and made of wicks soaked with methanol and toluene-methanol mixtures (0%, 13.8% and 20.7% toluene in methanol). The fuels of different radiant properties can consequently be simulated. The separations between the two burning walls were from 25 mm up to 413 mm in addition to the infinite case (single wall case).

They observed that as the separation decreased, the flames appeared to move closer to the burning surface; at the 38 mm wall separation the two flames merged. In addition, the

flame height increased slightly for decreasing wall separation.

From their analysis, the burning rate of the parallel burning walls increased up to about 40% over the single wall case. In addition, except for the case of pure methanol where the burning rate seems to remain constant over a fairly wide range of wall separations, the experiments with two methanol/toluene mixtures showed that the burning rate first increased as the separation was reduced (from infinite to 25 mm), then dropped. There was a value of separation for which the burning rate reached a maximum. They examined this observation and suggested that the maximum occurs when the wall separation is about 20 percent of the height of the pyrolysis region. The results suggested that the burning at low wall separations was controlled by convection because the burning rates of the different fuels (different percentages of toluene in methanol) at the same wall separation tended to approach the same value.

The aerodynamic and thermal structure of the flow developing between two vertical burning walls were studied by Most *et al.* (1989), examining the influence of different parameters such as channel width, burner length, gas supply flow rate and mass transfer driving force. The vertical burning walls used were gas-supplied and were 0.4 m wide and from 0.25 to 1.25 m high. Their results indicated that as the distance between both walls decreases, radiation is no longer the dominant mode of heat transfer. The character of the flow changes from natural to forced convection and there is a "relaminarisation" of the flow.

Foley and Drysdale (1995) carried out measurements of the heat flux distribution at the surface of a vertical wall exposed to flames from a 0.6 m long propane line burner between vertical parallel walls and against a wall. The experimental configuration is listed in Table 2.3.

The base type 'open' means that there was no "floor" at the foot of the walls so that air could flow under the wall and vertically upwards into the space between the 'walls'. On the contrary, 'closed' describes the configuration where the "walls" rested on a non-

combustible "floor" so that air could only enter horizontally from the sides into the space between the "walls".

Table 2.3- The experimental configurations investigated in the study of Foley and Drysdale (1995).

Separation	60 mm, 100 mm, ∞ (single wall case)
Burner position	centre, against instrumented wall, against opposite wall
Base type	Open, closed
Propane flowrate	5 *l*/min, 9 *l*/min

From their results, the following observations were made:

(1) The heat flux along the centerline increased with decreasing separation.

(2) Higher burner heat release rate yielded higher heat fluxes at the wall.

(3) The highest heat flux occurred with the burner against the instrumental wall, except the case of 60 mm separation with base closed where the highest flux occurred for the burner in the center of the gap. (In this special case, flame was seen to fill the entire width of the gap.)

(4) The heat flux distributions of the cases of open base and closed base were different. In the case of 60 mm separation with burner in center of separation, when the base was open, the flame was seen to behave more as a uniform sheet between the two walls. With the closed base, the flame tended to fill the gap, impinging directly on both walls.

Correlations of the measured heat flux and their dependence on the experimental variables were sought by the authors.

For single wall, burner against the instrumented wall

Open base, centreline fluxes

$$\dot{q}_w'' = 104.95\left(\frac{X}{Q_l^{*2/3}D}\right)^{-1.55} \tag{2.82}$$

where $\dot{q}_w''$ is the heat flux to the wall, Q_l^* is the dimensionless line burner heat release rate (Sec. 2.4.3.1), X is the height (Fig. 2.3) and D is the line burner length.

Closed base, centreline fluxes

$$\dot{q}_w'' = 51.07\left(\frac{X}{Q_l^{*2/3}D}\right)^{-1.29} \tag{2.83}$$

For two parallel wall case, burner against the instrumented wall,

Open base, centreline fluxes

$$\dot{q}_w'' = 104.53\left(\frac{X}{Q_l^{*2/3}D}\right)^{-1.4} \tag{2.84}$$

Closed base, centreline fluxes

$$\dot{q}_w'' = 89.5\left(\frac{X}{Q_l^{*2/3}D}\right)^{-1.16} \tag{2.85}$$

Taking the separation of the walls into account, a slight improvement of correlation coefficient was made, giving

Open base, centerline fluxes

$$\dot{q}_w'' = 42.18\left(\frac{X(a/D)^{0.36}}{Q_l^{*2/3}D}\right)^{-1.4} \tag{2.86}$$

Closed base, centreline fluxes

$$\dot{q}_w'' = 12.74\left(\frac{X(a/D)^{0.905}}{Q_l^{*2/3}D}\right)^{-1.16} \qquad (2.87)$$

Within the range of separations and conditions studied, altering the air flow pattern to the flame by preventing air entering under the 'walls' leads to significant increases in heat fluxes to the surfaces. When the base is open, cool air can flow upwards from the base. This effect is further enhanced by reducing the separation between the walls.

A numerical study was conducted by Wang *et al.* (1999) to estimate the flame radiation energy for parallel burning walls. The equations of turbulence, combustion, soot formation and energy were solved numerically with the associated boundary conditions. The burning rate distribution, flame structure and velocity profile on wall fires in a parallel configuration can be predicted for one and two burning walls (Fig. 2.12 (a) and (b)). There was good agreement with experimental data of velocity, temperature, stream wise driving pressure and profile of velocity fluctuation.

Fig. 2.12- The schematic diagram of vertical parallel wall fires with a buoyancy-induced flow. (a) single burning wall opposed against an inert wall; (b) two opposing burning walls.

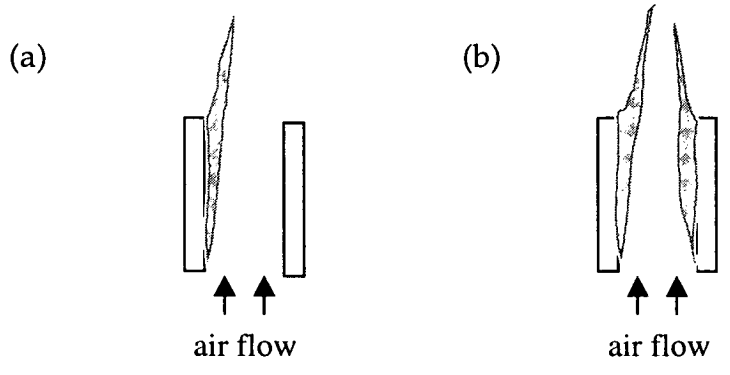

Some information was extracted by the model by considering two characteristic physical situations:

(1) When a burning wall opposes an inert wall, it is important to know how the geometry affects the ease with which the surface temperature of the inert wall can reach the ignition temperature.

(2) Once the facing wall has ignited, it is important to understand how the geometry influences the flame structure, and as a consequence, the convective / radiative fluxes and the accompanying burning rate, etc.

The temperature of an inert wall facing a burning wall (Fig.3.12(a)) was predicted by the model for different separation/height ratio (a/H) varying from 0.35 down to 0.062. From their prediction, the surface temperature of the inert wall increased with height. If assuming the material used was PMMA, the ignition temperature (600K) can only be reached if the value of a/H is less than 0.15. Therefore, for large separation (a/H>0.2), ignition of the opposing surface does not occur and the case of a single burning wall opposed an inert one (Fig.3.12(a)) has to be considered.

The effects of the confinement on convective and radiative heat transfer was evaluated using the model. For the case of two burning walls (Fig.3.12(b)), as the confinement is high (a/H<0.2), the convective heat flux was found to increase at first with increase of the a/H from 0.06 to 0.1, and decrease later with further increase of that to 0.15. The radiative heat flux predicted by the model showed that the highest values occur as (a/H) ratio equal to 0.1. The heat flux at the top of the sample as (a/H) =1 is c. 62 kW/m^2 for the PMMA fires, which is 3% and 41 % higher than that as (a/H) =0.062 and 0.15. It is seen that the convective and radiative heat transfer does not directly increase or decrease with the change of (a/H).

The burning rate was also predicted by the model. For two burning PMMA walls, the burning rate increases with height and depends on the separation, whilst for a single burning wall case, the burning rate is independent of the a/H ratio for a/H >0.2.

The mass flow rate of the unburned fuel at the exit of the channel was analysed since it will represent the potential flame height. In the case of a single burning wall, the a/H ratio has a weak effect and a negligible effect for $a/H>0.2$. However, a significant effect was predicted for the case of two burning walls.

2.7 Summary

As has been discussed, the flame height and heat flux from flame to the unburned surfaces of wall fires are the two important parameters determining the flame spread rate. These two parameters are influenced by several factors, however, geometry plays the most significant role. In the case of wall fires on vertical flat surfaces, many studies have been conducted. However, there still exists a need to carefully examine the previous correlations and modelling work. For the cases of wall fires in a corner and in confined parallel surfaces, very little attention has been paid. These two scenarios are worth more study because they are more hazardous.

Chapter 3

Experimental Work and Results

3.1 Introduction

The experimental programme was intended to expand the understanding of upward flame spread on vertical surfaces. The first part described in this chapter is the Cone Calorimeter test which provides quantitative data relevant to the response of combustible materials to fire conditions. The data will be used in modelling work in Chapter 4. The second part focuses on the wall fires on flat surfaces simulated by combustible solid strips and gas panels. Flames from combustible solid strips represent the real behaviour of wall fires. Gas panel test is capable of providing useful information under carefully controlled burning scenarios. The third part was designed to examine vertical flame spread in a corner and the effects of a nearby parallel wall because the presence of the extra wall (combustible or non-combustible) is known to affect flame spread rate of the wall fire. Flame height and heat flux distribution were the two primary parameters investigated in the experimental study due to their significant effects on fire growth and their use in modelling work (Chapter 4).

3.2 Cone Calorimeter Tests

Measurements were made using the Cone Calorimeter to provide data for modelling upward flame spread. The sample can be oriented horizontally or vertically. The vertical orientation was chosen because the sample will simulate the combustible solid on a wall.

3.2.1 Standard Cone Calorimeter Tests

The Cone Calorimeter has been described in Sec.1.3.1 and Fig. 1.1. During the tests, the ignition time is determined by the presence of a sustained flame on the sample surface, while burnout time is determined by the presence of a burnout region. In this

study, 6mm thick PMMA and 2.5mm thick cardboard were tested in the vertical orientation. Table 3.1 listed the test conditions (irradiance levels).

Table 3.1 - irradiance levels (kW/m^2) used for PMMA and cardboard cone tests

	6mm thick PMMA	2.5mm thick cardboard
Irradiance level (kW/m^2)	15, 20, 25, 30	20, 25

Material behaves like thermally thick, thermal thin or in between and material only behaves thermal thick for a limited time. Mikkola and Wichman (1989) have shown that the time to ignition of combustible materials can be expressed as follows:
For the thermally thick materials

$$t_{ig} = \frac{\pi}{4} k\rho c \frac{(T_{ig} - T_o)^2}{\dot{q}_r{}''^2} \tag{3.1}$$

and for thermally thin materials

$$t_{ig} = \rho c L_0 \frac{(T_{ig} - T_o)}{\dot{q}_r{}''} \tag{3.2}$$

where t_{ig} is the time to ignition, k is the conductivity, ρ is the density, c is the specific heat, T_{ig} is the ignition temperature, T_0 is the ambient temperature, L_0 is the sample thickness and $q_r^{"}$ is the irradiance.

3.2.2 Non-Standard Cone Calorimeter Tests

A non-standard Cone Calorimeter test procedure was developed for the modelling work of upward flame spread on vertical surfaces (Chapter 4). The usage and the development of the non-standard test will be discussed in Chapter 4. Here the test procedure and data are shown.

In the standard test, the cone heater exposes the vertical test specimen to thermal radiation during the whole test duration. In the non-standard test procedure, after the specimen was ignited, the cone heater was moved into a position in which the lowest edge of the heater was 2.5cm above the level of the top edge of the sample. Table 3.2 presents the residual radiant flux to the specimen surface measured in separate experiments under different effective irradiance levels. The maximum flux was obtained at the top edge of the sample and the minimum at the bottom.

Table 3.2 - The residual radiant flux from the cone heater to specimens under different initial irradiance levels.

Irradiance level with cone heater in normal position (kW/m^2)	Residual radiant flux when heater moved away (kW/m^2)
20	0.2-0.4
25	0.3-0.5
30	0.4-0.6

3.2.3 Experimental Results

Fig.3.1 shows the typical heat release rate measurements of PMMA under the irradiance of 15 kW/m^2 (standard and non-standard procedure), 20 kW/m^2 (standard procedure) and 25 kW/m^2 (standard procedure) and Fig.3.2 for cardboard under the irradiance of 20 kW/m^2 (standard and non-standard test procedures). For PMMA applying the standard procedure, it is seen that as the irradiance was higher, the time to ignition τ was shorter and the peak RHR $\dot{Q}''_{max}$ was higher. The former observation is because the surface temperature of the sample increased more rapidly as the sample was exposed to higher irradiance. The latter observation is because higher irradiance results in higher mass loss rate which will produce higher RHR. The experimental data of τ and $\dot{Q}''_{max}$ are summarised in Table 3.3.

As the irradiance was 15 kW/m^2, the time to ignition was almost identical in the two tests following the standard and non-standard test procedures (480 and 475 s). The peak rate of heat release for the curve using the non-standard test procedure was lower

than that using the standard one because the cone heater had been removed. The difference in the duration of burning should also be noted. Similar results for 2.5mm thick cardboard are shown in Fig.3.2: there is no significant difference in the RHR curves with and without an imposed heat flux of 20 kW/m^2 after ignition.

Table 3.3 – The comparison of the Cone Calorimeter data under different irradiances and applying the stand and non-standard test procedures.

	Time to ignition (s)	Burning time (s)	Peak RHR (kW/m^2)
15 kW/m^2 (non-standard procedure)	475	1164	190
15 kW/m^2 (standard procedure)	480	864	317
20 kW/m^2 (standard procedure)	182	-	422
25 kW/m^2 (standard procedure)	114	-	485

Brehob and Kulkarni (1989) observed that mass loss rates from different materials in the vertical orientation exhibit different sensitivities to external radiation when burning. Assuming that the heat of combustion remains constant during the burning process and independent of the imposed heat flux, mass loss rate is directly proportional to the rate of heat release (Equation 3.3) and similar sensitivities would be expected from measurements made in the Cone Calorimeter.

$$RHR = \dot{m}\ \Delta H_c \tag{3.3}$$

Conclusively, for the materials whose mass loss rate is easily affected by external radiation, the difference of the heat release rate measured by the Cone Calorimeter is apparent as the level of the external radiation changes. Cardboard is a material which consists of a sheet of fluted cardboard fixed between two outer layers and chars when heated. As one surface is exposed to heat, not much heat can be transferred to "inner

material". Therefore, as the intensity of heat transfer changes after ignition, the behaviour of the material would not change very much, which leads to similar RHR curves using the standard and non-standard test procedure.

Table 3.4 lists all the time to ignition data and their average for PMMA and cardboard under different irradiance levels. Fig.3.3 presents the thermally thick ignitability correlation for 6mm thick PMMA in the range 15 to 30 kW/m^2 because of the proportion of the $\dot{q}_r''$ and $t_{ig}^{-1/2}$ (Equation 3.1).

The different responses of PMMA and cardboard in the presence and absence of supporting radiation with modelling work will be discussed in Chapter 4.

Fig.3.1- The RHR of 6mm thick PMMA from the Cone Calorimeter under different irradiance (15, 20 and 25 kW/m^2) following the standard or non-standard test procedures

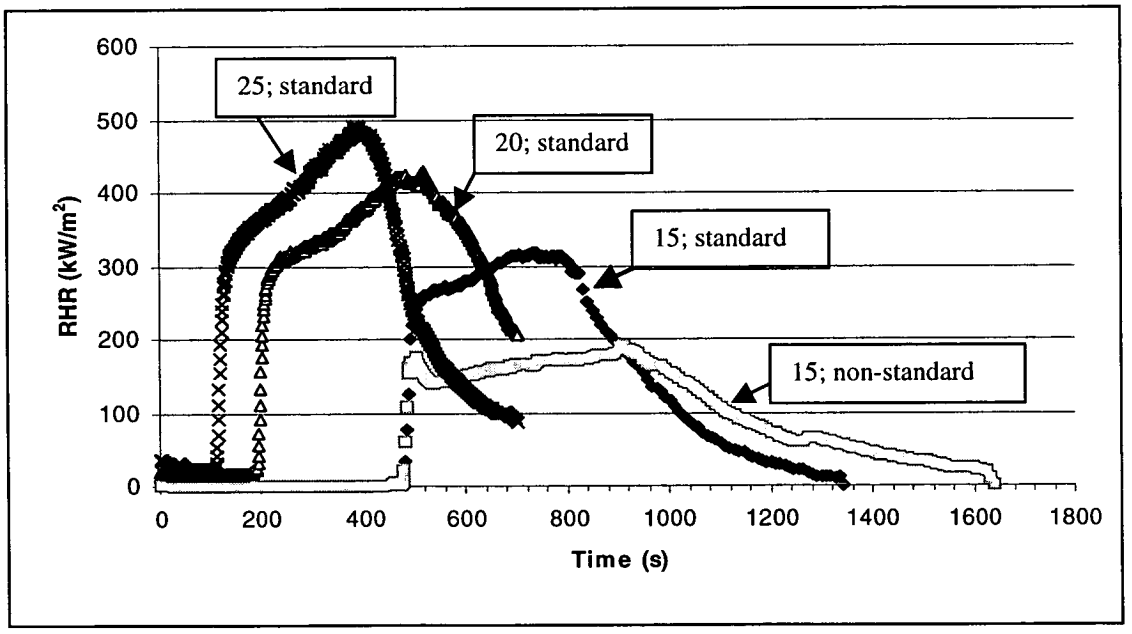

Fig.3.2- The RHR of 2.5mm thick cardboard from the cone calorimeter following the standard and non-standard test procedures (under irradiance of 20kW/m^2).

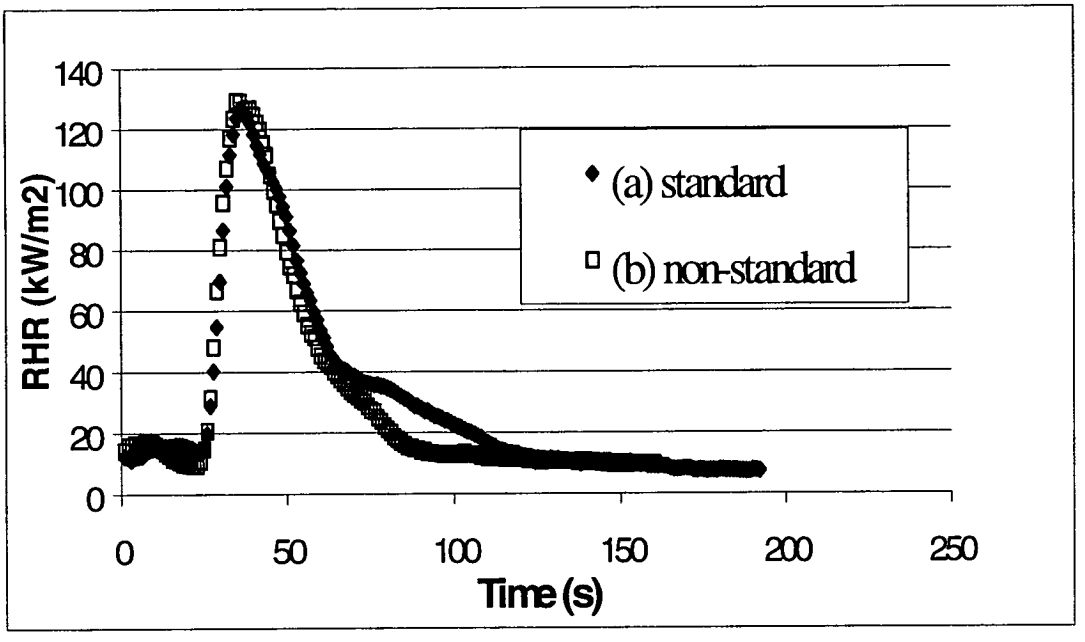

Table 3.4- The time to ignition data and its average for PMMA and cardboard under different irradiance levels.

Irradiance level (kW/m^2)	6mm thick PMMA			2.5mm thick cardboard		
	Time to ignition t_{ig} (s)		$1/t_{ig}^{1/2}$ ($s^{-1/2}$)	Time to ignition t_{ig} (s)		$1/t_{ig}^{1/2}$ ($s^{-1/2}$)
15	537 480 440	**average** 486	0.045	---	**average** ---	---
20	182 208 208	190	0.073	26 27 26	26.3	0.195
25	110 120 114	112	0.094	18 15 15	16	0.25
30	67 69 72	69	0.12	---	---	---

Fig.3.3- the thermally thick ignitability correlation for 6mm thick PMMA (Equation 3.1).

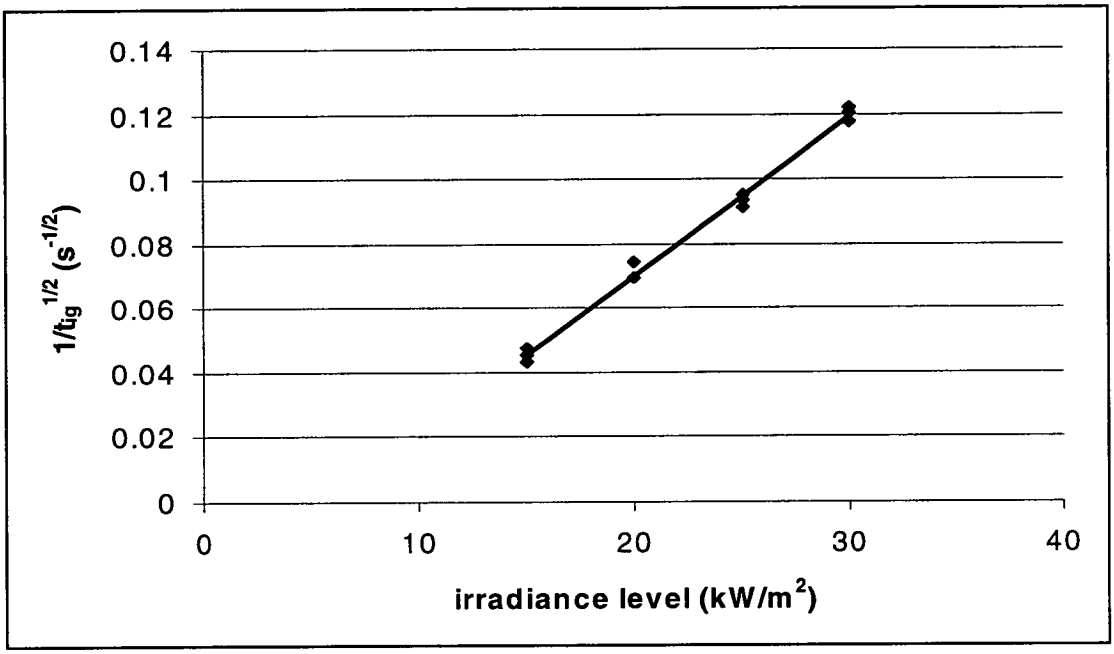

3.3 Measurement of Flame Height on Steady Burning Combustible Solid Strips

The objective of this study was to carry out flame height measurements under carefully controlled conditions to examine the validity of previous theoretical and experimental correlations and provide new insights into the flame height phenomenon. For the first time, the flame heights and heat release rates from the burning samples were measured directly and simultaneously in the same experiment.

3.3.1 Flame Heights of Steady Burning Wall Fires

The experimental rig located inside the Cone Calorimeter is shown in Figure 3.4 in schematic form. It was designed to hold vertical samples of combustible material at the lower edge of (and in the same plane as) a 60 cm high inert board. The sample was mounted on a 3 mm thick steel plate: in addition to preventing flame spreading up the back of the sample, it kept the rear face relatively cool and prevented distortion and slumping which would otherwise have occurred. The vertical edges of the sample were protected by 3mm thick mild steel strips designed to hold the sample against the backing plate. The rig was located below the hood of a Cone Calorimeter, thus allowing the rate of heat release from the burning sample to be measured directly. A hand-held butane-fuelled torch was used to ignite the surface of each sample uniformly. The inert wall was marked with a scale and a video camcorder was used to record each experiment. The flame height was determined subsequently by visual examination of the videorecordings which were then matched to the corresponding heat release rates. (The way to determine the height of a wall fire will be discussed in Sec.5.3.1).

The combustible material used was PMMA, as 6 mm thick slabs with heights ranging from 2.5 to 25 cm and widths of 4, 8 and 12 cm to simulate the early stages of vertical burning and to allow the effects of different aspect ratios to be studied. In addition, several samples of 12.5 and 25 mm thick were used to examine the thickness effect on flame height. By using sample heights up to 25 cm, the laminar, transition and turbulent burning regimes could be observed, as noted by Orloff *et al.* (1974) in their PMMA experiments.

Fig.3.4- The schematic of experimental rig located inside the chamber of the Cone Calorimeter

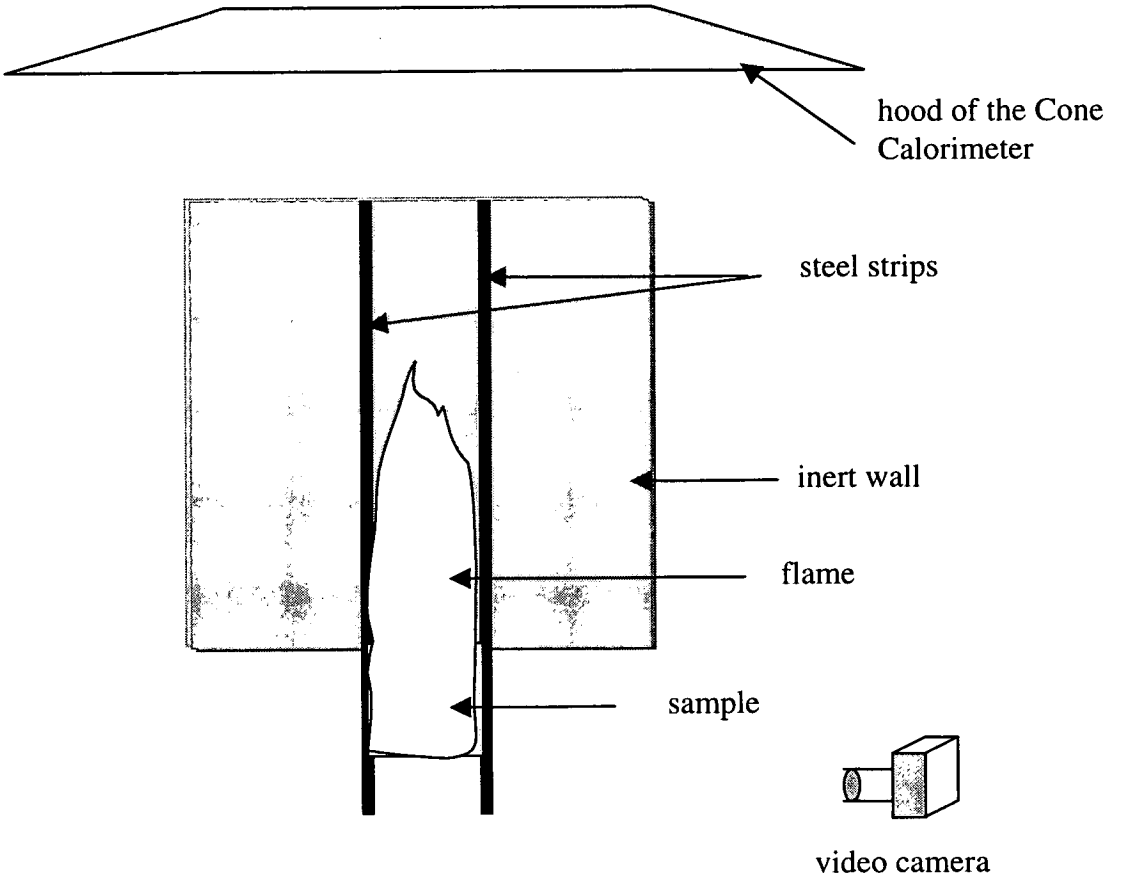

Modifications could be made to allow four different geometric configurations to be studied (see Fig.3.5 (A)-(D)). In three cases, the burning area was at the foot of the "wall". With Case A, there was a contiguous floor, but this was absent in Cases B and C. In Case B, the bottom edge was unprotected while in Case C the bottom edge was protected by a steel strip. In the fourth configuration (Case D), the sample represented a central burning area on an extended wall. The geometric configurations, heights and widths of PMMA samples of three thicknesses (6, 12.5 and 25mm) are summarised in Table 3.5, 3.6 and 3.7.

Fig.3.5 The four geometric configurations studied.

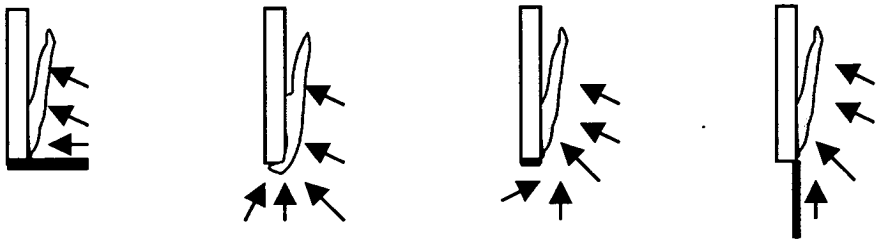

Table 3.5 - geometric configurations, heights and widths of 6mm thick PMMA samples

6mm thick PMMA		Width (m)		
		0.04	0.08	0.12
Height (m)	0.025	---	ABD	---
	0.05	ABD	ABC	A
	0.075	ABD	AB	---
	0.1	AB	ABCD	A
	0.15	---	ABCD	AD
	0.2	AD	ABCD	AD
	0.25	AB	ABC	AB

Table 3.6 - geometric configurations, heights and widths of 12.5mm thick PMMA samples

12.5mm Thick PMMA		Width (m)
		0.08
Height (m)	0.05	AB
	0.15	ABD
	0.25	ABD

Table 3.7 - Geometric configurations, heights and widths of 25mm thick PMMA samples

25mm Thick PMMA		Width (m)
		0.08
Height (m)	0.05	AB
	0.15	ABD
	0.25	AB

3.3.2. Results and Discussion

Figure 3.6 shows the typical RHR history for a burning PMMA sample, 8cm wide, 10cm high and 6mm thick in the configuration corresponding to Case A (with a contiguous floor). The ignition process took approximately 100 s and was followed by a period of unsteady burning (from 100s to 350s) during which the RHR increased to a steady peak value (corresponding to 150 kW/m^2 in this case) before burnout started (after 500s). The height of the flame during steady burning was determined (350-500s in Figure 3.6). The heights of the continuous flame and the flame tip were observed, but the flame height was recorded as the average of the visible flame height.

The effect of aspect ratio (R = height/width) on the correlation is shown in Figure 3.7 (a)-(d) for the four cases. These correlations indicate that the effect of R is negligible for $\dot{Q}' < 30$ kW/m^2 within the range of values of R used (0.3125 to 2.5).

The experimental data are in Appendix A-1. In Figures 3.8(a) and (b), the dependence of X_f on $\dot{Q}'$ for all four geometries is shown as normal and logarithmic plots. When $\dot{Q}'$ is less than c.10 kW/m, the data for all four configurations fall on the same line, but above c.10 kW/m, the data become scattered and systematic differences in the four series of flame height correlations can be observed.

Fig. 3.6- The typical RHR history of a 6mm thick, 8cm wide and 10cm high burning PMMA sample with a contiguous floor.

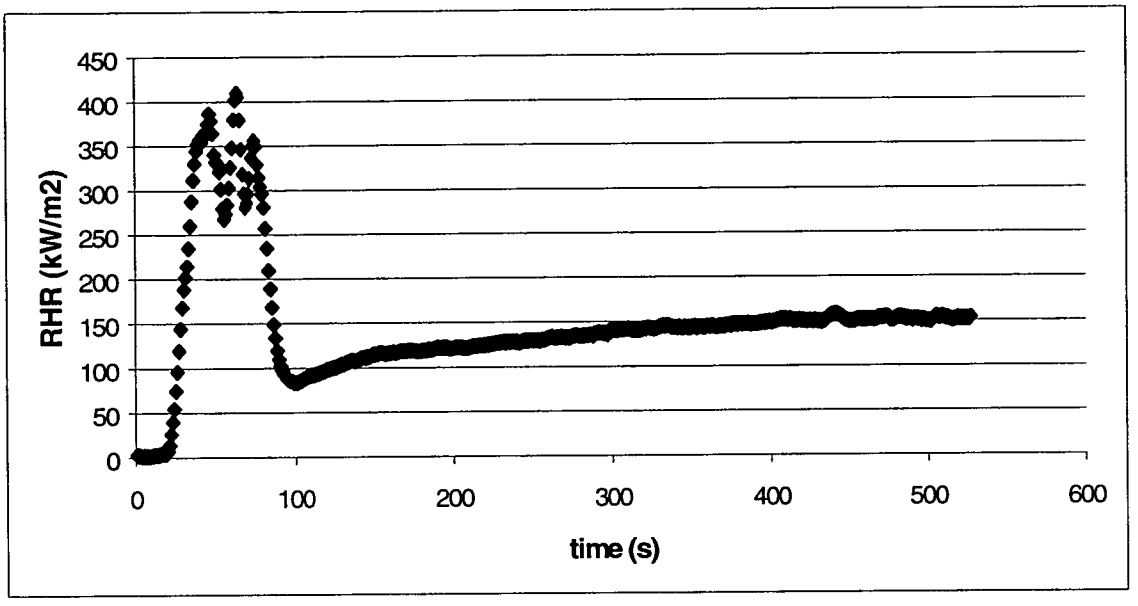

Fig. 3.7 (a)-(d)- The effect of aspect ratio on flame height correlation for the four geometric configurations.

(a)

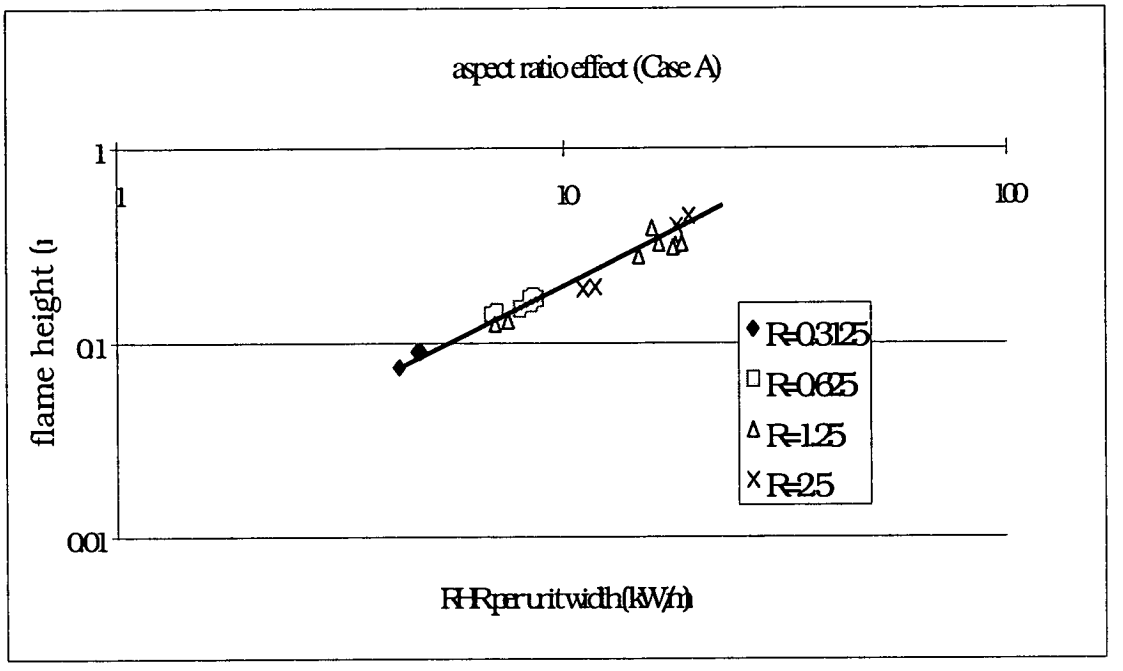

(b)

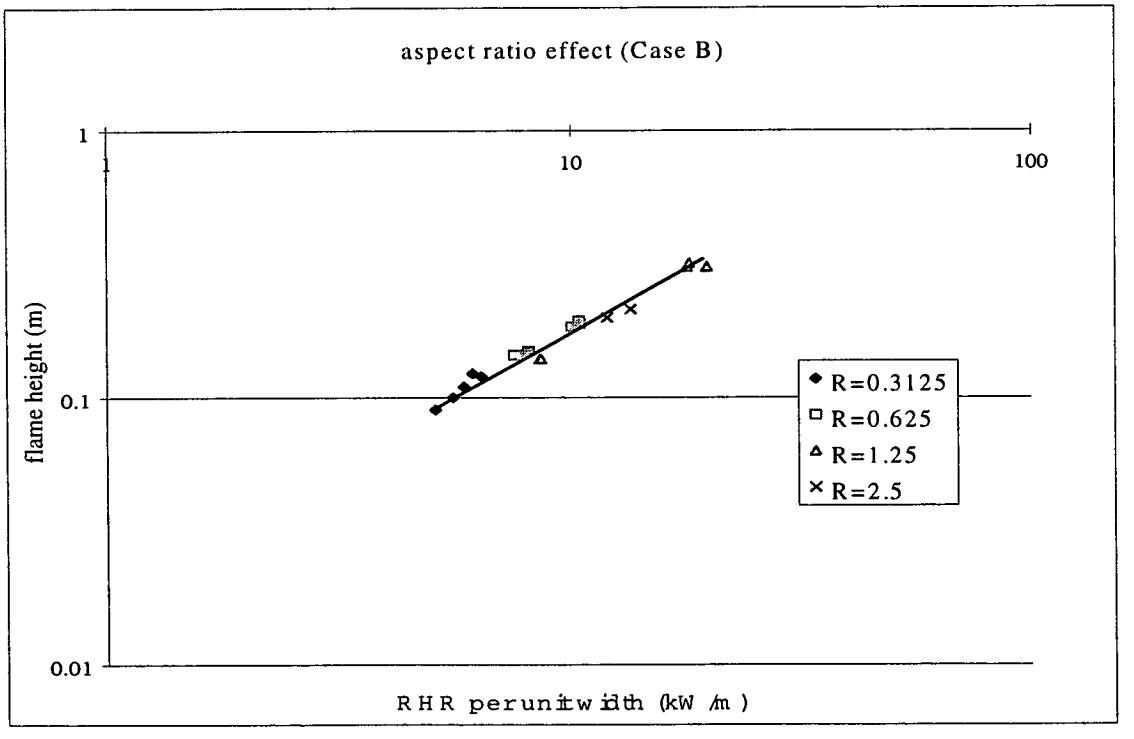

(c)

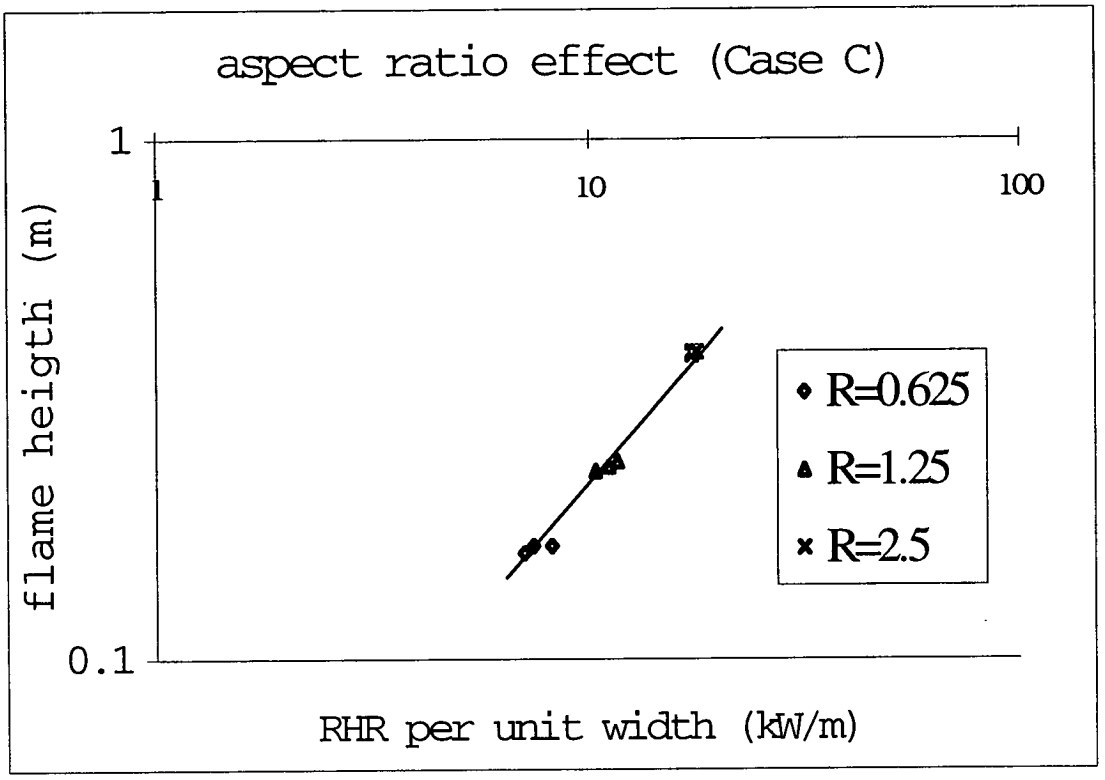
aspect ratio effect (Case C)
1
1
10
100
flame heigth (m)
0.1
R=0.625
R=1.25
R=2.5
RHR per unit width (kW/m)

(d)

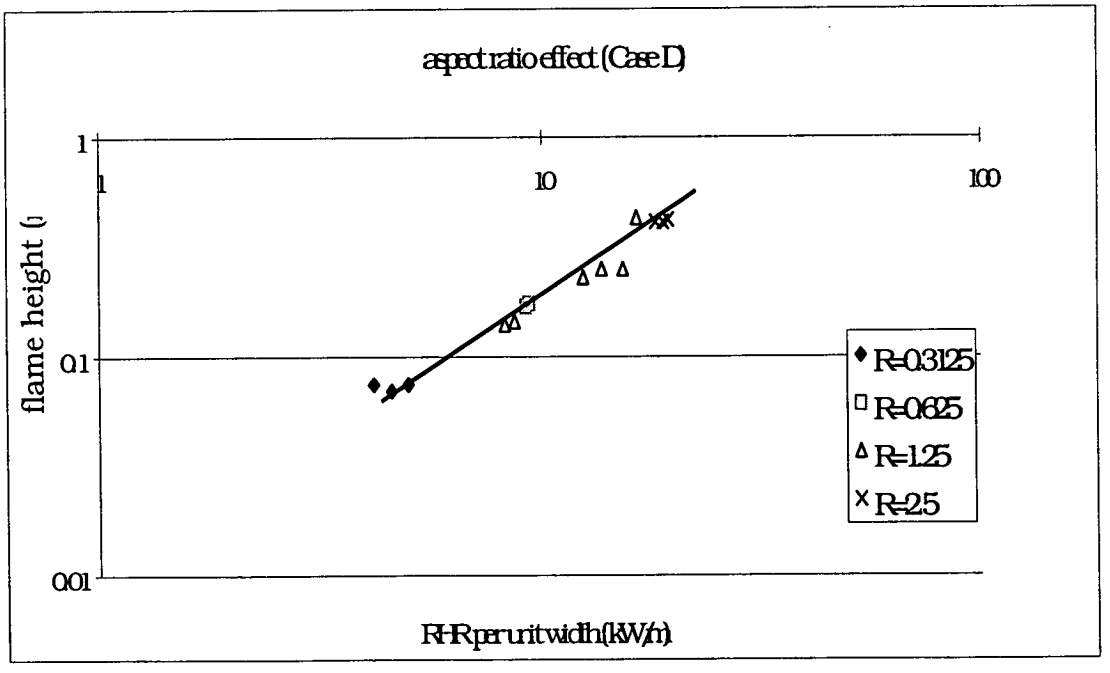
aspect ratio effect (Case D)
1
1
10
100
flame height (
0.1
0.01
R=0.3125
R=0.625
R=1.25
R=2.5
RHR per unit width (kW/m)

Fig.3.8 The dependence of flame height on RHR per unit width in normal (Fig.3.8(a))and logarithmic scale (Fig.3.8(b)).

(a)

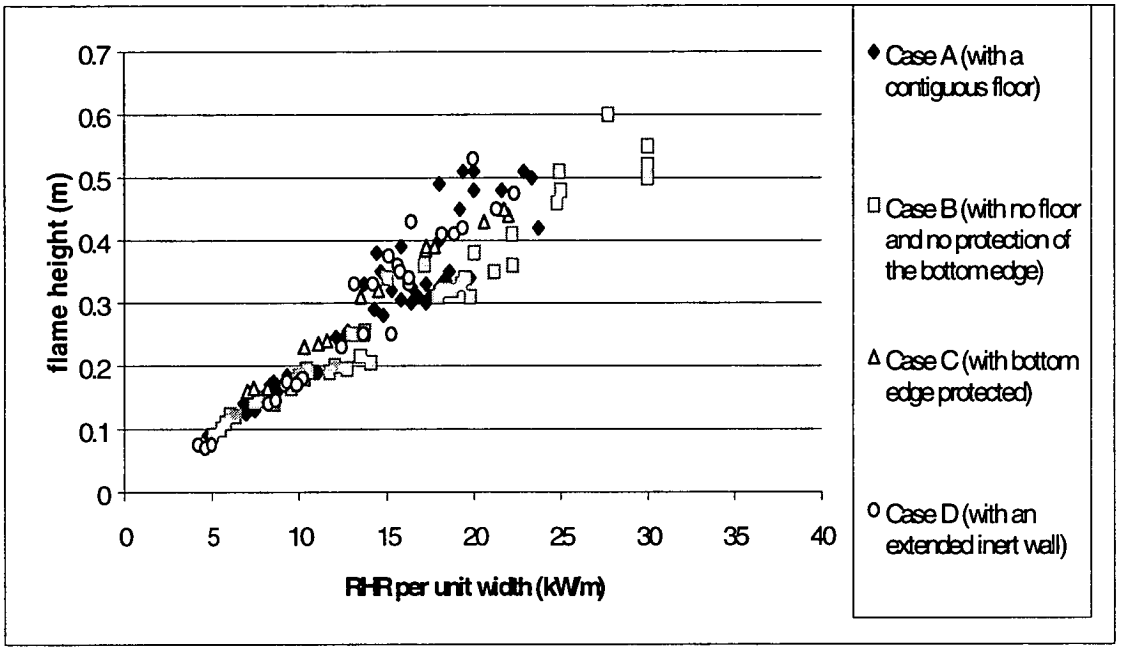

(b)

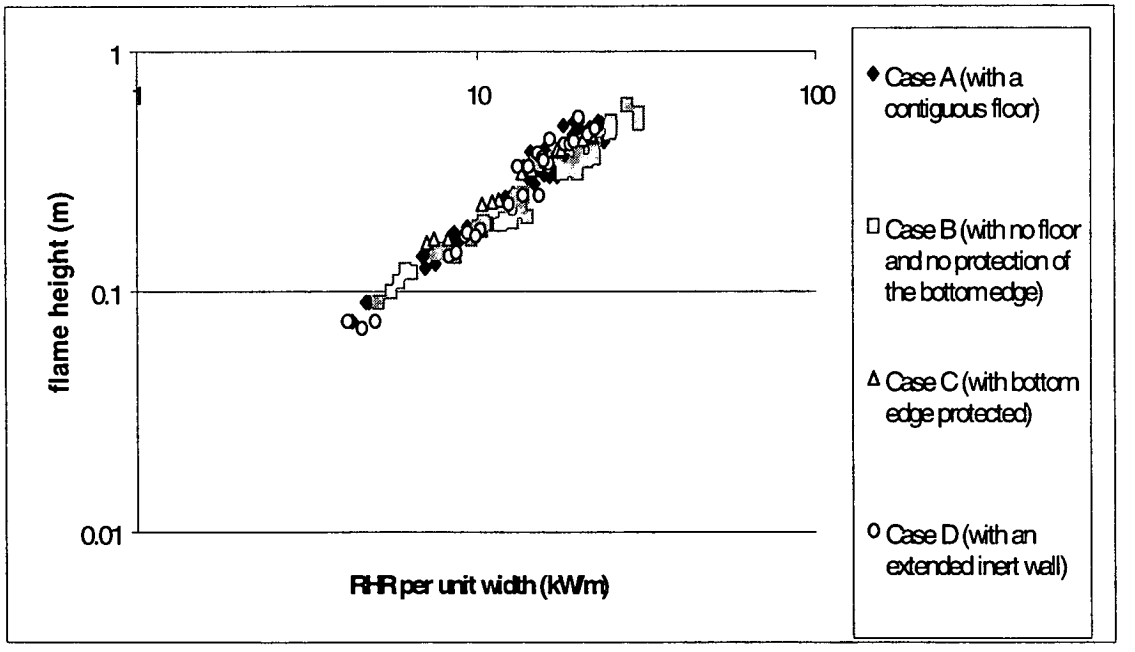

For Case A (a burning wall with a contiguous floor),

$$X_f = 0.016\dot{Q}'^{1.07} \tag{3.4}$$

For Case B (a burning wall with no floor and no protection of the bottom edge),

$$X_f = 0.018\dot{Q}'^{1.00} \tag{3.5}$$

For Case C (a burning wall with no floor but with the bottom edged protected)

$$X_f = 0.023\dot{Q}'^{0.98} \tag{3.6}$$

For Case D (a burning wall with an extended plate),

$$X_f = 0.011\dot{Q}'^{1.25} \tag{3.7}$$

The r^2 values for these four cases (Equations 3.4–3.7) are 0.931, 0.968, 0.987 and 0.963 respectively, and the values of power n are close to unity at least for Cases A, B and C. It can be seen that the burning walls set in an extended plate (Case D) produce the tallest flames (Figure 3.8). While further work would be required to explain this observation, it seems likely that it is a consequence of the fact that the burning area is part of a larger flat surface. The Case D flames may be less turbulent than those observed for Cases A, B and C. In general, turbulence tends to reduce the height of a diffusion flame (Delichatsios, 1984; this work), but the Case A flames are of similar height to the Case D flames, both being higher than Cases B and C (Figure 3.5(a)). Clearly, the effect of the lower edge boundary conditions needs to be studied in greater detail.

The steady values of $\dot{Q}'$ obtained for the different geometric configurations are listed in Table 3.8 (a) and plotted in Fig. 3.9. Samples with a lower-edge protection (Case C) produced the lowest values of $\dot{Q}'$ while Case B samples produced the highest. It

may be that the increased burning area due to the involvement of the lower edge would account for this observation. When PMMA samples burned with a contiguous floor (Case A), the lowest 10 mm of the flame was blue in colour, suggestive of a well-mixed region producing "premixed-like" burning. This may have caused higher local heat transfer and thus a higher local rate of burning, consequently producing a higher value of $\dot{Q}'$. This is consistent with observations made by Foley and Drysdale (1995) on the effect of a "floor" on the rate of heat transfer to a vertical wall exposed to a line burner.

In Table 3.8 (b), the steady-state rate of burning (expressed as a mass flux, $\dot{m}''$ g/m^2.s) of PMMA slabs of different heights are compared for these four configurations. The mass fluxes were calculated from the steady state values $\dot{Q}'$, assuming the heat of combustion of PMMA to be constant at 24.89 kJ/g (Drysdale, 1998). The burning rate is found to decrease as the height of the burning sample increases. This is consistent with the study carried out by Orloff *et al.* (1976) on the burning of thick vertical slabs of PMMA, 0.91 m wide and $\geq$ 1.5 m high. Their configuration corresponded to Case A. They also found that the rate of burning decreased with height over the first 20 cm from the bottom edge although the decrease was not so pronounced (about 15%).

The effect of the thickness of test samples on the flame height correlation was investigated. PMMA slabs of three thicknesses (6, 12.4 and 25 mm) with width of 8 cm and heights of 5, 15 and 25 cm were tested in two geometric configurations (A and B). Table 3.9 (a), (b) and (c) list the steady state RHR per unit width, steady state mass loss rate (with the assumption of constant heat of combustion) and time to reach steady state (after ignition) of these three sets of tests. It can be observed that, for different thickness of samples in different geometric configuration, the steady state RHR per unit width and the mass loss rate changed. However, there was no consistent trend to be observed as thickness or geometric configuration was changed. In addition, it took a longer time to reach steady state (after ignition) for thicker samples.

In Table 3.9 (b), a generally lower steady state mass loss rate was observed for longer samples in both the two geometric configurations (A and B). This coincided with the

measurement Orloff *et al.* (1976) carried out on the early stage (height < 25 cm) of upward spreading PMMA fires. Furthermore, Fig.3.10 (a) and (b) display the dependence of the RHR per unit width and flame heights for these 6, 12.5 and 25 mm thick samples (Case A and B). The best-fit correlations for these two cases (dashed lines in Fig. 3.10 (a) and (b)) are also shown for comparison. No significant thickness effect on the flame height correlation was shown, compared with data of the 6 mm thick samples although the steady state RHR per unit width, steady state mass loss rate and the time to reach steady state (after ignition) were different (shown in Fig.3.11, Table 3.9 (a), (b) and (c)).

3.3.3 Conclusion

The flame height correlation of wall fires on their early stages of development ($\dot{Q}'$ < 30kW/m) under different geometric configurations has been shown to conform to a correlation of the form of Equation 2.9 and be independent of the aspect ratio of the burning surface in the range of parameters studied. For the first time, rates of heat release and flame heights were measured directly in the same experiments. The correlation was found to depend on the lower edge configuration. Data for $\dot{Q}'$ > 30 kW/m need to be obtained to investigate the correlation for fully developed turbulent wall flames. The limited space within the test section of the Cone Calorimeter prevented such measurements being carried out in this part of the project.

The configurations which have been studied represent four possible scenarios that may exist during the early stage of fire development on a wall. The correlations were derived from steady flames although a flame height correlation for a spreading wall fire would be closer to the real situation

Fig. 3.9- The steady-state RHR per unit width of 8cm wide PMMA slabs with different heights under the four geometric configurations.

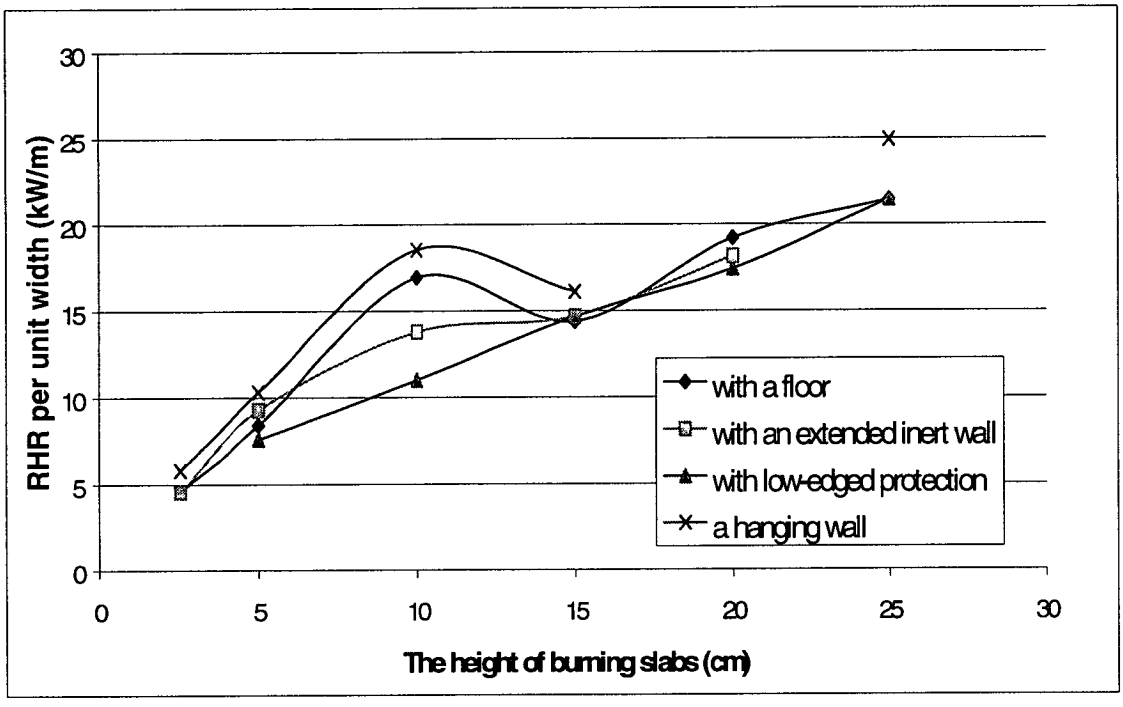

Table 3.8 - (a) and (b) The steady RHR per unit width and mass loss rate of 6mm thick, 8cm wide PMMA samples with different geometric configurations.

(a) RHR per unit width (kW/m)

Height, X_f (cm)	**(Case A)** with a floor 	**(Case B)** without lower edge protection (hanging wall) 	**(Case C)** with lower edge protection 	**(Case D)** with an extended surface 
2.5	4.6 ± 0.3	5.8 ± 0.7	---	4.6 ± 0.4
5	8.4 ± 0.4	10.3 ± 0.3	7.6 ± 0.6	9.3 ± 0.1
10	16.9 ± 2.1	18.5 ± 1.3	11.0 ± 0.7	13.8 ± 1.5
15	14.4 ± 0.3	16.1 ± 1.1	14.7 ± 1.3	14.7 ± 1.6
20	19.19	---	17.4 ± 0.3	18.1
25	21.4 ± 1.4	24.9	21.4 ± 0.9	---

(b) Mass loss rate m" (g/m^2 s)

(with assumption of the H_c of PMMA: 24.89 kJ/g)

Height X_f (cm)	**Case A**	**Case B**	**Case C**	**Case D**
2.5	7.38	9.34	---	7.34
5	6.76	8.28	6.09	7.46
10	6.80	7.44	4.42	5.54
15	3.85	4.31	3.93	3.93
20	3.85	---	3.50	3.64
25	3.44	4.01	3.45	---

Table 3.9 - (a), (b) and (c) The RHR per unit width, mass loss rate and time to reach steady state (after ignition) for different thickness of samples with geometric configuration cases (A) and (B).

3.9(a) RHR per unit width (kW/m)

	Thickness: 6mm		Thickness: 12.4mm		Thickness: 25mm	
Geometric configuration	A	B	A	B	A	B
Height : 5cm	8.7	10.3	8.9	12.2	8.9	---
Height : 15cm	14.4	---	14.4	19.7	13.7	15.0
Height : 25cm	20.0	24.9	21.5	28.8	24.8	24.8

3.9(b) Mass Loss Rate($g/m^2.s$)

	Thickness: 6mm		Thickness: 12.4mm		Thickness: 25mm	
Geometric configuration	A	B	A	B	A	B
Height : 5cm	7.0	8.3	7.2	9.8	7.2	---
Height : 15cm	3.7	---	3.9	5.3	3.7	4.0
Height : 25cm	3.2	4.0	3.5	4.6	4.0	4.0

(with the assumption of the heat of combustion of PMMA: 24.89kJ/g)

3.9(c) Time to reach steady state (after ignition) (s)

	Thickness: 6mm	Thickness: 12.4mm	Thickness: 25mm
Height : 5cm	50-100	200-240	300-350
Height : 15cm	80-100	200-250	300-400
Height : 25cm	80-100	300-330	300-400

Fig.3.10 (a) and (b)- The thickness effect on flame height correlation with geometric configuration Case A and B. (dashed lines show the best fit correlations in Fig. 3.7(a) and (b))

(a)

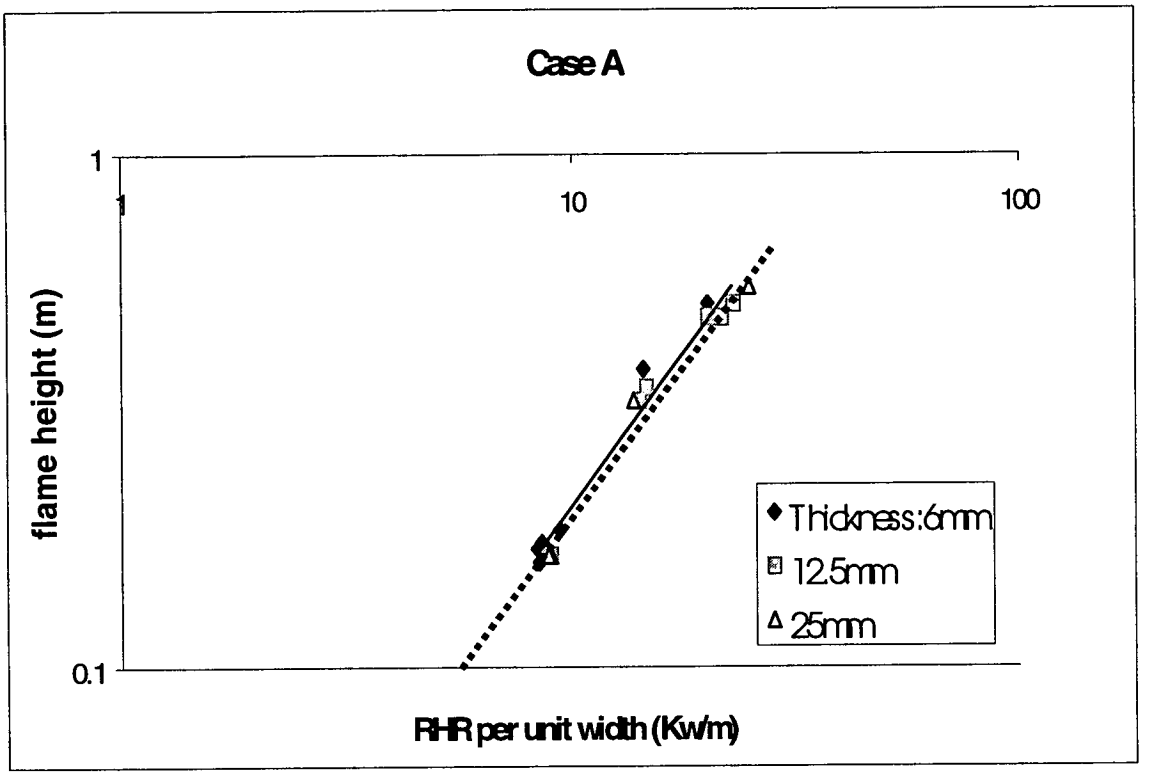

(b)

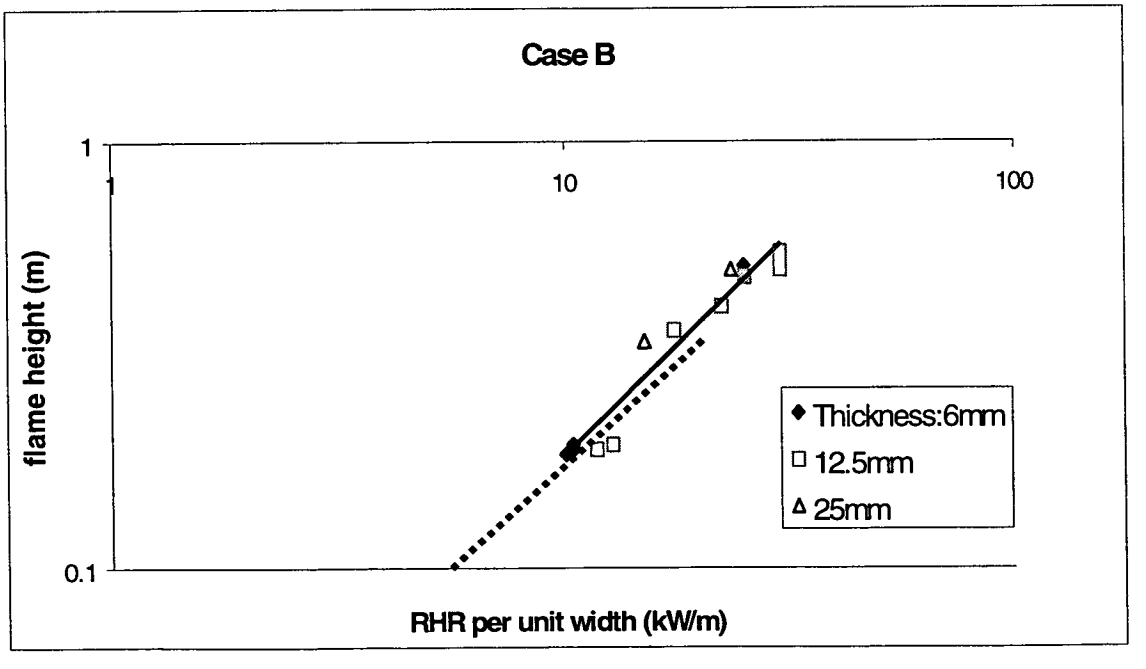

Fig. 3.11- The RHR per unit width of PMMA slabs of different thickness in the geometric configurations A and B.

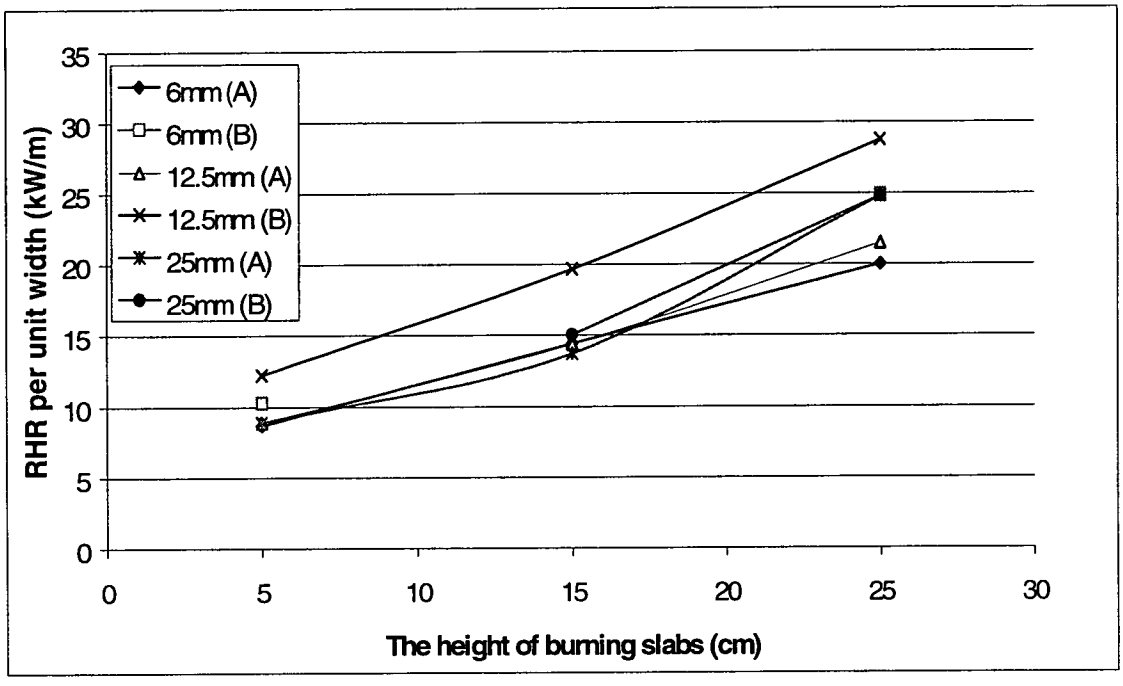

3.4 Single Wall Case Simulated by Spreading Wall Fires on PMMA Strips

The aim of the experimental work carried out was to look in detail at the flame height, heat flux from the flame to the unburned surfaces and flame spread rate on a spreading wall fire. The behaviour of a spreading flame is closer to that of a real fire.

3.4.1 Experimental Design

The experimental rig, shown in Fig. 3.12 in a schematic form, was designed to allow samples to be ignited horizontally and then to be rotated into a vertical position at the start of the test. This design can prevent extra heating on the region ahead of the 3 mm ignition zone. The combustible material used was PMMA, as 6 mm thick slabs with width of 7 cm and varying heights of 20, 30, 40 and 50 cm. The sample was marked with a scale so that the height of pyrolysis and flame tips can be determined by eye. The sample was held against a 2 mm thick steel plate: in addition to preventing flame spreading up the back of the sample, it kept the rear face relatively cool and prevented

distortion and slumping which would otherwise have occurred. A 5 mm wide slot was cut along the centreline of the backing plate to allow the pyrolysis front to be observed from the back of the sample by the appearance of bubbles. A heat flux meter was located at 2 cm from the top of the samples to measure heat flux from flame to unburned surface. The heat flux was recorded particularly while the flame tip and pyrolysis front reached the heat flux meter. A hand-held butane-fuelled torch was used to ignite the 3 mm ignition zone. After ignition, the sample was rotated to the vertical position, the flame height was observed visually and the time was noted while the pyrolysis front advanced one centimeter.

Modifications could be made to allow **either** 3 mm thick 15 mm wide mild steel strips **or** 25.4 mm thick 15 mm wide inert walls to be used to protect the vertical edges of the samples and hold the samples against the backing plate. The latter configuration, which will be called "with sidewalls" in this thesis, can help prevent lateral air entrainment along the burning sample.

Fig. 3.12 - The experimental rig. The dashed line frame represents the horizontally oriented rig during ignition and then moved to vertical after ignition (solid line). The flame and pyrolysis heights were observed by eye from the front and back surfaces of the burning samples.

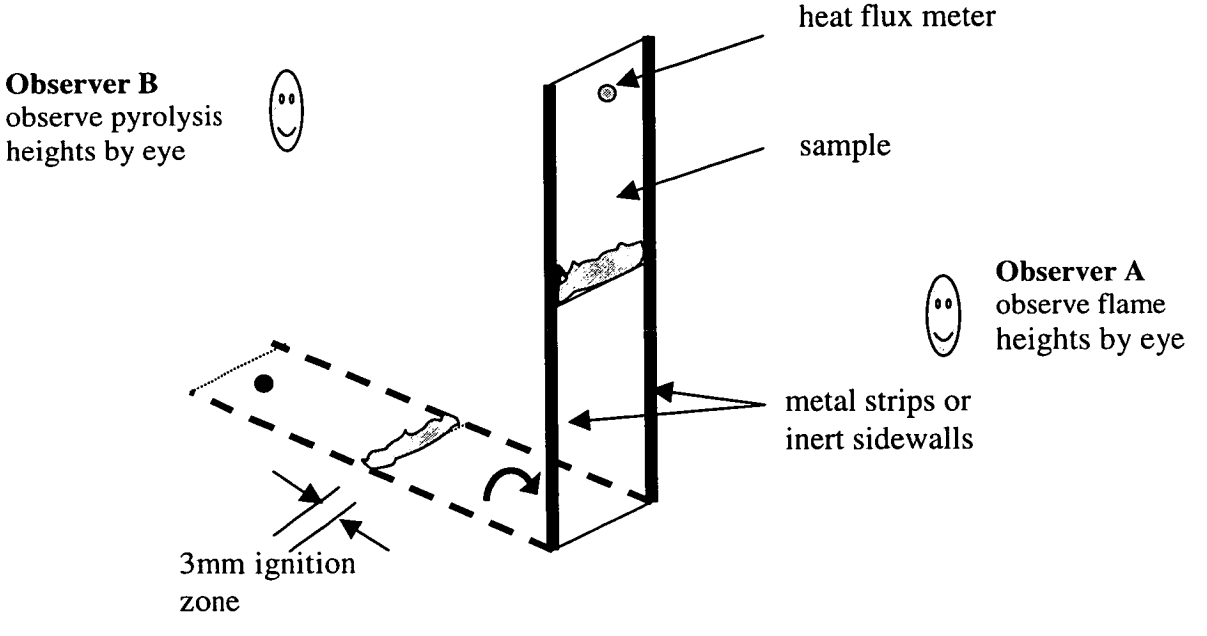

3.4.2. Results and Discussion

All the experimental data are presented in Appendix A-2, and a typical time elapsed and corresponding flame height measurement as the pyrolysis front advanced 1 cm and time-dependent heat flux measurement on and at 2 cm from the top of a 50 cm high burning PMMA slab without sidewalls are shown in Fig.3.13 and Fig.3.14. In Fig.3.13, the flame height is extrapolated linearly beyond upper edge of the samples, following the trend of the data. In Fig.3.14, the heat flux was marked when the flame tip and pyrolysis front passed the heat flux meter. The following section presents the relations of these parameters, which were averaged over three or four measurements.

3.4.2.1 Time history of pyrolysis front and flame spread rate

Fig. 3.15 shows the time history of the pyrolysis front on a 50 cm high PMMA slab with and without sidewalls, and Fig. 3.16 shows the flame spread rate. The wall fire with sidewalls spread faster than that without sidewalls. However, the difference is not apparently significant before 280 s.

Fig.3.13- Typical measurement of time elapsed and corresponding flame height as a function of pyrolysis height for a 50 cm high burning PMMA slab (without sidewalls).

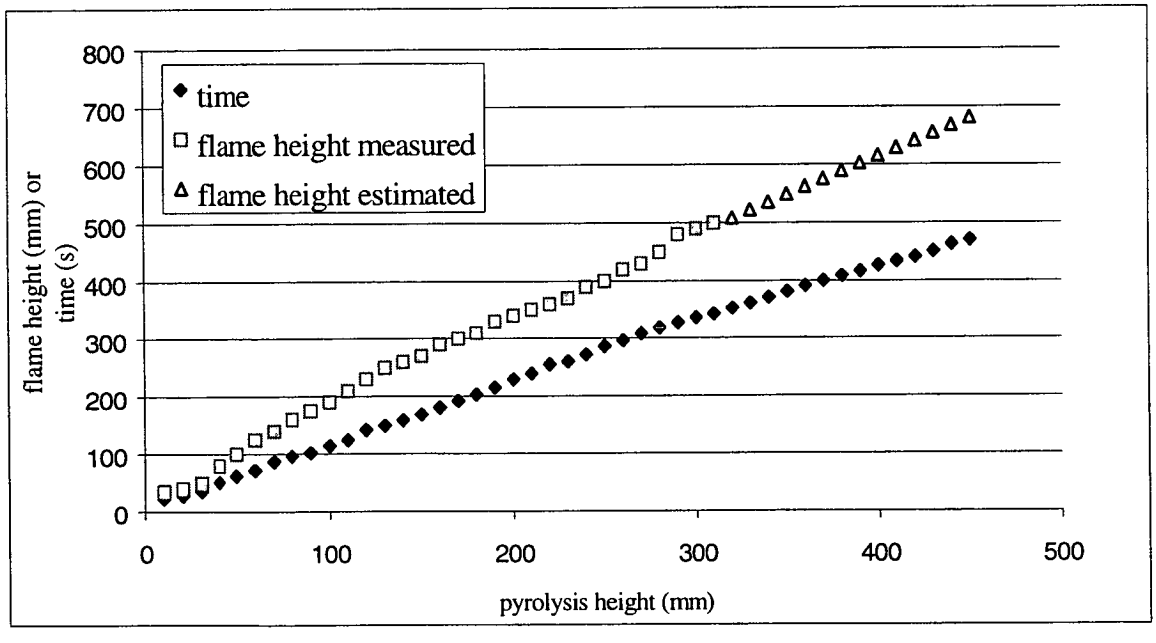

Fig.3.14- A typical heat flux measurement at the top of a 50 cm high burning PMMA slab without sidewalls.

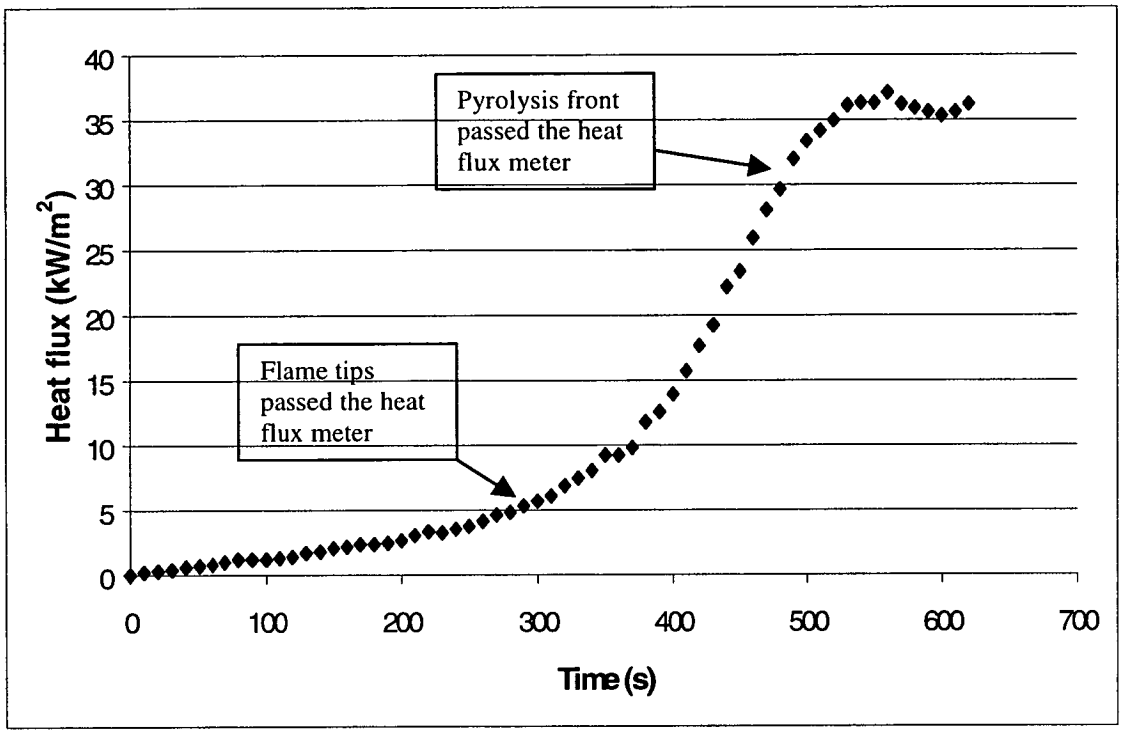

Fig.3.15- The time history of pyrolysis front position with and without sidewalls.

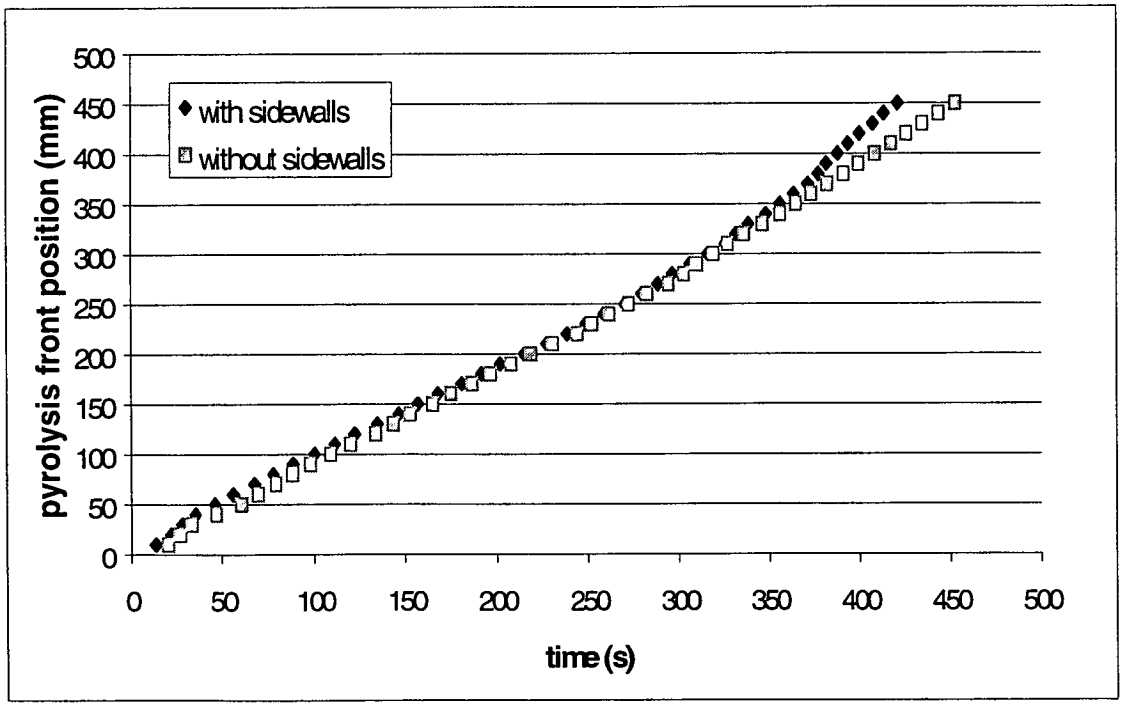

Fig. 3.16- The flame spread rate of PMMA fires with and without sidewalls.

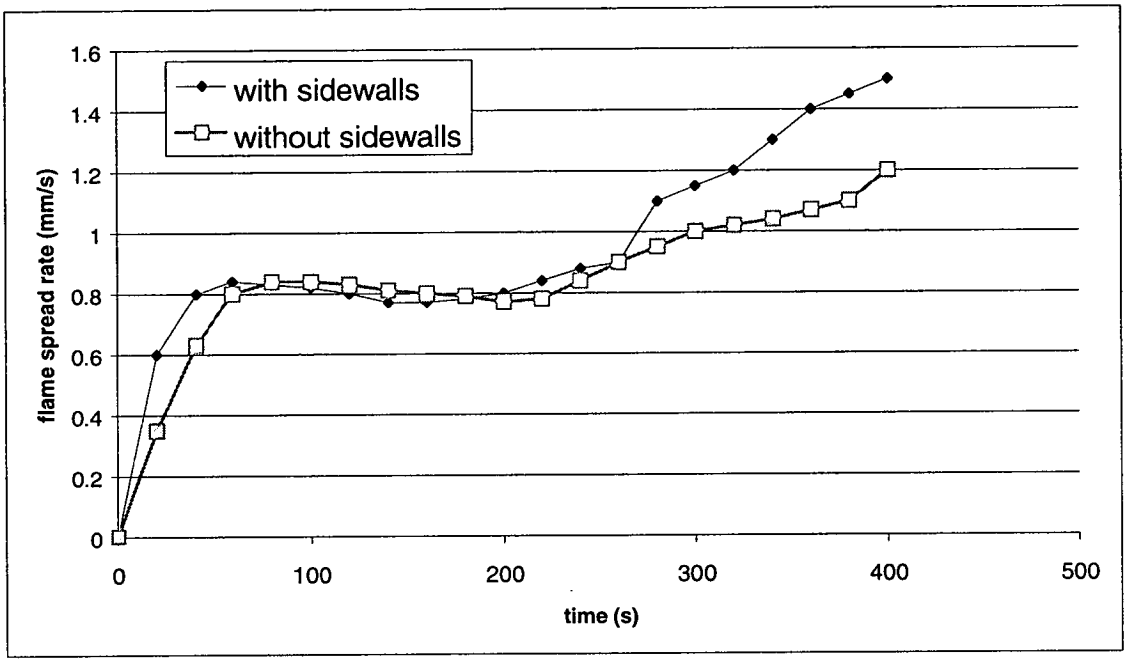

3.4.2.2 Pyrolysis front vs. flame height

Fig.3.17 shows the dependence of flame height on pyrolysis height with sidewalls present and absent. The flame height was more sensitive to pyrolysis height if sidewalls were present. This is because sidewalls have helped maintain one-dimensional air entrainment close to the burning surface. For the case in which sidewalls were present,

$$X_f = 1.72 X_p^{0.97} \tag{3.8}$$

where X_f and X_p are flame and pyrolysis height in meters. For the case without sidewalls,

$$X_f = 1.35 X_p^{0.87} \tag{3.9}$$

Fig.3.17- The dependence of flame height on pyrolysis height with sidewalls present or absent.

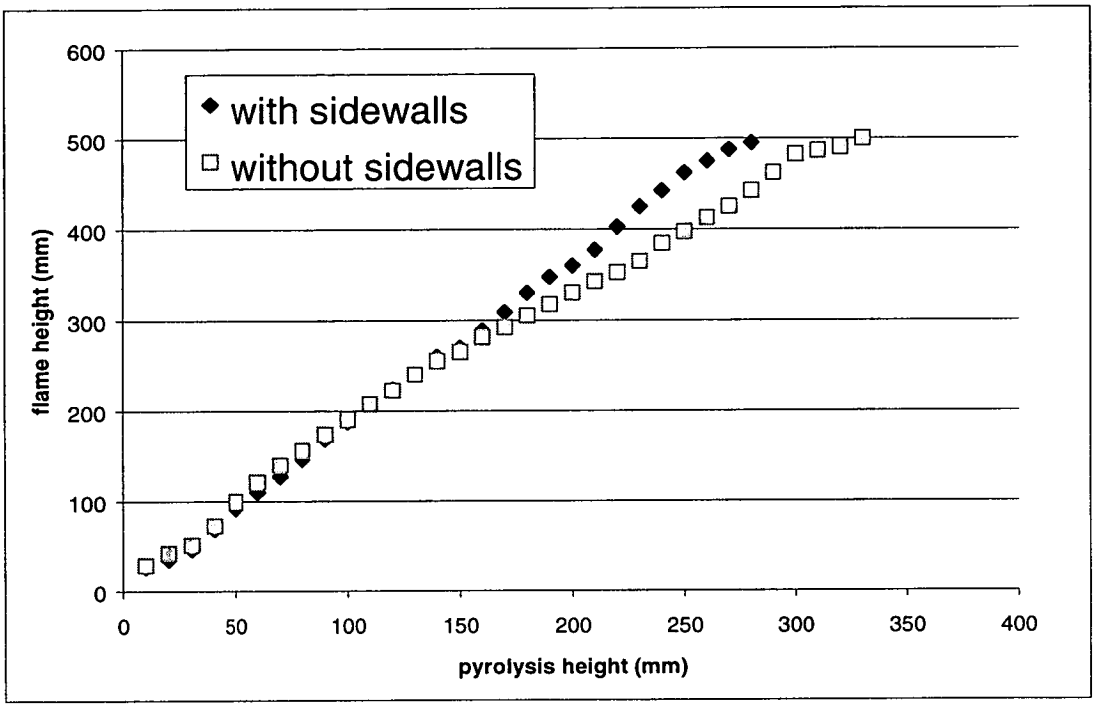

3.4.2.3 Heat flux

Fig.3.18 presents the heat flux measurements (average of three tests) from the heat flux meter located 2 cm from the top of the 20, 30, 40 and 50 cm high samples without sidewalls present. t_f and t_p respectively correspond to the time when the flame tip and pyrolysis front reached the heat flux meter. The duration between t_f and t_p represents the time during which the preheating region is exposed to heat (Fig.2.3).

The heat flux measured at t_f and t_p for different heights of PMMA samples is listed in Table 3.10. The heat flux corresponding to t_f decreased as the burning samples were longer. This was consistent with the observations of Qian *et al.* (1994) dealing with upward flame spread along vertical corner walls and Brehob *et al.* (1998) concerning upward flame spread with external radiation.

Fig.3. 18 - Variation of heat flux 20 mm from the top of the 20, 30, 40 and 50 cm sample in the absence of sidewalls.

(→ marks the time when the flame tips reached the heat flux meters; ⇢ indicates when the pyrolysis front reached the heat flux meters)

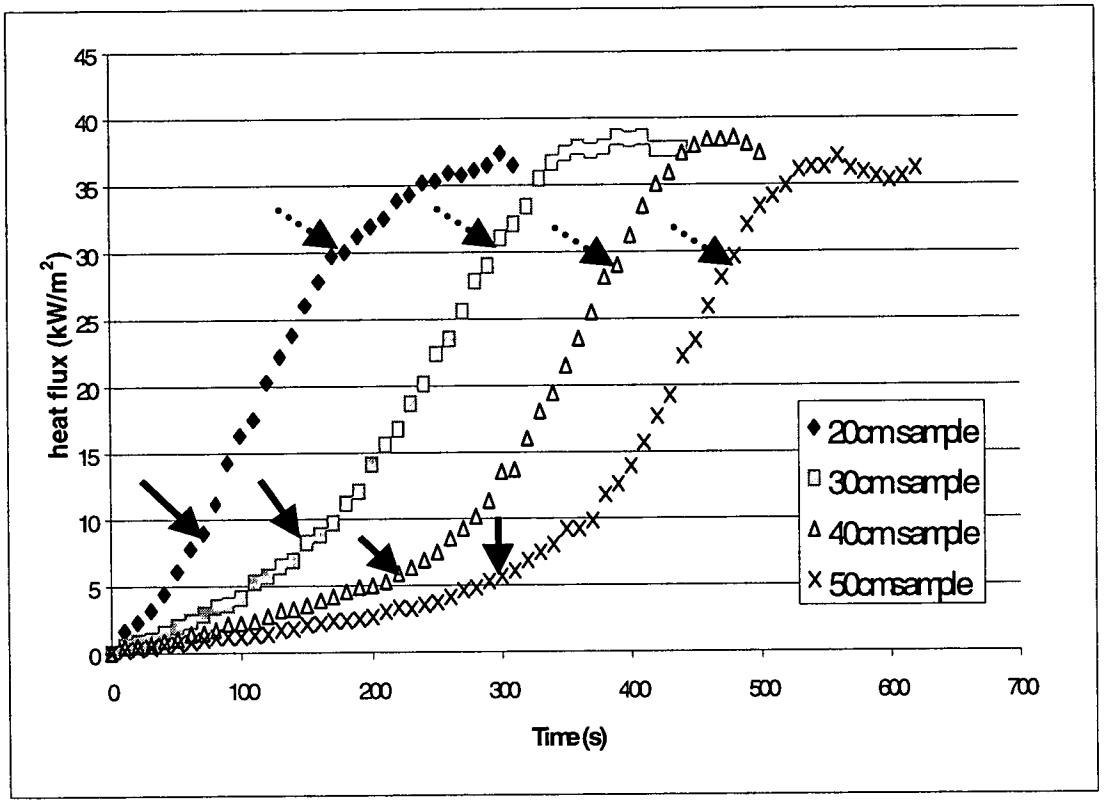

Table 3.10 - The heat flux measured at t_f and t_p for different heights of samples (without sidewalls).

height of heat flux meter (cm)	heat flux corresponding to t_f (kW/m^2)	heat flux corresponding to t_p (kW/m^2)
20	9.6	31
30	8.8	30
40	6.5	29
50	6.4	29

The heat fluxes corresponding to t_p were very close (Table 3.10), and could be regarded as "typical heat flux for upward flame spread". At these locations radiation plays a primary role. Furthermore, Fig.3.18 illustrates that the maximum heat flux occurred below pyrolysis fronts where the samples were undergoing pyrolysing. A uniform terminal heat flux (around 38 kW/m^2) was produced.

The heat fluxes from the spreading PMMA wall fires to the unburned zone with and without sidewalls present are compared. Fig.3.19 plots the heat flux against X/X_f. The best-fit functions are

For with sidewalls, with r^2=0.942

$$\dot{q}_w'' = 7.26 \left(\frac{X}{X_f}\right)^{-2.57} \tag{3.10}$$

For without sidewalls with r^2=0.875

$$\dot{q}_w'' = 8.27 \left(\frac{X}{X_f}\right)^{-2.72} \tag{3.11}$$

Fig. 3.20 plots the heat fluxes following the procedure used by Brehob *et al.* (2001). The best-fit functions are

For with sidewalls

$$\frac{\dot{q}_w''}{\dot{q}_{wo}''} = 0.18\left[\frac{X - X_p}{X_f - X_p}\right]^{-0.83} \tag{3.12}$$

and for the case without sidewalls,

$$\frac{\dot{q}_w''}{\dot{q}_{wo}''} = 0.21\left[\frac{X - X_p}{X_f - X_p}\right]^{-0.81} \tag{3.13}$$

It is seen that the heat flux distribution without sidewalls present was higher than that with sidewalls (about 15%). The presence of sidewalls restricts the air entrained laterally, which may result in less vigorous burning and lower heat fluxes. In addition, the heat flux corresponding to t_f and t_p for the case with sidewalls is very close to that without sidewalls, giving 7.8 and 29.8 kW/m^2 respectively. The representative heat flux in this preheating region (Fig. 2.3) could consequently be estimated to be c.18.8 kW/m^2. In addition, the maximum terminal heat flux (41 kW/m^2) with sidewalls present is higher than that without sidewalls (38 kW/m^2).

Fig.3.19 - The heat flux distribution of the spreading PMMA wall fires with and without sidewalls plotted against X/X_f.

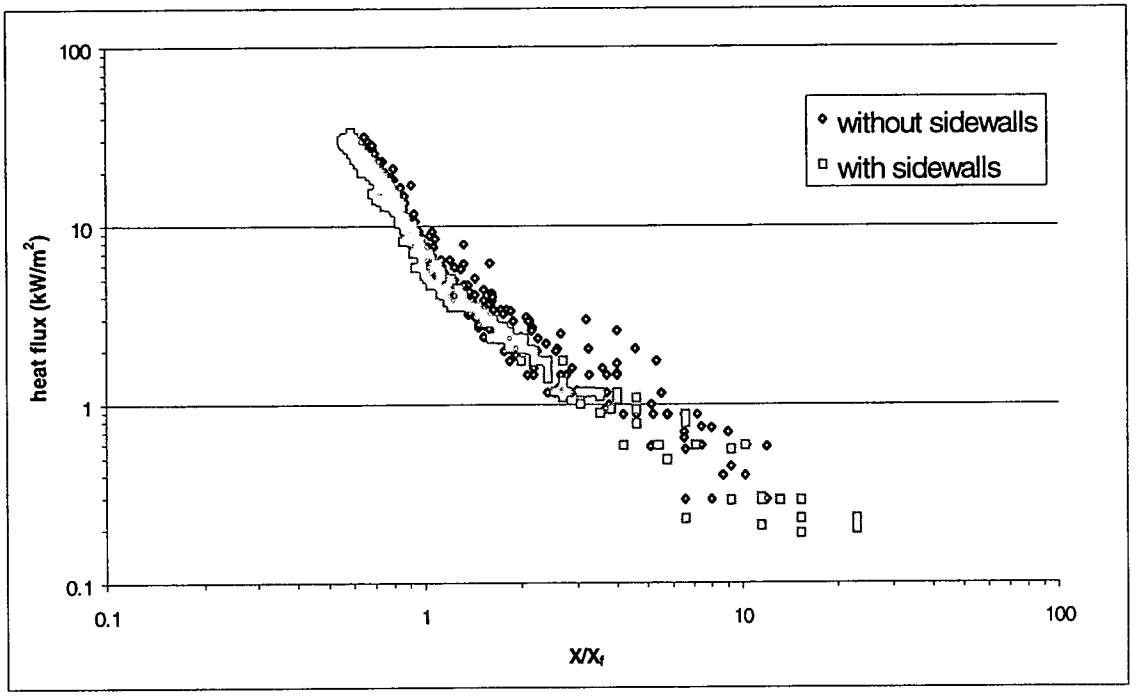

Fig.3.20 - The heat flux distribution of the spreading PMMA wall fires with and without sidewalls following the expression of Brehob *et al.* (2001).

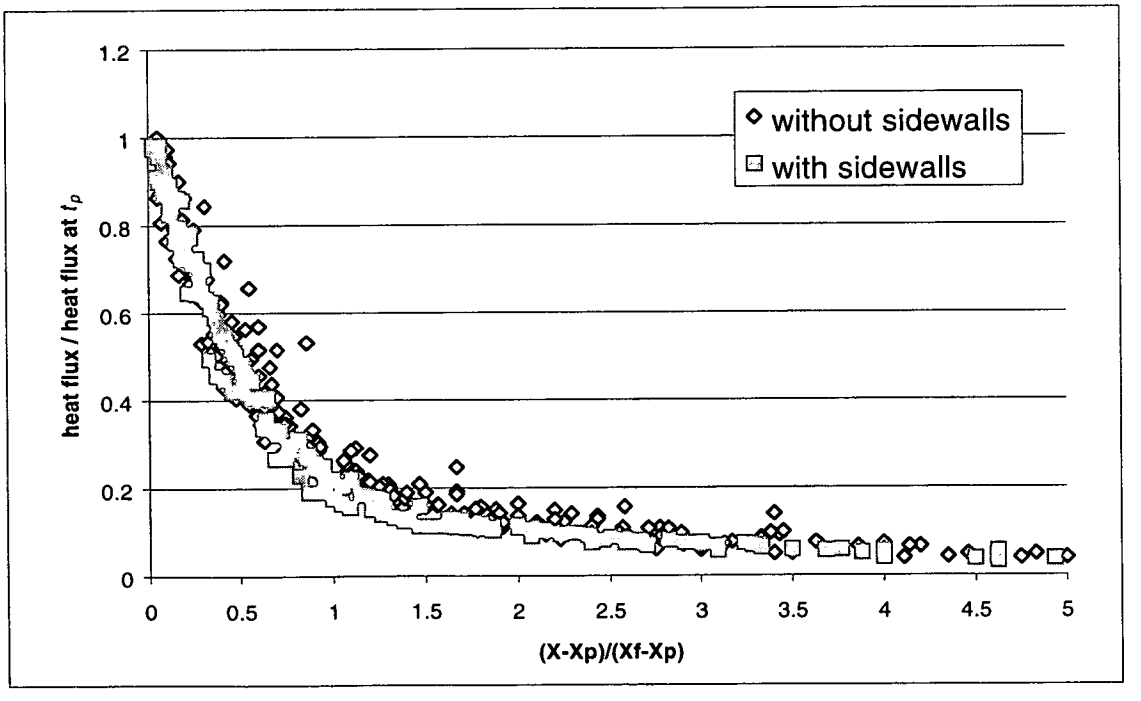

3.5 Single Wall Case Simulated by Gas Panel

3.5.1 Experimental Design

The experimental rig is shown in Fig. 3.21. A propane fuelled vertical panel (60 cm high and 84 cm wide) was constructed from 14 separate porous ceramic burners, four measuring 0.15 × 0.15 m and 10 measuring 0.15 × 0.30 m, as shown in Fig. 3.21. An inert board located above and in the same plane as the burner was held in a frame consisting of two metal channels which allowed the board to be moved sideways. These 14 burners were controlled individually by valves and the total flow of gas to the panel was controlled by a mass flow controller (Chell, CFD 100 flow controller)*. Prior to an experiment, a selection of valves was opened to provide a burner of the required area and aspect ratio for studying flame height as a function of fuel flowrate (in *l*/min). Three heat flux meters were located on the centreline of the inert wall at 20, 60 and 100 cm above the gas panel. By moving the inert wall horizontally along the channel frame, these heat flux meters were able to measure the heat flux on the centreline of the burning areas. The inert board was marked with a scale which allows flame heights to be determined by eye.

Table 3.11 lists the burning area and gas flow rate in *l*/min. The rate of heat release per unit width $\dot{Q}'$ was calculated using idea gas law

$$PV = nRT \tag{3.14}$$

where V is the volume (l) occupied by n moles of gas at a pressure P (atm) and temperature T (K), to calculate the mass flow rate and converted to $\dot{Q}'$ using the equation

$$\dot{Q}' = \dot{m}' \Delta H_c \tag{3.15}$$

with the assumption of complete combustion and the ΔH_c of propane is 46.45 kJ/g (Drysdale, 1998).

---

* Although it was a mass flow controller, calibrated for propane, its calibration was expressed as l/min at STP

Fig. 3.21 – Diagram showing the gas panel. Each rectangle represents a burner which has an individual control valve.

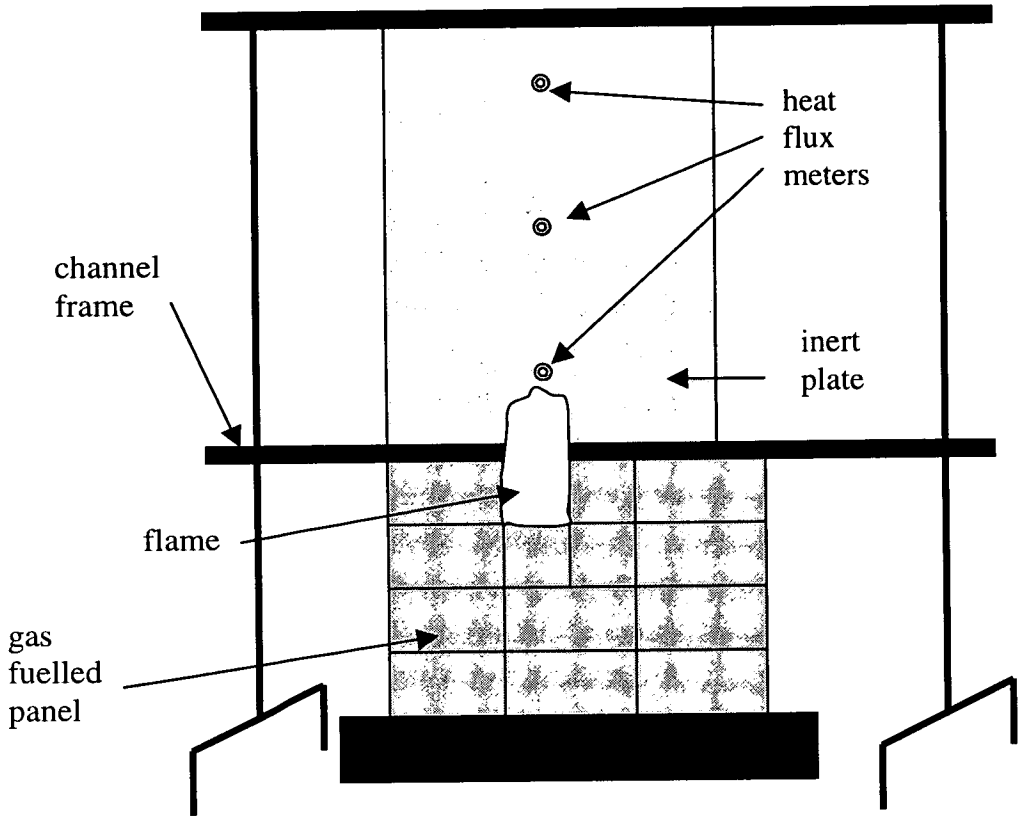

Table 3.11 - Burning areas and gas flowrates used in the gas panel tests.

Height (m)	Width (m)	H/W	Gas flow rate (L/min)
0.15	0.15	1	2.5, 3, 3.5, 4, 4.5, 5, 5.5, 6, 6.5, 7, 7.5, 8, 8.5, 9, 9.5, 10, 10.5, 11.5, 12.5, 13.5
0.3	0.15	2	3.5, 4, 4.5, 5, 5.5, 6, 6.5, 7, 7.5, 8, 8.5, 9, 9.5, 10, 10.5, 11, 12, 13, 14, 15, 16, 17, 19, 21
0.15	0.3	0.5	4, 4.5, 5, 5.5, 6, 7, 8, 9, 10, 11, 12, 13, 14, 15,16
0.3	0.3	1	7, 8, 9, 10, 11, 12, 13, 15, 17, 19, 21, 23, 25, 27
0.45	0.3	1.5	10, 10.5, 11, 12, 13, 14, 15, 16, 17, 18, 20, 22, 24, 26, 28, 30, 32, 35,
0.6	0.3	2	13, 15, 17, 19, 22, 25, 27, 29, 31, 33, 35, 37, 39, 41, 43
0.15	0.57	0.263	6.5, 7, 7.5, 8, 9, 10, 11, 12, 14, 16, 18, 20, 22, 25, 28, 30, 32, 34, 37, 40
0.3	0.57	0.526	12, 14, 16, 18, 20, 23, 26, 29, 32, 35, 38, 41, 44, 46, 48
0.45	0.57	0.789	16, 18, 20, 22, 24, 26, 29, 32, 35, 38, 41, 45, 48, 51

3.5.2 Experimental Results

All the experimental data are presented in Appendix A-3. Fig.3.22 (a) and (b) shows the dependence of X_f on $\dot{Q}'$ for different burning areas in normal and logarithmic scale. It can be seen that the flame height correlates with $\dot{Q}'$, however, divergence exists following the width of the burning areas.

For fires produced by 15 cm wide burners,

$$X_f = 0.058\dot{Q}'^{0.646} \tag{3.16}$$

For fires produced by 30 cm wide burners,

$$X_f = 0.07\dot{Q}'^{0.616} \tag{3.17}$$

For fires produced by 57 cm wide burners,

$$X_f = 0.061\dot{Q}'^{0.655} \tag{3.18}$$

The r^2 for these three correlations are 0.965, 0.989 and 0.991 respectively and the values of n are close to the theoretical value of 0.66 which was determined by Delichatsios (1984), Quintiere *et al.* (1986) and Eklund (1986) (see Section 2.4.3.1). The fires from wider burning areas produced higher flames. Actually, the same observation can be seen in Hasemi's work (Fig.3, 1985) using line burners with different widths although the width effect was not discussed. The reason for this is not known but might be because of change in the turbulent structure of the flame.

Fig. 3.22 (a) and (b) - The relation of X_f and $\dot{Q}'$ on vertical propane fires of different burning areas in normal and logarithmic scale. On the legend, h15w15 represents the burner as 15cm high and 15cm wide.

(a)

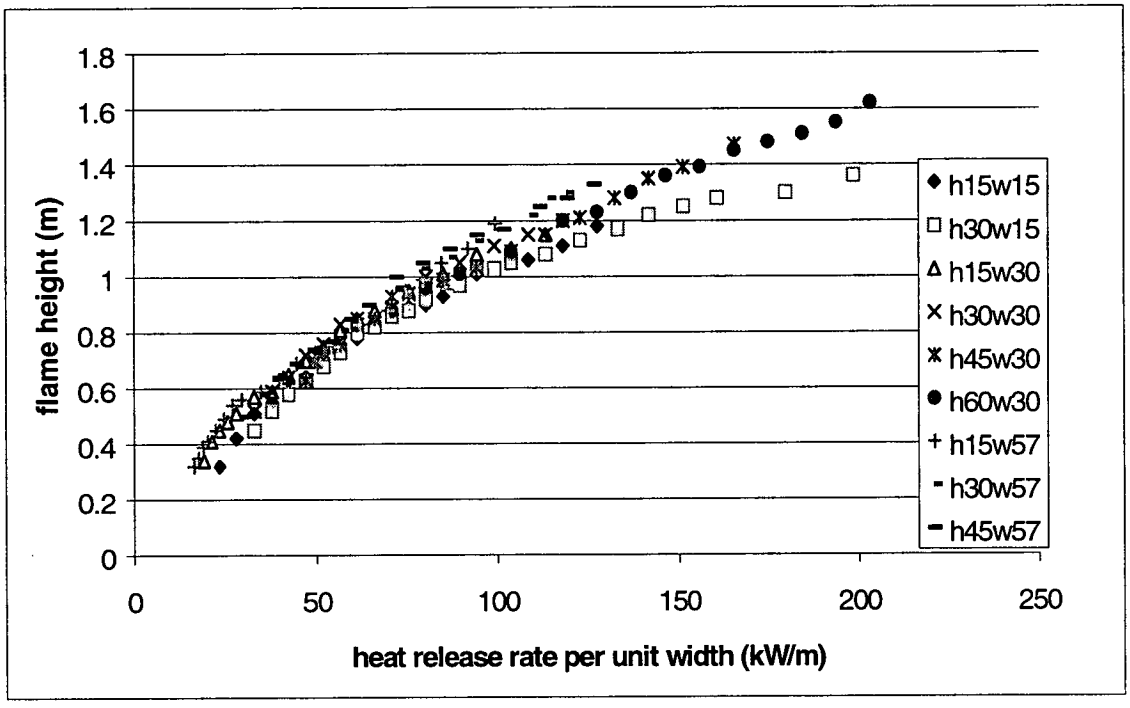

(b)

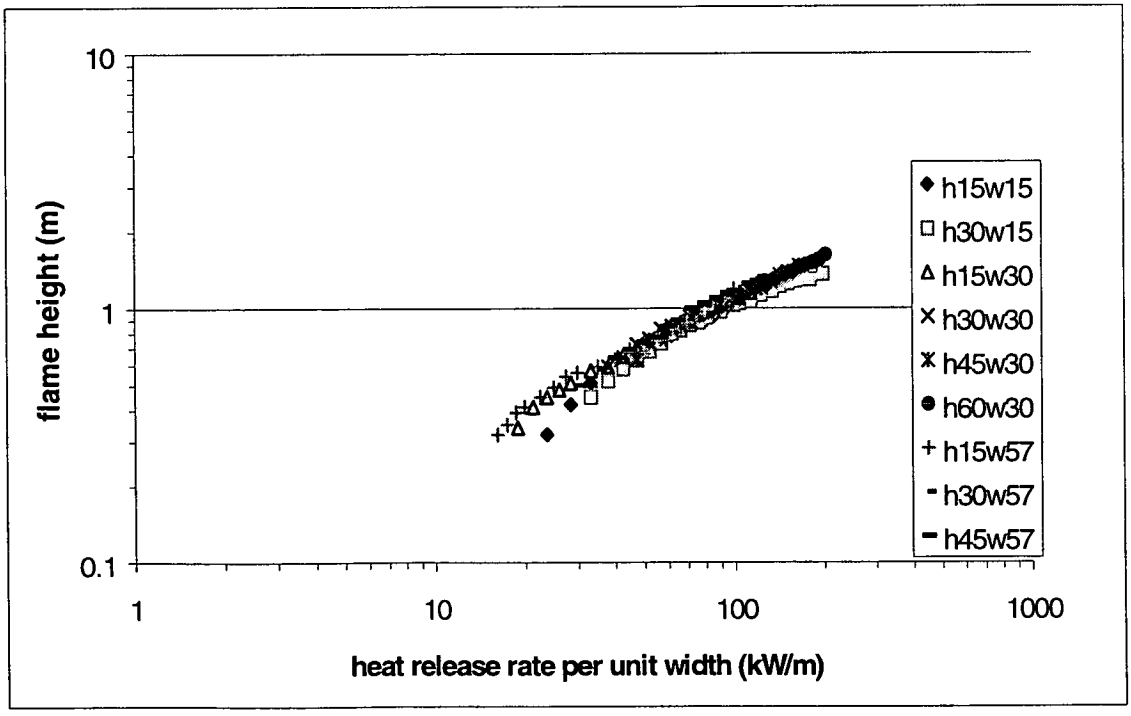

Heat flux distribution

The heat fluxes from the flames to the unburned surfaces along the centerline of the flames were measured and plotted against the position normalised by the flame height (X/X_f). For clarity, Fig.3.23 (a) shows the heat flux distributions for the 15 cm and 30 cm wide flames and Fig.3.24 (a) for width of 30 cm and 57 cm. Fig.3.23 (b) and Fig.3.24 (b) present the correlations in logarithm scale. In both Fig.3.23 and 3.24, three regions can be seen with the heat flux distributions of these 15, 30 and 57 cm wide flames: for X/X_f < c. 0.5-0.6, the heat flux was almost constant, for 0.5-0.6 < X/X_f < 1.1-1.2, the heat flux decreases with X/X_f, while for X/X_f > 1.1-1.2, the heat flux also decreases with X/X_f but less steeply. In addition, the scatter of the heat flux distributions is obvious.

In Fig.3.23 (a), it can be seen that the heat fluxes from 30 cm wide flames were higher than those from 15 cm wide ones. The average heat flux in the region where the heat flux is almost constant is approximately 25 kW/m^2 for the 15 cm wide flames and c.27 kW/m^2 for the 30 cm wide ones although this region is for X/X_f <0.5 for 15 cm ones while is 0.6 for 30 cm ones. The straight line sections of the heat flux distributions for c.0.6< X/X_f <c.1.2 for the 15 and 30 cm wide fires can be fitted by Equations 3.19 and 3.20 with correlation coefficients of 0.897 and 0.843.

$$\dot{q}'' = 4.60 \left(\frac{X}{X_f}\right)^{-2.40} \tag{3.19}$$

$$\dot{q}'' = 6.12 \left(\frac{X}{X_f}\right)^{-2.93} \tag{3.20}$$

In Fig.3.24 (a), the 30 cm wide flames also produced higher heat flux than 57 cm wide ones. The average heat flux produced from the 57 cm wide flames for X/X_f <0.5 is c. 23 kW/m^2. This is lower than that from the 30 cm wide flames (and 15 cm wide flames). For X/X_f greater than 0.8, the heat flux distributions for the 30 and 57 cm wide flames almost overlapped although the heat flux from 30 cm wide flames decreased more steeply. The straight line section for c.0.5< X/X_f <c.1.2 for the 57 cm wide fires can be fitted by Equation 3.21 with correlation coefficient of 0.836:

$$\dot{q}'' = 5.81 \left(\frac{X}{X_f} \right)^{-2.59} \tag{3.21}$$

There is width effect on the heat flux distributions. However, no clear trend was found.

Fig.3.23 - The heat flux distributions for the 15 cm and 30 cm wide flames. Fig.3.23 (a) in normal scale; Fig.3.23 (b) in logarithm scale.

(a)

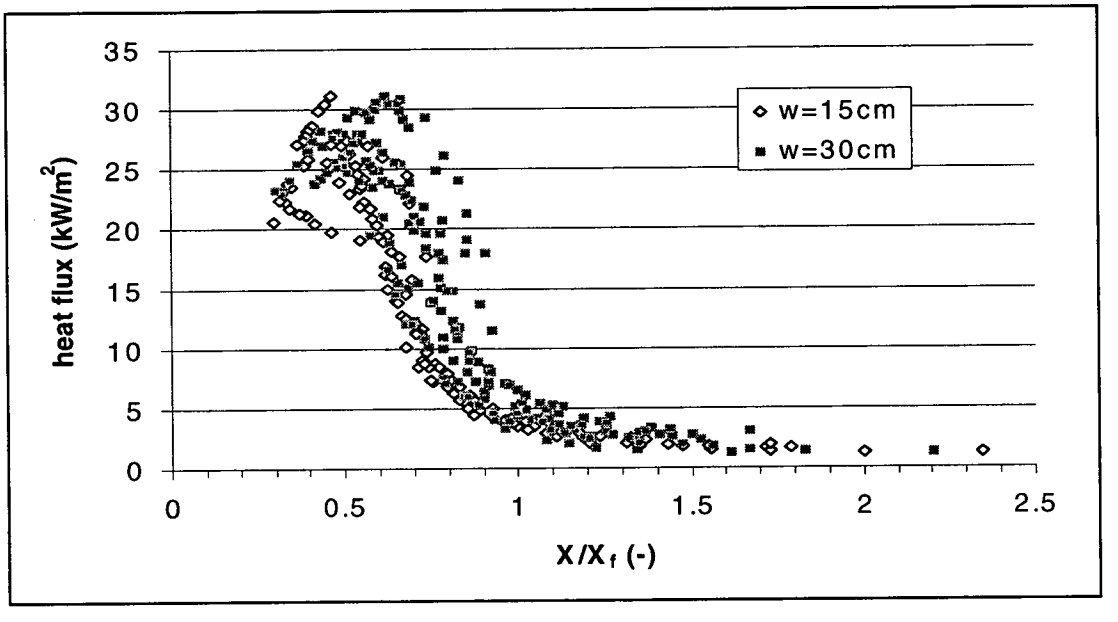

(b)

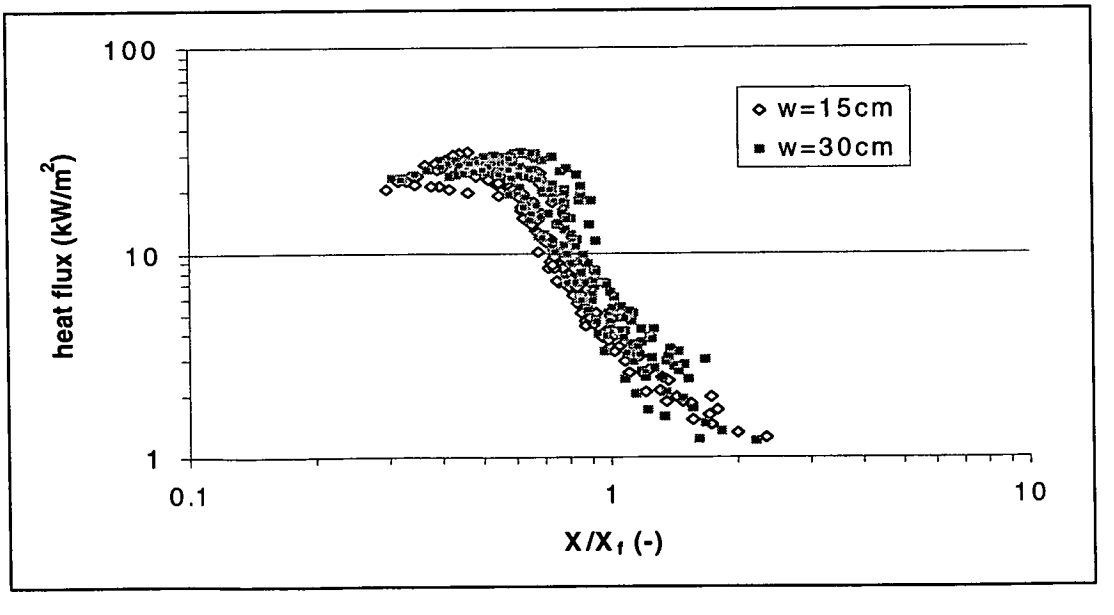

Fig.3.24 - The heat flux distributions for the 30 cm and 57 cm wide flames Fig.3.24 (a) in normal scale; Fig.3.24 (b) in logarithm scale.

(a)

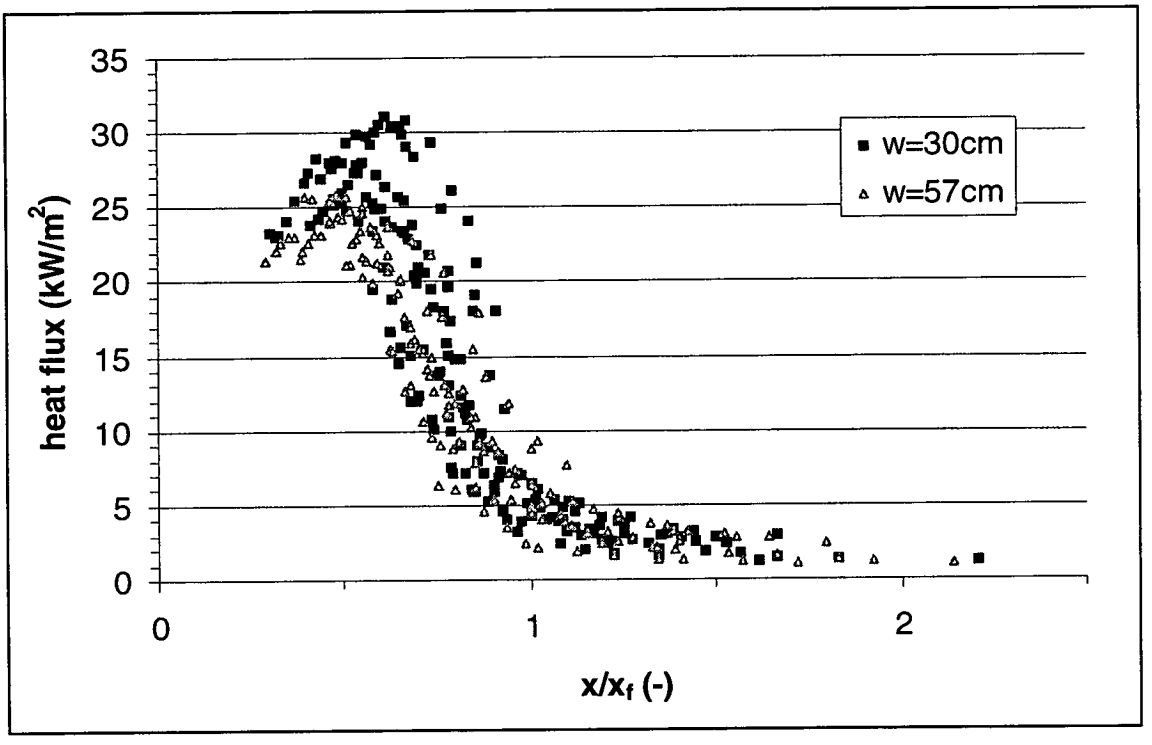

(b)

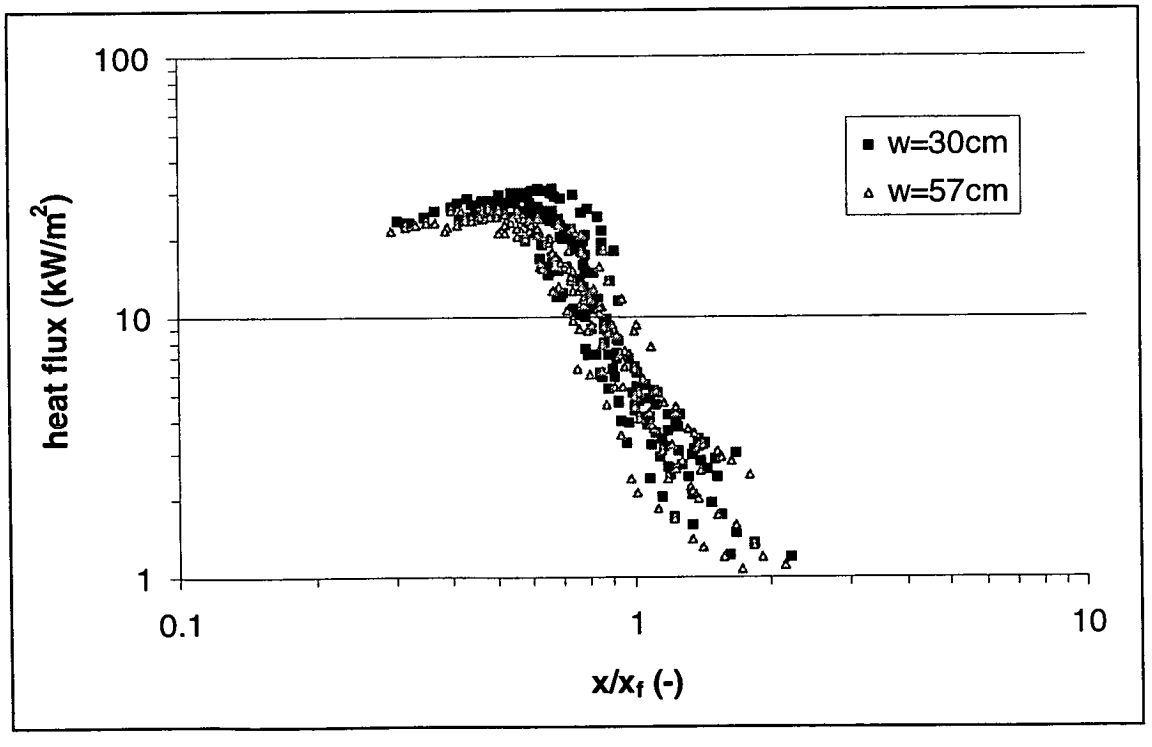

3.6 Corner Case

Upward flame spread on vertical walls in a corner has been demonstrated to result in more rapid fire growth than that on flat surfaces (Sec.2.5). However, only a few experiments and prediction models have been carried out and proposed for corner fires. Thus, experiments were designed to gain more understanding of this phenomenon and provide a database on which predictive models can be constructed.

Measurements primarily made were the flame height and heat flux as they were to be used in modelling work. In addition, the flame spread rate was measured for comparison with that on flat surfaces (Chapter 5) and with future modelling results.

3.6.1 Experimental Set-ups

An experimental rig was designed to hold two vertical combustible samples perpendicular to each other (see Fig. 3.25). The combustible material used was 6 mm thick PMMA slabs with height of 0.26, 0.5 and 1m and width of 0.1m. The two samples were mounted and fixed against two perpendicularly connected metal backing plates by two metal slabs which overlapped the samples by 0.02 m. Consequently the effective width exposed for burning was 0.08 m. The metal plates can prevent flame spreading up to the back of the samples, keep the rear face of the samples relatively cool and prevent distortion and slumping which would otherwise have occurred. The two metal plates protect the edges of the samples and fix two inert walls in addition to fixing the samples. The two inert walls were used as an extension to help maintain smooth air entrainment to the corner. In addition, a scale was marked on it and a video camcorder was used to record each experiment. The flame height was determined subsequently by visual examination of the videorecordings. An infrared camera was used to measure the surface temperature of the combustible walls, from which the position of pyrolysis front can be deduced by tracing the 360^0C isotherms. A hole was drilled at 0.24, 0.48 or 0.86 m high and 2 cm from the corner on each of the 0.26, 0.5 or 1 m high PMMA slabs and three pairs of holes on the backing plates at the corresponding locations so that heat flux meters can be located through these holes to measure the heat flux from the flame to the unburned surface.

The experiment started with the ignition of the bottom edges (0.02 m high and 0.08 m wide) of the two corner walls by a butane/propane fuelled torch, and finished with extinguish by a CO_2 fire extinguisher when pyrolysis fronts reached top of the sample.

Fig. 3.25 – The experimental rig for the corner/ wall tests.

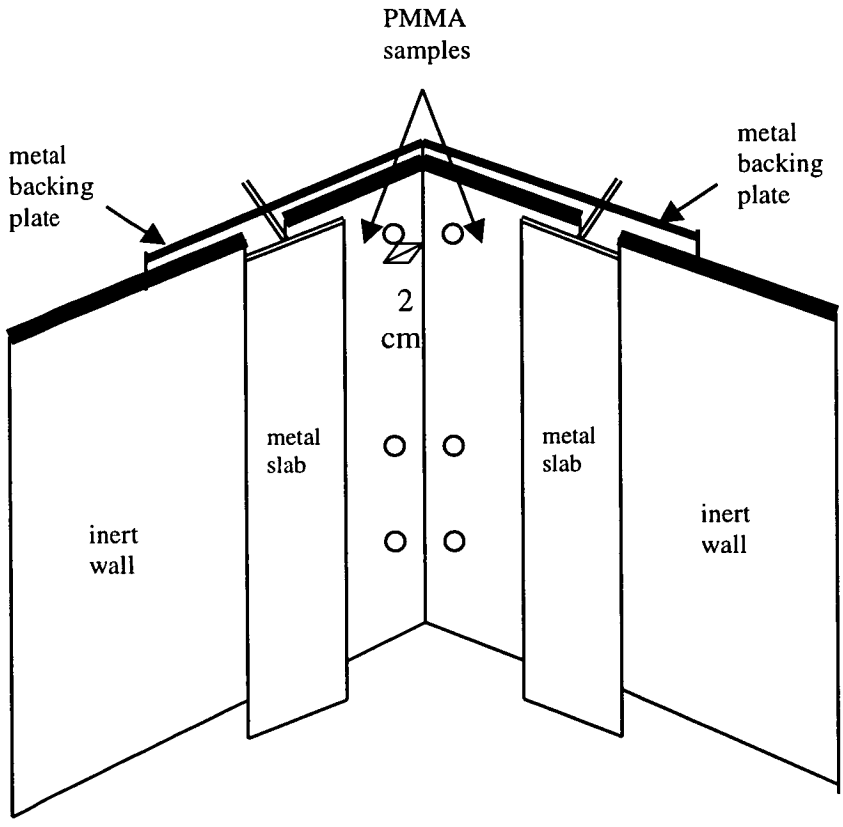

3.6.2 Experimental Results and Discussion

From the infrared imaging of the pyrolysis region, a clear M-shape was observed with the peak pyrolysis fronts occurring at 2 cm from the corner. This is because only the fuel vapours released away from the corner for a certain distance can be diffused with air to produce a diffusion flame. Along the corner, poor mixing of the pyrolysis products and air occurred, forming a volume of fuel rich mixture between the corner and the flame reducing the heat transfer into the corner. This coincides with the observation of Qian *et al.* (1994).

However, the corner did pyrolyse on its lower portion, which was not noticed by Qian *et al.* (1994). It was observed from the samples after extinction that, for the 1 m high corner, about 25 cm of the lower portion had undergone pyrolysis. This may be due to a change of the fuel vapour/ air mixture as burnout occurred at the bottom section of the sample and a long heating from the flame. The top view of the corner/wall fire can be illustrated in Fig. 3.26 (a) for the lower portion and Fig. 3.26 (b) for the upper portion. From the videorecordings, it can be seen that the flames on the two samples merged even at the upper portion where a separation existed between the two pyrolysing regions (Fig. 3.27).

Fig. 3.26 (a) and (b)- The schematic diagrams (top view) of the corner/wall fire. Fig. 3.26 (a) demonstrates the lower portion of the corner walls where pyrolysis occurred along the corner; Fig. 3.26 (b) demonstrates the upper portion where pyrolysis has not occurred along the corner.

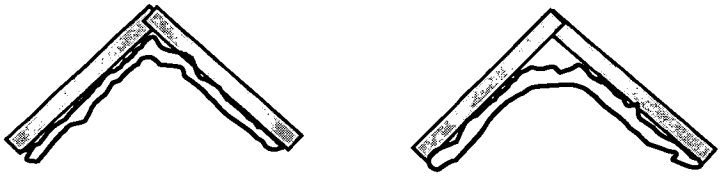

The relation of the peak of the pyrolysis front X_{pp} and flame height X_f with time t

Fig.3.28 shows the time history of the flame tips and pyrolysis front. An accelerating flame spread was demonstrated. The best-fit correlations with time t of the peak of the pyrolysis front X_{pp} (in cm) and flame height X_f (in cm) are in Equation 3.22 and 3.23.

$$X_{pp} = 0.0006t^2 + 0.1t + 4.39 \tag{3.22}$$

$$X_f = 0.0003t^2 + 0.21t + 13.3 \tag{3.23}$$

Fig. 3.27 – A videorecording taken during the corner test (next page).

The r^2 for Equation 3.22 and 3.23 are 0.9897 and 0.9938.

Qian *et al.* (1994) reported that there was an ignition effect for X_{pp} less than 20 cm in their PMMA tests. The PMMA slabs were 1.6 m high, 0.3 m wide and 0.02 m thick.

Excluding the data of the initial stage (<20 cm), the pyrolysis front X_{pp} and flame height X_f can be re-written to correlate with t in a power function for the comparison with the data of Qian *et al.* (1995).

$$X_{pp} = 0.0036t^{1.71} \tag{3.24}$$

$$X_f = 0.21t^{1.098} \tag{3.25}$$

The growth rate of the heights of the pyrolysis front peak and flame tips (ignition width: 8 cm) are lower than those reported by Qian *et al.* (1994) who deriving correlations for ignition width > 20 cm (Equation 2.72 and 2.79 in Sec. 2.6). The present result is consistent with the observation of Qian *et al.* (1994): that the flame spread rate increases with increasing ignition width from a spot to 20 cm, while remaining constant for ignition width of 20, 30 and 40 cm.

Fig. 3. 28 – The time history of the peak of the pyrolysis front X_{pp} and flame height X_f.

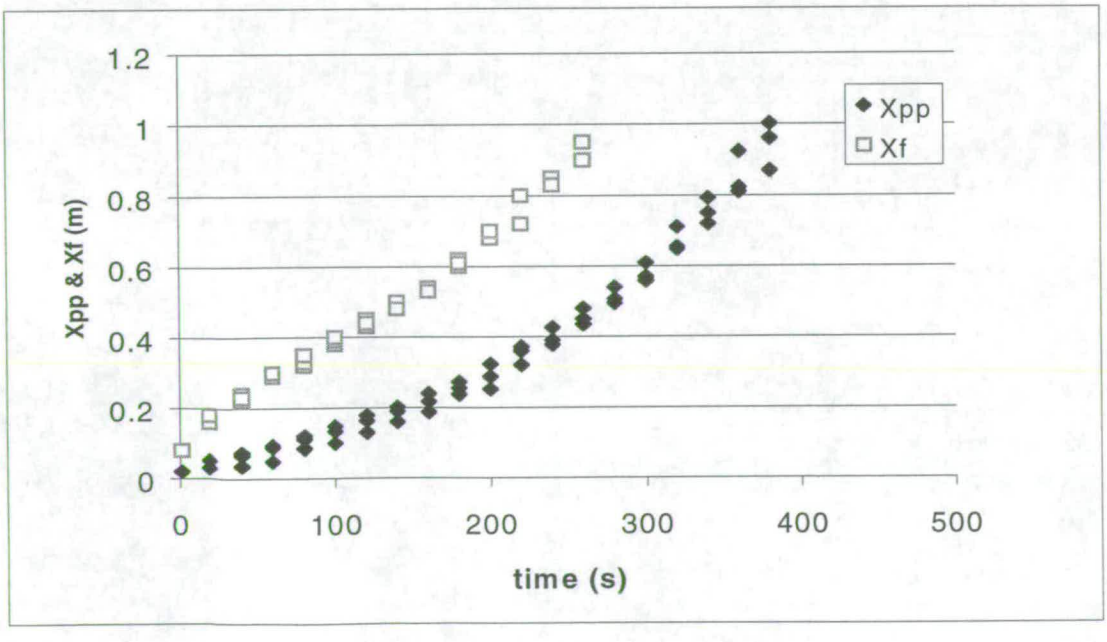

The relation of the peak of the pyrolysis front X_{pp} and flame height X_f

The relation of the peak of the pyrolysis front X_{pp} and flame height X_f is showed in Fig. 3.29, giving a correlation of Equation 3.26 with r^2 of 0.957

$$X_f = 1.47 X_{pp}^{0.64} \tag{3.26}$$

Fig. 3. 29 - The relation of the peak of the pyrolysis front X_{pp} and flame height X_f

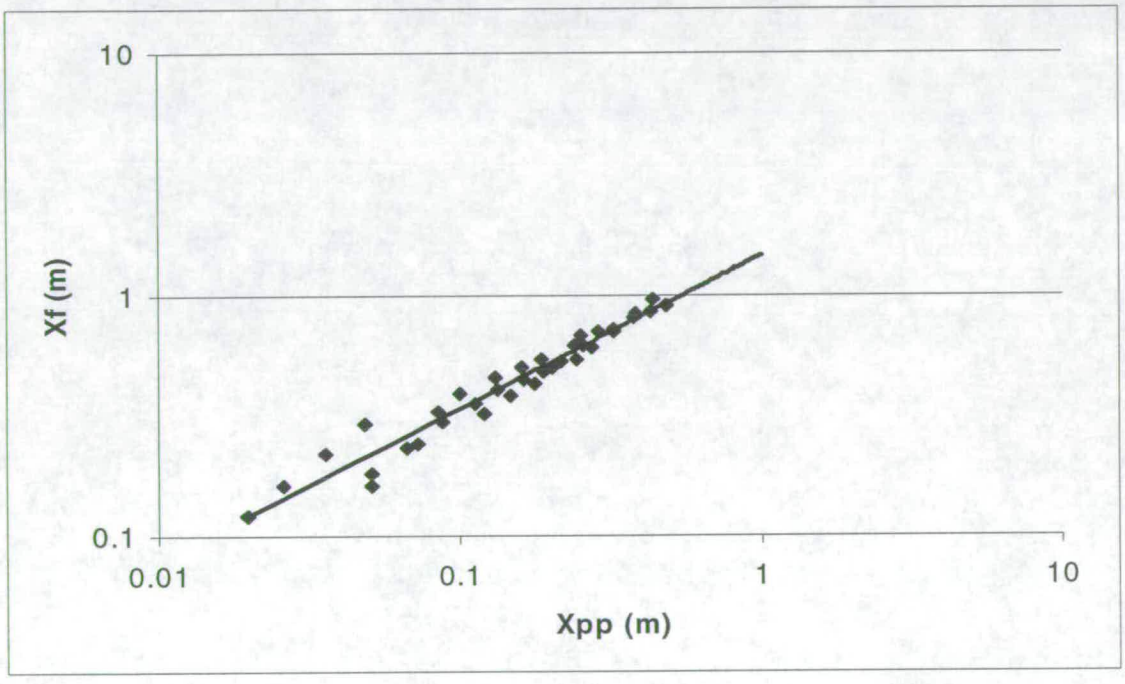

The relation of the spread rate of the pyrolysis front peak V_{pp} and time t

Fig. 3.30 – The time history of the spread rate of the pyrolysis front peak.

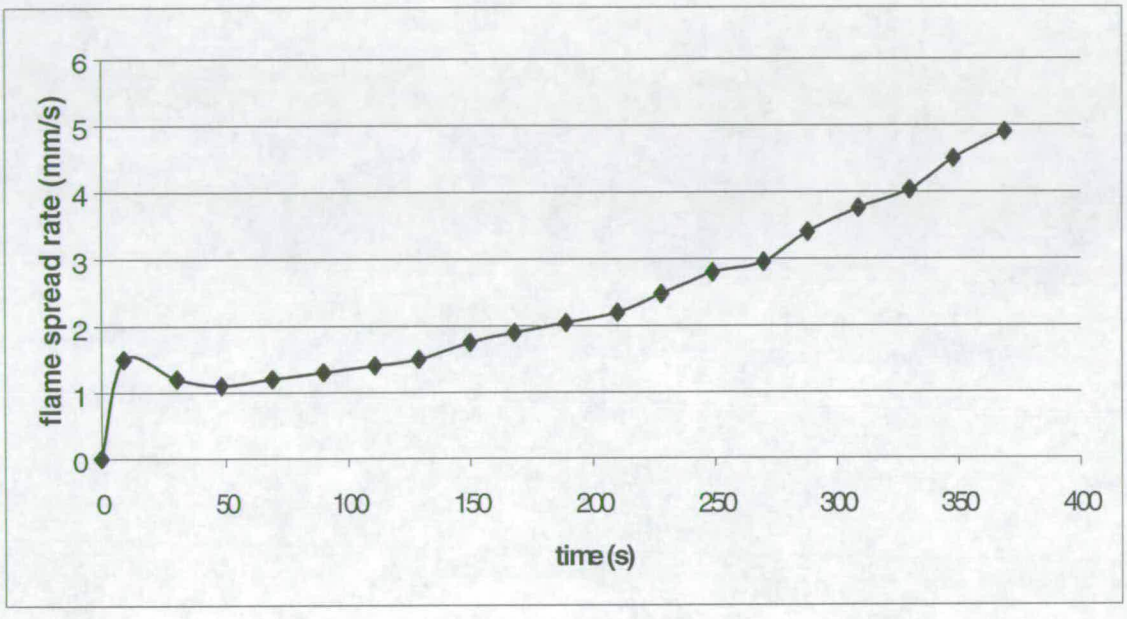

The high initial flame spread rate within 50 s, which is shown in Fig. 3.30, is a result of the heating effect of the torch.

The relation of the height and spread rate of the pyrolysis front peak X_{pp} and V_{pp}

The correlation between the X_{pp} and V_{pp} is

$$V_{pp} = 0.0048 X_{pp}^{0.66} \tag{3.27}$$

The r^2 is 0.848. This can be compared with the data of Qian *et al.* (1994), giving Equation 2.73

$$V_{pp} = 0.0134 X_{pp}^{0.944} \tag{2.73}$$

This spread rate in this study is much lower than that found by Qian *et al.* (1994) for ignition width between 20 and 40 cm. The power is also much lower. This shows again that the flame spread rate is strongly influenced by the width of the corner/wall fire.

Fig. 3. 31 - The relation of the height and spread rate of the pyrolysis front peak X_{pp} and V_{pp}

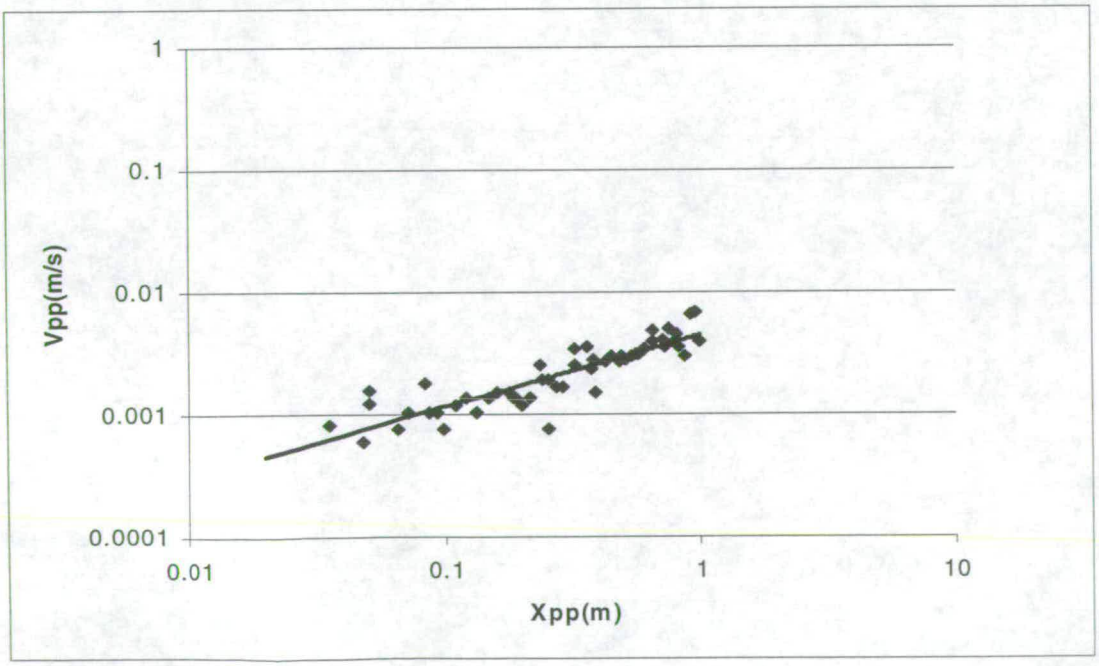

Heat flux distribution from the flame to the unburned surfaces

Fig.3.32 presents the heat flux measurements (average of three tests) from the heat flux meter at 24, 48 and 86 cm high of the 26, 50 and 100 cm samples. t_f and t_p respectively correspond to the time when the flame tip and pyrolysis front reached the heat flux meter. The duration between t_f and t_p represents the time when the preheating region is exposed to heat (Fig.2.3).

The heat flux measured at t_f and t_p for different heights of samples is listed in Table 3.12. The heat flux corresponding to t_f did not decrease as the length of the burning samples was increased. This was not consistent with the observations of Qian *et al.* (1994) dealing with upward flame spread along vertical corner PMMA walls, of Brehob *et al.* (1998) concerning upward flame spread with external radiation and discussed in Sec. 3.4.2.3 for wall fires on flat surfaces.

Fig.3. 32 - Variation of heat flux measured by heat flux meters at 24, 48 and 86 cm high of the 30, 50 and 100 cm samples.
(⋯▸ corresponds to the time when the flame tips reached the heat flux meters, t_f, and ⟶ indicates when the pyrolysis heights reached the heat flux meters, t_p)

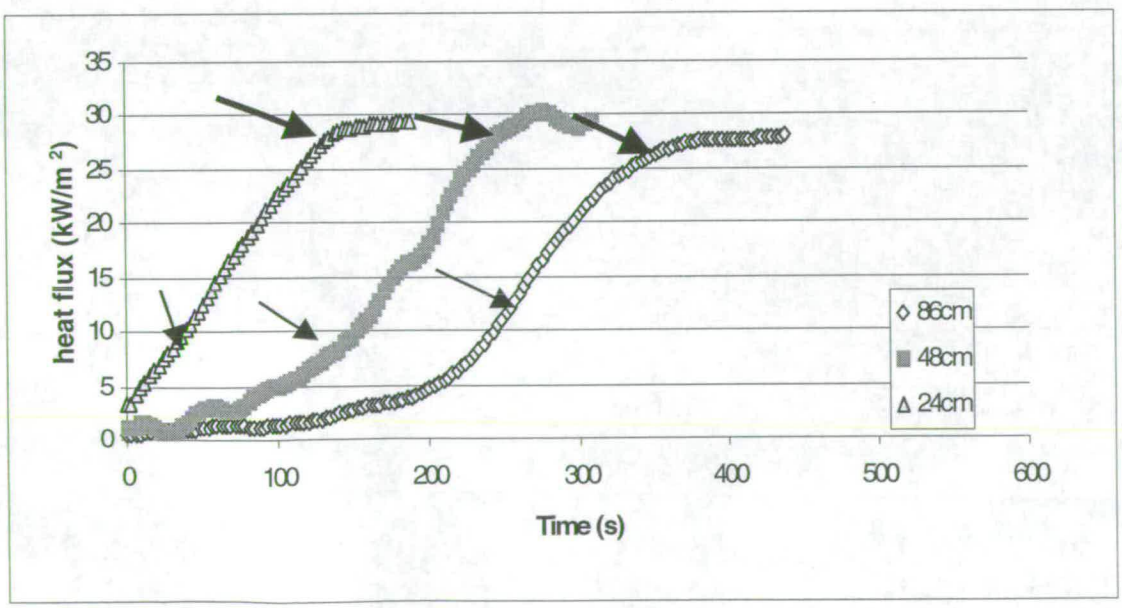

Table 3.12 - The heat flux measured at t_f and t_p with 6 mm thick and 8 cm wide PMMA fires.

height of heat flux meter (cm)	heat flux corresponding to t_f (kW/m^2)	heat flux corresponding to t_p (kW/m^2)
24	9.8	27.5
48	8.4	27.6
86	12.7	26.3

The averaged maximum terminal heat flux was found to be 28.9 ± 1.3 kW/m^2, which is lower than that on flat surfaces (30.6 ± kW/m^2, Sec. 3.4.2.3) in a similar scale (8 cm ignition length). A higher heat flux is expected because of cross-radiation between the two burning surfaces, but in this study, this effect was not significant. The study of Qian *et al.* (1994) with 20 cm ignition width reported the maximum to be 30.5 ± 2.0 kW/m^2. Their heat flux measured for corner/wall fires is not higher than that measured on flat surfaces (Sec.3.4.2.3) either.

Fig.3.33 presents the heat flux against the normalised flame height. In the straight line section of this diagram, the heat flux can be fitted by a power relation with a correlation coefficient of 0.837:

$$\dot{q}'' = 9.12\left(\frac{X}{X_f}\right)^{-2.59} \tag{3.28}$$

This is higher than the data of Qian *et al.* (1995). However, the ignition width was 8 cm in this study and 20 cm in the study of Qian *et al.* (1995).

Fig. 3.33- The heat flux against normalised flame height in the corner tests.

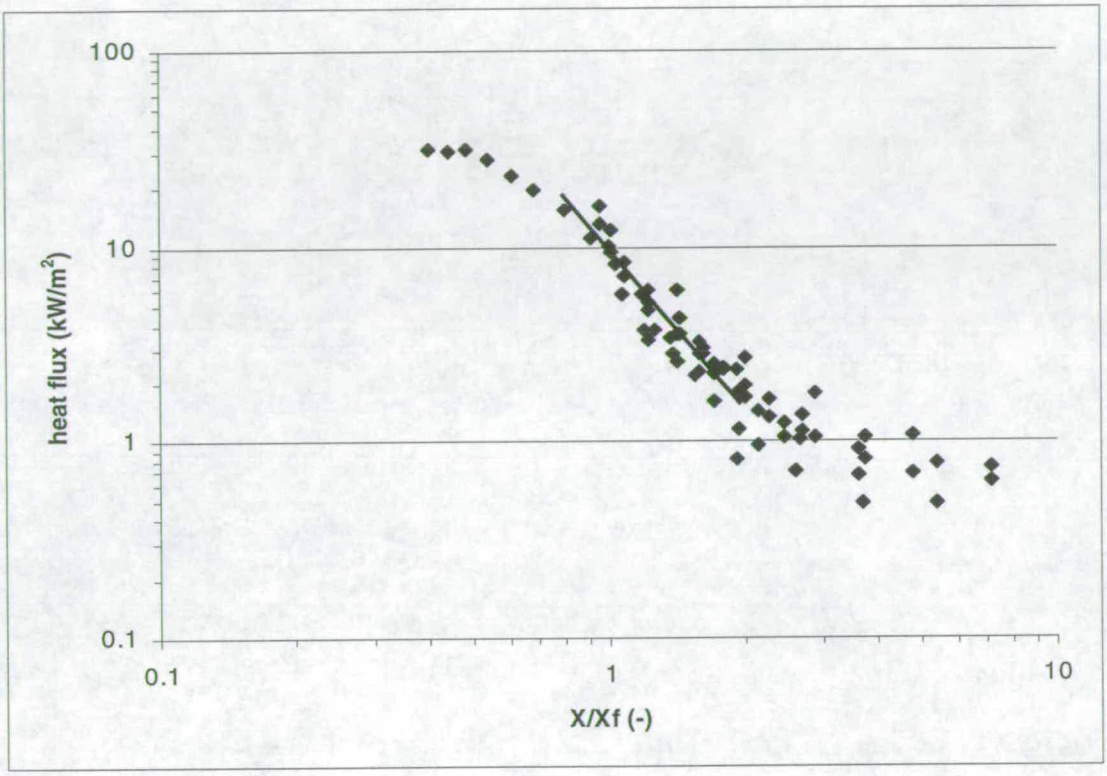

3.7 Wall Fires between Two Parallel Walls

Upward flame spread between two vertical parallel walls is a case which may lead to more rapid fire growth. A fire may start on a wall and grow under the influence of the other wall. If it is combustible, the adjacent wall may ignite as a result of heat transfer from the burning wall (Wang *et al.*, 1999). Experiments were designed to study the early stages of a wall fire under the influence of a parallel inert wall. Measurements made were of the flame height, of heat transfer from the flame to the unburned surface and to the parallel wall and of the flame spread rate. An important variable is the separation between the two walls which is believed to influence the air entrainment into the flame between the two walls.

3.7.1 Experimental Set-up

Two experiments were designed for different purposes. One was for measuring the heat flux and the other one for measuring the heights of the flame tips and pyrolysis fronts. Fig.3.34 shows the experimental set up of the first experiment, consisting of a steel rig and a parallel inert wall. The rig was designed to hold a combustible sample (0.08 m wide with height up to 1 m and thickness up to 25 mm) and a vertical backing plate secured in place so that the sample surface was flush with the rig surface using four clamps at the back of the rig. There was no gap between the walls and the floor. Two incombustible boards (1 m high and 0.4 m wide) were held in the rig to provide an extended plane surface, thus prevent the air being entrained from behind of the burning surfaces. The material used was 6 mm thick PMMA with heights of 0.26, 0.5 and 0.98 m. A Gardon-type total heat flux meter was located at 0.02 m below the top of the samples to measure the heat flux from the flame to the unburned surface.

The parallel inert wall was instrumented with three heat flux meters at heights of 0.15, 0.45 and 0.9 m for the measurements of heat flux from the flame to the opposing wall.

The experimental set up for the second experiment is shown in Fig. 3.35. The same rig holding combustible solids was used. Another rig, which acts as the parallel "wall", was built to allow a 10 cm wide slab of fire resistant glass to be located vertically along the centreline of the "wall" through which the visual flame heights

can be recorded by a camcorder. Two inert boards were also provided to form an extended plane surface, thus prevent the air being entrained from behind of the "parallel wall". An infra-red camera was used to measure the temperature of the burning surfaces, from which the position of pyrolysis front can be deduced by tracing the 360 ^{0}C isotherms.

Both experiments started with the ignition of a 1 cm high zone on the bottom of the solids by a butane/propane fuelled torch and ended with extinguishing when the pyrolysis fronts reached the top of the solids. The separation between the two "walls" was set to be 5, 15, 25 and 35 cm. The results were compared with those from a single burning wall (infinite separation).

Fig.3.34 - The set up of the heat flux experiment

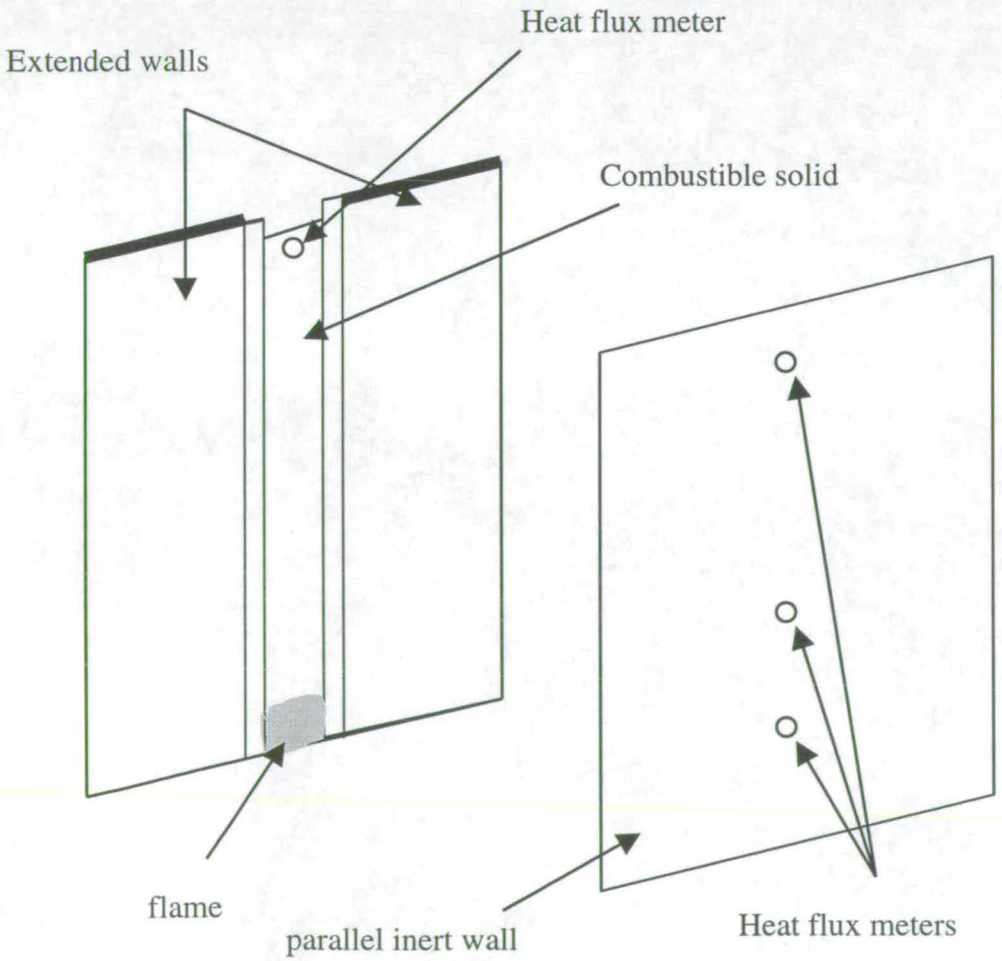

Fig.3.35 - The set up of the flame height/pyrolysis height experiment.

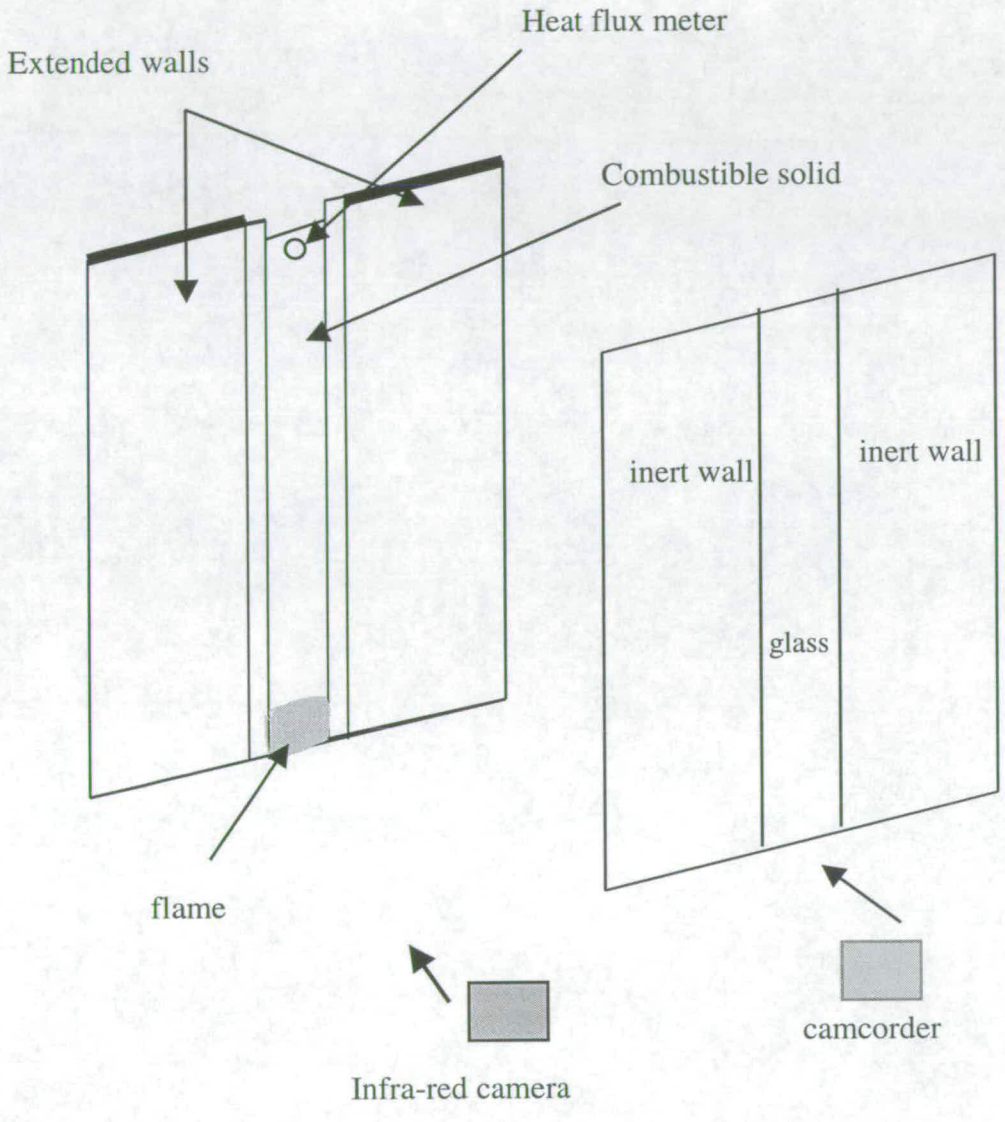

3.7.2 Experimental Results

Flame height correlation

All the experimental data are presented in Appendix A-5. Fig. 3.36 shows the dependence of the flame height X_f on the pyrolysis height X_p for different separations (5, 15, 25, 35 and "infinite").

From Fig.3.36 (a) and (b), it is seen that for separation a = infinite, the flames were the tallest and for separation a = 5 cm, the flames were the shortest. However, the difference between the flame height correlations for the different separations is not significant, especially for the turbulent flame region (X_p>20 cm from the experimental observation). The weaker influence in the laminar flame regions was expected because the confinement was relatively low compared with the turbulent flame regions. The individual correlation for the turbulent flame region for each separation is as follows:

For separation a = infinite, with $r^2 = 0.979$

$$X_f = 1.33 X_p^{0.69} \tag{3.29}$$

For separation a = 5 cm, with $r^2 = 0.964$

$$X_f = 1.18 X_p^{0.59} \tag{3.30}$$

For separation a = 15 cm, with $r^2 = 0.990$

$$X_f = 1.29 X_p^{0.69} \tag{3.31}$$

For separation a = 25 cm, with $r^2 = 0.973$

$$X_f = 1.20 X_p^{0.67} \tag{3.32}$$

For separation a = 35 cm, with $r^2 = 0.976$

$$X_f = 1.24 X_p^{0.65} \tag{3.33}$$

Fig. 3.36 - The dependence of the flame height X_f on the pyrolysis height X_p for different separations (5, 15, 25, 35 and infinite). (Fig.3.36(a) in normal scale; Fig.3.36(b) in logarithmic scale)

(a)

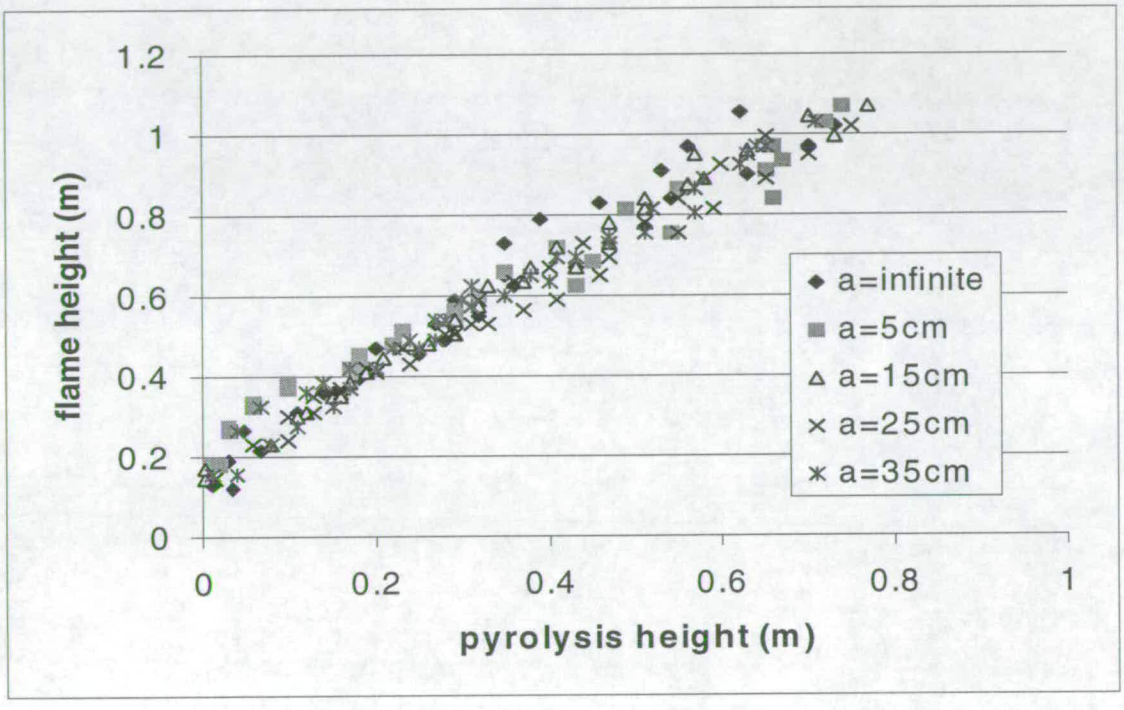

(b)

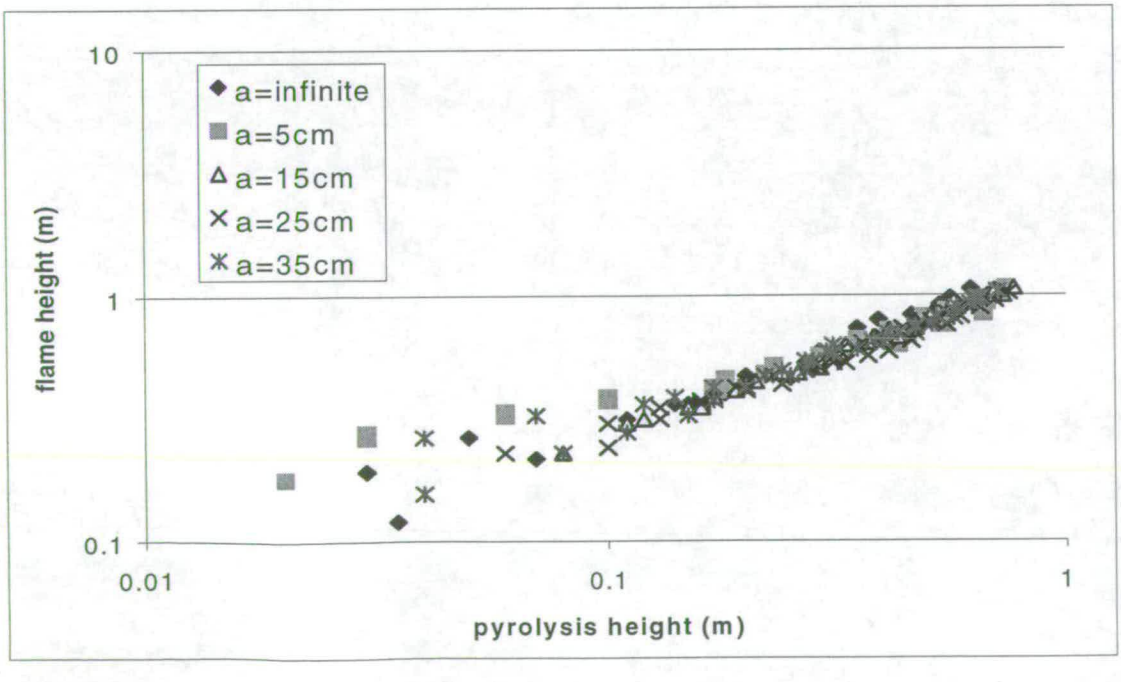

The heat flux to the unburned surfaces

Fig.3.37 presents the measurements of the heat flux from the flame to the unburned surfaces for different separations against the position normalised by the flame height (X/X_f) in the logarithmic scale. It is seen that there exists a uniform heat flux region for X/X_f <c.0.8. The heat flux in this region was between 30 to 40 kW/m^2. There was no significant difference which could be related to the different separations in this region.

A linear relation (in the logarithmic scale) appeared for c.0.8 < X/X_f >c.1.5. It is seen that the heat fluxes decreased when the separation was from 5 to 15 cm and increased when the separation was from 15 to 35 cm and then infinite. However, the effect of the separation on the heat flux distribution was not very significant. This is consistent with the observations of Foley and Drysdale (1995) and Wang *et al.* (1999), showing that the separation does have some but not strong influence on the heat fluxes generated at the wall although Foley and Drysdale (1995) used propane line fires while Wang *et al.* (1999) and the present work used PMMA. In the study of Foley and Drysdale (1995), the heat flux depended on (separation)$^{-1.05}$ for the separation of 6 and 10 cm. However, the experimental results in this study demonstrate that the heat flux was not directly proportional to the separation. The correlation for each separation (for c.0.8 < X/X_f >c.1.5) is as follows:

For separation a = infinite, with $r^2 = 0.930$

$$\dot{q}'' = 10.21 \left(\frac{X}{X_f}\right)^{-3.11} \tag{3.34}$$

For separation a = 5 cm, with $r^2 = 0.925$

$$\dot{q}'' = 9.13 \left(\frac{X}{X_f}\right)^{-3.89} \tag{3.35}$$

For separation a = 15 cm, with $r^2 = 0.926$

$$\dot{q}'' = 6.06 \left(\frac{X}{X_f} \right)^{-3.76} \tag{3.36}$$

For separation a = 25 cm, with $r^2 = 0.911$

$$\dot{q}'' = 8.17 \left(\frac{X}{X_f} \right)^{-3.51} \tag{3.37}$$

For separation a = 35 cm, with $r^2 = 0.890$

$$\dot{q}'' = 12.35 \left(\frac{X}{X_f} \right)^{-4.32} \tag{3.38}$$

For X/X_f >c.1.5, another straight line region is seen. The decrease of the heat flux (against X/X_f) was not as dramatic as for c.0.8 < X/X_f >c.1.5.

Fig.3.37 - The measurements of the heat flux from the flame to the unburned surfaces for different separations against the position normalised by the flame height (X/X_f) in the logarithmic scale.

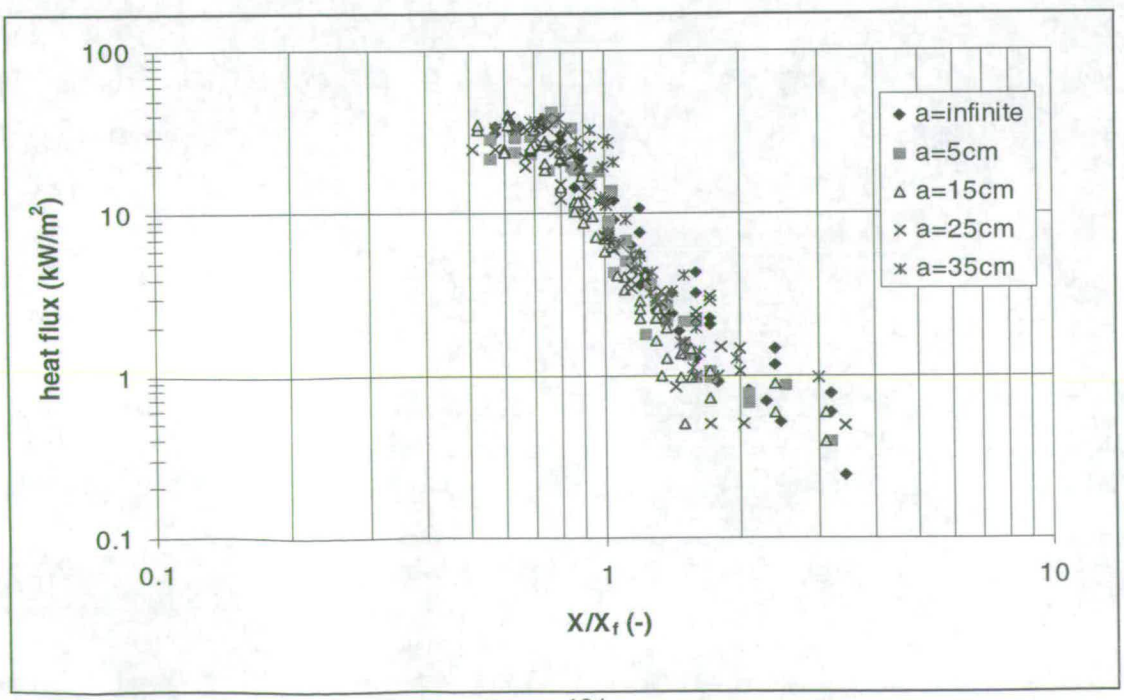

Flame spread rate

Fig.3.38 shows the flame spread rate for different separations on the 1m high, 0.08 m wide and 6 mm thick PMMA samples. For the initial 8 minutes, there was almost no difference, while after 8 minutes, the flames with an inert parallel wall 5 cm away spread most rapidly. In addition, there was still almost no difference of the flame spread rate between the other flames (for a= infinite, 15, 25 and 35 cm).

The slightly higher flame spread rate associated with the 5 cm separation was not accompanied by either the flame heights or the heat fluxes from the flames to the unburned surfaces, the two parameters determining the flame spread rate. The flames associated with the 5 cm separation did not appear to be taller and did not produce higher heat fluxes than the flames associated with other separations.

Fig.3.38 - The flame spread rate for different separations.

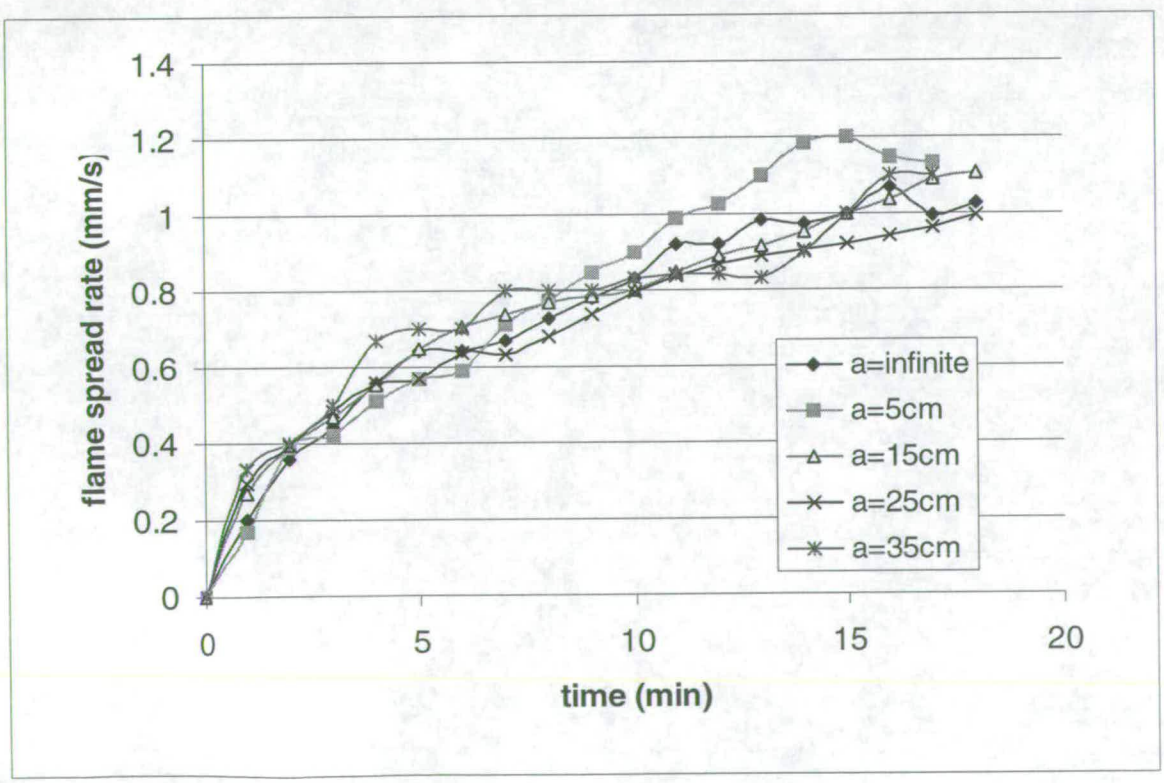

The heat flux to the opposing inert wall

The heat fluxes from the wall fires to the opposing inert wall at different separations were measured. The separation between the burning wall and the inert wall was 5, 15, 25 and 35 cm. Three heat flux meters were located at heights X' of 15, 45 and 90 cm along the centreline of the inert wall.

Fig.3.39 (a)-(d) show the heat flux distribution for these four separations measured at different values of X' against the ratio of the height of the heat flux meter X' and the flame heights (X'/X_f). It is seen that the heat flux measured at any heat flux meter located at X' increased less and less when the flame grew taller (the X'/X_f decreases). This is particularly significant for X'=15 cm and X'/X_f <0.2. This is expected because the radiation from the "new pyrolysing zone" was low due to a low configuration factor.

It is seen that the heat flux generated on the inert wall decreased when the (X'/X_f) was larger and increased when the separation a was shorter. The latter observation was consistent with that by Williamson *et al.* (1991), finding that the distance between the fire and the wall (heat receiver) affected the heat flux generated particularly significantly. However, no clear correlation was found between the heat flux and the parameters X', X_f and a.

For the 5 cm separation, when the flame height was 90 cm, the heat fluxes generated on the inert wall at X' = 90 cm reached c.8 kW/m^2 which was closer to those measured to the unburned surfaces (c.8 kW/m^2). A photo taken at that moment showed that the flame tips actually filled the gap between the two walls. The heat flux from the flame to the burning wall and to the opposing inert wall were then identical (only at X'=90 cm).

Fig.3.39 (a)-(d) - The heat flux distribution for four separations (5, 15, 25 and 35 cm) measured at different *X'* (15, 45 and 90 cm) against the ratio of the height of the measuring points *X'* and the flame heights (X'/X_f).

(a)

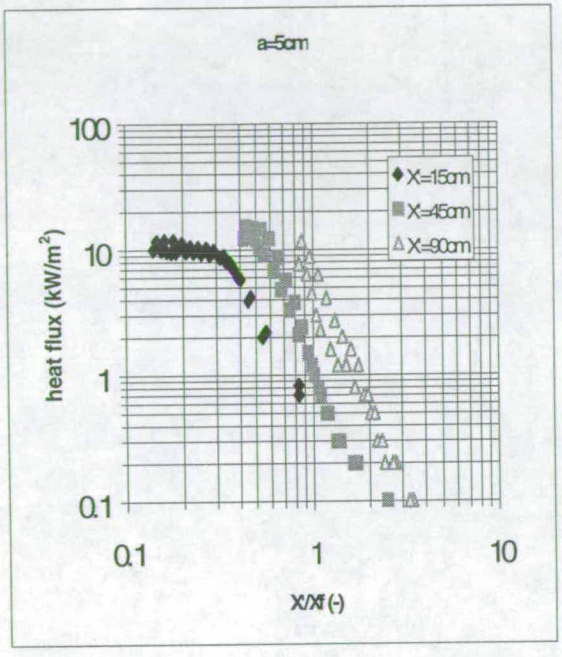

(b)

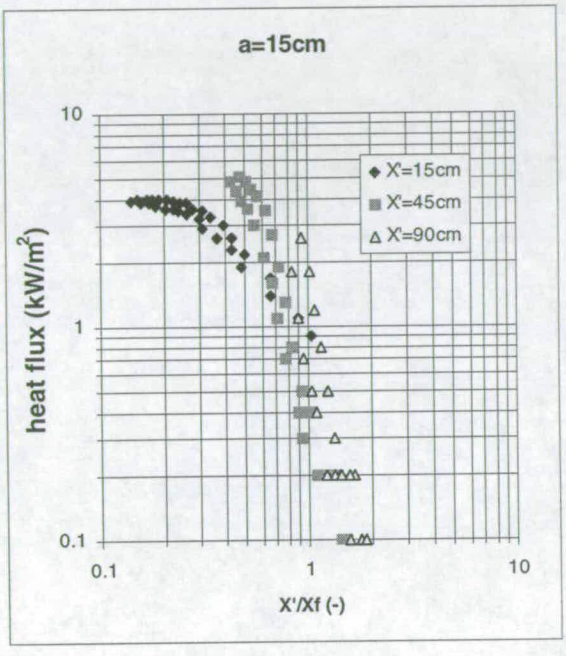

(c)

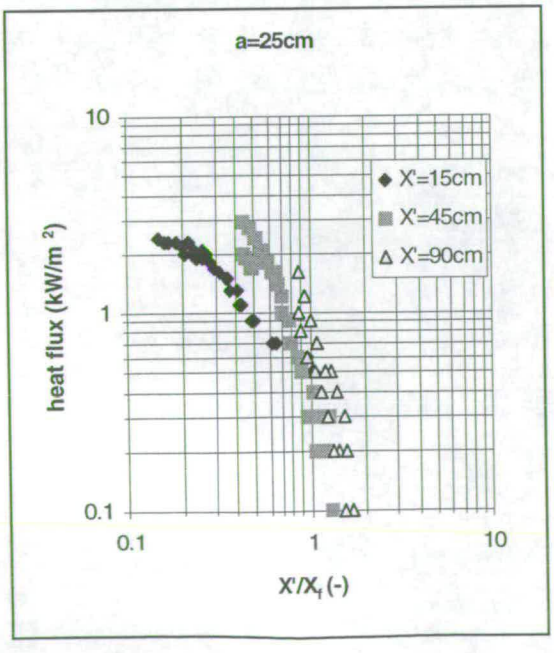

(d)

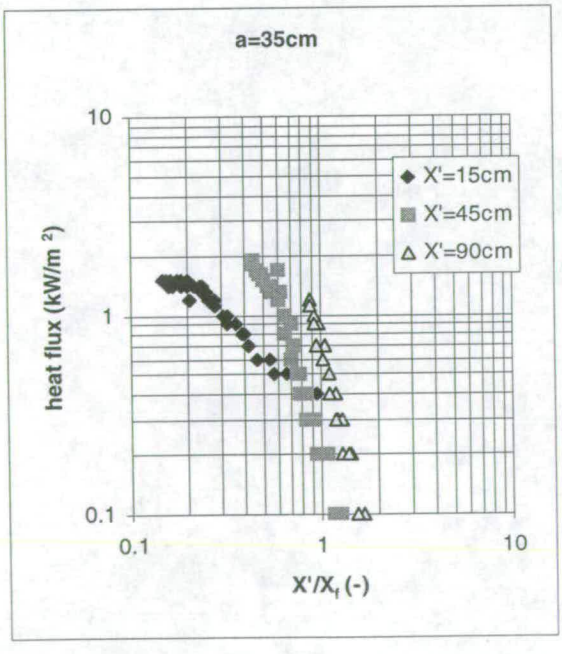

By using the configuration factor, the radiation emitted to the opposing inert wall can be estimated. The radiation is assumed to be contributed primarily from the pyrolysing zone because of a high emissivity. The surface temperature is estimated to be 350^0C and emissivity ε to be 0.85. Exemplifying the case (shown in Fig.3.40) of a 30 cm tall and 8 cm wide pyrolysing zone, the radiation to the point located 15 cm high (along the centreline) on a inert wall with separation = 5 cm is

$$\dot{q}_r'' = \phi\varepsilon\sigma T^4 = 0.6 \times 0.8 \times 5.67 \times 10^{-5} \times (400+273)^4 = 5.58(kW/m^2) \qquad (3.39)$$

where $\dot{q}_r''$ is the radiation from the pyrolysing zone, ϕ is the configuration factor and σ is the Stefan-Boltzmann constant (=5.67 10^{-5} kW/m^{2}K^4). The estimated radiation 5.58 kW/m^2 is higher than the measured total heat flux (=c.3 kW/m^2) but no account has been taken of the cooling effect of the induced flow of air.

Fig. 3.40 – The dimension of the case studied for the estimation of radiation by using the configuration factor.

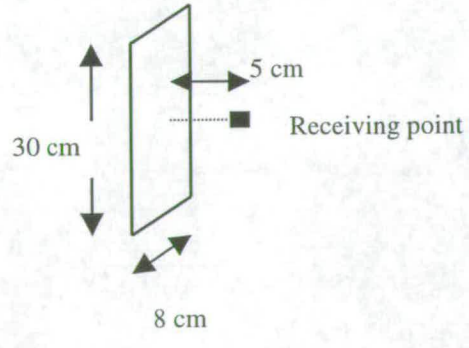

3.8 Conclusion

In this chapter, only the experimental results were presented. The comparison with other studies and among these geometries (wall fires on flat surfaces, in a corner, between two parallel walls) will be made in Chapter 5.

Chapter 4

Computer Modelling

4.1 Introduction

Mathematical modelling of flame spread phenomena has become an activity of increasing importance within the fire safety engineering community. This is due primarily to the growing awareness of the need for quantitative fire risk assessment, but also because such modelling has been made more practicable since the development of some small scale apparatus (reviewed in Sec. 2.4.5).

The Cone Calorimeter is the most commonly used apparatus which is capable of providing quantitative data relevant to the response of combustible materials under fire conditions (Sec. 1.3.1 and 3.2). However, there is still considerable debate on how it can best be used. Data have been used to model the response of wall lining materials in the Nordtest Apparatus (1986), and to predict the rate of upward flame spread on vertical surfaces. However, insufficient attention seems to have been paid to the relevance of the test scenario of these models. The Cone Calorimeter allows the time to ignition and the rate of heat release to be measured under a range of heat fluxes. Several suggestions have been made about how such data may be used for materials selection, but none has yet been accepted. One school of thought is that the data cannot be used simply to provide arbitrary ranking orders, but should be used in conjunction with flame spread models to assess the likely fire growth rate that could occur in the end-use scenario. The existing upward flame spread models provide a starting point for the development of a proper "engineering tool".

The modelling work of the upward flame spread on vertical flat surfaces has been reviewed in Sec. 2.4.5. In this chapter, Grant and Drysdale's model (1995) will be discussed because this model uses data from the Cone Calorimeter and includes burnout. Afterwards, this model will behave as a base to access the modelling work for the cases of in a corner and between two parallel walls (Chapter 5).

4.2 Grant and Drysdale's Model for Upward Flame Spread on Vertical Flat Surfaces

Based on the modelling work of Saito *et al.* (1985) and Karlsson (1993), Grant and Drysdale (1995) developed a model not only to include burnout but also to allow the heat release rate data from the Cone Calorimeter to be used directly as input, without using the approximate form as given in Equation 2.32. This resolves the problem which arises if the RHR can not be approximated by Equation 2.32 which assumed that the RHR reaches its maximum value as soon as the sample is ignited, then decreases with a decay coefficient λ (Sec. 2.4.5).

The development of Grant and Drysdale's model has been reviewed in Sec. 2.4.5. Before burnout occurs, the flame spread rate $V_p(t)$ can be expressed as an integral equation of the Volterra type (second kind) (Equation 2.31) and can be solved numerically.

$$V_p(t)=\frac{1}{\tau}\left[K\left\{X_{po}\dot{Q}''(t)+\int_0^t \dot{Q}''(t-t_p)V_p(t_p)dt_p\right\}^n-\left(X_{po}+\int_0^t V_p(t_p)dt_p\right)\right] \qquad (2.31)$$

but after burnout occurs, the velocity $V_p(t)$ becomes,

$$V_p(t)=\frac{1}{\tau}\left[K\left\{\int_{t-t_b}^t \dot{Q}''(t-t_p)V_p(t_p)dt_p\right\}^n-\left(\int_{t-t_b}^t V_p(t_p)dt_p\right)\right] \qquad (2.33)$$

where τ is the time to ignition, t_b is the burnout time, $\dot{Q}$" is the heat release rate of a burning material (carried out by the Cone Calorimeter), X_{po} is the initial height of the pyrolysis zone, n and K are constants.

To solve Equation 2.31 and 2.33, five pieces of information are needed:

(1) The constants n and K of a flame height correlation (see Equation 2.9).

(2) $\dot{Q}$" (kW/m^2)

(3) τ (s)

(4) t_b (s)

(5) X_{po} depending on the experimental set ups

In Grant and Drysdale's model, the values of n and K were taken as 2/3 and 0.0666, following the flame height correlation of Tu and Quintiere (1991). Values of $\dot{Q}''$, τ and t_b were provided by Cone Calorimeter tests with a heat flux 20 kW/m^2 (for cardboard). The X_{po} was set up to be 0.02m. Very satisfactory results were obtained for the rate of upward flame spread on vertical samples of cardboard.

4.2.1 The Flame Height Correlation

The flame height of wall fires on a flat surface has been studied experimentally and theoretically, which has been investigated in Sec. 2.4.3. One can see that all these correlations are in the form of Equation 2.9, however, difference exists between the values of the n and K.

$$X_f = K\dot{Q}''^n \tag{2.9}$$

The sensitivity of the flame height correlation to the modelling result is analysed associated with the data of $\dot{Q}''$ of 6 mm thick PMMA under the irradiance of 15 kW/m^2 (the RHR following the standard procedure in Fig. 3.1). The value of τ was 480 s, t_b was 802 s and X_{po} was set to be 0.002 m. The influence of n and K is examined separately.

4.2.1.1 The influence of power "*n*"

With the value of K set as 0.066, the values of n examined are listed in Table 4.1.

Table 4.1 – Values of *n* examined (with *K*=0.066).

	n	Steady state flame spread rate (mm/s)
Test 1	2/3	4.7
Test 2	0.8	>200
Test 3	1	Steady state not reached

The modelling results are shown in Fig. 4.1. The influence of the value of n is very significant. Numerically, for values of n greater than unity, the prediction of flame spread rate will increase exponentially and never reaches a steady state. However, even for n = 2/3 and 0.8, the influence of the value of n is also very significant, giving a steady state flame spread rates of 4.7 mm/s for n = 2/3 and over 200 mm/s for n = 0.8.

Fig. 4.1 – The flame spread rate prediction of Grant and Drysdale's model applying different values of n of the flame height correlation. In Fig.4.1 (a), the predictions for n = 2/3, 0.8 and 1 are presented while Fig.4.1 (b) only presents for n = 2/3 and 0.8 for clarity.

(a)

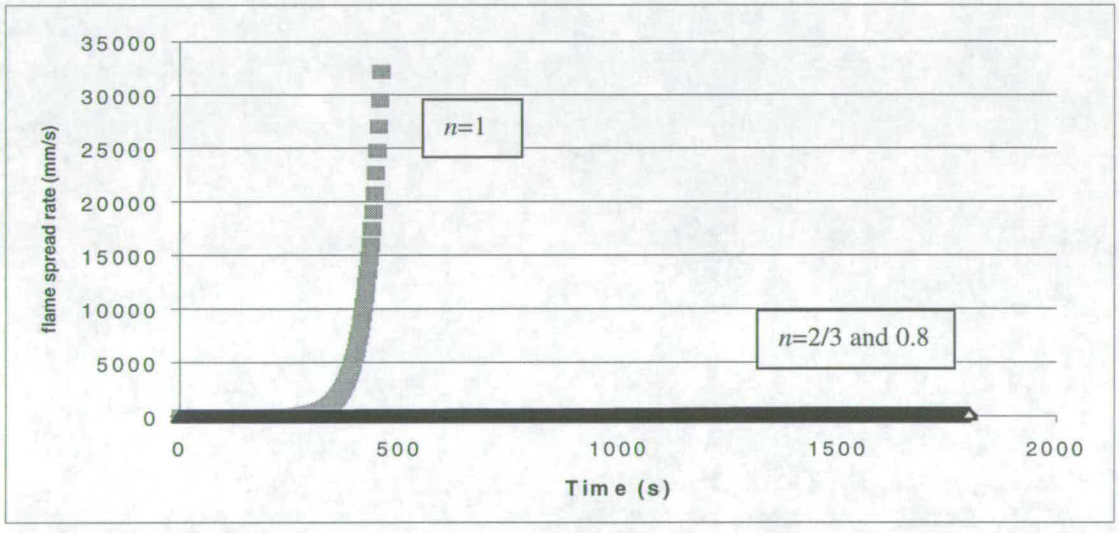

(b)

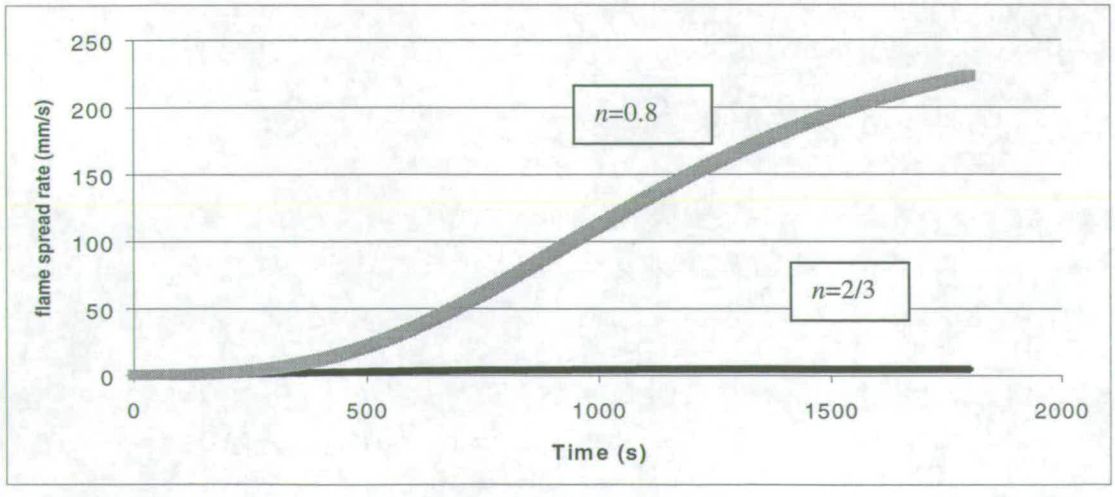

4.2.1.2 The influence of the constant "*K*"

With the value of n set to be 2/3, the values of K examined are listed in Table 4.2. The steady-state flame spread rates for values of K = 0.044, 0.055 and 0.066 are 1.37, 2.67 and 4.73 mm/s. It is seen that for the value of K increasing from 0.044 to 0.066, which is 50% greater, the steady-state spread rate is 245% greater. The influence of the value of K is also significant.

From Sec. 4.2.1.1 and 4.2.1.2, it can be seen that the determination of the flame height correlation is very important.

Table 4.2 – The values of *K* examined.

	K	Steady state flame spread rate (mm/s)
Test 1	0.044	1.37
Test 2	0.055	2.67
Test 3	0.066	4.73

Fig.4.2 – The influence of the value of *K* of the flame height correlation on the modelling prediction.

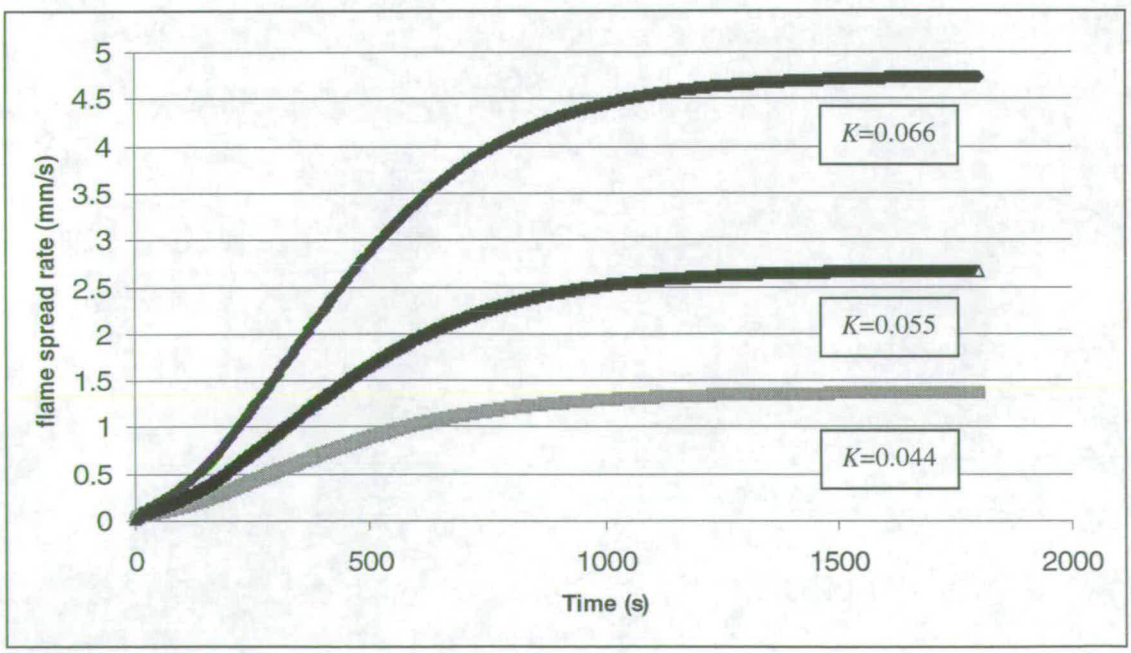

4.2.2 The Role of the Cone Calorimeter

The Cone Calorimeter is capable of providing the data of $\dot{Q}''$, τ and t_b under a selected irradiance level. During the tests, the vertical sample faces the cone heater, simulating the fire behaviour of the surface exposed to radiant heat from a nearby fire. The selected irradiance in the modelling work is the averaged heat flux which represents the assumed constant heat flux to the unburned surface in the preheating zone (Fig.2.3).

4.2.2.1 The Representative Heat Flux

The representative heat fluxes used in previous upward flame spread models have been summarised in Table 2.2 (Sec. 2.4.4.1), ranging from 20 to 30 kW/m^2. From the experimental investigation in Chapter 3, the averaged heat flux was determined to be around 15 kW/m^2. The influence of the representative heat flux is examined by applying the data of $\dot{Q}''$ obtained with different irradiances listed in Table 4.3. The values of n and K used in the model are 2/3 and 0.066.

The modelling prediction applying the three irradiances (15, 20 and 25 kW/m^2) are shown in Fig. 4.3. As to be expected, the larger the irradiance is applied, which represents the heating effect in upward flame spread, the higher the flame spread rate is produced. At 1800s, the flame spread rate is predicted to be 4.7, 24.8 and 56.8 mm/s applying the irradiances of 15, 20 and 25 kW/m^2 with the 6 mm thick PMMA samples.

Table 4.3 – The effect of changing the irradiance value.

	Irradiance (kW/m^2)	flame spread rate at 1800 s (mm/s)
Test 1	15	4.7
Test 2	20	24.8
Test 3	25	56.8

Fig. 4.3 - The modelling prediction applying three irradiances (I= 15, 20 and 25 kW/m^2).

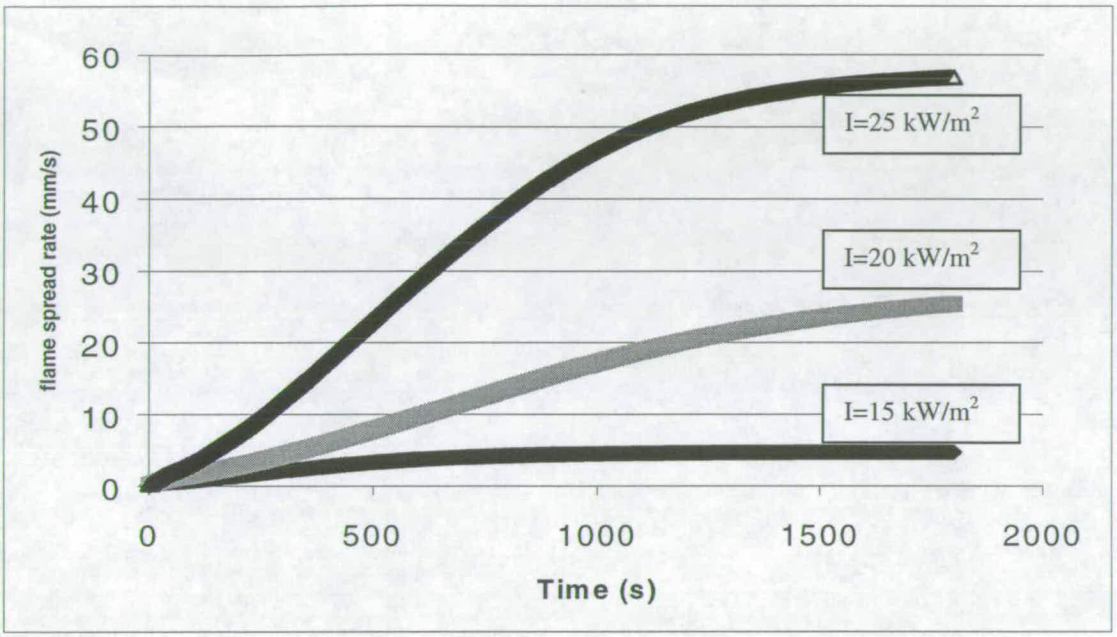

4.2.2.2 The Role of the Cone Heater

In the upward flame spread modelling work, the cone heater in the Cone Calorimeter simulates the heating effect from the flame to the unburned surfaces. Therefore, the irradiance of the cone heater is determined to be the average heat flux in the preheating region. The schematic of the roles of heat feedback from the flame and the cone heater is presented in Fig.4.4.

Before ignition, the sample is exposed to the heater, simulating the preheating behaviour of the unburned region ahead of the pyrolysis front. However, once burning, the process is self-sustaining and the rate of burning (hence the RHR) is controlled by heat transfer from the flames at the burning surface. No additional heat input is present. The flame spread model still requires data on the time to ignition under an imposed heat flux which models that from the flame in the preheating region (X_f - X_p), but after ignition occurs the RHR in the absence of an imposed heat flux should be used.

To test this hypothesis, appropriate data have to be obtained using the Cone Calorimeter in an unconventional manner. The ignition delay is first determined, but then the cone heater is moved immediately after ignition has occurred, leaving the sample to burn without any supplementary heating. The heater is required only to simulate the heat flux from the flame to the surface in the region (X_f - X_p).

Fig.4.4 - The schematic of the roles of heat feedback from the flame and the cone heater.

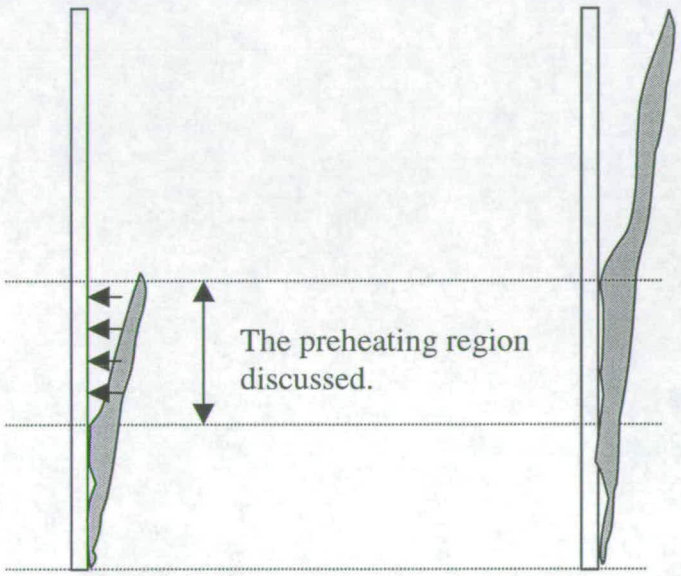

(a) the unburned region before ignition (b) the unburned region after ignition

(a') the sample before ignition (b') the sample after ignition

The Modified Procedure using the Cone Calorimeter

The relevant data were obtained by moving the cone heater away from the sample immediately after ignition. Ideally, it should be removed completely, but this is not possible within the standard equipment. Instead, it was moved upwards by the manually operated screw mechanism into a position in which the lowest edge of the heater was 2.5 cm above the top edge of the sample. This took about 10 s. In separate experiments the residual radiant flux to the surface was found to be 0.3~0.6 kW/m^2 (Table 3.2, Sec.3.2.2) when the power of the heater was set to give 30 kW/m^2. To a first approximation, it is assumed that the "residual" radiation can be neglected, particularly when the heater is operating at a lower power (15 kW/m^2 at the sample surface).

Typical data on the transient rate of heat release of PMMA samples exposed to 15 kW/m^2 in the standard and "modified" tests have been shown in Fig.3.1 and discussed in Sec.3.2.3. The comparison between the experimental results and the flame spread rates predicted from Equations 2.31 and 2.33 are shown in Fig 4.5. It is clear that the result obtained from the model with the RHR data from the modified procedure is in much better agreement with experiment. The early rate of spread appears to be underpredicted, but it is likely that the additional heat provided by the ignition source would affect the early stages of flame spread. This would give a higher initial RHR at the beginning of each experiment.

Given this result, it is surprising that Grant and Drysdale (1995) obtained such good agreement for upward flame spread on cardboard when the standard procedure was used to obtain RHR data in the Cone Calorimeter. Using the same model, Anderson and McKeever (1996) found good agreement for hardboard, plywood and wallpaper-covered wood surfaces, albeit with a much higher irradiance from the cone heater (35 kW/m^2). The reason may lie in the sensitivity of the rate of heat release to external radiation for these materials.

Fig. 4.5 - The comparison of the experimental measurement of the flame spread rate of 6mm thick PMMA slabs and the prediction from Grant and Drysdale's model with the standard and non-standard test procedures.

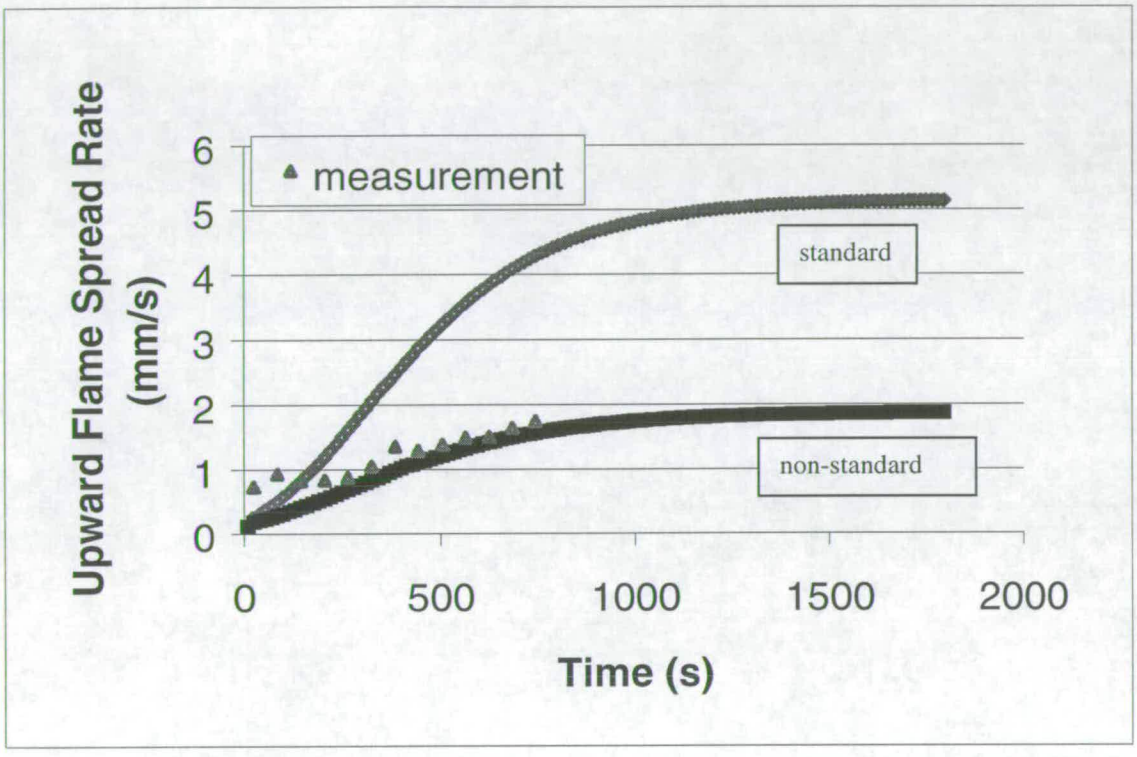

Brehob and Kulkarni observed that mass loss rates from different materials in the vertical orientation exhibit different sensitivities to external radiation when burning (1989). Assuming that the heat of combustion remains constant during the burning process, mass loss rate is directly proportional to the rate of heat release (Equation 4.1) and similar sensitivities would be expected from measurements made in the Cone Calorimeter.

$$RHR = \dot{m}\ \Delta H_c \tag{4.1}$$

For 6mm thick PMMA (see Fig.3.1), the rates of heat release differ markedly in the presence and absence of supporting radiation. Similar results for 2.5mm thick cardboard are shown in Fig.3.2: there is no significant difference in the RHR curves with and without an imposed heat flux of 15 kW/m^2. The reason has been discussed

in Sec.3.1. As a result, there is no difference in the predicted rates of upward flame spread on cardboard (Fig.4.6).

Fig.4.6 - Upward flame spread rate of 2.5mm thick cardboard predicted by Grant and Drysdale's model with the standard and non-standard Cone Calorimeter test procedures.
(The two predictions using the standard and non-standard procedures overlap.)

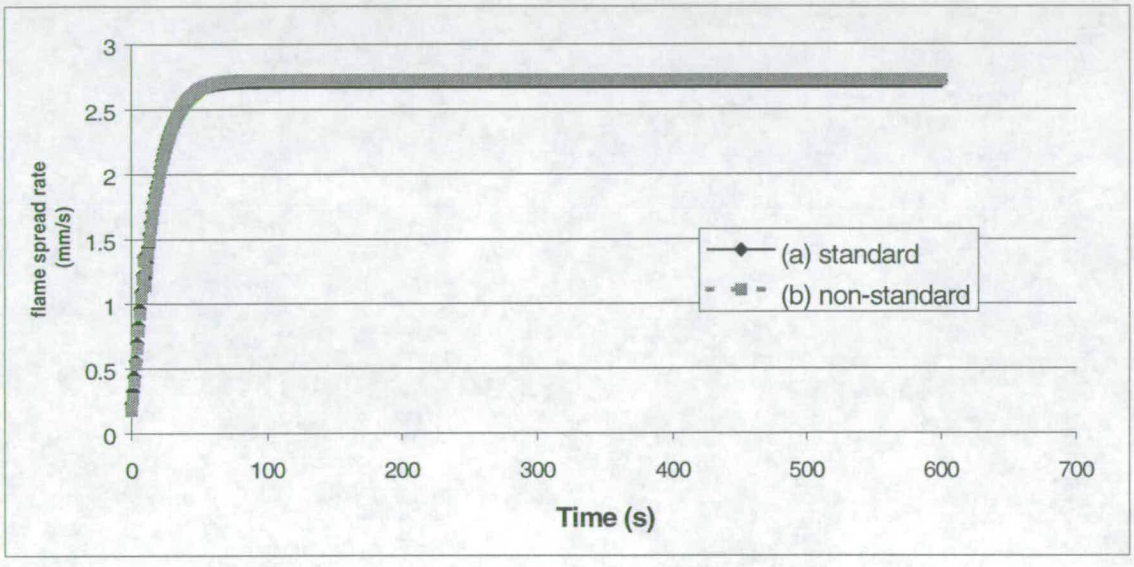

4.2.2.3 The data of $\dot{Q}''$, τ and t_b

After the irradiance has been determined, the value of $\dot{Q}''$ can be measured directly in the Cone Calorimeter using the non-standard test procedure, while the values of τ and t_b are determined by the observer. (The value of τ is determined by the presence of a sustained flame and the value of t_b by the presence of a burnout region on the sample surface.)

4.2.3 The initial ignition zone X_{po}

The initial ignition zone X_{po} depends on the experimental set up. Its effect on the modelling work can be examined numerically. Table 4.4 lists the heights of the

ignition zone examined on 6 mm thick PMMA slabs. Fig. 4.7 shows the prediction results with values of n and K to be 2/3 and 0.066 and applying the standard test procedure.

From Fig. 4.7, it can be seen that for these two heights of ignition zone, only the initial flame spread rate is influenced and afterwards, reaches almost identical steady state flame spread rate (4.72 mm/s). The results are expected.

Table 4.4 – The X_{po} examined.

	X_{po} (m)	Steady state flame spread rate (mm/s)
Test 1	0.002	4.72
Test 2	0.02	4.72

Fig. 4.7 – The modelling predictions applying two different heights of the initial ignition zone.

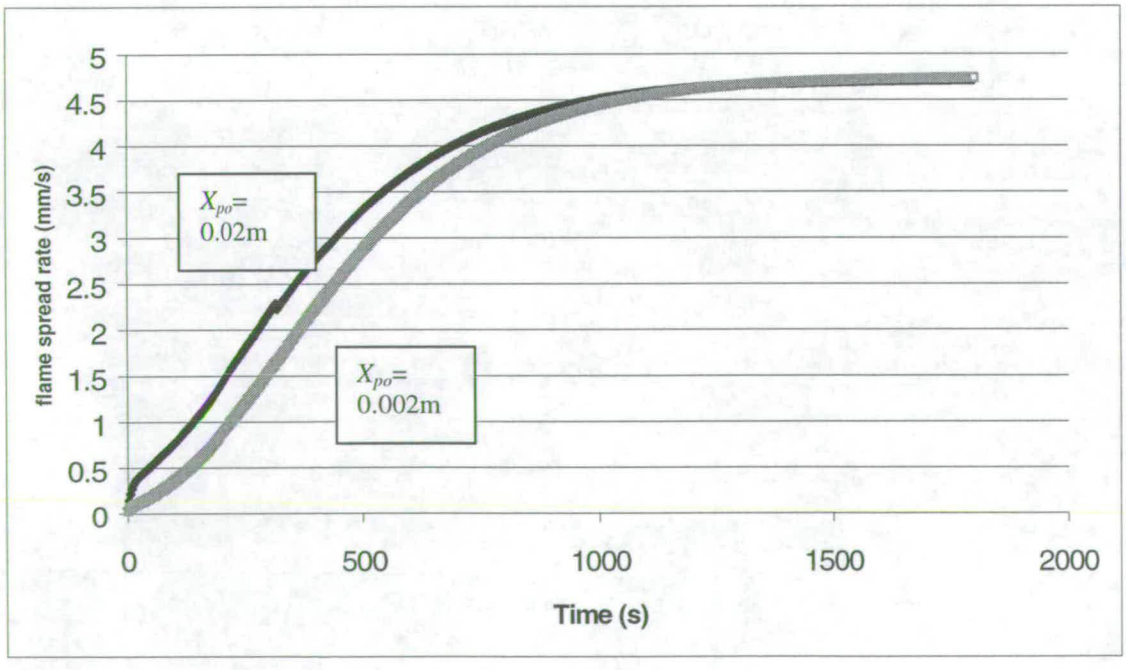

4.2.4 The Modelling Work Considering the Two Distinct Regions of the Flame Height Correlations

The flame height correlation of a wall fire has been reviewed in Chapter 2 and determined experimentally in Chapter 3 (using PMMA slabs of different aspect ratios and gas burners). The results clearly show two distinct regions for values of $\dot{Q}'$ greater than and less than 20 kW/m (The results are summarised in Fig. 5.4, Sec. 5.3.2). For $\dot{Q}' < 20$ kW/m, the value of n (Equation 2.9) is approximately 1, while for $\dot{Q}' > 20$ kW/m it is c.2/3.

Modelling work in earlier studies (Sec. 2.4.5) and in the previous sections of this chapter apply the flame height correlation for $\dot{Q}' > 20$ kW/m for the entire range of values of $\dot{Q}'$, ignoring the different correlation for $\dot{Q}' < 20$ kW/m.

The flame height correlations carried out for $\dot{Q}' < 20$ kW/m are considered using Equations 3.5 and 3.7. These two equations were carried out for PMMA wall fires with $\dot{Q}' < 30$ kW/m and represent the two extreme cases producing the tallest and shortest flames (Case B and Case D) among the four different lower edge configurations studied in Section 3.3.2. With Case B, no floor and no protection of the bottom edge were present, while with Case D the burning wall was with an extended plate.

For Case B,

$$X_f = 0.018\dot{Q}'^{1.00} \tag{3.5}$$

For Case D,

$$X_f = 0.011\dot{Q}'^{1.25} \tag{3.7}$$

Fig. 4.8 shows the predictions for the early stages of flame spread when $\dot{Q}' < 20$ kW/m, applying the flame height correlations of Case B and Case D (Equation 3.5 and 3.7). The RHR curve used for this modelling work was from the Cone Calorimeter for 6 mm thick PMMA under 15 kW/m^2 irradiance applying the non-standard test procedure. The prediction using Tu and Quintiere's correlation (1991) (for c.15 kW/m $< \dot{Q}' <$ c.200 kW/m) is included for comparison, which gives the values of n and K (Equation 2.9) to be 2/3 and 0.066. Fig. 4.5 has shown a good agreement between the prediction applying Tu and Quintiere's correlation (1991) and experimental data.

It is seen that the predictions of flame spread rate obtained by applying Equation 3.5 and 3.7 (Case B and D) are much lower in the early stages than when Tu and Quintiere's correlation (1991) is applied. It is expected that the flame spread rate prediction applying Equation 3.5 and 3.7 will be higher than that using Tu and Quintiere's correlation after a certain time because the power n in Equation 3.5 and 3.7 is ≥ 1, which will predict an exponential increase (see Fig.4.1). Logically, Equation 3.5 or 3.7 should be adopted for $\dot{Q}' < 20$ kW/m and the model run with this correlation until $\dot{Q}' = 20$ kW/m. Then Tu and Quintiere's correlation would be applied for $\dot{Q}' > 20$ kW/m. Grant and Drysdale's model needs to be developed to incorporate the flame height correlations for different values of $\dot{Q}'$. Figure 4.8 shows clearly that applying Tu and Quintiere's correlations (1991) for values of $\dot{Q}' < 20$ kW/m actually overestimates the flame spread rate in the early stage.

The predictions of flame spread rate obtained by applying Equation 3.5 and 3.7 (Case B and D) are also much lower than the experimental data shown in Fig.4.5. However, it has to be noticed that the initial *measured* rate of spread (Fig. 4.5) is high because of a strong initial heating by a blow torch. In a real fire, ignition source often continues for some time after the combustible material ignites. More research is needed to examine the ignition process, which can provide more realistic information for its modelling work.

The two discontinuities which appeared at 423 s with the predictions for Case B and D are because burnout of the lowest section of the sample occurred at that moment, which results in a sudden drop of the pyrolysis area and of the flame spread rate prediction. This is a numerical problem. However, the initial peak at about 10 s and the subsequent fall in the predicted flame spread rate are a result of the non-standard Cone Calorimeter test procedure. Immediately after ignition, the cone heater is moved away and the imposed heat flux falls from 15 kW/m^2 to almost zero. The decrease can be explained by a slight cooling of the surface until the flame becomes established at the surface (see the curve of 15 kW/m^2 irradiance and non-standard test procedure in Fig.3.1).

Fig. 4.8 - The modelling predictions applying the flame height correlations of Case B and Case D (Equation 3.5 and 3.7) and Tu and Quintiere (1991).

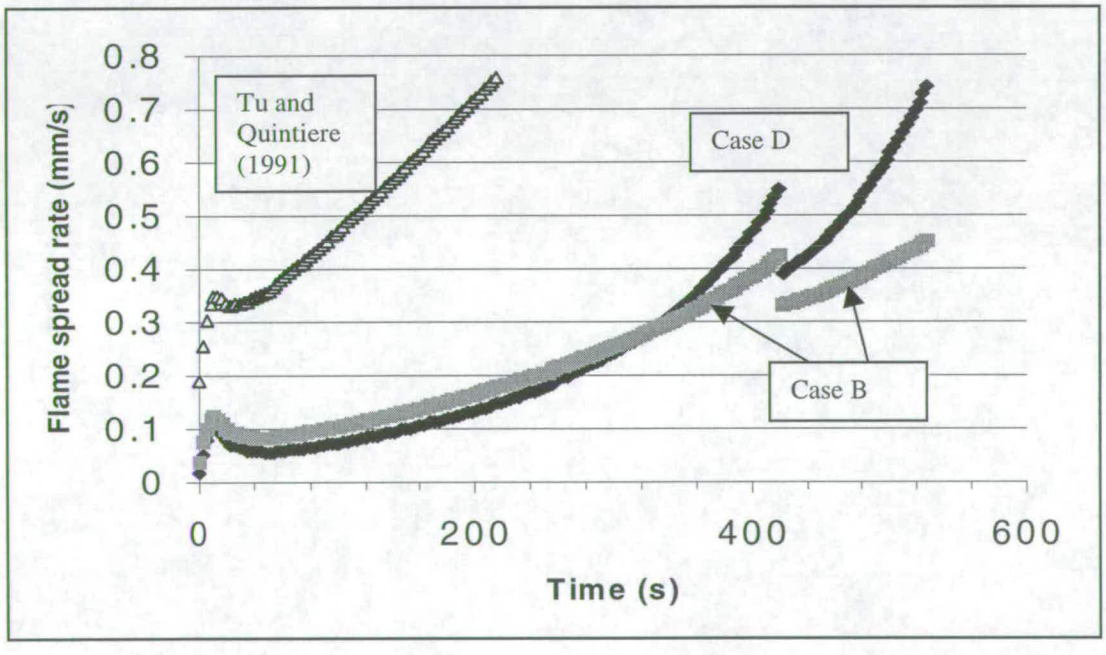

4.2.5 Conclusions

Grant and Drysdale's model (1995) has been discussed in this chapter, and the following conclusions can be made.

(1) The flame height correlation can influence the modelling results very significantly.

(2) The irradiance applied in the Cone Calorimeter, which simulates the heat transfer to the unburned region, also has great influences on the prediction.

(3) The RHR data obtained with the non-standard test procedure is more relevant to the real heat transfer behaviour in the preheating region.

Chapter 5

Discussion

5.1 Introduction

The objectives of this study were to contribute towards the understanding of wall fires on flat surfaces, in a corner and with the influences of a parallel wall. The behaviour of the wall fires was investigated experimentally by determining important parameters. The upward flame spread rate of the wall fires can be predicted by using a model with these parameters as input data.

In this chapter, an overall discussion will be conducted to examine the adequacy of the experimental apparatus, methods, modelling work, etc.

5.2 Apparatus to Simulate the Upward Flame Spread on Vertical Surfaces

To simulate a wall fire, several types of experiments have been carried out:

(1) gas line burner against an inert wall (Hasemi, 1985; Sugawa, 1991),

(2) vertical panel fuelled by gas, e.g. natural gas, propane (Coutin *et al.* 1999; this work),

(3) vertical combustible solid ignited uniformly over the whole surface (this work) and

(4) vertical combustible solid ignited on its bottom edge (Quintiere *et al.*, 1986; this work).

Here the physical burning area of the fires and the RHR released from the fires associated with these experiments are discussed because these two parameters determine the flame height and heat flux from the flame to the unburned surface which are required for the modelling work.

5.2.1 Gas line burner against an inert wall

The schematic diagram of a line fire against a wall is in Fig. 5.1 (Hasemi, 1985; Sugawa, 1991). The rate of supply of the gaseous fuel (m^3/s or g/s) can be controlled by a rotameter or a mass flow controller. By adjusting the gas flow, different mass flow rates, which will determine the RHR (Equation 5.1), can be produced to simulate different rates of burning.

The burning area of a line fire against a wall is not an 'area' if compared with other solid combustible materials. In addition, the source of flame is horizontal. This is different from burning walls, where combustible vapours are released from a vertical surface. Hasemi (1985) noticed that the behaviour of flame near the line burner may be different from that of a vertical fuel.

The RHR per unit width $\dot{Q}'$ transferred from the line fire is calculated by Equation 5.1.

$$\dot{Q}' = \dot{m}' \chi \Delta H_c \tag{5.1}$$

where $\dot{m}'$ is the mass flow rate of the gas fuel per unit length (g/s •m), χ is the completeness of combustion and ΔH_c is the net heat of combustion. For a line burner, $\dot{m}'$ is set up manually and will not change during burning. The value of χ is determined by the geometry, air entrainment, cooling by the environment, etc. and depends on the fuel, and ΔH_c also depends on the fuel.

Fig. 5.1 – The schematic diagram of a line fire produced by a line burner against an inert board. (⋯► Gaseous fuel emerging from the line burner)

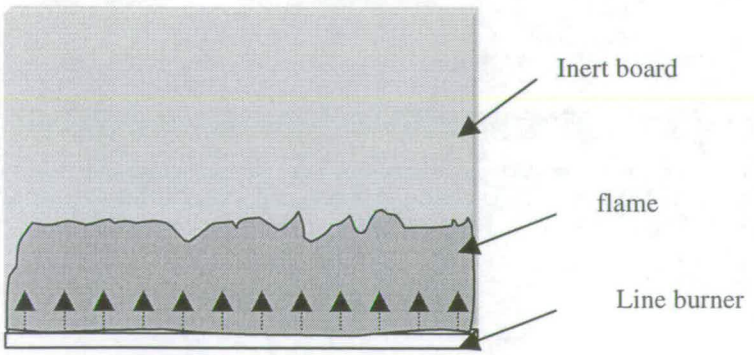

5.2.2 Gas Panel Simulation

The schematic diagram of a fire produced by a vertical gas panel is in Fig. 5.2. Like a line burner, the flow rate of fuel is controlled, either using a rotameter or a mass flow controller. By adjusting the gas flow, different mass flow rate can be produced to simulate different rates of burning.

One advantage of the gas panel simulation, compared with using a line burner, is that the gas panel produces a vertical burning surface from which the gaseous fuel emerges. This is closer to a real wall fire.

The total mass flow rate is also fixed during burning once the flow rate is set up. The value of χ can be determined by the geometry, air entrainment, cooling by the environment, etc., and ΔH_c depends on the fuel used.

Fig. 5.2 – The schematic diagram of a wall fire produced by a vertical gas panel. (→ Gaseous fuel emerging from the panel)

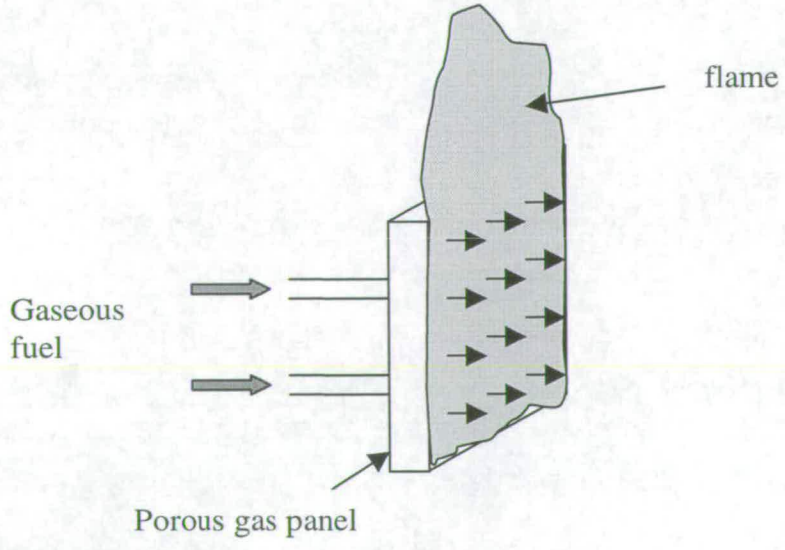

5.2.3 Simulation by Vertical Combustible Solids Initially Ignited Uniformly

Using a vertical combustible solid (this work) is definitely closer to real wall fires. If the solid is initially ignited uniformly over its whole surface, the initial mass flow rate is expected to be uniform. However, the local mass flow rate will change depending on the local heat transfer from the flame (and external heat sources) and will not be uniform over the surface.

To simulate different burning rates, an external radiation is usually applied, which can increase the local mass flow rate by increasing the radiative heat transfer. The schematic diagram of the simulation by a vertical burning solid is shown in Fig. 5.3.

The RHR per unit width of the vertical burning solid is determined by Equation 5.2.

$$\dot{Q}' = \dot{m}'' \chi \Delta H_c X_p \tag{5.2}$$

where X_p is the height of the burning surface. The value of χ is affected by the geometry, the air entrainment, cooling from the environment, etc. The local and total mass flow rate are self-determining and can only be changed by the external radiation. This is different from the line burner and gas panel, with which the total mass flow rate is fixed by the experimentalist.

Fig. 5.3 - The schematic diagram of the simulation by a vertical burning solid.

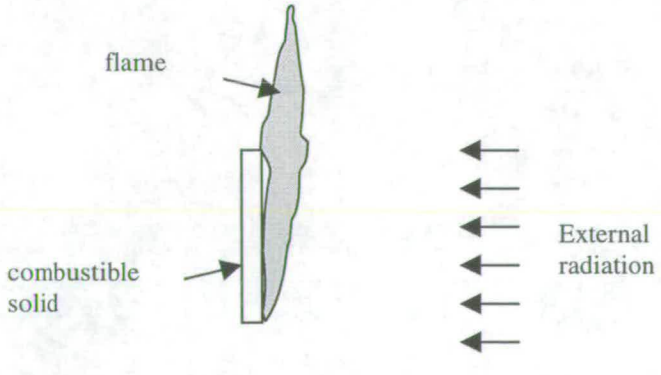

5.2.4 Simulation by Vertical Combustible Solids Ignited along the Lower Edge

A combustible solid ignited along its lower edge could produce an upward spreading fire. This kind of fire is a real wall fire in real fire conditions. However, compared with the vertical burning solid initially ignited uniformly, this fire may not produce a specific shape of burning area.

5.2.5 Comparison of These Four Simulations

Table 5.1 summarises the comparison of some properties of these four simulations. For line burners and gas panels, the total mass flow rate of gaseous fuel is controlled manually. Once set up, the mass flow rate is fixed and does not change by other factors, e.g. geometry. On the contrary, for burning solids, the mass flow rate is determined by the heat transfer to the burning surface, which is influenced by geometry, external heat source, etc.

Those simulations with which the shape of the burning area is fixed can be controlled more easily to produce systematic investigation. However, the difference between those simulations and real spreading wall fires should be kept in mind.

Table 5.1 - The comparison of some properties of different simulations.

	Line burner	Gas panel	Combustible solid	
			Ignited initially uniformly	Ignited on the bottom edge
Total mass flow rate during burning	fixed	fixed	various	
Completeness of combustion	May be changed by other factors	May be changed by other factors	May be changed by other factors	
burning area	Horizontal; shape fixed	Vertical; shape fixed	Vertical; shape fixed	Vertical; shape varied

5.3 Flame Height

In Sec.4.2.1, it can be seen that the flame height correlation plays a very important role in upward flame spread modelling. In Chapter 3, the flame height was measured on vertical steady burning solids (for $\dot{Q}'$<30 kW/m), spreading flames and on fires from a gas panel (for 10 kW/m < $\dot{Q}'$<110 kW/m). In addition, the flame height of fires in a corner and with the influence of an inert parallel wall has been investigated. In this section, all the flame height measurement will be discussed together.

5.3.1 Determination of Flame Height

The visible flame height of a wall fire, especially as it is turbulent, is not easily determined because of the fluctuation. Sugawa *et al.* (1991) summarised four methods, which have been reviewed in Sec.2.4.3.1: (1) infrared-images, (2) judgement by eye, (3) normal photographs and (4) video tape recordings. Saito *et al.* (1985) used another method detecting the sharp increase of thermocouple temperature. The flame heights depend strongly on the observation or record methods. In addition, personal difference in eye-averaged flame heights seemed to be unavoidable. Chitty and Cox (1979) defined flame height on a statistical basis and designed an experiment which was able to analyse the positive ion current drawn by a electrostatic probe immersed in the fire plume. Flame height was then determined to be the location where flame being present for 50 % of the time. Their measurement was consistent with the eye-averaged flame height for a methane diffusion flame above a 0.3 m square porous burner. Moreover, Zukoski *et al.* (1984) used measurements of flame persistency to determine flame height of pool fires. Coutin *et al.* (1999) applied an objective methodology using a CCD camera to map flame luminosity for measuring wall flame heights. This kind of objective methodology should be able to produce more accurate flame height correlations.

5.3.2 Comparison of Previous Flame Height Correlations on Flat Surfaces and Those in This Study

All the experiments for wall fires on flat surfaces have shown that the flame height correlation conforms to the form (Equation 2.9):

$$X_f = K\dot{Q}'^n \tag{2.9}$$

The type of experiments (Sec.5.2) and the geometric configuration may affect the values of K and n.

Fig. 5.4 - The comparison of previous flame height correlations and those in this study

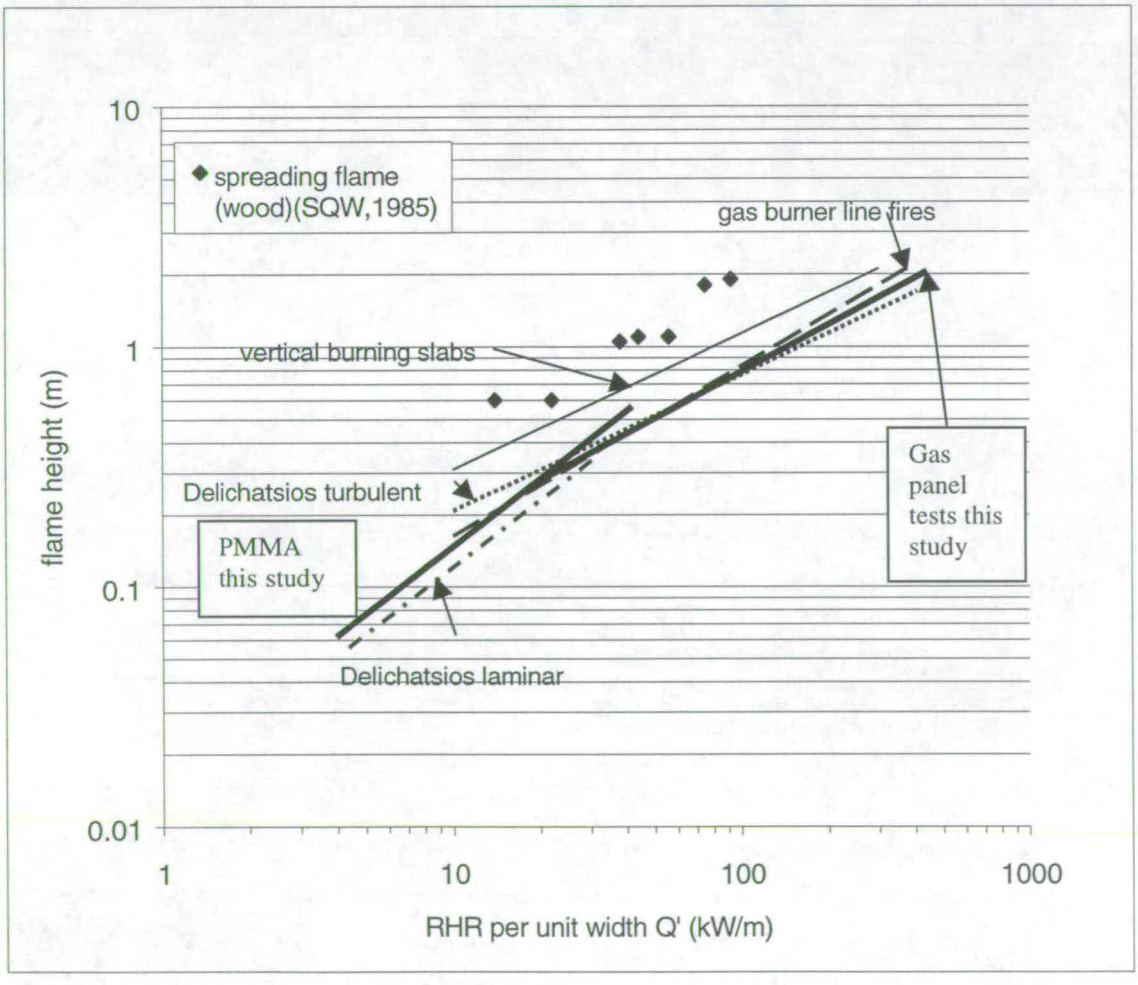

The flame height correlations carried out for steady burning PMMA fires (for $\dot{Q}'$ <30 kW/m) and from a gas panel (for 10 kW/m < $\dot{Q}'$<110 kW/m) are compared with previous ones derived theoretically or experimentally (Fig. 5.4). The correlation of the gas burner line fires is from Fig. 2.3, that of the vertical burning solid is from Fig. 2.5, and the spreading flame data and the Delichatsios correlations (laminar and turbulent) are from the studies of Saito *et al.* (SQW, 1985) and Delichatsios (1984). It can be seen that the correlations obtained in this study show very good agreement with the previous ones.

There are two distinct regions of correlation. For $\dot{Q}'$ < c. 20 kW/m, the power n of the flame height correlation (Equation 2.9) is about 1, while for $\dot{Q}'$ > c. 20 kW/m, the value of n is about 2/3. These regions of correlation are actually associated with laminar or turbulent flames. Wall fires were observed to be turbulent when the flames were higher than approximately18 cm (Orloff *et al.*, 1976), which is approximately for $\dot{Q}'$ > c. 20 kW/m.

5.3.3 Effect of Geometric Configurations on the Flame Height

The geometries investigated experimentally in Chapter 3, which may affect the flame height correlation, are as follow.

- lower edge configurations (on a flat surface)
- sidewalls (on a flat surface)
- the width of a burning area (on a flat surface)
- in a corner
- with a parallel inert wall nearby (on a flat surface)

The effect of each geometric configuration has been shown individually in previous chapters. Some conclusions for wall fires on flat surfaces can be made:

1. The lower edge configuration of a wall fire changes the air entrainment pattern, which influences the formation of boundary layers and then the flame height (at least for PMMA with height <30 cm).

2. The presence of sidewalls increases the flame height as sidewalls help maintain one-dimensional air entrainment along the vertical burning surface (at least for PMMA with height <50 cm).
3. The fires from wider burning areas produce higher flames (at least for propane fires with $\dot{Q}'$ <200 kW/m).

The flame height correlations for a flat surface, in a corner and between two parallel walls are compared in Fig. 5.5. The details of these cases are listed in Table 5.2. The experimental data are from PMMA fires. The PMMA slabs were 8 cm wide and 6 mm thick with height of 0.5 m or 1 m.

Table 5.2 – The geometrical arrangements of the flame height experiments using PMMA.

	Correlation (X_f and X_p in meters)	
On a flat surface (no floor)	$X_f=1.35X_p^{0.87}$ (Equation 3.9)	For $0<X_p<0.35$ m
In a corner (with floor)	$X_f=1.47X_p^{0.64}$ (Equation 3.26)	For $0<X_p<0.7$ m
Parallel case (separation: infinite; with floor)	$X_f=1.33X_p^{0.69}$ (Equation 3.29)	For $0<X_p<0.7$ m
Parallel case (separation: 5 cm; with floor)	$X_f=1.18X_p^{0.59}$ (Equation 3.30)	For $0<X_p<0.7$ m

It is seen that the wall fires in a corner produced the tallest flames for a given pyrolysis height X_p. In addition, the influence of a parallel wall was not very strong. Note that, the only difference between the two sets of experiments involving a flat surface (described as "flat surface on its own", and "flat surface with a parallel wall at infinite separation") was that the former did not have a floor present, while the latter was directly on a floor. It would appear that the presence of a floor increases the height of a flame. This is consistent with the observation of flame height made in the

Cone Calorimeter for PMMA samples shorter than 30 cm with $\dot{Q}'$ <30 kW/m (Sec. 3.3.2). The flame associated with Case A (with floor) is higher than that with Case B (no floor).

Fig. 5.5 – The comparison of the flame height correlations shown in Table 5.2 for the cases of on a flat surface, in a corner and between two parallel walls.

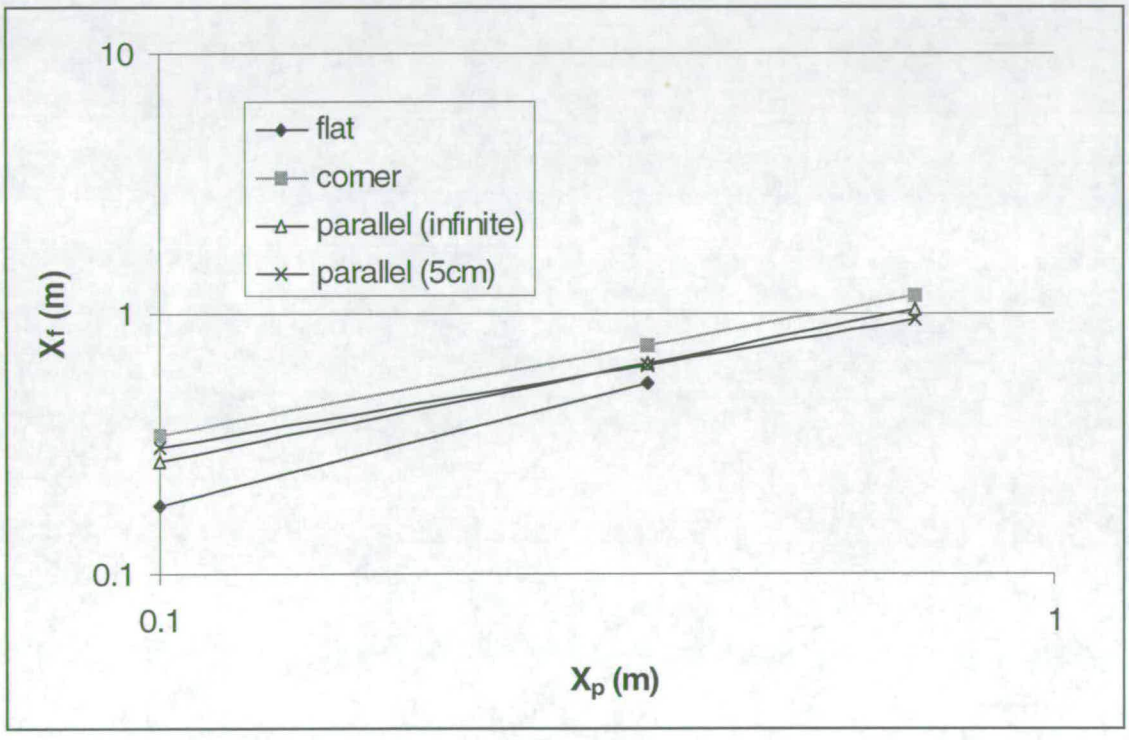

The flame height correlation discussed here is against the pyrolysis height X_p, giving

$$X_f = K_1 X_p^{\,n} \tag{5.3}$$

However, the form (Equation 2.9) in which the flame height is correlated against the heat release rate per unit width $\dot{Q}'$ is more useful for the analysis of the flame spread rate of a wall fire. Section 5.3.2 has shown that the flame height correlation for wall fires on flat surfaces conform to this form (Equation 2.9). In this study, however, the values of $\dot{Q}'$ were not measured in the experiments of wall fires in a corner and with the influence of a parallel inert wall.

For the cases of wall fires on a flat surface and with the influence of a parallel inert wall, the relationship of the flame height correlated against X_p and $\dot{Q}'$ can be seen in Equation 5.4.

$$X_f = K\dot{Q}'^n = K(\dot{m}''\chi\Delta H_c X_p)^n \tag{5.4}$$

where $\dot{m}''$ is the mass flow rate of the gas fuel per unit area (g/ m^2• s), χ is the completeness of combustion and ΔH_c is the net heat of combustion.

Therefore, Equation 5.3 can be re-arranged, giving Equation 5.5

$$X_f = K_1 \left(\frac{\dot{Q}'}{\dot{m}''\chi\Delta H_c}\right)^n = \frac{K_1}{(\dot{m}''\chi\Delta H_c)^n}\dot{Q}'^n \tag{5.5}$$

It can be seen that even the value of K_1 is higher in a flame height correlation, after the correlation is re-arranged to be set against $\dot{Q}'$, the value of K may be lower if the value of ($\dot{m}''\chi\ \Delta H_c$) is higher. $\dot{m}''$and χ are self-determining in the PMMA experiments. Thus, the sequence of flame height correlation shown in Fig. 5.5 may not directly determine that of the flame spread rate. For this analysis, the values of $\dot{m}''$ and χ are needed.

Hasemi has obtained data (1996) of the flame heights in a corner, giving

$$X_f/H = 6.0Q_v^{*0.60} \tag{2.71}$$

where

$$Q_v^* = \frac{\dot{Q}}{\rho CpTo(gH)^{1/2}(WH)} \tag{2.70}$$

H is the height of the burning area and can be expressed by X_p. W is the width of the burning area.

Therefore,

$$X_f = K_2 \dot{Q}'^{0.6} X_p^{0.1} = K_3 \dot{Q}''^{0.6} X_p^{0.7} \tag{5.6}$$

where K_2 and K_3 are constants. It was found that the flame height in a corner is not only related to $\dot{Q}'$.

5.4 Heat Flux

5.4.1 Effect of Geometric Configuration

The heat fluxes measured ahead of the pyrolysis front for different geometric configurations have been presented in previous chapters. Every heat flux distribution plotted against the ratio X/X_f in a logarithmic scale forms the shape as shown in Fig. 5.6 (see Fig. 3.19, 3.23, 3.24,3.33 and 3.37). There are three regions:

1. Region I: The heat flux is approximately constant.
2. Region II: The heat flux decreases linearly.
3. Region III: The heat flux decreases linearly, but less rapidly than in Region II.

Only the heat transfer in Region I and II will be discussed because of their contribution to the upward flame spread.

Fig. 5.6 – The shape of heat flux distribution against the X/X_f.

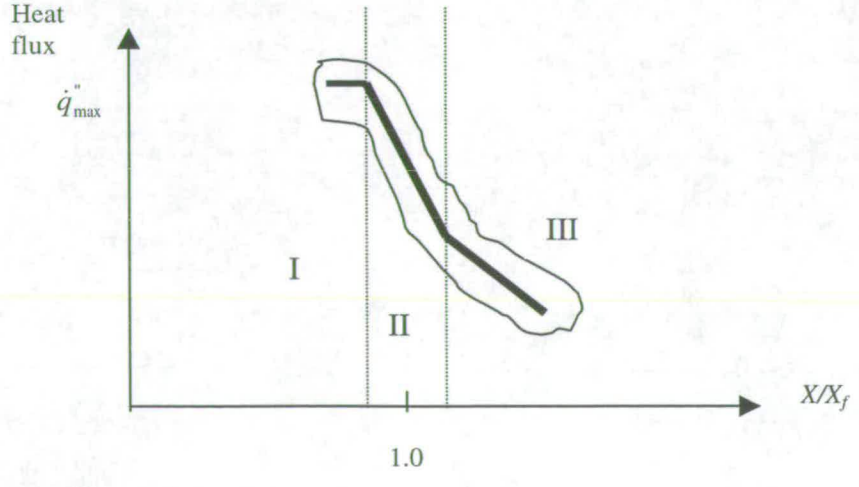

Table 5.3 summarises the heat flux correlations in this and previous studies. Details are given in previous chapters. The geometric configurations correspond to a wall fire on a flat surface, in a corner and between parallel walls. $\dot{q}''_{max}$ is the averaged heat flux in Region I.

For wall fires on flat surfaces, the values of $\dot{q}''_{max}$ (Region I) in all the experiments was between 25 to 30 kW/m^2 for X/X_f <0.5-0.6. The comparison of the heat flux correlations for wall fires on flat surfaces in Section II are shown in Fig. 5.7. A good agreement can be seen between the correlations in this (PMMA, gas panel tests) and previous studies (Hasemi, 1984; Quintiere *et al.* 1986). The heat fluxes in the study of Quintiere *et al.* (1986) and Hasemi (1985) were generally low. This may because the heat flux meters were mounted in a water-cooled copper plate above the burning surface in the study of Quintiere *et al.* (1986), and in Hasemi's study (1985), the vertical wall was a water-cooled "isothermal" wall. The water-cooled copper plate and isothermal wall absorbed some heat which would otherwise have been carried upwards. The heat flux measured on the wall above consequently was reduced.

The effects of the width of a burning surface and the presence of sidewalls on the heat flux distribution have been described in Sec.3.4 and 3.5 by using PMMA slabs and a gas panel. The presence of sidewalls was found to decrease the heat flux (c.15% in the PMMA experiment in Fig.5.7). In addition, there was an effect of width. However, no clear trend of the width effect was found for the wall fires with widths between 15, 30 and 57 cm. The 30 cm wide flames produced higher heat fluxes than the 15 and 57 cm wide flames. More data are needed.

Table 5.3 – The heat flux correlations discussed.

	experiment	Region I	Region II	
Wall fire on a flat surface	PMMA (0.5 m long, 7 cm wide, 6 mm thick) (Without sidewalls)	$\dot{q}''_{max} \approx 30$ kW/m^2 $\left(\frac{X}{X_f}\right)<0.63$	$\dot{q}'' = 8.27\left(\frac{X}{X_f}\right)^{-2.72}$ $0.63<\left(\frac{X}{X_f}\right)<1.4$	Width= 7 cm
	PMMA (0.5 m long, 7 cm wide, 6 mm thick) (With sidewalls)	$\dot{q}''_{max} \approx 30$ kW/m^2 $\left(\frac{X}{X_f}\right)<0.62$	$\dot{q}'' = 7.26\left(\frac{X}{X_f}\right)^{-2.57}$ $0.62<\left(\frac{X}{X_f}\right)<1.4$	Width= 7 cm
	Gas panel tests (propane)	$\dot{q}''_{max} \approx 25$ kW/m^2 $\left(\frac{X}{X_f}\right)<0.5$	$\dot{q}'' = 4.6\left(\frac{X}{X_f}\right)^{-2.40}$ $0.5<\left(\frac{X}{X_f}\right)<1.1$	Width= 15 cm
	Gas panel tests (propane)	$\dot{q}''_{max} \approx 27$ kW/m^2 $\left(\frac{X}{X_f}\right)<0.6$	$\dot{q}'' = 6.12\left(\frac{X}{X_f}\right)^{-2.93}$ $0.6<\left(\frac{X}{X_f}\right)<1.2$	Width= 30 cm
	Propane line burner Hasemi (1984)	$\dot{q}''_{max} \approx 26$ kW/m^2 $\left(\frac{X}{X_f}\right)<0.46$	$\dot{q}'' = 5.1\left(\frac{X}{X_f}\right)^{-2.5}$ $0.46<\left(\frac{X}{X_f}\right)<1.66$	Width= 8.2 cm
	Six materials Quintiere *et al.* (1986)	$\dot{q}''_{max} \approx 25$ kW/m^2 $\left(\frac{X}{X_f}\right)<0.5$	$\dot{q}'' = 4.3\left(\frac{X}{X_f}\right)^{-2.4}$ $0.5<\left(\frac{X}{X_f}\right)<1.6$	Width= 28.5 cm

In a corner	PMMA (1 m high, 8 cm wide, 6 mm thick)	$\dot{q}''_{max} \approx 30$ kW/m^2 $\left(\frac{X}{X_f}\right)<0.6$	$\dot{q}'' = 9.12\left(\frac{X}{X_f}\right)^{-2.59}$ $0.6<\left(\frac{X}{X_f}\right)<2$	Width= 8 cm
	PMMA (0.45 m high, 20 cm wide, 2 cm thick), Qian *et al.* (1994)	$\dot{q}''_{max} \approx 32.5$ kW/m^2 $\left(\frac{X}{X_f}\right)<0.55$	$\dot{q}'' = 8.22\left(\frac{X}{X_f}\right)^{-2.29}$ $0.55<\left(\frac{X}{X_f}\right)<2$	Width= 20 cm
	Gas panel tests (propane), Hasemi (1996)	$\dot{q}''_{max} \approx 28$ kW/m^2 $\left(\frac{X}{X_f}\right)<0.55$	$\dot{q}'' = 5.8\left(\frac{X}{X_f}\right)^{-2.8}$ $0.55<\left(\frac{X}{X_f}\right)<2$	Width= 22.5 cm
Between parallel walls	PMMA (1 m long, 8 cm wide, 6 mm thick)	$\dot{q}''_{max} \approx 35$ kW/m^2 $\left(\frac{X}{X_f}\right)<0.7$	$\dot{q}'' = 10.21\left(\frac{X}{X_f}\right)^{-3.11}$ $0.7<\left(\frac{X}{X_f}\right)<1.5$	Separation =infinite
	PMMA (1 m long, 8 cm wide, 6 mm thick)	$\dot{q}''_{max} \approx 35$ kW/m^2 $\left(\frac{X}{X_f}\right)<0.7$	$\dot{q}'' = 9.13\left(\frac{X}{X_f}\right)^{-3.89}$ $0.7<\left(\frac{X}{X_f}\right)<1.5$	Separation =5 cm

The effect of the presence of a parallel inert wall on the heat flux distribution has been studied in Sec. 3.7. The material used was 6 mm thick, 8 cm wide and 1 m high PMMA. The experiment started with ignition of a 1 cm high zone on the bottom of the slabs. It was seen that in general the heat fluxes decreased when the separation was from 5 to 15 cm and increased when the separation was from 15 to 35 cm and then infinite. Fig. 5.8 presents the correlations in Region II (Fig.5.6) for the two extreme cases: separation = 5 cm and infinite (without a parallel wall).

Fig. 5.7 - The comparison of the heat flux correlations in Region II for wall fires on flat surfaces.

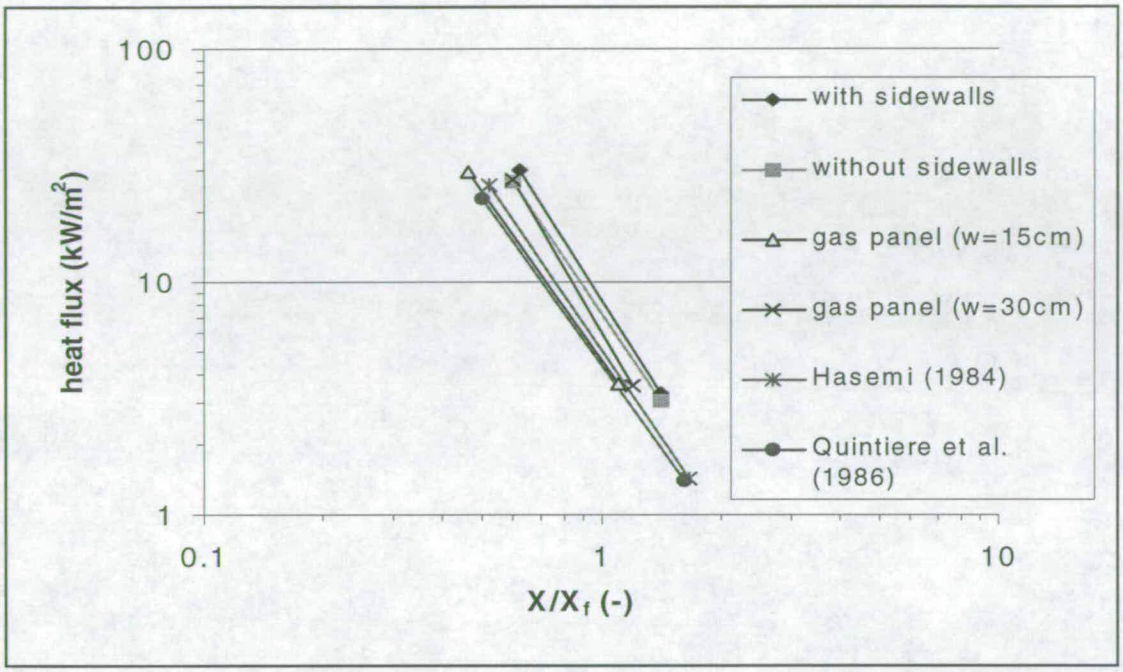

Fig. 5.8 also shows the heat flux distributions of wall fires (Region II) for a corner obtained in this and previous studies (Qian *et al.*, 1994; Hasemi, 1996). There is good agreement between these correlations. The widths of the burning surfaces in these studies were different: 8 cm wide PMMA slabs in this study, 20 cm wide PMMA slabs in the study of Qian *et al.* (1994) and 22.5 cm propane fires in Hasemi's (1996). It seems that the width effect on the heat flux distribution of a corner/wall fire is not large at least for width <c.20 cm.

From Table 5.3 and Fig. 5.8, the comparison of the heat flux distributions (in Region I and II) in a corner, between parallel walls and a single wall (parallel case with infinite separation) can be shown. Surprisingly, the difference between these geometric configurations is not significant. Even for the corner/wall fires, the cross radiation from the other wall fires does not increase the heat flux at least for the wall fires with width < 20 cm.

Several conclusions can be made according to those observations discussed above:

(at least for wall fires on 1 m high and 20 cm wide samples)

1. The heat flux distributions for wall fires on flat surfaces, in a corner and with the influence of a parallel inert wall are similar when plotted against X/X_f.
2. There exist three regions as demonstrated in Fig. 5.6.
3. The levels of $\dot{q}''_{max}$ (Region I) are between 25 to 35 kW/m^2 for wall fires on flat surfaces, in a corner and with the influence of a parallel inert wall. However, 25 kW/m^2 was obtained when water-cooler plates were used (Hasemi, 1985; Quintiere *et al.*, 1986). Only one of the experimental data sets in this present work falls this low (gas panel tests with width of 30 cm, Table 5.3). Therefore, 30-35 kW/m^2 might be an acceptable range.
4. The results appear to be independent of the nature of the fuel (at least for PMMA and propane).

Fig. 5.8 – The heat flux distributions of wall fires for a corner and between two parallel walls.

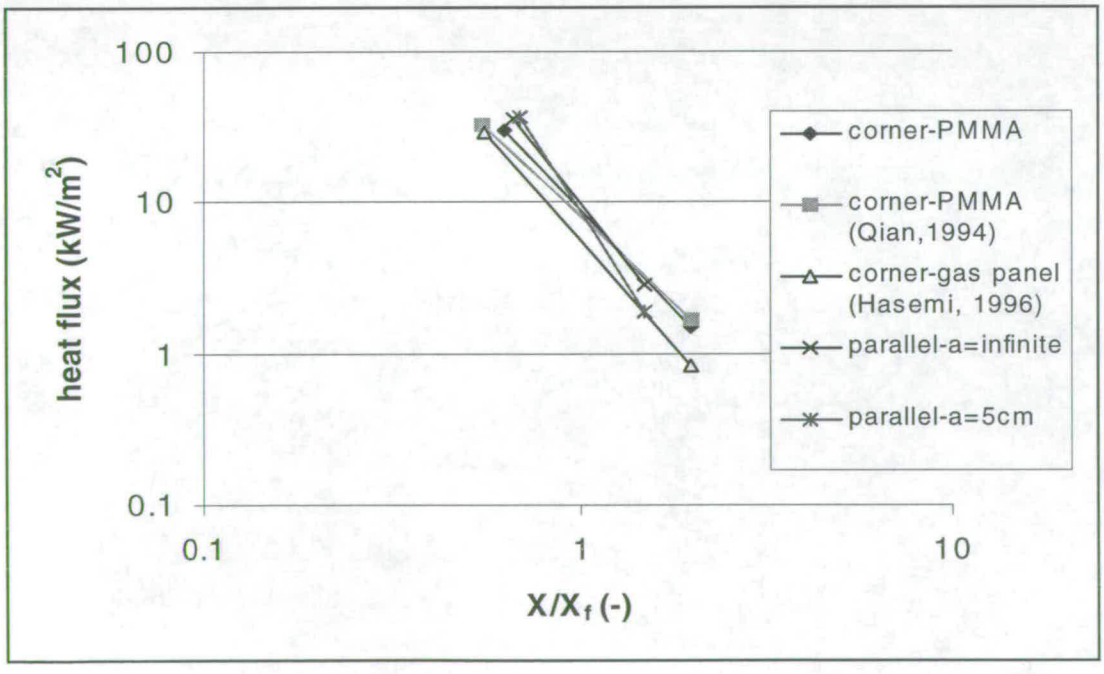

5.5.Flame Spread Rate

The methods for deducing the position of the pyrolysis front are as follows:

(1) monitor the surface temperature of a burning wall by thermocouples

(2) monitor the surface temperature of a burning wall by a infra-red camera

(3) for PMMA, the pyrolysis front can be observed from the back of the material by the appearance of bubbles.

In this study, the third method was adopted in the spreading PMMA experiment (Sec.3.4), while the experiments of PMMA wall fires in a corner and between two parallel walls used the second method. For the first and second methods, the ignition temperature of a material has to be known. The ignition temperature of PMMA was estimated to be 360^0C in this study.

The upward flame spread rates of the PMMA wall fires on a flat surface, in a corner and between two walls are compared in Fig.5.9. The PMMA samples were 6 mm thick, 8 cm wide and from 0.5 to 1 m high. However, the heights of the ignition zone (at the "foot" of the slabs) were 2 mm in the spreading PMMA tests and 1 cm for the corner and between two walls. The ignition effect is believed to only affect the early stage, which has been shown by the analysis of the modelling work in Sec. 4.2.3.

The wall fires in a corner spread most rapidly while the fires between two parallel walls spread most slowly. This observation was made according to three tests of the experiments. The flame spread rate can be analysed by the heat flux and flame height correlations (against $\dot{Q}'$) associated with these geometries. Fig. 5.10 combines the heat flux data of PMMA wall fires on flat surfaces (with and without sidewall), in a corner and with the influence of a parallel wall, showing the difference of the heat fluxes ahead of the burning zone associated with these geometries. Fig. 5.5 has already shown that the flames (as a function of the pyrolysis height) associated with the corner/wall fires are the tallest while with a flat surface being the shortest. Table 5.4 lists the sequences of the flame height correlation (as a function of the pyrolysis height), heat flux distribution and flame spread rate measured.

Fig.5.9. - The upward flame spread rates of the PMMA wall fires on a flat surface, in a corner and between two walls.

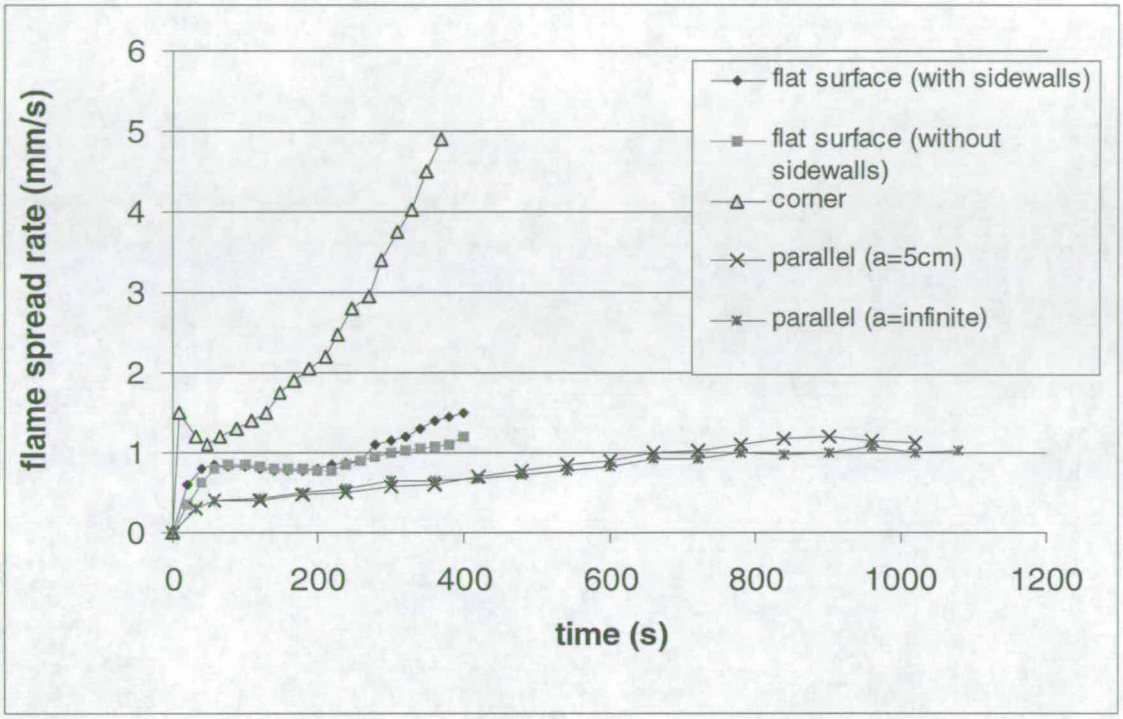

Fig. 5.10 – The comparison of the heat flux distributions (Region II only) of PMMA wall fires on flat surfaces (with and without sidewalls), in a corner and with the influence of a parallel wall.

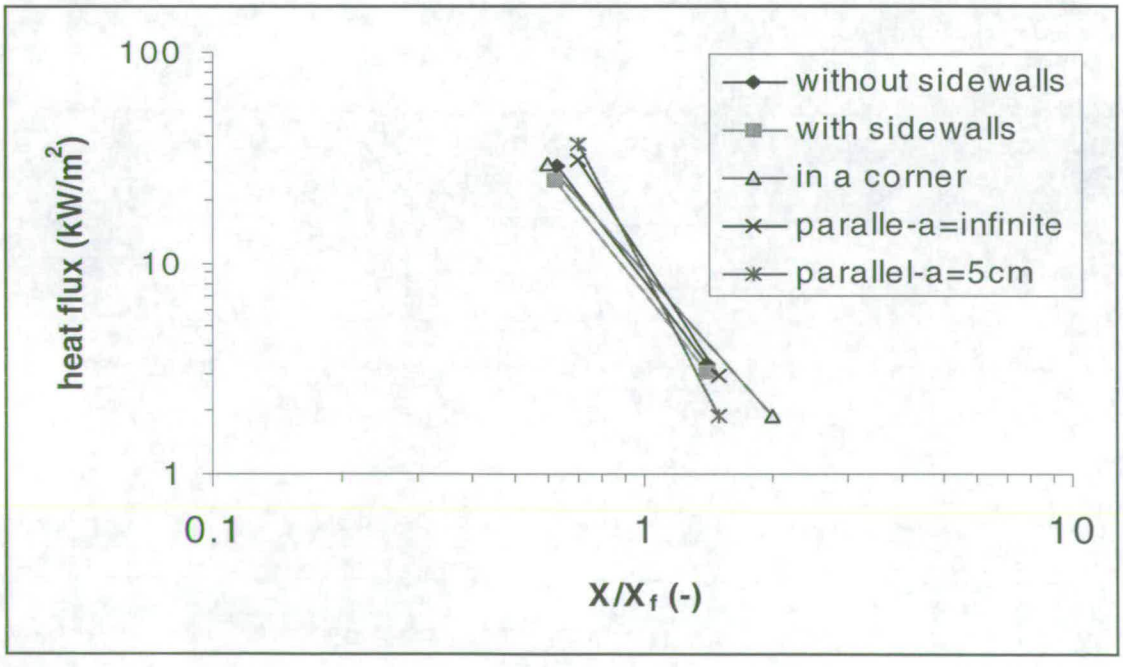

Table 5.4 - The sequences of the flame height correlation (as a function of the pyrolysis height), heat flux distribution and flame spread rate measured.

	Flame height correlation (as a function of X_p)	flame heat flux distribution	flame spread rate measured
On a flat surface (with sidewalls: no floor)	4	5	2
On a flat surface (without sidewalls: no floor)	5	4	3
In a corner (with floor)	1	3	1
Parallel case a=infinite (with floor)	3	2	5
Parallel case a=5 cm (with floor)	2	1	4

The sequence of measured flame spread rate (Fig. 5.9) associated with these geometries could not be explained directly by the sequences of flame height correlation and heat flux distribution. Most surprisingly, the flame spread rates of wall fires under the influence of a parallel wall were lower than those on flat surface. The flames under the influence of a parallel wall were taller and the heat fluxes were higher. More research is needed to understand the geometry effect in details. The experiment of wall fires without a floor with a parallel inert wall nearby is recommended to compare the data in this study.

In addition, the information of $\dot{m}''$, for estimating X_f as a function of $\dot{Q}'$, is lacking. As discussed in Sec.5.3.3, the sequence of flame height correlation as a function of X_p may be changed if the flame height expressed as a function of $\dot{Q}'$ after $\dot{m}''$ is taken into account. It may be reasonable to infer that the value of $\dot{m}''$, influenced by the geometries, plays an important role. Thus, the measurement of $\dot{m}''$ is recommended. Further research is needed to understand how $\dot{m}''$ is affected by geometry.

5.6 Modelling Work

5.6.1 Modelling Work of Upward Flame Spread on Vertical Flat Surfaces

In Chapter 4, the modelling work of wall fires on flat surfaces has been discussed and the following conclusions have been made associated with Grant and Drysdale's model (1995):

(1) The flame height correlation can influence the modelling results very significantly.

(2) The irradiance applied in the Cone Calorimeter, which simulates the heat transfer to the unburned region, also has great influences on the prediction. In addition, a lower value of the representative heat flux was suggested to be between 15 to 20 kW/m^2 rather than a value between 25 to 30 kW/m^2 as used by others.

(3) The RHR data obtained with the non-standard test procedure are more relevant to the real heat transfer behaviour in the preheating region (Fig.2.3).

5.6.1.1 Further Discussion

Flame Height Correlation

It has been demonstrated that the flame height correlation is affected by the geometry (lower edge configuration, width of the burning area, etc.), and two distinct regions were found for $\dot{Q}' >$ c.20 kW/m and $\dot{Q}' <$ c. 20 kW/m. More accurate prediction is expected using the flame height correlations for specific geometric configurations and regions for $\dot{Q}'$ greater or less than c. 20 kW/m.

Heat Flux Distribution

In the modelling work, the conical heater in the Cone Calorimeter was used to simulate the heat transfer ahead of the pyrolysis front to the unburned surface. The irradiance is fixed implying an assumption of constant heat flux in this preheating

region and zero elsewhere. In fact, the heat flux is not constant and the heat transfer from the buoyant plume is ignored, being less than 10 kW/m^2 (Sec.3.4.2.2). However, it is convenient to apply a constant irradiance for the benefit of using the Cone Calorimeter.

Other Fuels

In this study, only PMMA was used. Other materials like wood should be tested against the model prediction (with the non-standard Cone Calorimeter test procedure).

Scale

In this study, the width of the PMMA sample was 7-8 cm. Good agreement was shown against the model prediction using data from 10 cm square samples in the Cone Calorimeter adopting the non-standard Cone Calorimeter test procedure and a lower irradiance of 15 kW/m^2. However, Anderson *et al.* (1996) used the Grant and Drysdale's model (1995) (with standard Cone Calorimeter test procedure) and adopted a higher irradiance of 35 kW/m^2. A good agreement was shown in their flame spread rate tests of hardboard, plywood and wall paper covered wood surfaces. A question may arise: why the standard test procedure and the higher irradiance did not make an overestimation of the flame spread rate. The standard test procedure and another higher irradiance of 25 kW/m^2 were applied by Kokkala *et al.* (1997). Their prediction of the RHR was consistent with the experimental data. The same question may arise.

Table 5.5 lists the conditions of these models (in this study, Anderson *et al.* 1996 and Kokkala *et al*, 1997) and materials they tested. The experiments of the flame spread rate were actually carried out with very different materials and test conditions. In the present work, PMMA was used, while wood products were used in the studies of Anderson *et al.* (1996) and Kokkala *et al.* (1997). Wood products chars during flame spread process. In addition, the width of the sample for flame spread rate experiments was also very different to be was from 7 to 120 cm. The wider flames are expected to be thicker, producing higher heat fluxes to the unburned surface and resulting in a higher flame spread rate. The models of Anderson *et al* (1996) and Kokkala *et al.* (1997) did not overestimate the flame spread rate may be because for wider flames, a higher irradiance is reasonable. However, the non-standard test procedure is still

more relevant to the real heat transfer behaviour in the preheating region. Further analysis of the width effect is needed.

In addition, as the wall is wider, in addition to the modification of the flame height correlation and heat flux representation, the adoption of the 10 cm square sample in the Cone Calorimeter may not be proper. Further research is needed to examine this hypothesis.

Table 5.5 - The conditions of three upward flame spread models

Modelling work	irradiance (kW/m^2)	Cone Calorimeter test	burning slab used for flame spread rate experiments			
			width (cm)	height (cm)	thickness (mm)	material
This study	15	Non-standard	7-8	100	6	PMMA
Anderson *et al.* (1996)	35	standard	60	120	4	Wood products
Kokkala *et al.* (1997)	25	standard	120	240	9-11	Wood products

5.6.2 The Modelling Work of the Corner/Wall Fires

Grant and Drysdale's model (1995) was reviewed as to whether or not it can be used to predict the flame spread rate of a corner/wall fire. The assumptions involved have to be examined. A representative value of the heat flux to the unburned surface can be estimated according to the heat flux measurement (Sec.3.6.2). However, the flame height correlation for corner/wall fires has been shown to be not in the form of Equation 2.9 which correlates the flame height against the RHR per unit width but in the form of Equation 5.6 (Sec.5.3.3)

$$X_f = K_2 \dot{Q}'^{0.6} X_p^{0.1} \qquad (5.6)$$

where K_2 is a constant.

Thus, Grant and Drysdale's model could not work for this scenario because the flame height in its present form is not only dependent on the heat release rate per unit width but also on the pyrolysis height X_p.

5.6.3 The Modelling Work of the Wall Fires between Two Parallel Walls

The flame spread rate of a wall fire with the influence of a parallel inert wall could be predicted by Grant and Drysdale's model (1995) with the non-standard Cone Calorimeter test procedure. However, no flame height correlation was carried out in this study in the form of Equation 2.9. It is recommended for further research.

5.6.4 Proposals for the Modelling Work of Wall Fires under External Radiation

In fact, Equation 2.31 and 2.33 (the flame spread rate expressed as integral equations of the Volterra type) are the common forms for the upward flame spread modelling. By choosing proper values of n and K, and inputting the transient rate of heat release which can imitate the real scenario, other types of upward flame spread should be able to be simulated. In Chapter 4, the modelling work for upward flame spread on flat surfaces was discussed. The values of n and K are chosen to be 2/3 and 0.066, and the transient rate of heat release was measured by the Cone Calorimeter with the non-standard test procedure.

Upward flame spread on flat surfaces with external radiation is a scenario which can lead to more severe fire hazard. It may be simulated by adopting another non-standard Cone Calorimeter test procedure. After examining the assumptions for the modelling work discussed in Chapter 2 and 4, one of them should be highlighted that the heat flux only occurs in the region (X_f-X_p). Thus, if the effect from the external radiation above the flame front is too small to be considered, for example below 10 kW/m^2, the following method could work.

Fig.5.11 presents an upward flame spread with external radiation. Before the surface is ignited, the unburned region (X_f -X_p) is exposed to both the flame and the external radiation. Consequently, the heater should simulate both the two heating effects. After ignition, the flame is established. The heater should only simulate the external radiation. Therefore, a second non-standard Cone Calorimeter procedure is derived. Before ignition, the irradiance of the cone heater acts as the sum of the heat flux from the flame and the external radiation, while after ignition, the cone heater only simulates the external radiation.

Practically, it is difficult to set up different irradiances of the cone heater for two periods of time in a standard Cone Calorimeter. A new design would be required. Three proposals are provided here. First, an additional cone heater is involved to play the role of the flame, and the original one is used to simulate the heat released by the external radiation (see Fig.5.11). Before the sample ignites, two heaters release heat together. After ignition, the cone heater simulating the flame is removed. The rate of flame spread on flat surfaces with external radiation could be predicted by Grant and Drysdale's model (1995) with the transient rate of heat release measured in this way as input.

The second proposal requires a cone heater which can be moved away from the surface (Fig.5.12). Before ignition, the heater is located where the heater can release heat fluxes which is the sum of from the flame and the external radiation. After ignition, the heater is moved away from the surface to a location where the heater can releases heat fluxes only simulating the external radiation. There is no doubt that the locations of the heater have to be deduced so that the sample can receive defined heat fluxes which are expected. The rate of flame spread can subsequently be predicted by Grant and Drysdale's model (1995) applying RHR data from the Cone Calorimeter using this non-standard test procedure.

The third proposal needs data from two Cone Calorimeter tests. One test (Test A) measures time to ignition t_{ig} under the irradiance acting as the sum of the external radiation and the flame. The other (Test B) measures RHR under the irradiance only acting the external radiation. The "modified RHR", combining these two data from Test A and B, would not be exactly the same as that in the first and second proposals

because the heating times before ignition in Test A and B are different. The temperature profile inside the sample is different. However, the data produced in this way might be a reasonable approximation.

These three methods have to be examined by experiments.

Fig.5.11 - The schematic of the roles of heat feedback from the flame and the cone heater in the modelling work of the wall fires under external radiation.

← :heat from the flame ⬅ :heat from the external radiation

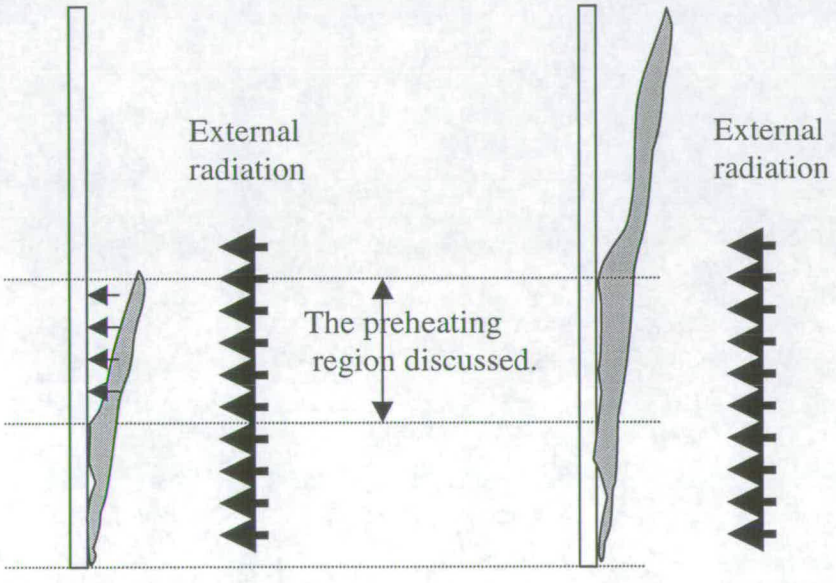

(a) the unburned region before ignition (b) the unburned region after ignition

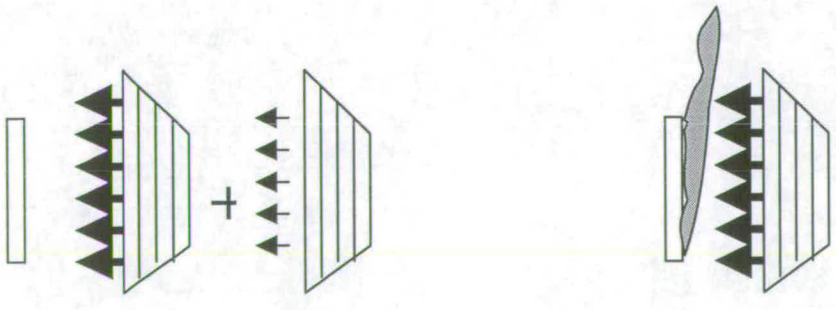

(a') the sample before ignition (b') the sample after ignition

Fig. 5.12 – The schematic diagram of the second proposal for the modelling work of wall fires under external radiation.

Before ignition

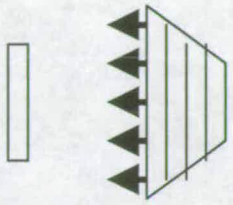

After ignition

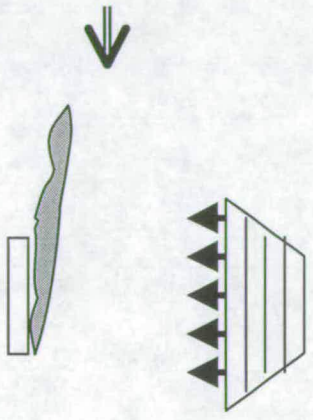

Chapter 6

Conclusions and Recommendations for Future Work

6.1 Introduction

Upward flame spread on vertical flat surfaces, in a corner and with the influence of a parallel inert wall have been studied by carrying out experiments and modelling work. The details of these experiments were shown in Chapter 3, of the modelling work were demonstrated in Chapter 4 and an overall discussion was presented in Chapter 5. This chapter will highlight the conclusions obtained in this study and provide recommendations for future work.

6.2 Flame Height

The flame height and heat flux from the flame to unburned surfaces are the two important parameters determining the spread rate of the flame. All the experimental data have been analysed to see whether or not there exists a similarity among the flame height correlations and heat flux distributions of wall fires on vertical flat surfaces, in a corner and with the influence of a parallel inert wall. The conclusions are as follows:

1. All the flame height correlations except in a corner conform to the form (Equation 2.9):

$$X_f = K\dot{Q}'^n \tag{2.9}$$

where X_f is the flame height, $\dot{Q}'$ is the heat release rate per unit width and n and K are constants. However, the values of K and n are affected by the geometric

configuration and the range of values of $\dot{Q}'$.

In addition, for the wall fire in a corner

$$X_f = K_2 \dot{Q}'^n X_p^m \tag{5.6}$$

where X_p is the height of pyrolysis zone.

2. The lower edge configuration of a wall fire changes the air entrainment pattern, which influences the formation of boundary layers and then the flame height (at least for PMMA fires on flat surfaces with height <30 cm) (Sec. 3.3.1).

3. The presence of sidewalls slightly increases the flame height as sidewalls help maintain one-dimensional air entrainment along the vertical burning surface (at least for PMMA fires on flat surfaces with height <50 cm) (Sec. 3.4.2.3).

4. The fires from wider burning areas produce higher flames (at least for propane fires produced on flat surfaces with $\dot{Q}'$ <200 kW/m) (Sec. 3.5.2).

5. The influence of a parallel wall on the flame height correlation is not very strong (at least for wall fires with pyrolysis height shorter than 1 m) (Sec. 3.7.2).

6. The presence of a floor increases the height of a flame (at least for wall fires with pyrolysis height shorter than 1 m) (Sec. 5.3.3).

7. While the flame height correlations expressed against the pyrolysis height X_p, the wall fires in a corner produced the tallest flames (at least for wall fires with pyrolysis height shorter than 1 m) of the geometries studied (wall fires on a flat surfaces, in a corner and with the influence of a parallel wall) (Sec. 5.3.3).

6.3 Heat Flux

For the heat flux distribution, (at least for wall fires on up to 1 m high and 20 cm wide samples)

1. The heat flux distributions for wall fires on flat surfaces, in a corner and with the influence of a parallel inert wall are similar when plotted against X/X_f (Sec. 3.4.2.3, 3.5.2, 3.6.2 and 3.7.2).

2. There exist three regions as demonstrated in Fig. 5.6.

3. The levels of $\dot{q}''_{max}$ (Region I in Fig. 5.6) are between 25 to 35 kW/m^2 for wall fires on flat surfaces, in a corner and with the influence of a parallel inert wall (Sec. 2.4.4, 3.4.2.3, 3.5.2, 3.6.2 and 3.7.2). Values of approximately 25 kW/m^2 were observed in the studies of Hasemi (1985) and Quintiere *et al.* (1986) using water-cooled isothermal board and copper plate. The water-cooled isothermal board and copper plate absorbed some heat which would otherwise have been carried upwards.

4. The results appear to be independent of the nature of the fuel (at least for PMMA and propane) (Sec. 3.4.2.3, 3.5.2, 3.6.2 and 3.7.2).

5. There are slight effects of the presence of sidewalls and the width of the burning area. The presence of sidewalls decreases the heat flux (about 15%) (Sec. 3.4.2.3).

6.4 The Modelling Work

In Chapter 4, the modelling work of wall fires on flat surfaces has been discussed and the following conclusions have been made associated with Grant and Drysdale's model (1995):

1. The flame height correlation can influence the modelling results very significantly (Sec. 4.2.1).

2. The irradiance applied in the Cone Calorimeter, which simulates the heat transfer to the unburned region, also has a great influence on the prediction of the flame spread rate (Sec.4.2.2). In addition, a lower value of the representative heat flux was suggested to be between 15 to 20 kW/m^2 rather than the commonly accepted value between 25 to 30 kW/m^2 (Sec. 3.4.2.3).

3. The RHR data obtained with the non-standard test procedure which reduces the applied heat flux to almost zero after ignition is more relevant to the real heat transfer behaviour in the preheating region (Sec. 4.2.2.2).

6.5 Recommendations for Future Work

1. In this study, the height of a flame was determined by eye. An objective methodology would produce more reliable flame height correlations.

2. It is obvious that the height of a flame is influenced by the geometric configuration which affects the flow characteristics, the accessibility of air, the heat transfer behaviour, etc. These factors can interact with one another and affect the burning rate (or mass loss rate $\dot{m}''$), the completeness of combustion χ and the structure of the flame. More research is needed to understand how these mechanisms interact.

3. It has been seen that there exist effects of the width of a burning surface, the geometric configuration, etc. on the heat flux distribution from the flame to the unburned surface. The heat fluxes measured in this study were the total heat flux. It would be better to analyse the geometry effect on the convective and radiative heat fluxes separately. The results may help predict the heat transfer behaviour as the geometry changes.

4. The sequence of measured flame spread rate (Fig. 5.9) associated with all the geometries could not be explained directly by the consequences of flame height correlation and heat flux distribution. More research is needed to understand the geometry effect in details. In addition, the information of $\dot{m}''$, for estimating X_f as a function of $\dot{Q}'$, is lacking. It may be reasonable to infer that the value of $\dot{m}''$, influenced by the geometries, plays an important role. Thus, the measurement of $\dot{m}''$ is recommended. Further research is needed to understand how $\dot{m}''$ is affected by geometry.

5. It has been demonstrated that the flame height correlation is affected by the geometry (lower edge configuration, width of the burning area, etc.), and two distinct regions were found for $\dot{Q}'$ > c.20 kW/m and $\dot{Q}'$ < c. 20 kW/m. More accurate prediction is expected using the flame height correlations for specific geometric configurations and regions for $\dot{Q}'$ greater or less than c. 20 kW/m.

6. In this study, only PMMA was used. Other materials like wood should be tested against the model prediction (with the non-standard Cone Calorimeter test procedure).

7. As discussed in 5.6.1.1, good agreement has been shown between modelling prediction and experimental data in this work, studies of Anderson *et al.* (1996) and Kokkala *et al.* (1997) although the conditions of these models, materials they tested and the geometry of the sample for flame spread rate experiments were very different (see Table 5.5). The present work applied a lower irradiance for the Cone Calorimeter tests and a non-standard Cone Calorimeter test procedure. A question may arise: why the standard test procedure and the higher irradiance did not make an overestimation of the flame spread rate in the studies of Anderson *et al.* (1996) and Kokkala *et al.* (1997). A reason possibly lies in the difference of materials tested. In the present work, PMMA was used, while wood produces were used in the studies of Anderson *et al.* (1996) and Kokkala *et al.* (1997). Wood produces chars during flame spread process. Another possible reason is the width of the sample for flame spread rate experiments. The width of the burning slabs was 7 cm in this work, 60 cm in the study of Anderson *et al.* (1996) and 120

cm in the study of Kokkala *et al.* (1997). The wider flames are expected to be thicker, producing higher heat fluxes to the unburned surface and resulting in a higher flame spread rate. A higher irradiance may be reasonable. However, the non-standard test procedure is still more relevant to the real heat transfer behaviour in the preheating region. Further analysis of the width effect is needed.

8. As the wall is wider, in addition to the modification of the flame height correlation and heat flux representation, the adoption of the 10 cm square sample in the Cone Calorimeter may not be proper. Further research is needed to examine this hypothesis.

9. The flame spread rate of a wall fire with the influence of a parallel inert wall could be predicted by Grant and Drysdale's model (1995) with the non-standard Cone Calorimeter test procedure. However, no flame height correlation was carried out in this study in the form of Equation 2.9. It is recommended for further research.

10. Three proposals for the modelling work of wall fires under external radiation have been provided in Sec.5.6.3. The modelling prediction applying these three non-standard Cone Calorimeter test procedures are recommended to compare with experimental measurement.

6.6 Summary

Upward flame spread on vertical surfaces can lead directly to flashover (Hasemi, 1999). In order to prevent the occurrence of hazardous wall fires, there is a need to select materials which satisfy performance-based regulations. This approach needs information from reliable fire models which simulate accurately the fire behaviour of materials in their end-use configuration.

This study focuses on the early stages of the upward flame spread. An existing model which uses data directly from the Cone Calorimeter test was examined. A non-standard test procedure was developed which gives results capable of giving better predictions from the model. The flame height and heat feedback to the unburned

wall were also examined and more information obtained. It was found that the geometry associated with a wall fire affect the flame height and heat transfer. However, further research is still needed to understand the geometry effect.

With the modifications according to the geometry, the model was found to give good agreement with experimental measurements of vertical spread on sheets of PMMA. Two additional cases were studied: wall fires influenced by an inert parallel wall and by the proximity of a corner (with a floor). The measurement of flame height and heat feedback provides data for further investigation and modelling work.

Chapter 7

References

Ahmad T and Faeth GM, Turbulent wall fires, 17th Symposium (International) on combustion, pp. 1149~1160, 1978

Akita K, Some Problem of Flame Spread along a Liquid Surface, 14th Symposium (International) on combustion, pp. 1075~1083, 1973

Altenkirch RA, Eichhorn R and Shang PC, Buoyancy Effects on Flames Spreading Down Thermally Thin Fuels, Combustion and Flame, Vol. 37, pp. 71~83, 1980

Anderson M and McKeever C, An Experimental study of upward flame spread on cellulosic materials, Proceedings of the Seventh International Fire Safety and Engineering Conference INTERFLAM'96, pp. 169-178, 1996

Annamalai K and Sibulkin M, Flame spread over combustible surfaces for laminar flow system II: flame heights and fire spread rate, Combustion Science and Technology, Vol. 19, pp. 185, 1979

Babrauskas V, The cone calorimeter, Chap.3, Sec.3, The SFPE Handbook of Fire Protection Engineering, 2nd Edition, pp. 3-37~3-52, 1995

Beck VR, Performance based fire safety design- recent development in Australia, Fire Safety Journal, Vol. 23, pp. 133-158, 1994

Beyler CL, Hunt SP, Iqbal N and Williams FW, A computer model of upward flame spread on vertical surfaces, Fire Safety Science- Proceedings of the Fifth International Symposium, pp. 297-308, 1997

Bhattacharjee S, Altenkirch RA, Olson SL and Sotos RG, J. of Heat Transfer, Vol. 113, pp. 670, 1991

Brehob EG, Kim CI and Kulkarni AK, Numerical model of upward flame spread on practical wall materials, Fire safety Journal, Vol. 36, pp.225-240, 2001

Brehob EG and Kulkarni AK, Time dependent mass loss rate behavior of wall materials under external radiation, Fire and Materials, Vol. 17, 249-254, 1989

Brehob E and Kulkarni AK, Experimental Measurements of Upward Flame Spread on a Vertical Wall with External Radiation, Fire Safety Journal, Vol.31, pp.181-200, 1998

BSI, Fire safety engineering in buildings, Draft for development, DD240, 1997

Chitty R and Cox G, A method for measuring combustion intermittency in fires, Fire and Materials, Vol. 3, pp. 238-242, 1979

Coutin M, Most JM, Delichatsios MA and Delichatsios MM, Flame heights in wall fires: effects of width, confinement and pyrolysis length, Fire Safety Science- Proceedings of the Sixth International Symposium, pp. 729-740, 1999

Cox G, Compartment Fire Modelling, Combustion Fundamentals of Fires, Chapter 6, editor: G. Cox, 1995

Cox G and Kumar S, Modelling enclosure fires using CFD, SFPE handbook, 3rd edition, 2000

Custer RLP and Meacham BJ, Introduction to performance-based fire safety, SFPE and NFPA, 1997

Delichatsios MA, Strong turbulent plumes I: similarity, Combustion Science and Technology, Vol. 24, pp. 191, 1981

Delichatsios MA, Turbulent convective flows and burning on vertical walls, 19th Symposium (International) on combustion, pp. 855~868, 1982

Delichatsios MA, Flame heights in buoyant diffusion flames and a new material flammability number, FMRC, 1983

Delichatsios MA, Flame Heights in Turbulent Wall Fires with Significant Flame Radiation, Combustion Science and Technology, Vol. 39, pp. 195-214, 1984

Delichatsios MA and Chen Y, Flame spread on charring materials: numerical predictions and critical conditions, Fire Safety Science- Proceedings of the Fourth International Symposium, pp. 457-468, 1995

Delichatsios MA and Delichatsios MM, Effects of transient pyrolysis on wind-assisted and upward flame spread, Combustion and Flame, Vol. 89, pp. 5-16, 1992

Delichatsios MA and Delichatsios MM, Upward flame spread and critical conditions for PE/PVC cables in a tray configuration, Fire Safety Science- Proceedings of the Fourth International Symposium, pp. 433-444, 1995

Delichatsios MA, Delichatsios MM and Chen Y, Simularity solutions and applications to turbulent upward flame spread on noncharring materials, Combustion and Flame, Vol. 102, pp. 357-370, 1995

Delichatsios MM, Mathews MK and Delichatsios MA, An Upward Fire Spread and Growth Simulation, Fire Safety Science- Proceedings of the Third International Symposium, pp. 207-216, 1991

Delichatsios MM and Saito K, Upward fire spread: Key flammability properties, simularity solutions and flammability indices, Fire Safety Science- Proceedings of the Third International Symposium, pp. 217-226, 1991

de Ris, JN, Spread of a laminar diffusion flame, 12th Symposium (International) on combustion, pp. 241~252, 1968

de Ris JN and Orloff L, The role of buoyancy direction and radiation in turbulent diffusion flames on surfaces, 15th Symposium (International) on combustion, pp. 175~182, 1974

Drysdale DD, An Introduction to Fire Dynamics, pp. 233~262, 1998

Drysdale DD and Macmillan AJR, Flame spread on inclined surfaces, Fire safety Journal, Vol. 18, pp. 245-254, 1992

Eklund TI, A Vortex Model for Wall Flame Height, Journal of Fire Sciences, Vol.4-January/February, pp.4-14, 1986

Fernandez-Pello AC, A theoretical model for the upward laminar spread of flames over vertical fuel surfaces, Combustion and Flame, Vol.31, pp. 135~148, 1978

Fernandez-Pello AC, Flame spread modeling, Combustion Science and Technology, Vol. 39, pp. 119-134, 1984

Fernandez-Pello AC, The Solid Phase, Combustion Fundamentals of Fire (editor: Cox, G), Chapter 2, pp. 31~100, 1995

Fernandez-Pello AC and Hirano T, Controlling mechanisms of flame spread, Combustion Science and Technology, Vol. 32, pp.1-31, 1983

Fernandez-Pello AC and Quintiere J, A simplified model of radiating-turbulent-upward flame spread over the surface over a charring combustible, Fall meeting Eastern Section of the Combustion Institute, Altantic city, 1982

Fernandez-Pello AC and Williams FA, Experimental techniques in the study of laminar flame spread over solid combustibles, Combustion Science and Technology, Vol. 14, pp.155-167, 1976

Foley M and Drysdale DD, Heat Transfer from Flames between Vertical Parallel Walls, Fire Safety Journal, Vol.24, pp. 53-73, 1995

Friedman R, A survey of knowledge about idealized fire spread over surfaces, Fire Research Abstracts and Reviews, Vol. 10, pp. 1-8, 1968

FPA, Fire Protection Yearbook 1998/9, The Loss Prevention Council, Library of Fire Safety, Vol.1, 1998

Glassman I And Dryer FL, Flame Spreading across Liquid Fuels, Fire Safety J., Vol. 3, pp. 123~138, 1980

Goransson U and Wickstrom U, Flame spread predictions in the room/corner test based on the Cone Calorimeter, Interflam'90, pp. 211-219, 1990

Grant G and Drysdale D, Numerical Modelling of Early Flame Spread in Warehouse Fires, Fire Safety Journal, Vol.24, pp. 247-278, 1995

Hasemi Y, Experimental Wall Flame Heat Transfer Correlations for the Analysis of Upward Wall Flame Spread, Fire Science and Technology, Vol.4, No.2, pp. 75-90, 1984

Hasemi Y, Thermal Modeling of Upward Wall Flame Spread, Fire Safety Science-Proceedings of the First International Symposium, pp. 87-96, 1985

Hasemi Y, Diffusion flame modelling as a basic for the rational fire safety design of built environments, Fire Safety Science-Proceedings of the Sixth International Symposium, pp. 3~22, 2000

Hasemi Y and Tokunaga T, Some experimental aspects of turbulent diffusion flames and buoyant plumes from fire sources against a wall and in a corner of walls, Combustion Science and Technology, Vol.40, pp.1-17, 1984

Hasemi Y, Yoshida M, Nohara A. and Nakabayashi T., Unsteady-State Upward Flame Spreading Velocity along Vertical Combustible Solid and Influence of External Radiation on the Flame Spread, Fire Safety Science-Proceedings of the Third International Symposium, pp. 197~206, 1991

Hasemi Y, Yoshida M, Yasui N and Parker WJ, Upward flame spreading along a vertical solid for transient local heat release rate, Fire Safety Science-Proceedings of the Fourth International Symposium, pp. 385~396, 1995

Hasemi Y, Yoshida M, Takashima S, Kikuchi R and Yokobayashi Y, and Flame length and flame heat transfer correlations in corner-wall and corner-wall-ceiling configurations, Interflam'96, Seventh International Fire Science and Engineering Conference, 1996

Hirano T, Noreikis SE and Waterman TE, Postulations of flame spread mechanisms, Combustion and Flame, Vol. 22, pp. 353-363, 1974

Hirano T, Flame Propagation across Liquids-A Review of Gas Phase Phenomena, Fire Safety J., Vol. 21, pp. 207~229, 1993

Hokugo A, Hasemi Y, Hayashi Y and Yoshida M, Mechanism for the upward flame spread through balconies based on an investigation and experiments for a multi-story fire in high-rise apartment building, Fire Safety Science-Proceedings of the sixth International Symposium, pp. 649-660, 2000

Hottel HC and Hawthorne WR, 3rd Symposium (International) on Combustion, pp. 255-266, 1949

Huggett C, Estimation of rate of heat release by means of oxygen consumption measurement, Fire and Materials, Vol.4, No.2, pp. 61-65, 1980

Huggett C, von Elbe G, and Haggerty W, The combustiblity of materials in oxygen-helium and oxygen-nitrogen atmospheres, Brooks Air force Base, Report SAM-TR-66-85, 1965

ISO 5657, 'Fire Tests, Reaction to Fire. Ignitability of building products'. International Organisation for Standardisation, Geneva, 1997

ISO 5658, 'Fire Tests, Reaction to Fire. Lateral ignition and flame spread of building products'. International Organisation for Standardisation, Geneva, 1993

ISO 5660, 'Fire Tests, Reaction to Fire. Rate of heat release from building products'. International Organisation for Standardisation, Geneva, 1993

ISO 9705, Fire tests- 'full-scale room test for surface products', International Organisation for Standardisation, Geneva, 1993

Kanury A, Ignition of liquid Fuels, SFPE Handbook of Fire Protection engineering, Society of Fire Protection Engineers, First Edition, pp. 1-315-325, 1988

Karlsson B, A Mathematical Model for Calculating Heat Release Rate in the Room Corner Test, Fire Safety Journal, Vol.20, pp. 93-113, 1993

Karlsson B, Models for calculating flame spread on wall lining materials and the resulting heat release rate in a room, FSJ, Vol. 23, pp. 365-386, 1994

Karlsson B and Magnusson SE, Combustible wall lining materials: numerical simulation of room fire growth and the outline of a reliability based classification procedure, Fire Safety Science- Proceedings of the Third International Symposium, pp. 667-678, 1991

Karlsson B, Magnusson SE and Andersson B, Numerical simulation of room fire growth on combustible linings and a rational classification model, Interflam'90, pp. 43-54, 1990

Kashiwagi T, A study of flame spread over a porous material under external radiation fluxes, The Proceedings of the Fifteenth Symposium (International) on Combustion, pp.255-265, 1974

Kim JS, de Ris J and Kroesser FW, Laminar free-convective burning of fuel surfaces, The Proceedings of the 13th Symposium (International) on Combustion, pp.949-961, 1971

Kim JS, de Ris J and Kroesser FW, Laminar burning between parallel fuel surfaces, Int. J. of Heat Transfer, Vol.17, pp. 439-451, 1974

Kim CI, Upward flame spread on vertical walls, PhD Thesis, The Pennsylvania State University, University Park, PA, 1992

Kokkala MA, Characteristics of a flame in an open corner of walls, Interflam'93 Conference, 1993

Kokkala MA, Baroudi D and Parker WJ, Upward Flame Spread on Wooden Surface Products: Experiments and Numerical Modelling, Fire Safety Science- Proceedings of the Fifth International Symposium, pp. 309-320, 1997

Kulkarni A and Fisher SJ, Upward flame spread on vertical walls: an approximate but complete model and experiments, Heat Transfer and Combustion System- ASME Winter Meeting, pp. 53-61, 1989

Kung H-C, The burning of vertical wooden slabs, The Proceedings of the Fifteenth Symposium (International) on Combustion, pp.243-253, 1974

Lewis B and von Elbe G, Combustion, Flames and Explosions of Gases, 3rd edition, Academic Press, Orlando, FL, 1987

Lewis MJ, Rubini PA and Moss JB, Field modelling of non-charring flame spread, Fire Safety Science- Proceedings of the Sixth International Symposium, pp. 683-694, 1999

Liburdy JA and Faeth GM, Heat transfer and mean structure of a turbulent thermal plume along a vertical isothermal wall, Journal of Heat Transfer, Vol.100, pp. 177-183, 1978

Loh HT and Fernandez-pello AC, A study of the mechanisms of flow assisted flame spread, The Proceedings of the 20th Symposium (International) on Combustion, pp.1575, 1984

Mackinven R, Hansel J and Glassman I, Combustion Science and Technology, Vol.1, p293, 1970

Magee RS and McAlevy RF, The Mechanism of Flame Spread, J. of Fire and Flammability, Vol. 2, pp. 271~297, 1971

Markstein GH and de Ris J, Upward fire spread over textiles, 14th Symposium (International) on combustion, pp. 1085~1097, 1973

McAlevy RF and Magee RS, The Mechanism of Flame Spreading over the Surface of Ignition Condensed-Phase Materials, 12th Symposium (International) on combustion, pp. 215~227, 1969

Mitler HE, Algorithm for the mass loss rate of a burning wall, Fire Safety Science-Proceedings of the Second International Symposium, pp. 179-188, 1989

Mitler HE, Predicting the spread rates of fires on vertical surfaces, 23rd Symposium (International) on combustion, pp. 1715~1721, 1990

Most JM, Bellin B, Joulain P and Sztal B, Interaction between two burning vertical walls, Fire Safety Science- Proceedings of the Second International Symposium, pp. 285-294, 1989

Mowrer FW and Williamson RB, Flame spread evaluation for thin interior finish materials, Fire Safety Science- Proceedings of the Third International Symposium, pp. 689-698, 1991

Nakakuki A, Flame Spread over Solid and Liquid Fuels, J. of Fire and Flammability, Vol.7, pp.19~40, 1976

Nordtest, Surface products: Room fire tests in full scale, Nortest method NT Fire 025, 1986

Ohlemiller TJ and Cleary TG, Upward Flame spread on Composite Materials, ASC Symposium Series 599, Fire and Polymers II, American Chemical Society, Vol.32, pp.422-434, 1995

Ohlemiller TJ and Cleary TG, Upward Flame spread on Composite Materials, Fire Safety Journal, Vol.32, pp.159-172, 1999

Ohlemiller TJ, Cleary TG and Sheilds J, Effect of ignition conditions on upward flame spread on a composite material in a corner configuration, Fire Safety Journal, Vol.31, pp.331-344, 1998

Orloff L, de Ris J and Markstein GH, Upward turbulent fire spread and burning of fuel surface, 15th Symposium (International) on combustion, pp. 183~192, 1974

Orloff L, Modak AT and Alpert RL, Burning of large-scale vertical surfaces, 16th Symposium (International) on combustion, pp. 1345~1354, 1976

Ostman BAL and Nussbaum RM, Correlation between small-scale rate of heat release and full-scale room flashover for surface linings, Fire Safety Science- Proceedings of the Second International Symposium, pp. 823-832, 1989

Qian C, Ishida H and Saito K, Upward flame spread along PMMA vertical corner walls partII: Mechanism of "M" shape pyrolysis front formation, Combustion and Flame, Vol. 99, pp. 331-338, 1994

Qian C and Saito K, An empirical model for upward flame spread over vertical flat and corner walls, Fire Safety Science- Proceedings of the Fifth International Symposium, pp. 285-296, 1997

Quintiere JG, A simulation model for fire growth on materials subject to a room-corner test, Fire Safety Journal, Vol. 20, pp. 313-340, 1993

Quintiere JG, Surface Flame Spread, The SFPE Handbook of Fire Protection Engineering 2nd Edition, Section 2, Chapter 14, pp.2-205~2-216, 1995

Quintiere JG, Fire Growth: An Overview, J. of Fire Technology, pp.7~31, 1998

Quintiere JG and Cleary TG, Heat flux from flames to vertical surfaces, J. of Fire Technology, pp.209~231, 1994

Quintiere JG, Harkleroad M, New concept for measuring flame spread properties, NBSIR 84-2943, NBS, 1985

Quintiere JG, Harkleroad M and Hasemi Y, Wall Flames and Implications for Upward Flame spread, Combustion Science and Technology, Vol. 48, pp. 191-222, 1986

Quintiere JG and Lee CH, Ignitor and thickness effects on upward flame spread, Fire Technology, Vol.34, No.1, pp.18-38, 1998

Ray SR, Fernandez-Pello AC and Glassman I., A study of the heat transfer mechanisms in horizontal flame propagation, J. of Heat Transfer, Vol. 102, pp. 357-363, 1980

Saito K, Quintiere JG and Williams FA, Upward Turbulent Flame Spread, Fire Safety Science- Proceedings of the First International Symposium, pp. 75-86, 1985

Sibulkin M, Kim J The dependence of flame propagation on surface heat transfer: II upward burning, Combustion Science and Technology, Vol.17, pp.39~49, 1977

Sibulkin M, Kim J and Creeden JV Jr., The dependence of flame propagation rates on surface heat transfer, Combustion Science and Technology, Vol.14, pp.43~, 1975

Simms DL, On the pilot ignition of wood by radiation, Combustion and Flame, Vol.7, pp.253-261, 1963

Sirignano WA and Glassman I, Flame Spreading above Liquid Fuels: Surface-Tension-Driven Flows, Combustion Science and Technology, Vol.1, pp.307~312, 1970

Smith DA, Measurements of flame length and flame angle in an inclined trench, Fire Safety Journal, Vol. 18, pp. 231-244, 1992

Smith EE and Satija S, Release rate model for developing fires, J. of Heat Transfer, Vol.105, pp. 281-287, 1983

Steward FR, Linear flame heights for various fuels, Combustion and Flame, Vol. 8, pp. 171-178, 1964

Sugawa O, Satoh H and Oka Y, Flame Height from Rectangular Fire Sources Considering Mixing Factor, Fire Safety Science- Proceedings of the Third International Symposium, pp. 435-444, 1991

Sundstrom B, Classification of Wall and Ceiling Linings, Proceedings of EUREFIC Seminar, pp. 23-33, 1991

Suzuki M, Dobashi R and Hirano T, Behaviour of fire spreading downward over thick paper, 25th Symposium (International) on combustion, pp. 1439~1446, 1994

Tamanini F, A numerical model for the prediction of radiation-controlled turbulent wall fires, 17th Symposium (International) on combustion, pp. 1075~1085, 1978

Tamanini F and Ahmad T, Modeling of buoyant turbulent flames over combustible walls, 7th International Colloquium on gas dynamics of explosions and reactive systems, W Germany, 1979

Tamanini F and moussa AM, Experiments on the turbulent burning of vertical parallel walls, Combustion Science and Technology, Vol. 23, pp. 143-151, 1980

Thomas PH, On concurrent upward surface spread of flame, Fire Safety J, Vol. 22, pp. 89-99, 1994

Thomas PH, The growth of fire- ignition to full involvement, Combustion Fundamentals of Fire (editor: Cox, G), Chapter 5, pp. 273~328, 1995

Thomas PH, Webster CT and Raftery MM, Some experiments on buoyant diffusion flames, Combustion and Flame, Vol.5, pp. 359-367, 1961

Thornton WM, The relation of oxygen to the heat of combustion of organic compounds, Philosophical Magazine, Vol.33, pp. 196-203, 1917

Tu KM and Quintiere JG, Wall Flame Heights with External Radiation, Fire Technology, pp.195-203, 1991

Turnbull J and Will G, 4th Year Honours Thesis, Spread of flame on wall lining materials, School of Civil and Environmental Engineering, the University of Edinburgh, 1999.

Wang HY, Torero JL and Joulain P, Calculation of vertical parallel wall fires with buoyancy-induced flow, Fire Safety Science- Proceedings of the Sixth International Symposium, pp. 671-682, 1999

Watson L and Gamble J, Fire Statistics United Kingdom 1998, Home Office Statistical Bulletin, 1999

Wichman IS, Review of flame spread, Progress in Energe and Combustion Science, Vol. 18, pp. 553, 1992

Williams FA, Mechanism of Fire Spread, 16th Symposium (International) on combustion, pp. 1281~1294, 1977

Williamson RB and Dembsey NA, Advances in assessment methods for fire safety, Proceedings of the Interflam' 90 Conference, pp. 389-416, 1990

Woodburn PJ and Drysdale DD, Fires in inclined trenches: the dependence of the critical angle on the trench and burner geometry, Fire Safety Journal, Vol.31, pp. 143-164, 1998

Wu PK, Delichatsios MM and de Ris J, Upward fire spread over PMMA walls- A model/experiment comparison, 1993 Annual Conference on fire research, NIST, pp. 7-10, 1993

Zabetakis MG, Flammability characteristics of combustible gases and vapours, US Bureau of Mines, Bulletin 627, 1965

Zukoski EE, Properties of fire plumes, Combustion Fundamentals of Fires, (editor: Cox, G), pp.101-220, 1995

Appendix A

Experimental Data

A-1 Measurements of Flame Heights and Corresponding RHR per unit width on Steady Burning PMMA Samples

A-2 Measurements of Pyrolysis Heights, Flame Heights and Heat Fluxes Carried out on Spreading PMMA Fires

A-3 Measurements of Flame Heights and Heat Fluxes to the Unburned Surfaces in Gas Panel Tests

A-4 Measurements of Flame Heights and Heat Fluxes to the Unburned Surfaces on PMMA Wall Fires in a Corner

A-5 Measurements of Flame Heights, Heat Fluxes to the Unburned Surfaces and Heat Fluxes to the Opposing Wall on PMMA Wall Fires with the influence of a Parallel Inert Wall

A-1 – Measurements of flame heights and corresponding RHR per unit width on steady burning PMMA samples

Case A

Height (m)	Width (m)	Total RHR Q (kW)	RHR per unit width Q'(kW/m)	Thickness (mm)	Flame height (m)
0.025	0.08	0.3424	4.28	6	0.075
0.025	0.08	0.3832	4.79	6	0.09
0.025	0.08	0.376	4.7	6	0.09
0.05	0.04	0.3	7.5	6	0.13
0.05	0.04	0.2808	7.02	6	0.125
0.05	0.08	0.6976	8.72	6	0.17
0.05	0.08	0.6376	7.97	6	0.15
0.05	0.08	0.676	8.45	6	0.16
0.05	0.08	0.5496	6.87	6	0.14
0.05	0.08	0.6688	8.36	6	0.17
0.05	0.08	0.684	8.55	6	0.175
0.05	0.08	0.5672	7.09	6	0.145
0.05	0.085	0.7956	9.36	6	0.185
0.05	0.135	1.1664	8.64	6	0.14
0.05	0.135	1.39185	10.31	6	0.18
0.05	0.14	1.526	10.9	6	0.19
0.075	0.04	0.3832	9.58	6	0.175
0.075	0.04	0.388	9.7	6	0.18
0.075	0.08	0.9688	12.11	6	0.245
0.075	0.08	1.0224	12.78	6	0.255
0.075	0.08	1.0048	12.56	6	0.245
0.1	0.04	0.4424	11.06	6	0.19
0.1	0.04	0.472	11.8	6	0.195
0.1	0.08	1.4152	17.69	6	0.31
0.1	0.08	1.3136	16.42	6	0.325
0.1	0.08	1.38	17.25	6	0.33
0.1	0.08	1.3984	17.48	6	0.31
0.1	0.08	1.4608	18.26	6	0.335
0.1	0.08	1.2648	15.81	6	0.305
0.1	0.08	1.1416	14.27	6	0.29
0.1	0.08	1.4736	18.42	6	0.32
0.1	0.08	1.3432	16.79	6	0.31
0.1	0.08	1.48	18.5	6	0.325
0.1	0.08	1.3792	17.24	6	0.3
0.1	0.08	1.2224	15.28	6	0.32
0.1	0.08	1.4376	17.97	6	0.325
0.1	0.08	1.3112	16.39	6	0.3
0.1	0.08	1.3992	17.49	6	0.31
0.1	0.08	1.452	18.15	6	0.325

0.1	0.08	1.5496	19.37	6	0.335
0.1	0.08	1.1824	14.78	6	0.28
0.1	0.08	1.4328	17.91	6	0.32
0.1	0.14	2.5732	18.38	6	0.335
0.1	0.14	2.5998	18.57	6	0.35
0.15	0.08	1.1528	14.41	6	0.38
0.15	0.12	1.8996	15.83	6	0.39
0.2	0.04	0.7912	19.78	6	0.34
0.2	0.08	1.44	18	6	0.4
0.2	0.08	1.5352	19.19	6	0.45
0.2	0.12	2.16	18	6	0.49
0.2	0.12	2.3256	19.38	6	0.51
0.25	0.04	0.9488	23.72	6	0.42
0.25	0.04	1.1164	27.91	6	0.45
0.25	0.04	1.2	30	6	0.44
0.25	0.04	1.508	37.7	6	0.5
0.25	0.08	1.6	20	6	0.51
0.05	0.08	0.716	8.95	12.5	0.165
0.05	0.08	0.7072	8.84	12.5	0.165
0.15	0.08	1.1704	14.63	12.5	0.35
0.15	0.08	1.128	14.1	12.5	0.33
0.25	0.08	1.6	20	12.5	0.48
0.25	0.08	1.7272	21.59	12.5	0.48
0.05	0.08	0.716	8.95	25	0.165
0.05	0.08	0.708	8.85	25	0.165
0.15	0.08	1.0968	13.71	25	0.33
0.25	0.08	1.8656	23.32	25	0.5

Case B

Height (m)	Width (m)	Total RHR Q (kW)	RHR per unit width Q'(kW/m)	Thickness (mm)	Flame height (m)
0.025	0.08	0.4456	5.57	6	0.1
0.025	0.08	0.512	6.4	6	0.12
0.025	0.08	0.408	5.1	6	0.09
0.025	0.08	0.4904	6.13	6	0.123
0.025	0.08	0.4696	5.87	6	0.11
0.05	0.04	0.3424	8.56	6	0.14
0.05	0.04	0.3444	8.61	6	0.14
0.05	0.08	0.6032	7.54	6	0.145
0.05	0.08	0.8328	10.41	6	0.195
0.05	0.08	0.612	7.65	6	0.145
0.05	0.08	0.8032	10.04	6	0.185
0.05	0.08	0.6472	8.09	6	0.15
0.05	0.08	0.8352	10.44	6	0.19
0.075	0.04	0.5632	14.08	6	0.205
0.075	0.04	0.4124	10.31	6	0.18
0.075	0.08	1.0448	13.06	6	0.25
0.075	0.08	1.0936	13.67	6	0.25
0.075	0.08	0.768	9.6	6	0.165
0.075	0.08	1.0984	13.73	6	0.255
0.1	0.04	0.54	13.5	6	0.215
0.1	0.04	0.48	12	6	0.2
0.1	0.08	1.5832	19.79	6	0.31
0.1	0.08	1.4328	17.91	6	0.31
0.1	0.08	1.4488	18.11	6	0.32
0.1	0.08	1.556	19.45	6	0.34
0.1	0.08	1.5	18.75	6	0.32
0.1	0.08	1.692	21.15	6	0.35
0.1	0.08	1.7776	22.22	6	0.36
0.1	0.08	1.54	19.25	6	0.33
0.25	0.04	0.8	20	6	0.38
0.25	0.08	1.9936	24.92	6	0.51
0.25	0.12	3.3276	27.73	6	0.6
0.05	0.085	1.08205	12.73	12.5	0.195
0.05	0.085	0.99705	11.73	12.5	0.19
0.15	0.08	1.7752	22.19	12.5	0.41
0.15	0.08	1.3712	17.14	12.5	0.36
0.25	0.08	2.4	30	12.5	0.5
0.25	0.08	2.4	30	12.5	0.52
0.25	0.08	2	25	12.5	0.48
0.25	0.08	2.4	30	12.5	0.55
0.15	0.08	1.2008	15.01	25	0.34
0.25	0.08	1.9832	24.79	25	0.46

Case C

Height (m)	Width (m)	Total RHR Q (kW)	RHR per unit width Q'(kW/m)	Thickness (mm)	Flame height (m)
0.05	0.08	0.656	8.2	6	0.165
0.05	0.08	0.5672	7.09	6	0.16
0.05	0.08	0.5952	7.44	6	0.165
0.1	0.08	0.9272	11.59	6	0.24
0.1	0.08	0.8256	10.32	6	0.23
0.1	0.08	0.8864	11.08	6	0.235
0.15	0.08	1.1608	14.51	6	0.32
0.15	0.08	1.2744	15.93	6	0.35
0.15	0.08	1.0824	13.53	6	0.31
0.2	0.08	1.3784	17.23	6	0.385
0.2	0.08	1.3808	17.26	6	0.39
0.2	0.08	1.4176	17.72	6	0.39
0.25	0.08	1.7592	21.99	6	0.44
0.25	0.08	1.7392	21.74	6	0.45
0.25	0.08	1.6464	20.58	6	0.43

Case D

Height (m)	Width (m)	Total RHR Q (kW)	RHR per unit width Q'(kW/m)	Thickness (mm)	Flame height (m)
0.025	0.08	0.3328	4.16	6	0.075
0.025	0.08	0.3656	4.57	6	0.07
0.025	0.08	0.3992	4.99	6	0.075
0.05	0.04	0.33	8.25	6	0.14
0.05	0.04	0.3472	8.68	6	0.145
0.075	0.04	0.4084	10.21	6	0.18
0.075	0.04	0.3964	9.91	6	0.17
0.1	0.08	0.9936	12.42	6	0.23
0.1	0.08	1.2208	15.26	6	0.25
0.1	0.08	1.0936	13.67	6	0.25
0.15	0.08	1.25	15.62	6	0.36
0.15	0.08	1.26	15.75	6	0.35
0.15	0.08	1.208	15.1	6	0.375
0.15	0.12	1.9692	16.41	6	0.43
0.2	0.04	0.6504	16.26	6	0.33
0.2	0.08	1.4504	18.13	6	0.41
0.2	0.12	2.3952	19.96	6	0.53
0.2	0.08	1.5	18.85	6	0.41
0.2	0.08	1.539	19.35	6	0.42
0.25	0.08	1.702	21.28	6	0.45
0.25	0.08	1.7856	22.32	6	0.475
0.15	0.08	1.1352	14.19	12.5	0.33
0.15	0.08	1.0528	13.16	12.5	0.33
0.05	0.085	0.782	9.2	25	0.17
0.05	0.085	0.7956	9.36	25	0.175
0.15	0.08	1.3024	16.28	25	0.34

A-2 - Measurements of Pyrolysis Heights, Flame Heights and Heat Fluxes Carried out on Spreading PMMA Fires

20 cm high PMMA samples without sidewalls

(test 1)

Xp (mm)	Time (s)	Rate of Spread (mm/s)	Flame height (mm)	X/Xf	(X-Xp)/ (Xf-Xp)	X-Xf (m)	Heat Flux (kW/m^2)	HF/HF_0
10	19	0.53	30	5.33	7.5	0.13	1.76	0.055
20	24	2.00	40	4	7	0.12	1.5	0.046875
30	30.5	1.54	50	3.2	6.5	0.11	1.17	0.036563
40	42	0.87	75	2.13	3.428	0.085	2.96	0.0925
50	54.5	0.80	100	1.6	2.2	0.06	3.67	0.114688
60	64.5	1.00	120	1.33	1.666	0.04	6.15	0.192188
70	77.5	0.77	150	1.06	1.125	0.01	7.65	0.239063
80	89.5	0.83	170	0.94	0.888	-0.01	10.6	0.33125
90	96.5	1.43	190	0.84	0.7	-0.03	13	0.40625
100	110.5	0.71	200	0.8	0.6	-0.04	16.49	0.515313
110	123	0.80	204.17	0.78	0.530	-0.044	18	0.5625
120	130.5	1.33	220.81	0.72	0.396	-0.060	20	0.625
130	140.5	1.00	237.30	0.67	0.279	-0.077	21	0.65625
140	154.5	0.71	253.67	0.63	0.175	-0.093	25	0.78125
150	171	0.61	269.92	0.59	0.083	-0.109	27.6	0.8625

(test 2)

Xp (mm)	Time (s)	Rate of Spread (mm/s)	Flame height (mm)	X/Xf	(X-Xp)/ (Xf-Xp)	X-Xf (m)	Heat Flux (kW/m^2)	HF/HF_0
10	19	0.53	35	4.57	6	0.125	2.06	0.064375
20	24	2.00	40	4	7	0.12	2.6	0.08125
30	32	1.25	50	3.2	6.5	0.11	3	0.09375
40	43.5	0.87	60	2.66	6	0.1	4.5	0.140625
50	54.5	0.91	100	1.6	2.2	0.06	8.2	0.25625
60	65.5	0.91	120	1.33	1.666	0.04	7.9	0.246875
70	78	0.80	150	1.06	1.125	0.01	9.3	0.290625
80	88.5	0.95	175	0.91	0.842	-0.015	17	0.53125
90	101.5	0.77	190	0.84	0.7	-0.03	16.5	0.515625
100	113.5	0.83	200	0.8	0.6	-0.04	18.2	0.56875
110	123.5	1.00	200.0	0.79	0.55	-0.04	21	0.65625
120	136.5	0.77	215.7	0.74	0.417	-0.05	23	0.71875
130	150.5	0.71	231.2	0.69	0.29	-0.07	27	0.84375
140	160.5	1.00	246.7	0.64	0.187	-0.08	27.6	0.8625
150	172	0.87	261.9	0.61	0.089	-0.10	30.6	0.95625

30 cm high PMMA samples without sidewalls

(test 1)

Xp (mm)	Time (s)	Rate of Spread (mm/s)	Flame height (mm)	X/Xf	(X-Xp)/ (Xf-Xp)	X-Xf (m)	Heat Flux (kW/m^2)	HF/HF_0
10	17	0.59	35	7.428	10	0.225	0.59	0.019032
20	23	1.67	40	6.5	12	0.22	0.7	0.022581
30	29	1.67	45	5.777	15.33	0.215	0.88	0.028387
40	45	0.63	65	4	8.8	0.195	1.7	0.054839
50	55	1.00	80	3.25	7	0.18	2.06	0.066452
60	65	1.00	115	2.26	3.636	0.145	2.35	0.075806
70	75	1.00	125	2.08	3.454	0.135	3.1	0.1
80	86	0.91	145	1.793	2.769	0.115	3.4	0.109677
90	97	0.91	160	1.625	2.428	0.1	4.2	0.135484
100	107	1.00	180	1.444	2	0.08	5.1	0.164516
110	117	1.00	200	1.3	1.666	0.06	5.75	0.185484
120	132	0.67	215	1.209	1.473	0.045	6.47	0.20871
130	141	1.11	230	1.130	1.3	0.03	6.47	0.20871
140	153	0.83	240	1.083	1.2	0.02	8.5	0.274194
150	165	0.83	250	1.04	1.1	0.01	8.83	0.284839
160	179	0.71	280	0.928	0.833	-0.02	11.77	0.379677
170	191	0.83	290	0.896	0.75	-0.03	11.18	0.360645
180	201	1.00	300	0.866	0.666	-0.04	13.53	0.436452
190	211	1.00	307.3	0.845	0.59	-0.04	14.12	0.455484
200	225	0.71	321.4	0.808	0.494	-0.06	15.3	0.493548
210	235	1.00	335.3	0.775	0.398	-0.075	16.3	0.525806
220	247	0.83	349.8	0.744	0.309	-0.089	20	0.645161
230	260	0.77	362.9	0.716	0.225	-0.102	21.2	0.683871
240	266	1.67	376.6	0.690	0.146	-0.11	22.5	0.725806
250	274	1.25	390.2	0.666	0.071	-0.13	25	0.806452

(test 2)

Xp (mm)	Time (s)	Rate of Spread (mm/s)	Flame height (mm)	X/Xf	(X-Xp)/ (Xf-Xp)	X-Xf (m)	Heat Flux (kW/m^2)	HF/HF_0
10	16	0.63	35	7.428	10	0.225	0.75	0.024194
20	19	3.33	40	6.5	12	0.22	0.88	0.028387
30	22	3.33	45	5.777	15.33	0.215	0.88	0.028387
40	39	0.59	70	3.714	7.333	0.19	1.47	0.047419
50	49	1.00	100	2.6	4.2	0.16	2.06	0.066452
60	62	0.77	120	2.166	3.333	0.14	2.7	0.087097
70	72	1.00	140	1.857	2.714	0.12	3.35	0.108065
80	81	1.11	160	1.625	2.25	0.1	3.82	0.123226
90	88	1.43	170	1.529	2.12	0.09	3.5	0.112903
100	98	1.00	190	1.368	1.777	0.07	3.21	0.103548
110	110	0.83	210	1.238	1.5	0.05	5.89	0.19
120	122	0.83	230	1.130	1.272	0.03	6.47	0.20871
130	137	0.67	250	1.04	1.083	0.01	7.4	0.23871
140	149	0.83	270	0.966	0.923	-0.01	9.4	0.303226
150	163	0.71	290	0.896	0.785	-0.03	9.8	0.316129
160	171	1.25	300	0.866	0.714	-0.04	10.6	0.341935
170	185	0.71	304.3	0.854	0.669	-0.044	12	0.387097
180	195	1.00	320.3	0.811	0.570	-0.060	13	0.419355
190	204	1.11	336.2	0.773	0.478	-0.076	16	0.516129
200	214	1.00	352.0	0.738	0.394	-0.092	18.5	0.596774
210	223	1.11	367.7	0.707	0.317	-0.107	21	0.677419
220	237	0.71	383.3	0.678	0.244	-0.123	24.5	0.790323
230	248	0.91	398.9	0.651	0.177	-0.138	25.2	0.812903
240	258	1.00	414.4	0.627	0.11	-0.154	28	0.903226
250	268	1.00	429.8	0.604	0.055	-0.169	30	0.967742

(test 3)

Xp (mm)	Time (s)	Rate of Spread (mm/s)	Flame height (mm)	X/Xf	(X-Xp)/ (Xf-Xp)	X-Xf (m)	Heat Flux (kW/m^2)	HF/HF_0
10	16	0.63	30	8.666	12.5	0.23	0.4	0.012903
20	23	3.33	40	6.5	12	0.22	0.65	0.020968
30	29	3.33	50	5.2	11.5	0.21	0.88	0.028387
40	40	0.59	70	3.714	7.333	0.19	1.17	0.037742
50	53	1.00	90	2.888	5.25	0.17	1.6	0.051613
60	66	0.77	120	2.166	3.333	0.14	2.6	0.083871
70	74	1.00	130	2	3.166	0.13	2.4	0.077419
80	86	1.11	150	1.733	2.571	0.11	3.4	0.109677
90	95	1.43	160	1.625	2.428	0.1	4	0.129032
100	105	1.00	170	1.529	2.285	0.09	4.4	0.141935
110	115	0.83	190	1.321	1.87	0.07	4.7	0.151613
120	125	0.83	210	1.238	1.555	0.05	5	0.16129
130	136	0.67	230	1.130	1.3	0.03	6	0.193548
140	147	0.83	250	1.04	1.090	0.01	7.1	0.229032
150	160	0.71	270	0.962	0.916	-0.01	8.83	0.284839
160	170	1.25	290	0.896	0.769	-0.03	10.59	0.341613
170	185	0.71	300	0.866	0.692	-0.04	11.5	0.370968
180	201	1.00	300.53	0.865	0.663	-0.040	14.72	0.474839
190	211	1.11	315.27	0.8246	0.558	-0.055	15.3	0.493548
200	226	1.00	329.93	0.7880	0.461	-0.069	18	0.580645
210	234	1.11	344.51	0.7546	0.371	-0.084	19.2	0.619355
220	249	0.71	359.00	0.7242	0.287	-0.099	21.787	0.702806
230	261	0.91	373.43	0.6962	0.209	-0.113	22.37	0.721613
240	271	1.00	387.78	0.6704	0.135	-0.12	24.72	0.797419
250	280	1.00	402.06	0.6466	0.065	-0.142	27.07	0.873226

40 cm high PMMA samples without sidewalls

(test 1)

Xp (mm)	Time (s)	Rate of Spread (mm/s)	Flame height (mm)	X/Xf	(X-Xp)/ (Xf-Xp)	X-Xf (m)	Heat Flux (kW/m^2)	HF/HF_0
10	18	0.56	30	12	17.5	0.33	0.58	0.019333
20	21	3.33	35	10.28	22.66	0.325	0.59	0.019667
30	26	2.00	45	8	22	0.315	0.74	0.024667
40	38	0.83	65	5.538	12.8	0.295	1.16	0.038667
50	52	0.71	90	4	7.75	0.27	1.47	0.049
60	64	0.83	110	3.272	6	0.25	1.47	0.049
70	74	1.00	130	2.769	4.833	0.23	1.47	0.049
80	83	1.11	150	2.4	4	0.21	1.7	0.056667
90	95	0.83	160	2.25	3.857	0.2	2	0.066667
100	109	0.71	180	2	3.25	0.18	2.06	0.068667
110	117	1.25	190	1.894	3.125	0.17	2.2	0.073333
120	129	0.83	205	1.756	2.823	0.155	3.23	0.107667
130	139	1.00	220	1.636	2.555	0.14	2.94	0.098
140	150	0.91	240	1.5	2.2	0.12	2.94	0.098
150	162	0.83	250	1.44	2.1	0.11	3.65	0.121667
160	173	0.91	260	1.384	2	0.1	4.1	0.136667
170	188	0.67	290	1.241	1.583	0.07	4.7	0.156667
180	200	0.83	310	1.161	1.384	0.05	4.7	0.156667
190	212	0.83	320	1.125	1.307	0.04	6	0.2
200	226	0.71	340	1.058	1.142	0.02	6.8	0.226667
210	240	0.71	350	1.028	1.071	0.01	7.65	0.255
220	249	1.11	370	0.972	0.933	-0.01	8.83	0.294333
230	260	0.91	380	0.947	0.866	-0.02	9.4	0.313333
240	273	0.77	400	0.9	0.75	-0.04	10.4	0.346667
250	281	1.25	405.1	0.888	0.708	-0.04	11.2	0.373333
260	293	0.83	419.9	0.857	0.625	-0.05	12.5	0.416667
270	307	0.71	434.6	0.828	0.546	-0.07	14.6	0.486667
280	315	1.25	449.3	0.801	0.472	-0.08	16.4	0.546667
290	324	1.11	463.9	0.775	0.402	-0.10	18.6	0.62
300	334	1.00	478.5	0.752	0.33	-0.11	18.8	0.626667
310	344	1.00	493.0	0.730	0.27	-0.13	20	0.666667
320	356	0.83	507.5	0.709	0.213	-0.14	23	0.766667
330	366	1.00	522.0	0.689	0.156	-0.16	27	0.9
340	375	1.11	536.4	0.671	0.101	-0.17	29.2	0.973333
350	385	1.00	550.8	0.653	0.049	-0.19	31.5	1.05

(test 2)

Xp (mm)	Time (s)	Rate of Spread (mm/s)	Flame height (mm)	X/Xf	(X-Xp)/ (Xf-Xp)	X-Xf (m)	Heat Flux (kW/m^2)	HF/HF_0
10	13	0.77	40	9	11.66	0.32	0.7	0.0233
20	20	1.43	50	7.2	11.33	0.31	0.88	0.0293
30	22	5.00	50	7.2	16.5	0.31	0.88	0.0293
40	34	0.83	70	5.142	10.66	0.29	1	0.0333
50	45	0.91	85	4.235	8.857	0.275	1.32	0.3896
60	56	0.91	100	3.6	7.5	0.26	1.6	0.0533
70	67	0.91	140	2.571	4.142	0.22	2	0.0666
80	75	1.25	150	2.4	4	0.21	2.2	0.0733
90	89	0.71	170	2.117	3.375	0.19	2.94	0.098
100	99	1.00	190	1.894	2.888	0.17	2.94	0.098
110	109	1.00	200	1.8	2.777	0.16	2.64	0.088
120	123	0.71	220	1.636	2.4	0.14	3.4	0.1133
130	136	0.77	235	1.531	2.190	0.125	3.85	0.1283
140	146	1.00	250	1.44	2	0.11	4.12	0.1373
150	156	1.00	260	1.384	1.909	0.1	4.3	0.1433
160	169	0.77	270	1.333	1.818	0.09	4.7	0.1566
170	184	0.67	300	1.2	1.461	0.06	4.7	0.1566
180	190	1.67	310	1.16	1.384	0.05	5.29	0.1763
190	199	1.11	320	1.125	1.307	0.04	5.89	0.1963
200	210	0.91	340	1.058	1.142	0.02	5.89	0.1963
210	222	0.83	350	1.028	1.071	0.01	6.5	0.2166
220	238	0.63	370	0.972	0.933	-0.01	7.65	0.255
230	250	0.83	380	0.947	0.866	-0.02	8.83	0.2943
240	262	0.83	400	0.9	0.75	-0.04	9.5	0.3166
250	272	1.00	406.33	0.885	0.703	-0.04	10.3	0.3433
260	283	0.91	419.94	0.857	0.625	-0.05	11.5	0.3833
270	293	1.00	433.47	0.830	0.550	-0.07	12.8	0.4266
280	303	1.00	446.91	0.805	0.479	-0.08	14.3	0.4766
290	312	1.11	460.28	0.782	0.411	-0.10	15	0.5
300	325	0.77	473.58	0.760	0.345	-0.11	18.6	0.62
310	335	1.00	486.80	0.739	0.282	-0.12	18.8	0.6266
320	346	0.91	499.96	0.720	0.222	-0.13	20	0.6666
330	356	1.00	513.05	0.701	0.163	-0.15	23	0.7666
340	369	0.77	526.0	0.684	0.107	-0.16	28.25	0.9416
350	377	1.25	539.0	0.667	0.052	-0.17	29.5	0.9833

(test 3)

Xp (mm)	Time (s)	Rate of Spread (mm/s)	Flame height (mm)	X/Xf	(X-Xp)/ (Xf-Xp)	X-Xf (m)	Heat Flux (kW/m^2)	HF/HF_0
10	13	0.77	30	12	17.5	0.33	0.294	0.0098
20	20	1.43	45	8	13.6	0.315	0.294	0.0098
30	25	2.00	55	6.545	13.2	0.305	0.294	0.0098
40	40	0.67	70	5.142	10.66	0.29	0.588	0.0196
50	54	0.71	95	3.789	6.888	0.265	1	0.0333
60	62	1.25	120	3	5	0.24	1.2	0.04
70	70	1.25	135	2.666	4.461	0.225	1.47	0.049
80	81	0.91	150	2.4	4	0.21	1.77	0.059
90	93	0.83	180	2	3	0.18	1.77	0.059
100	103	1.00	195	1.846	2.736	0.165	2.35	0.0783
110	114	0.91	210	1.714	2.5	0.15	2.6	0.0866
120	125	0.91	220	1.636	2.4	0.14	2.94	0.098
130	139	0.71	235	1.531	2.190	0.125	2.94	0.098
140	148	1.11	245	1.469	2.095	0.115	3.51	0.117
150	157	1.11	260	1.384	1.909	0.1	3.53	0.1176
160	173	0.63	280	1.285	1.666	0.08	3.7	0.1233
170	183	1.00	280	1.285	1.727	0.08	4.12	0.1373
180	194	0.91	300	1.2	1.5	0.06	4.7	0.1566
190	205	0.91	320	1.125	1.307	0.04	4.7	0.1566
200	219	0.71	330	1.090	1.230	0.03	5.29	0.1763
210	230	0.91	350	1.028	1.071	0.01	5.88	0.196
220	244	0.71	365	0.986	0.965	-0.005	5.89	0.1963
230	258	0.71	380	0.947	0.866	-0.02	7.6	0.2533
240	267	1.11	400	0.9	0.75	-0.04	8	0.2666
250	277	1.00	405.26	0.888	0.708	-0.04	8.24	0.2746
260	287	1.00	419.24	0.858	0.627	-0.05	9.2	0.3066
270	298	0.91	433.15	0.831	0.551	-0.07	11.7	0.39
280	306	1.25	447.00	0.805	0.479	-0.08	12.1	0.4033
290	315	1.11	460.77	0.781	0.409	-0.10	12.9	0.43
300	329	0.71	474.4	0.758	0.343	-0.11	15.3	0.51
310	340	0.91	488.14	0.737	0.280	-0.12	15.89	0.5296
320	347	1.43	501.73	0.717	0.220	-0.14	19.3	0.6433
330	355	1.25	515.26	0.698	0.161	-0.15	20.6	0.6866
340	370	0.67	528.7	0.680	0.105	-0.16	22.94	0.7646
350	378	1.25	542.17	0.663	0.052	-0.18	25.9	0.8633

50 cm high PMMA samples without sidewalls

(test 1)

Xp (mm)	Time (s)	Rate of Spread (mm/s)	Flame height (mm)	X/Xf	(X-Xp)/ (Xf-Xp)	X-Xf (m)	Heat Flux (kW/m^2)	HF/HF_0
10	23	0.43	35.00	13.14	18	0.425	0.29	0.01
20	28	2.00	40.00	11.5	22	0.42	0.29	0.01
30	35	1.43	50.00	9.2	21.5	0.41	0.45	0.015
40	51	0.63	80.00	5.75	10.5	0.38	0.88	0.030
50	62	0.91	100.00	4.6	8.2	0.36	0.88	0.030
60	72	1.00	125.00	3.68	6.153	0.335	0.95	0.032
70	87	0.67	140.00	3.285	5.571	0.32	1.17	0.040
80	96	1.11	160.00	2.875	4.75	0.3	1.17	0.040
90	102	1.67	175.00	2.628	4.352	0.285	1.25	0.043
100	114	0.83	190.00	2.421	4	0.27	1.47	0.05
110	124	1.00	210.00	2.190	3.5	0.25	1.6	0.055
120	142	0.56	230.00	2	3.090	0.23	1.76	0.06
130	149	1.43	250.00	1.84	2.75	0.21	1.76	0.060
140	158	1.11	260.00	1.769	2.666	0.2	2	0.068
150	168	1.00	270.00	1.703	2.583	0.19	2.33	0.080
160	180	0.83	290.00	1.586	2.307	0.17	2.35	0.081
170	192	0.83	300.00	1.533	2.230	0.16	2.4	0.082
180	203	0.91	310.00	1.483	2.153	0.15	2.7	0.093
190	215	0.83	330.00	1.393	1.928	0.13	3.25	0.112
200	229	0.71	340.00	1.352	1.857	0.12	3.53	0.121
210	239	1.00	350.00	1.314	1.785	0.11	3.53	0.121
220	255	0.63	360.00	1.277	1.714	0.1	4.12	0.142
230	260	2.00	370.00	1.243	1.642	0.09	4.12	0.142
240	272	0.83	390.00	1.179	1.466	0.07	4.5	0.155
250	286	0.71	400.00	1.15	1.4	0.06	5.5	0.189
260	296	1.00	420.00	1.095	1.25	0.04	5.88	0.202
270	308	0.83	430.00	1.069	1.18	0.03	6.3	0.217
280	318	1.00	450.00	1.022	1.058	0.01	7.6	0.262
290	327	1.11	480.00	0.958	0.894	-0.02	7.65	0.263
300	336	1.11	490.00	0.938	0.842	-0.03	8	0.275
310	342	1.67	500.00	0.92	0.789	-0.04	9	0.310
320	352	1.00	508.53	0.904	0.742	-0.048	10	0.344
330	361	1.11	522.12	0.881	0.676	-0.062	10	0.344
340	371	1.00	535.65	0.858	0.613	-0.076	10	0.34
350	381	1.00	549.12	0.83	0.552	-0.089	12.4	0.427
360	391	1.00	562.53	0.817	0.493	-0.102	12.9	0.444
370	400	1.11	575.89	0.798	0.43	-0.11	13.53	0.466
380	408	1.25	589.20	0.780	0.382	-0.129	14.6	0.503
390	416	1.25	602.46	0.763	0.329	-0.142	15.5	0.534
400	426	1.00	615.68	0.747	0.278	-0.155	18.4	0.634
410	434	1.25	628.84	0.731	0.228	-0.168	20	0.689
420	441	1.43	641.96	0.716	0.180	-0.181	21.78	0.751

430	451	1.00	655.03	0.702	0.133	-0.195	24.13	0.832
440	463	0.83	668.06	0.688	0.087	-0.208	27	0.931
450	470	1.43	681.05	0.675	0.043	-0.22	28.25	0.974

(test 2)

Xp (mm)	Time (s)	Rate of Spread (mm/s)	Flame height (mm)	X/Xf	(X-Xp)/ (Xf-Xp)	X-Xf (m)	Heat Flux (kW/m^2)	HF/HF_0
10	15	0.67	30	15.33	22.5	0.43	0.29	0.01
20	19	2.50	40	11.5	22	0.42	0.29	0.01
30	23	2.50	45	10.22	28.66	0.415	0.4	0.013
40	38	0.67	70	6.571	14	0.39	0.56	0.01
50	51	0.77	90	5.111	10.25	0.37	0.58	0.02
60	61	1.00	110	4.181	8	0.35	0.88	0.030
70	73	0.83	130	3.538	6.5	0.33	0.9	0.031
80	83	1.00	150	3.066	5.428	0.31	1.17	0.040
90	95	0.83	180	2.555	4.111	0.28	1.17	0.040
100	106	0.91	190	2.421	4	0.27	1.17	0.040
110	121	0.67	210	2.190	3.5	0.25	1.47	0.050
120	134	0.77	220	2.090	3.4	0.24	1.47	0.050
130	145	0.91	240	1.916	3	0.22	1.9	0.065
140	155	1.00	250	1.84	2.909	0.21	2.06	0.07
150	168	0.77	260	1.769	2.818	0.2	2.32	0.08
160	184	0.63	275	1.672	2.608	0.185	2.5	0.086
170	192	1.25	290	1.586	2.416	0.17	2.66	0.091
180	205	0.77	300	1.533	2.333	0.16	2.8	0.096
190	213	1.25	310	1.483	2.25	0.15	2.8	0.096
200	225	0.83	320	1.437	2.166	0.14	3.1	0.106
210	239	0.71	340	1.352	1.923	0.12	3.53	0.121
220	253	0.71	350	1.314	1.846	0.11	3.7	0.127
230	265	0.83	360	1.277	1.769	0.1	4.42	0.152
240	275	1.00	380	1.210	1.571	0.08	4.7	0.162
250	285	1.00	390	1.179	1.5	0.07	4.7	0.162
260	299	0.71	410	1.121	1.333	0.05	5.29	0.182
270	311	0.83	420	1.095	1.266	0.04	5.3	0.182
280	323	0.83	430	1.069	1.2	0.03	6.2	0.213
290	330	1.43	450	1.022	1.062	0.01	6.47	0.223
300	338	1.25	470	0.978	0.941	-0.01	6.47	0.223
310	346	1.25	480	0.958	0.882	-0.02	7.35	0.253
320	354	1.25	490	0.977	0.82	-0.03	7.9	0.272
330	367	0.77	500	0.92	0.764	-0.04	8.6	0.296
340	381	0.71	521.88	0.881	0.659	-0.061	10	0.344
350	390	1.11	535.38	0.859	0.593	-0.075	10.59	0.365
360	397	1.43	548.83	0.838	0.529	-0.088	12.2	0.42
370	405	1.25	562.24	0.81	0.468	-0.102	13.8	0.475
380	415	1.00	575.60	0.799	0.408	-0.115	15	0.517
390	424	1.11	588.92	0.781	0.351	-0.128	16	0.551

400	433	1.11	602.21	0.763	0.296	-0.142	18	0.620
410	441	1.25	615.45	0.742	0.243369	-0.155	20	0.689
420	451	1.00	628.65	0.731	0.191706	-0.168	22.36	0.771
430	459	1.25	641.82	0.716	0.14163	-0.181	22.95	0.791
440	466	1.43	654.95	0.702	0.093045	-0.194	25.5	0.87
450	479	0.77	668.05	0.688	0.045862	-0.20	28.25	0.974

50 cm high PMMA samples with sidewalls

(test 1)

Xp (mm)	Time (s)	Rate of Spread (mm/s)	Flame height (mm)	X/Xf	(X-Xp)/ (Xf-Xp)	X-Xf (m)	Heat Flux (kW/m^2)	HF/HF_0
10	16	0.63	20.00	23	45	0.44	0.2	0.005
20	22	1.67	30.00	15.33	44	0.43	0.19	0.0055
30	28	1.67	40.00	11.5	43	0.42	0.21	0.0061
40	42	0.71	70.00	6.571	14	0.39	0.23	0.0067
50	57	0.67	80.00	5.75	13.66	0.38	0.49	0.0144
60	65	1.25	100.00	4.6	10	0.36	0.78	0.0229
70	76	0.91	120.00	3.833	7.8	0.34	0.94	0.0276
80	89	0.77	150.00	3.066	5.42	0.31	1.01	0.0297
90	99	1.00	170.00	2.705	4.625	0.29	1.1	0.0323
100	109	1.00	190.00	2.421	4	0.27	1.4	0.0411
110	125	0.63	200.00	2.3	3.88	0.26	1.77	0.0520
120	137	0.83	210.00	2.190	3.77	0.25	2.01	0.0591
130	149	0.83	230.00	2	3.3	0.23	2.35	0.0691
140	158	1.11	250.00	1.84	2.909	0.21	2.56	0.0752
150	172	0.71	260.00	1.769	2.818	0.20	2.74	0.0805
160	188	0.63	280.00	1.642	2.5	0.18	2.98	0.0876
170	198	1.00	310.00	1.483	2.071	0.15	3.23	0.0
180	210	0.83	330.00	1.393	1.866	0.13	3.53	0.1038
190	220	1.00	340.00	1.352	1.8	0.12	3.62	0.1064
200	233	0.77	350.00	1.314	1.733	0.11	3.71	0.1091
210	246	0.77	360.00	1.277	1.666	0.10	3.78	0.1111
220	254	1.25	390.00	1.179	1.411	0.07	4.51	0.1326
230	267	0.77	410.00	1.121	1.277	0.05	5.28	0.1552
240	280	0.77	420.00	1.095	1.222	0.04	6.1	0.1794
250	294	0.71	450.00	1.022	1.05	0.01	7	0.2058
260	304	1.00	470.00	0.978	0.952	-0.01	7.66	0.2252
270	310	1.67	480.00	0.958	0.904	-0.02	8.2	0.2411
280	316	1.67	490.00	0.938	0.857	-0.03	9.1	0.2676
290	325	1.11	514.53	0.89	0.757	-0.05	10	0.2941
300	335	1.00	532.33	0.864	0.688	-0.07	11.2	0.3294
310	345	1.00	550.13	0.836	0.624	-0.09	13.6	0.4
320	354	1.11	567.93	0.809	0.564	-0.11	15.1	0.4441
330	362	1.25	585.73	0.785	0.508	-0.13	16.48	0.4847
340	375	0.77	603.53	0.762	0.455	-0.14	17.6	0.5176
350	381	1.67	621.33	0.740	0.4054	-0.16	18.8	0.5529
360	389	1.25	639.13	0.728	0.356	-0.18	20.02	0.5888
370	403	0.71	656.93	0.700	0.313	-0.20	21.5	0.6323

380	408	2.00	674.73	0.681	0.271	-0.21	23.1	0.6794
390	410	5.00	692.53	0.664	0.231	-0.23	24.3	0.7147
400	414	2.50	710.33	0.647	0.193	-0.25	25.1	0.7382
410	418	2.50	728.13	0.631	0.157	-0.27	27.07	0.7961
420	424	1.67	745.93	0.61	0.122	-0.29	29.12	0.8564
430	433	1.11	763.73	0.602	0.089	-0.30	31.2	0.9176
440	438	2.00	781.53	0.588	0.058	-0.32	33.3	0.9794
450	450						35.32	1.0388
460	480						41.21	1.2120
470	510						41.21	1.2120
480	540						42.38	1.2464
490	570						42.97	1.2638

(test 2)

Xp (mm)	Time (s)	Rate of Spread (mm/s)	Flame height (mm)	X/Xf	(X-Xp)/ (Xf-Xp)	X-Xf (m)	Heat Flux (kW/m^2)	HF/HF_0
10	10	1.00	20.00	23	45	0.44	0.23	0.007
20	28	0.56	30.00	15.33	44	0.43	0.23	0.007
30	46	0.56	50.00	9.2	21.5	0.41	0.56	0.018
40	49	3.33	70.00	6.571	14	0.39	0.79	0.026
50	57	1.25	100.00	4.6	8.2	0.36	0.94	0.031
60	67	1.00	115.00	4	7.27	0.345	1.08	0.036
70	79	0.83	130.00	3.538	6.5	0.33	1.11	0.037
80	90	0.91	145.00	3.172	5.846	0.315	1.18	0.039
90	100	1.00	170.00	2.705	4.62	0.29	1.34	0.044
100	110	1.00	190.00	2.421	4	0.27	1.57	0.052
110	122	0.83	210.00	2.190	3.5	0.25	1.77	0.059
120	134	0.83	230.00	2	3.090	0.23	2.06	0.068
130	144	1.00	240.00	1.916	3	0.22	2.3	0.076
140	158	0.71	260.00	1.769	2.666	0.2	2.42	0.080
150	166	1.25	270.00	1.703	2.583	0.19	2.5	0.083
160	176	1.00	290.00	1.586	2.307	0.17	2.92	0.097
170	192	0.63	310.00	1.483	2.071	0.15	3.21	0.107
180	201	1.11	320.00	1.43	2	0.14	3.5	0.116
190	215	0.71	340.00	1.352	1.8	0.12	3.6	0.12
200	227	0.83	360.00	1.277	1.625	0.1	3.69	0.123
210	237	1.00	390.00	1.179	1.388	0.07	3.77	0.125
220	253	0.63	410.00	1.121	1.263	0.05	4.2	0.14
230	260	1.43	440.00	1.045	1.095	0.02	4.7	0.156
240	268	1.25	460.00	1	1	0	5.3	0.176
250	284	0.63	470.00	0.978	0.954	-0.01	6.1	0.203
260	292	1.25	470.00	0.978	0.952	-0.01	6.9	0.23
270	300	1.25	480.00	0.958	0.9047	-0.02	7.65	0.255
280	308	1.25	515.83	0.891	0.7632	-0.055	8.6	0.286
290	324	0.63	534.23	0.861	0.6960	-0.074	9.6	0.32
300	332	1.25	552.63	0.832	0.6337	-0.092	10.64	0.354
310	342	1.00	571.03	0.805	0.574	-0.111	12.1	0.403
320	351	1.11	589.43	0.780	0.519	-0.129	13.8	0.46
330	357	1.67	607.83	0.779	0.4679	-0.147	15.3	0.51
340	369	0.83	626.23	0.734	0.4192	-0.166	16.3	0.543
350	376	1.43	644.63	0.713	0.373	-0.184	17.3	0.576

360	386	1.00	663.03	0.693	0.33	-0.203	18.3	0.61
370	392	1.67	681.43	0.675	0.288	-0.221	19.32	0.644
380	398	1.67	699.83	0.657	0.2501	-0.239	21.4	0.713
390	404	1.67	718.23	0.640	0.2132	-0.258	23.5	0.783
400	412	1.25	736.63	0.624	0.1782	-0.276	25.7	0.856
410	420	1.25	755.03	0.609	0.1449	-0.295	25.9	0.863
420	426	1.67	773.43	0.594	0.1131	-0.313	26.7	0.89
430	432	1.67	791.83	0.580	0.0829	-0.331	27.6	0.92
440	438	1.67	810.23	0.56	0.054	-0.350	28.5	0.9
450	446	1.25	828.63	0.555	0.0264	-0.368	29.5	0.983
460	450						30.61	1.020
470	480						37.68	1.256
480	510						42.38	1.4126
490	540						42.38	1.412
500	570						42.38	1.412

(test 3)

Xp (mm)	Time (s)	Rate of Spread (mm/s)	Flame height (mm)	X/Xf	(X-Xp)/ (Xf-Xp)	X-Xf (m)	Heat Flux (kW/m^2)	HF/HF_0
10	16	0.63	30.00	15.33	22.5	0.43	0.29	0.009
20	23	1.43	40.00	11.5	22	0.42	0.3	0.009
30	28	2.00	45.00	10.22	28.66	0.415	0.59	0.018
40	43	0.67	70.00	6.571	14	0.39	0.88	0.027
50	56	0.77	100.00	4.6	8.2	0.36	1.09	0.0340
60	69	0.77	115.00	4	7.272	0.345	1.17	0.0365
70	79	1.00	130.00	3.538	6.5	0.33	1.17	0.0365
80	90	0.91	150.00	3.066	5.428	0.31	1.17	0.0365
90	102	0.83	170.00	2.705	4.625	0.29	1.77	0.0553
100	117	0.67	190.00	2.421	4	0.27	1.77	0.0553
110	125	1.25	215.00	2.139	3.333	0.245	2.03	0.0634
120	135	1.00	225.00	2.044	3.238	0.235	2.35	0.0734
130	149	0.71	240.00	1.916	3	0.22	2.35	0.0734
140	163	0.71	270.00	1.703	2.461	0.19	2.6	0.0812
150	173	1.00	280.00	1.642	2.384	0.18	2.94	0.0918
160	183	1.00	300.00	1.533	2.142	0.16	3.25	0.1015
170	197	0.71	315.00	1.460	2	0.145	3.53	0.1103
180	207	1.00	330.00	1.393	1.866	0.13	3.53	0.1103
190	217	1.00	350.00	1.314	1.687	0.11	4.09	0.1278
200	232	0.67	360.00	1.277	1.625	0.1	4.4	0.13
210	244	0.83	380.00	1.210	1.470	0.08	5.09	0.1590
220	255	0.91	410.00	1.121	1.263	0.05	5.55	0.1734
230	267	0.83	430.00	1.069	1.15	0.03	5.88	0.183
240	277	1.00	440.00	1.045	1.1	0.02	6.98	0.2181
250	287	1.00	460.00	1	1	0	7.06	0.2206
260	297	1.00	470.00	0.978	0.952	-0.01	8.24	0.25
270	310	0.77	490.00	0.938	0.863	-0.03	8.83	0.2759
280	322	0.83	500.00	0.92	0.818	-0.04	10	0.31
290	331	1.11	528.59	0.87	0.712	-0.068	10.59	0.3309
300	340	1.11	546.59	0.841	0.648	-0.086	12.95	0.4046
310	347	1.43	564.59	0.814	0.589	-0.104	12.95	0.4046

320	357	1.00	582.59	0.789	0.53	-0.122	14.6	0.456
330	365	1.25	600.59	0.765	0.480	-0.140	15.89	0.4965
340	371	1.67	618.59	0.743	0.430	-0.158	17.09	0.5340
350	380	1.11	636.59	0.72	0.383	-0.176	17.66	0.5518
360	388	1.25	654.59	0.70	0.339	-0.194	20.01	0.6253
370	398	1.00	672.59	0.683	0.297	-0.212	22.37	0.6990
380	404	1.67	690.59	0.666	0.257	-0.23	23.21	0.725
390	412	1.25	708.59	0.649	0.219	-0.248	24.72	0.7725
400	420	1.25	726.59	0.633	0.183	-0.266	23.54	0.735
410	426	1.67	744.59	0.61	0.149	-0.284	24.32	0.76
420	432	1.67	762.59	0.603	0.116	-0.302	27.09	0.846
430	440	1.25	780.59	0.589	0.085	-0.320	29.43	0.919
440	446	1.67	798.59	0.576	0.055	-0.338	30.61	0.956
450	453	1.43	816.59	0.563	0.027	-0.356	31.2	0.975
460	470						34.14	1.066
470	490						36.5	1.140
480	510						37.68	1.177
490	530						38.85	1.214
500	550						38.85	1.214

(test 4)

Xp (mm)	Time (s)	Rate of Spread (mm/s)	Flame height (mm)	X/Xf	(X-Xp)/ (Xf-Xp)	X-Xf (m)	Heat Flux (kW/m^2)	HF/HF_0
10	12	0.83	35.00	13.14	18	0.425	0.29	0.009
20	20	1.25	40.00	11.5	22	0.42	0.29	0.009
30	24	2.50	50.00	9.2	21.5	0.41	0.29	0.009
40	37	0.77	65.00	7.07	16.8	0.395	0.59	0.019
50	51	0.71	85.00	5.411	11.71	0.375	0.59	0.019
60	61	1.00	110.00	4.181	8	0.35	0.59	0.019
70	73	0.83	130.00	3.538	6.5	0.33	0.9	0.029
80	81	1.25	140.00	3.285	6.333	0.32	1.18	0.038
90	95	0.71	165.00	2.787	4.933	0.295	1.18	0.038
100	107	0.83	180.00	2.555	4.5	0.28	1.18	0.038
110	119	0.83	205.00	2.243	3.684	0.255	1.77	0.057
120	129	1.00	230.00	2	3.090	0.23	1.77	0.057
130	143	0.71	250.00	1.84	2.7	0.21	2.12	0.068
140	155	0.83	260.00	1.769	2.666	0.2	2.35	0.075
150	166	0.91	270.00	1.703	2.583	0.19	2.35	0.075
160	176	1.00	285.00	1.614	2.4	0.175	2.35	0.075
170	190	0.71	300.00	1.533	2.230	0.16	2.94	0.094
180	203	0.77	340.00	1.352	1.75	0.12	3.53	0.113
190	211	1.25	360.00	1.277	1.58	0.1	3.53	0.113
200	225	0.71	370.00	1.243	1.529	0.09	3.53	0.113
210	239	0.71	380.00	1.210	1.470	0.08	3.53	0.113
220	252	0.77	400.00	1.15	1.333	0.06	4.12	0.132
230	263	0.91	420.00	1.095	1.210	0.04	4.71	0.151
240	273	1.00	450.00	1.022	1.047	0.01	5.1	0.164
250	282	1.11	470.00	0.978	0.954	-0.01	5.89	0.19
260	292	1.00	490.00	0.9387	0.8695	-0.03	5.89	0.19
270	302	1.00	500.00	0.92	0.8260	-0.04	7.06	0.2277
280	311	1.11	519.40	0.8856	0.751	-0.0594	8.24	0.2658

290	319	1.25	538.00	0.8550	0.6854	-0.078	8.24	0.2658
300	332	0.77	556.60	0.8264	0.6235	-0.0966	10.4	0.3354
310	346	0.71	575.20	0.7997	0.5656	-0.1152	12.5	0.4032
320	349	3.33	593.80	0.774	0.5113	-0.1338	12.96	0.4180
330	355	1.67	612.40	0.7511	0.460	-0.1524	12.98	0.418
340	367	0.83	631.00	0.729	0.4123	-0.171	13.8	0.4451
350	377	1.00	649.60	0.7081	0.3671	-0.1896	14.13	0.4558
360	383	1.67	668.20	0.6884	0.3244	-0.2082	15.3	0.4935
370	389	1.67	686.80	0.6697	0.2840	-0.2268	20.01	0.6454
380	395	1.67	705.40	0.6521	0.2458	-0.2454	20.01	0.6454
390	402	1.43	724.00	0.6353	0.2095	-0.264	20.01	0.6454
400	409	1.43	742.60	0.6194	0.1751	-0.2826	22.37	0.7216
410	415	1.67	761.20	0.6043	0.1423	-0.3012	23.67	0.7635
420	423	1.25	779.80	0.5898	0.1111	-0.3198	25.6	0.8258
430	430	1.43	798.40	0.5761	0.0814	-0.3384	27.08	0.8735
440	438	1.25	817.00	0.5630	0.053	-0.357	28.25	0.911
450	446	1.25	835.60	0.5505	0.0259	-0.3756	30.2	0.9741
460	470						32.97	1.0635
470	490						37.67	1.2151
480	510						40.03	1.291
490	530						40.03	1.291
500	550						41.21	1.3293
	570						41.21	1.3293

A-3 Measurements of Flame Heights and Heat Fluxes to the Unburned Surfaces in Gas Panel Tests

H=0.15 m, W=0.15 m, H/W=1

flow rate (L/min)	RHR (kW)	Q' (kW/m)	Xf (m)	bottom	middle	top
2.5	3.5425	23.61667	0.32	15.28	1.6	1.25
3	4.251	28.34	0.42	15.67	2.12	1.71
3.5	4.9595	33.06333	0.51	22.14	2.92	1.86
4	5.668	37.78667	0.55	23.07	3.43	2.37
4.5	6.3765	42.51	0.63	24.21	4.4	2.51
5	7.085	47.23333	0.64	25.04	6.14	3.08
5.5	7.7935	51.95667	0.73	25.36	7.17	3.24
6	8.502	56.68	0.76	25.84	9.06	3.69
6.5	9.2105	61.40333	0.78	25.64	11.31	3.99
7	9.919	66.12667	0.74	25.49	13.77	4.81
7.5	10.6275	70.85	0.88	25.81	14.9	5.03
8	11.336	75.57333	0.89	25.1	16.19	5.56
8.5	12.0445	80.29667	0.9	25.37	18.9	5.61
9	12.753	85.02	0.93	24.3	20.38	7.35
9.5	13.4615	89.74333	1	23.55	23.72	7.33
10	14.17	94.46667	1.01	23.7	24.91	8.38
10.5	14.8785	99.19	1.03	23.81	25.32	8.7
11.5	16.2955	108.6367	1.06	22.34	26.24	11.17
12.5	17.7125	118.0833	1.11	22.38	26.97	12.47
13.5	19.1295	127.53	1.18	20.68	27.15	16.09

H=0.3 m, W=0.15 m, H/W=2

flow rate (L/min)	RHR (kW)	Q' (kW/m)	Xf (m)	bottom	middle	top
3.5	4.9595	33.06333	0.45	8.66	1.52	1.31
4	5.668	37.78667	0.52	14.93	1.85	1.43
4.5	6.3765	42.51	0.58	12.27	2.09	1.82
5	7.085	47.23333	0.63	20.49	2.6	1.97
5.5	7.7935	51.95667	0.68	17.66	3.35	2.45
6	8.502	56.68	0.73	24.45	3.88	2.65
6.5	9.2105	61.40333	0.8	19.52	4.65	3.02
7	9.919	66.12667	0.82	26	5.42	3.34
7.5	10.6275	70.85	0.86	20.93	6.17	3.43
8	11.336	75.57333	0.88	26.95	6.75	3.92
8.5	12.0445	80.29667	0.92	21.87	8.71	4.15
9.1	12.8947	85.96467	0.98	27.35	8.48	4.45
9.5	13.4615	89.74333	0.97	22.91	11.64	5.02
10	14.17	94.46667	1.03	27.96	10.07	5.08
10.5	14.8785	99.19	1.03	23.92	14.59	5.71
11	15.587	103.9133	1.05	27.64	12.78	5.91
12	17.004	113.36	1.08	31.18	13.99	6.74
13	18.421	122.8067	1.13	30.5	16.94	7.85
14.1	19.9797	133.198	1.17	29.86	19.33	8.45
15	21.255	141.7	1.22	28.7	21.73	9.64
16	22.672	151.1467	1.25	28.17	22.21	11.27
17	24.089	160.5933	1.28	27.76	23.4	12.15
19	26.923	179.4867	1.3	27.46	24.62	15.74
21	29.757	198.38	1.36	27.13	25.19	17.75

H=0.3 m, W=0.3 m, H/W=1

flow rate (L/min)	RHR (kW)	Q' (kW/m)	Xf (m)	bottom	middle	top
7	9.919	33.06333	0.52	14.17	2.07	1.96
8	11.336	37.78667	0.59	18	2.63	2.41
9	12.753	42.51	0.64	20.69	3.22	2.79
10	14.17	47.23333	0.72	22.47	3.89	3.06
11	15.587	51.95667	0.76	23.4	4.74	3.62
12	17.004	56.68	0.83	24.94	6.09	4.1
13	18.421	61.40333	0.85	24.9	7.15	4.14
15	21.255	70.85	0.89	25.7	9.96	5.35
17	24.089	80.29667	1	25.98	12.34	6.3
19	26.923	89.74333	1.05	25.54	17.03	7.96
21	29.757	99.19	1.11	24.78	18.81	8.96
23	32.591	108.6367	1.15	24.26	21.03	10.93
25	35.425	118.0833	1.2	23.83	23.47	13.78

H=0.15 m, W=0.3 m, H/W=0.5

flow rate (L/min)	RHR (kW)	Q' (kW/m)	Xf (m)	bottom	middle	top
4	5.668	18.89333	0.34	16.22	1.22	1.2
4.5	6.3765	21.255	0.41	19.15	1.59	1.34
5	7.085	23.61667	0.45	19.67	1.71	1.47
5.5	7.7935	25.97833	0.48	21.81	2.04	1.74
6	8.502	28.34	0.51	23.88	2.4	1.91
7	9.919	33.06333	0.57	26.38	3.26	2.43
8	11.336	37.78667	0.59	27.24	4	2.7
9	12.753	42.51	0.65	27.93	5.97	3.42
10	14.17	47.23333	0.7	27.98	7.5	3.86
11	15.587	51.95667	0.75	28	10.74	4.6
12	17.004	56.68	0.81	28.23	12.01	4.63
13	18.421	61.40333	0.85	27.35	14.58	5.28
14	19.838	66.12667	0.88	26.62	16.65	5.89
16	22.672	75.57333	0.95	25.39	19.49	7.08
18	25.506	85.02	1.01	24.08	24.08	10.1
20	28.34	94.46667	1.08	23.19	24.82	11.99
22	31.174	103.9133	1.1	22.99	25.35	15.07
24	34.008	113.36	1.15	23.3	25.15	15.56

H=0.45 m, W=0.3 m, H/W=1.5

flow rate (L/min)	RHR (kW)	Q' (kW/m)	Xf (m)	bottom	middle	top
10	14.17	47.23333	0.63	13.21	2.94	2.99
10.5	14.8785	49.595	0.7	11.43	2.59	2.83
11	15.587	51.95667	0.73	13.71	3.16	3.25
12	17.004	56.68	0.76	21.33	3.56	3.37
13	18.421	61.40333	0.83	17.42	4.78	4.23
14	19.838	66.12667	0.85	24.96	4.35	3.88
15	21.255	70.85	0.93	19.92	6.87	5.07
16	22.672	75.57333	0.94	28.44	5.86	4.59
17	24.089	80.29667	0.97	29.14	7.16	4.81
18	25.506	85.02	0.99	29.87	9.06	5.43
20	28.34	94.46667	1.03	30.4	11.12	6.04
22	31.174	103.9133	1.09	30.61	15.1	7.1
24	34.008	113.36	1.15	29.8	18.36	8.28
26	36.842	122.8067	1.21	29.93	21.03	9.77
28	39.676	132.2533	1.28	29.38	23.28	11.58
30	42.51	141.7	1.35	28.15	23.74	13.08
32	45.344	151.1467	1.39	27.64	24.04	13.94
35	49.595	165.3167	1.52	26.93	25.34	15.52

H=0.6 m, W=0.3 m, H/W=2

flow rate (L/min)	RHR (kW)	Q' (kW/m)	Xf (m)	bottom	middle	top
13	18.421	61.40333	0.83	13.19	2.45	2.62
15	21.255	70.85	0.88	18.02	2.92	3.09
17	24.089	80.29667	0.96	24.13	4.05	3.76
19	26.923	89.74333	1.01	26.18	5.07	4.2
22	31.174	103.9133	1.09	29.35	7.21	5.19
25	35.425	118.0833	1.2	30.8	11.76	6.44
27	38.259	127.53	1.23	30.47	14.76	6.95
29	41.093	136.9767	1.3	31.11	18.02	8.08
31	43.927	146.4233	1.36	29.96	19.58	8.88
33	46.761	155.87	1.39	29.16	20.62	9.7
35	49.595	165.3167	1.45	27.97	20.46	10.78
37	52.429	174.7633	1.48	27.38	22.89	12.32
39	55.263	184.21	1.51	27.27	25.49	14.84
41	58.097	193.6567	1.55	26.48	25.66	15.94
43	60.931	203.1033	1.62			

H=0.3 m, W=0.3 m, H/W=1 (lower)

flow rate (L/min)	RHR (kW)	Q' (kW/m)	Xf (m)	bottom	middle	top
9	12.753	42.51	0.54	4.9	1.56	1.87
10	14.17	47.23333	0.59	6.05	1.83	2.11
11	15.587	51.95667	0.66	7.11	2.03	2.29
12	17.004	56.68	0.7	8.43	2.2	2.46
13	18.421	61.40333	0.77	9.94	2.52	2.63
14	19.838	66.12667	0.79	11	2.65	2.78
16	22.672	75.57333	0.85	15.41	3.59	3.34
18	25.506	85.02	0.89	17.74	4.2	3.75
20	28.34	94.46667	0.95	20	4.91	4.12
22	31.174	103.9133	1.02	22.31	6.52	4.81
24	34.008	113.36	1.09	23.91	7.75	5.35

H=0.15 m, W=0.57 m, H/W=2.63

flow rate (L/min)	RHR (kW)	Q' (kW/m)	Xf (m)	bottom	middle	top
6.5	9.2105	16.15877	0.32	7.65	1.08	0.93
7	9.919	17.40175	0.35	8.77	1.19	1.11
7.5	10.6275	18.64474	0.39	9.32	1.31	1.19
8	11.336	19.88772	0.41	10.97	1.4	1.33
9	12.753	22.37368	0.45	12.5	1.68	1.58
10	14.17	24.85965	0.49	15.25	1.83	1.72
11	15.587	27.34561	0.54	19.25	2.11	2.01
12	17.004	29.83158	0.56	21.05	2.38	2.16
14	19.838	34.80351	0.59	23.14	3.53	2.78
16	22.672	39.77544	0.63	25	4.59	2.38
18	25.506	44.74737	0.69	25.75	6.01	3.85
20	28.34	49.7193	0.73	25.86	6.36	4.05
22	31.174	54.69123	0.75	25.48	9.62	4.5
25	35.425	62.14912	0.83	25.63	12.65	5.39
28	39.676	69.60702	0.88	25.66	15.46	6.16
30	42.51	74.57895	0.95	23.04	19.89	8.77
32	45.344	79.55088	0.99	23.02	20.26	9
34	48.178	84.52281	1.05	22.55	22.6	10.61
37	52.429	91.9807	1.1	22.08	24.23	13.06
40	56.68	99.4386	1.19	21.35	24.09	15.41

H=0.3 m, W=0.57 m, H/W=5.26

flow rate (L/min)	RHR (kW)	Q' (kW/m)	Xf (m)	bottom	middle	top
12	17.004	29.83158	0.5	14.69	2.56	2.46
14	19.838	34.80351	0.58	17.93	3.2	2.87
16	22.672	39.77544	0.65	20.55	4.27	3.18
18	25.506	44.74737	0.68	21.83	5.12	3.74
20	28.34	49.7193	0.73	22.77	6.45	4.24
23	32.591	57.17719	0.81	23.74	9.13	5.22
26	36.842	64.63509	0.9	24.62	11.77	6.26
29	41.093	72.09298	0.96	24.72	13.67	7.09
32	45.344	79.55088	1.03	24.42	16.97	8.68
35	49.595	87.00877	1.07	24	20.13	10.27
38	53.846	94.46667	1.1	23.22	21.81	11.78
41	58.097	101.9246	1.14	23.21	22.63	13.12
44	62.348	109.3825	1.22	22.64	23.73	14.9
46	65.182	114.3544	1.28	22.12	23.44	15.44
48	68.016	119.3263	1.3	21.51	22.91	16.18

H=0.45 m, W=0.57 m, H/W=7.89

flow rate (L/min)	RHR (kW)	Q' (kW/m)	Xf (m)	bottom	middle	top
16	22.672	39.77544	0.64	9.34	2.21	2.78
18	25.506	44.74737	0.69	11.82	2.62	3.05
20	28.34	49.7193	0.74	13.66	3.05	3.22
22	31.174	54.69123	0.77	15.53	3.7	3.6
24	34.008	59.66316	0.85	17.66	4.9	4.5
26	36.842	64.63509	0.9	18.1	5.42	4.69
29	41.093	72.09298	1	20.03	7.85	5.77
32	45.344	79.55088	1.05	20.67	9.24	6.31
35	49.595	87.00877	1.1	21.23	11.2	7.37
38	53.846	94.46667	1.15	21.47	12.68	8.55
41	58.097	101.9246	1.17	21.65	14.16	9.31
45	63.765	111.8684	1.25	21.16	15.88	10.92
48	68.016	119.3263	1.28	21.14	17.7	12.79
51	72.267	126.7842	1.33			

A-4 Measurements of Flame Heights and Heat Fluxes to the Unburned Surfaces on PMMA Wall Fires in a Corner

Sample height: 100cm; the height of heat flux meter: 86 cm. (Test 1)

Time (s)	Xpp (m)	Xf (m)	Vpp (m/s)	Heat flux (kW/m^2)	Heat flux (kW/m^2)
0	0.02	0.12		0.63	0.36
10			0.00155	0.67	0.39
20	0.051	0.16		0.78	0.48
30			0.00105	0.85	0.57
40	0.072	0.24		0.92	0.67
50			0.00105	1.00	0.77
60	0.093	---		1.12	0.90
70			0.00135	1.22	0.99
80	0.12	0.32		1.38	1.13
90			0.00135	1.51	1.23
100	0.147	0.38		1.65	1.34
110			0.0015	1.81	1.51
120	0.177	0.43		1.95	1.69
130			0.0012	2.15	1.90
140	0.201	0.5		2.52	2.26
150			0.00195	2.89	2.55
160	0.24	0.54		3.27	2.83
170			0.00165	3.67	3.12
180	0.273	0.6		4.36	3.63
190			0.00255	4.97	4.17
200	0.324	0.7		6.04	5.25
210			0.0024	7.10	6.18
220	0.372	0.8		8.45	7.16
230			0.0027	10.06	8.04
240	0.426	0.85		12.26	9.38
250			0.0027	13.95	10.74
260	0.48	0.9		16.25	13.11
270			0.003	18.15	15.17
280	0.54			19.94	17.01
290			0.00345	22.17	19.17
300	0.609			23.44	20.39
310			0.0041	24.55	21.46
320	0.711			25.70	22.46
330			0.00395	26.40	23.08
340	0.792			27.05	23.57
350			0.0066	27.62	24.0
360	0.924			28.22	24.28
370			0.0039	28.34	24.36
380	1.002			28.26	24.38
390				28.2	24.31
400				28.29	24.08
410				28.39	23.52
420				28.40	23.13
430				28.39	22.82
440				28.41	22.53

Sample height: 100cm; the height of heat flux meter: 86 cm. (Test 2).

Time (s)	Xpp (m)	Xf (m)	Vpp (m/s)	Heat flux (kW/m^2)	Heat flux (kW/m^2)
0	0.02	0.12		7.44E-02	0.49
10				9.95E-02	0.53
20	0.006	0.16		1.90E-01	0.60
30			0.0015	6.36E-01	0.65
40	0.036	0.22		1.06E+00	0.70
50			0.0006	1.38E+00	0.74
60	0.048	0.29		1.42E+00	0.83
70			0.0018	1.19E+00	0.91
80	0.084	0.33		7.07E-01	1.07
90			0.00075	4.51E-01	1.23
100	0.099	0.39		3.49E-01	1.40
110			0.0015	4.22E-01	1.56
120	0.129	0.45		8.13E-01	1.76
130			0.0015	1.14E+00	1.93
140	0.159	0.5		1.60E+00	2.28
150			0.00135	1.93E+00	2.48
160	0.186	0.54		2.32E+00	2.68
170			0.00255	2.61E+00	2.88
180	0.237	0.62		2.85E+00	3.37
190			0.00075	3.10E+00	4.01
200	0.252	0.68		3.81E+00	5.02
210			0.00345	4.65E+00	5.74
220	0.321	0.72		5.71E+00	6.56
230			0.00285	6.82E+00	7.63
240	0.378	0.83		8.26E+00	9.78
250			0.00285	9.39E+00	11.70
260	0.435	0.95		1.12E+01	13.91
270			0.003	1.29E+01	15.32
280	0.495			1.47E+01	16.88
290			0.00315	1.64E+01	18.65
300	0.558			1.86E+01	20.73
310			0.0048	2.03E+01	21.92
320	0.654			2.24E+01	23.27
330			0.00495	2.34E+01	24.10
340	0.75			2.41E+01	24.89
350			0.0036	2.47E+01	25.55
360	0.822			2.53E+01	25.98
370			0.0069	2.54E+01	25.96
380	0.96			2.50E+01	26.05
390				2.49E+01	26.17
400				2.49E+01	26.11
410				2.50E+01	25.83
420				2.49E+01	25.7
430				2.47E+01	25.80
440				2.42E+01	25.71
450				2.38E+01	24.17
460				2.33E+01	21.00
470				2.31E+01	17.77

Sample height: 100cm; the height of heat flux meter: 86 cm. (Test 3)

Time (s)	Xpp (m)	Xf (m)	Vpp (m/s)	Heat flux (kW/m^2)	Heat flux (kW/m^2)
0	0.02			0.58	0.02
10			0.00155	0.61	0.02
20	0.051	0.18		0.68	1.07
30			0.00075	0.74	0.96
40	0.066	0.23		0.81	1.04
50			0.00105	0.90	1.15
60	0.087	0.3		1.04	1.77
70			0.0012	1.15	1.69
80	0.111	0.35		1.24	1.04
90			0.00105	1.31	0.87
100	0.132	0.4		1.41	0.97
110			0.0015	1.57	1.11
120	0.162	0.44		1.80	1.16
130			0.00135	1.99	1.51
140	0.189	0.48		2.28	2.39
150			0.00135	2.52	2.87
160	0.216	0.53		2.84	3.06
170			0.00195	3.12	2.78
180	0.255	0.61		3.58	2.57
190			0.00165	3.97	2.79
200	0.288	0.7		4.74	3.3
210			0.0036	5.46	3.76
220	0.36			6.40	4.14
230			0.0015	7.58	4.81
240	0.39			9.54	6.37
250			0.003	11.30	7.93
260	0.45			13.95	10.45
270			0.00285	15.88	12.48
280	0.507			17.68	14.16
290			0.00315	19.32	15.67
300	0.57			21.23	17.81
310			0.0039	22.72	19.60
320	0.648			24.64	21.4
330			0.0036	25.92	22.11
340	0.72			26.85	22.92
350			0.0045	27.31	24.10
360	0.81			27.56	25.58
370			0.003	27.72	26.55
380	0.87			28.11	27.18
390			0.0054	28.21	27.28
400	0.978			28.13	27.18
410				28.20	27.12
420				28.52	27.17
430				28.80	27.35
440				28.41	22.53
450				28.44	22.31
460				27.59	21.44
470				23.08	17.77

Sample height: 50cm; the height of heat flux meter: 48 cm. (Test 1 and 2)

Time (s)	Xpp (m)	Xf (m)	Vpp (m/s)	Heat flux (kW/m^2)	Xpp (m)	Vpp (m/s)	Heat flux (kW/m^2)
0	0.02	0.13		0.497	0.002		1.75
10			0.0032	1.05		0.0032	1.90
20	0.084	0.18		1.04	0.066		0.89
30			0.0009	1.42		0.0012	0.05
40	0.102	0.25		2.34	0.09		0.84
50			0.0013	2.70		0.00135	3.15
60	0.138	0.31		2.20	0.117		3.82
70			0.00135	2.34		0.00135	2.99
80	0.165	0.35		3.39	0.144		3.84
90			0.0015	3.66		0.0015	5.40
100	0.195	0.4		3.73	0.174		6.14
110			0.00135	4.26		0.00135	6.60
120	0.222	0.45		5.74	0.201		7.07
130			0.00145	6.77		0.0018	7.52
140	0.251			7.83	0.237		8.82
150			0.0026	9.02		0.00195	9.91
160	0.303			10.63	0.276		11.30
170			0.00225	12.30		0.0018	13.16
180	0.348			15.04	0.312		15.93
190			0.00225	16.77		0.00195	15.95
200	0.393	0.7		18.27	0.351		17.90
210			0.00355	20.71		0.0024	21.06
220	0.464	0.75		23.71	0.399		22.87
230			0.0026	26.06		0.00495	23.69
240	0.516	0.83		28.74	0.498		25.36
250				30.34			26.16
260			0.0054	31.19			27.25
270				31.15			28.88
280				31.04			29.27
290				30.81			27.64
300				30.63			27.07
310				31.17			27.49
320				31.56			
330				31.18			
340				31.18			

Sample height: 30cm; the height of heat flux meter: 24 cm. (Test 1 and 2)

Time (s)	Xf (m)	Heat flux (kW/m^2)	Heat flux (kW/m^2)
0	0.12	3.74	2.73
10		5.87	3.83
20	0.17	7.92	6.00
30		8.94	8.13
40	0.24	10.4	10.0
50		12.13	12.75
60	0.3	13.51	15.3
70		15.34	17.5
80	0.35	17.62	19.72
90		19.52	21.44
100	0.39	21.02	23.40
110		22.53	25.80
120	0.44	23.71	27.84
130		24.6	29.61
140	0.49	25.54	31.50
150		26.38	31.24
160	0.54	27.28	30.8
170		27.46	31.10
180	0.6	27.36	31.28
190		27.63	31.32
200		27.94	
210		27.31	

A-5 - Measurements of Flame Heights, Heat Fluxes to the Unburned Surfaces and Heat Fluxes to the Opposing Wall on PMMA Wall Fires with the influence of a Parallel Inert Wall

Measurements of heat flux to unburned surfaces

Sample height : 24 cm

Time	a = ∞		a=5cm		a=15 cm		a= 25 cm		a=35 cm
(min)	Test 1	Test 2	Test 1	Test 2	Test 1	Test 2	Test 1	Test 2	Test 1
0	0	0	0	0	0	0	0	0	0
0.33	1.46	1.02	0.48	0.48	0.48	0.48	1.46	0.68	0.77
0.66	2.63	1.94	0.59	1.26	1.16	0.87	2.23	1.65	1.75
1	4.38	3.21	0.97	2.14	1.46	0.97	3.11	2.92	2.53
1.33	6.33	3.89	1.84	3.21	2.33	2.14	4.28	3.89	3.50
1.66	8.18	5.45	2.92	4.76	3.21	3.79	5.84	5.25	4.76
2	10.71	7.59	4.38	6.52	4.57	5.64	7.39	7.20	5.93
2.33	14.32	9.35	6.32	10.02	6.52	7.30	9.14	9.34	7.88
2.66	18.99	12.27	8.26	13.23	8.56	8.95	10.70	10.80	11.09
3	23.38	14.61	10.90	18.68	10.31	11.77	12.26	15.18	13.72
3.33	27.08	18.02	14.01	21.90	12.75	14.60	14.60	18.10	18.39
3.67	29.91	22.11	15.86	22.09	14.60	17.22	17.03	20.92	19.85
4	31.66	25.42	18.49	26.37	18.59	20.24	19.27	22.09	23.36
4.33	34.68	29.71	21.41	28.03	20.63	21.41	20.34	25.21	26.67
4.66	35.85	32.15	23.16	29.38	22.48	23.55	23.16	25.50	29.78
5	36.34	33.90	23.36	29.68	24.33	25.01	24.72	24.91	32.99
5.33	35.95	35.17	23.65	29.68	25.30	25.89	25.98	23.45	34.55
5.66	34.58	35.56	23.75	29.68	25.50	24.82	25.69	20.92	34.45
6	31.27	34.10	23.75	29.59	24.91	24.14	25.21		33.58
6.33			23.26	29.00	24.33	23.26	19.27		32.60
6.66			23.16	28.90	23.45				
7			21.99	28.90					
7.33			21.90						
7.66									
8									

Sample height : 48 cm

Time (min)	a = ∞		a=5cm		a=15 cm		a= 25 cm	a= 35 cm
	Test 1	Test 2	Test 1	Test 2	Test 1	Test 2	Test 1	Test 1
0	0	0	0	0	0	0	0	0
0.33	0.29	0.48	0.29	0.19	0.19	0.29	0.19	0.38
0.66	0.48	0.68	0.29	0.29	0.29	0.48	0.38	0.87
1	0.58	0.77	0.38	0.38	0.38	0.58	0.48	0.97
1.33	0.97	0.87	0.50	0.48	0.38	0.68	0.68	1.07
1.66	1.16	0.97	0.68	0.58	0.48	0.87	0.77	1.16
2	1.46	1.16	0.77	0.68	0.58	0.87	1.07	1.26
2.33	1.65	1.55	0.87	0.77	0.68	0.87	1.16	1.46
2.66	1.84	2.04	0.97	0.87	0.68	0.97	1.26	1.75
3	2.04	2.23	1.07	0.97	0.73	1.07	1.46	1.94
3.33	2.23	2.43	1.26	1.07	0.77	1.16	1.65	2.43
3.67	2.33	2.72	1.75	1.26	0.87	1.26	1.75	2.82
4	2.43	3.21	2.14	1.55	0.97	1.36	1.84	3.30
4.33	2.72	3.69	2.33	1.84	1.07	1.55	1.94	3.50
4.66	3.30	4.08	2.43	1.94	1.16	1.75	2.23	3.89
5	3.89	4.38	2.72	2.14	1.26	1.94	2.43	4.38
5.33	4.18	4.86	2.92	2.43	1.36	2.14	2.53	4.57
5.66	4.76	5.35	3.21	3.11	1.46	2.23	2.72	4.96
6	5.15	6.32	3.60	3.69	1.65	2.23	2.92	5.54
6.33	5.84	8.07	3.89	3.89	1.84	2.33	4.18	6.32
6.66	7.30	9.34	4.38	4.38	1.94	2.43	4.96	6.8
7	9.24	11.97	5.06	5.06	2.23	2.92	6.03	7.59
7.33	10.99	15.28	6.22	5.93	2.72	3.01	6.81	7.10
7.66	13.72	18.29	7.30	6.81	3.11	3.50	7.68	9.83
8	17.22	21.70	8.95	7.78	3.40	4.08	8.46	12.07
8.33	19.46	24.91	10.80	9.24	3.89	4.96	9.44	14.11
8.66	23.55	27.84	13.04	11.87	5.06	5.74	11.09	16.54
9	28.32	30.56	16.54	15.18	5.84	7.00	12.75	18.49
9.33	32.60	34.06	21.41	15.37	6.81	8.37	14.11	23.45
9.66	36.79	36.98	27.54	18.98	7.78	10.22	14.69	28.90
10	38.44	37.57	33.58	19.47	8.85	11.77	17.52	32.70
10.33	37.18	36.89	38.64	25.01	9.92	14.40	22.38	36.11
10.66	35.77	35.62	41.95	32.51	12.16	17.71	28.90	37.96
11		34.55	42.44	36.40	14.60	21.31	33.19	38.93
11.33			41.85	38.35	18.39	24.52	36.21	39.22
11.66			40.39	38.15	22.58	29.39	37.96	39.13
12				35.62	26.76	33.19	39.42	38.54
12.33				32.92	30.46	37.57	40.59	38.25
12.66					33.09	40.00	40.68	37.76
13					35.04	40.49	39.32	36.59
13.33					35.52	39.32	37.47	35.82
13.66					34.84	37.57	35.62	34.94
14					33.03	35.52		

Sample height: 96 cm

Time (min)	a = ∞			a=5cm	a=15 cm		a= 25 cm	a= 35 cm		
	Test 1	Test 2	Test 3	Test 1	Test 1	Test 2	Test 1	Test 1	Test 2	Test 3
0	0	0	0	1.11	0	0	0	0	1.2	0.3
1	0	0	0	0.65	0	0	0	0	1.3	0.6
2	0	0	0	1.44	0	0	0	0	1.3	0.5
3	0.03	0	0.24	1.91	0	0	0	0	0.8	0.5
4	0.27	0	0.05	1.85	0	0	0	0	0.3	0.6
5	0.20	0.01	0.51	2.65	0	0	0	0	0.5	0.6
6	0.38	0.01	0.68	2.67	0	0	0	0	0.5	0.5
7	0.49	0.02	0.80	3.63	0	0	0	0	0	0.9
8	0.16	0.05	0.91	4.58	0	0	0	0	0.3	1
9	0.73	0.05	1.27	5.59	0	0	0	0	1	1.6
10	0.67	0.12	1.86	6.94	0	0	0	0.6	1.4	2
11	0.72	0.24	2.49	8.74	0	0	0	1	1.1	2.5
12	1.03	0.30	3.65	13.33	0.6	0	0.7	1.4	1.6	3.3
13	1.28	0.35	5.05	21.76	6.6	0	1.3	3	2.2	3.8
14	2.03	0.50	6.72	31.31	8.2	4.2	1.6	3	2.9	5.5
15	1.76	0.91	11.95	35.63	9.6	7.1	2.7	3.2	4.7	8.2
16	3.53	1.36	21.42	37.44	11.9	17.1	5.2	5.5	6.5	12.8
17	6.32	1.79	31.79	38.53	21.7	24	9.7	9.3	11.4	21.6
18	15.48	2.44	34.16	39.19	26.9	28.3	17	20.9	19.4	29.6
19	21.02	3.72	32.69	38.51	25.6	25.4	24.7	28.6	26.4	32.1
20	18.85	6.92	31.53	31.69	20.2	29.4	26.3	32.9	27.4	31.6
21	20.62	13.21	30.41	29.13			24.5	27.9		31.2
22	18.11	21.58	28.60	30.59			23.4			29.9
23		26.78		29.94			22.4			31.9
24		26.64					23.4			
25		25.47								
26		24.72								
27		23.6								

Measurements of heat flux to the opposing wall

Separation=5 cm, measuring point *X'*= 15, 45 and 90 cm.

Time (min)	X'=15 cm		X'=45 cm		X'=90 cm	
	Test 1	Test 2	Test 1	Test 2	Test 1	Test2
0	0.38	0.4	0	0	0	0
1	0.83	0.7	0	0.1	0	0.1
2	2.2	2	0.2	0.2	0.1	0.1
3	4.2	3.9	0.3	0.3	0.2	0.2
4	5.8	6	0.5	0.5	0.2	0.3
5	7.1	7.7	0.7	0.8	0.3	0.5
6	8.1	8.9	1	1.2	0.5	0.7
7	8.7	9.8	1.5	2.4	0.7	1.2
8	9.1	10.2	2.1	3.8	0.8	1.6
9	9.3	10.4	3.3	5.7	1.2	2
10	9.5	10.5	4.8	8.7	1.2	2.7
11	9.6	11.2	6.7	12.2	1.6	4.1
12	9.6	11.8	9.1	14.5	2.3	6.3
13	9.5	11.8	10.7	14.8	3	8.8
14	9.7	11.7	12	15.3	4.5	11.7
15	9.9	11.3	12.5	15.6	6.3	13.9
16	10	11	12.2	15.8	7.7	15.1
17	10	10.7	11.9	15.6	8.6	15.1
18	9.9	10.5	12.5	15.2	10	15.1
19	9.7	10.1	12.9	13.6	10.7	13.1
20	9.4	9.5	12.8	12.1	10.6	11.4
21	9.2	9.3	12.8	11.6	10.8	11.3
22	8.8	8.8	13.1	11.8	11.7	11.8
23		8.3		11.8		12.2

Separation=15 cm, measuring point *X'*= 15, 45 and 90 cm.

time	X'=15 cm			X'=45 cm			X'=90 cm		
	Test 1	Test 2	Test 3	Test 1	Test 2	Test 3	Test 1	Test 2	Test 3
0	0.6	0.8	0.7	0.1	0.1	0.2	0.1	0.1	0.2
1	0.9	1.1	0.9	0.1	0.1	0.2	0.1	0.1	0.2
2	1.4	1.7	1.4	0.1	0.1	0.2	0.1	0.1	0.2
3	1.9	2.2	1.9	0.1	0.1	0.2	0.1	0.1	0.2
4	2.3	2.6	2.3	0.2	0.2	0.2	0.1	0.1	0.2
5	2.6	3	2.7	0.2	0.2	0.3	0.1	0.1	0.2
6	2.9	3.3	3.1	0.3	0.4	0.4	0.1	0.1	0.2
7	3.2	3.5	3.3	0.4	0.5	0.5	0.1	0.1	0.2
8	3.4	3.6	3.5	0.7	0.8	0.8	0.1	0.2	0.2
9	3.5	3.8	3.6	1.1	1.3	1.1	0.2	0.2	0.2
10	3.6	3.8	3.8	1.6	1.9	1.8	0.2	0.2	0.3
11	3.6	3.9	3.8	2.1	2.7	2.5	0.2	0.3	0.4
12	3.7	4	3.7	3	3.5	3.1	0.4	0.5	0.5
13	3.8	4	3.8	3.6	4.1	3.7	0.5	0.8	0.8
14	3.9	4	3.7	3.9	4.4	4.1	0.7	1.2	1.2
15	4	4	3.7	4.3	4.8	4.3	1.1	1.8	1.7
16	3.9	3.8	3.8	4.8	5.1	4.6	1.8	2.6	2.2
17	3.9	3.4	3.8	4.9	5.2	4.8	2.3	3.1	2.8
18	3.8	3.1	3.7	5	5.2	4.7	2.8	3.2	3.1
19	3.8	3	3.7	5.1	5.2	4.7	3.2	3.3	3.3
20	3.7	3	3.8	5.1	5.3	4.7	3.3	3.5	3.4
21		3.1	3.8		5.1	4.7		3.5	3.4
22			3.7			4.7			3.5
23			3.6			4.6			3.6

Separation=25 cm, measuring point *X'*= 15, 45 and 90 cm.

Time (min)	X'=15 cm		X'=45 cm		X'=90 cm	
	Test 1	Test 2	Test 1	Test 2	Test 1	Test2
0	0.4	0.6	0.1	0.3	0.1	0.4
1	0.5	0.6	0.1	0.3	0.1	0.4
2	0.7	0.7	0.1	0.3	0.1	0.3
3	0.9	0.9	0.1	0.3	0.1	0.3
4	1.1	1.1	0.1	0.3	0.1	0.3
5	1.3	1.3	0.2	0.3	0.1	0.3
6	1.5	1.5	0.2	0.4	0.1	0.3
7	1.6	1.7	0.3	0.5	0.1	0.3
8	1.7	1.8	0.5	0.6	0.1	0.3
9	1.8	2	0.6	0.7	0.1	0.3
10	1.9	2.1	0.7	0.9	0.1	0.3
11	1.9	2.1	1	1.2	0.2	0.4
12	2	2.3	1.4	1.6	0.2	0.5
13	2	2.2	1.6	1.8	0.3	0.5
14	1.9	2.3	1.8	2.1	0.4	0.7
15	1.4	2.3	1.8	2.4	0.5	0.9
16	1	2.3	1.7	2.7	0.6	1.2
17	0.8	2.4	1.9	2.9	0.8	1.6
18	0.7	2.4	2	3	1	1.8
19	0.7	2.4	2.1	3	1.3	2
20	0.7	2.3	2.2	2.9	1.5	2
21	0.7	2.2	2.1	2.9	1.5	2
22	0.7	2.2	2.1	2.9	1.5	2.2
23	0.7		2.1		1.5	
	0.7		2.1		1.5	

Separation=35 cm, measuring point *X'*= 15, 45 and 90 cm.

time	X'=15 cm			X'=45 cm			X'=90 cm		
	Test 1	Test 2	Test 3	Test 1	Test 2	Test 3	Test 1	Test 2	Test 3
0	0.3	0.3	0.4	0	0	0.2	0	0	0.1
1	0.4	0.4	0.4	0	0	0.1	0	0	0.1
2	0.5	0.5	0.5	0	0.1	0.2	0	0	0.1
3	0.6	0.6	0.6	0	0.1	0.2	0	0	0.1
4	0.6	0.7	0.7	0.1	0.1	0.2	0	0.1	0.1
5	0.8	0.8	0.9	0.1	0.1	0.2	0	0.1	0.1
6	0.9	0.9	1	0.2	0.2	0.3	0	0.1	0.1
7	0.9	1	1.1	0.2	0.2	0.3	0.1	0.1	0.2
8	1	1	1.3	0.3	0.3	0.4	0.1	0.1	0.2
9	1.2	1.1	1.4	0.3	0.4	0.6	0.1	0.1	0.2
10	1.2	1.2	1.5	0.4	0.5	0.7	0.1	0.1	0.2
11	1.3	1.3	1.5	0.5	0.7	0.9	0.1	0.2	0.3
12	1.4	1.4	1.6	0.6	0.9	1.1	0.2	0.2	0.3
13	1.4	1.4	1.6	0.8	1	1.3	0.2	0.3	0.4
14	1.2	1.4	1.6	1.3	1.2	1.5	0.3	0.3	0.5
15	1.5	1.4	1.6	1.7	1.3	1.6	0.4	0.4	0.7
16	1.5	1.4	1.4	1.4	1.5	1.6	0.5	0.6	0.8
17	1.5	1.4	1.3	1.4	1.6	1.6	0.7	0.7	0.9
18	1.5	1.5	1.4	1.6	1.7	1.8	0.9	0.9	1.1
19	1.5	1.5	1.6	1.7	1.9	1.9	1	1.1	1.3
20	1.5	1.5	1.6	1.8	1.9	1.9	1.2	1.1	1.3
21	1.5	1.6	1.7	1.9		1.9	1.2		1.3
22		1.6	1.6			1.9			1.3
23		1.6				2			1.4

Measurements of flame heights, pyrolysis heights and flame spread rates

Separation = infinite

time	Test 1			Test 2			Test 3	
	Xp	Xf	Vp	Xp	Xf	Vp	Xp	Vp
0	0.035	0.12	0.2	0.01	0.132	0.2	0.02	0.2
1	0.07	0.216	0.38	0.03	0.192	0.35	0.03	0.34
2	0.11	0.288	0.45	0.05	0.264	0.45	0.09	0.43
3	0.14	0.36	0.6	0.11	0.312	0.52	0.12	0.55
4	0.19	0.408	0.62	0.15	0.36	0.6	0.16	0.7
5	0.25	0.456	0.72	0.18	0.396	0.55	0.22	0.65
6	0.28	0.492	0.74	0.18	0.432	0.57	0.25	0.7
7	0.32	0.552	0.76	0.2	0.468	0.62	0.29	0.8
8	0.36	0.624	0.78	0.27	0.528	0.65	0.36	0.9
9	0.43	0.672	0.8	0.29	0.588	0.7	0.43	1
10	0.51	0.768	0.86	0.35	0.648	0.72	0.52	1.18
11	0.54	0.84	0.93	0.35	0.732	0.74	0.56	1.1
12	0.63	0.9	0.95	0.39	0.792	0.76	0.63	1.25
13	0.7	0.972	0.97	0.46	0.828	0.78	0.77	1.17
14	0.73	1.02	1	0.53	0.912	0.8	0.82	1.2
15	0.83		1.05	0.56	0.972	0.95	0.86	1.2
16	0.89		1.08	0.62	1.056	0.9	0.92	1
17	0.95		1.1	0.67		0.98	0.98	1
18	1		1.1	0.76		1		
19				0.8		1.1		
20				0.89				
21				1				
22								
23								

Separation = 5cm

time	Test 1			Test 2			Test 3	
	Xp	Xf	Vp	Xp	Xf	Vp	Xp	Vp
0	0.01	0.18	0.15	0.02	0.18	0.15	0.006	0.15
1	0.03	0.264	0.2	0.03	0.276	0.2	0.01	0.2
2	0.06	0.324	0.3	0.06	0.336	0.3	0.07	0.38
3	0.1	0.372	0.48	0.1	0.384	0.43	0.1	0.5
4	0.18	0.408	0.55	0.17	0.42	0.55	0.15	0.6
5	0.18	0.444	0.6	0.18	0.456	0.62	0.17	0.55
6	0.22	0.48	0.7	0.23	0.516	0.73	0.22	0.7
7	0.29	0.54	0.75	0.29	0.564	0.8	0.29	0.77
8	0.32	0.6	0.7	0.43	0.624	0.9	0.38	0.95
9	0.35	0.66	0.7	0.45	0.684	0.95	0.48	1.05
10	0.41	0.72	0.82	0.54	0.756	1.05	0.58	1.1
11	0.49	0.816	0.88	0.66	0.84	1.1	0.68	1.1
12	0.55	0.864	0.95	0.67	0.936	1.15	0.76	1.2
13	0.65	0.912	1.1	0.72	1.032	1.2	0.86	1.25
14	0.66	0.972	1.05	0.85		1.25	0.92	1.3
15	0.74	1.068	1.05	0.88		1.1	0.99	1.3
16	0.75		1	1		1.2	1	1.2
17	0.85		0.98			1.2		
18	0.96		1					
19	1		1.15					
20								
21								
22								
23								

Separation = 15cm

time	Test 1			Test 2			Test 3	
	Xp	Xf	Vp	Xp	Xf	Vp	Xp	Vp
0	0.003	0.144	0.4	0.003	0.168	0.3	0.005	0.1
1	0.08	0.228	0.52	0.08	0.228	0.47	0.01	0.2
2	0.12	0.312	0.55	0.11	0.3	0.56	0.06	0.3
3	0.15	0.348	0.6	0.16	0.348	0.61	0.12	0.45
4	0.19	0.408	0.66	0.17	0.384	0.65	0.16	0.63
5	0.24	0.48	0.77	0.21	0.444	0.7	0.19	0.65
6	0.29	0.504	0.8	0.26	0.48	0.73	0.21	0.68
7	0.32	0.576	0.82	0.29	0.54	0.76	0.24	0.73
8	0.37	0.636	0.84	0.32	0.576	0.78	0.3	0.74
9	0.43	0.672	0.85	0.33	0.624	0.8	0.33	0.75
10	0.47	0.732	0.87	0.38	0.672	0.83	0.4	0.84
11	0.51	0.816	0.88	0.41	0.72	0.84	0.46	0.95
12	0.56	0.876	0.89	0.47	0.78	0.86	0.55	1
13	0.57	0.948	0.92	0.51	0.84	0.88	0.63	1.06
14	0.73	0.996	0.95	0.58	0.888	0.9	0.7	1.15
15	0.77	1.068	1	0.63	0.96	0.95	0.76	1.16
16	0.78		1.1	0.7	1.044	1	0.83	1.17
17	0.89		1.1	0.74		1.05	0.89	1.17
18	0.95			0.8		1.1	0.99	1.18
19				0.9		1.15		
20				0.98		1.2		
21								
22								
23								

Separation = 25cm

time	Test 1			Test 2			Test 3	
	Xp	Xf	Vp	Xp	Xf	Vp	Xp	Vp
0	0.015	0.144	0.38	0.04	0.156	0.3	0.005	0.2
1	0.06	0.228	0.39	0.1	0.24	0.4	0.02	0.4
2	0.1	0.3	0.45	0.13	0.312	0.5	0.021	0.5
3	0.13	0.348	0.5	0.16	0.36	0.58	0.12	0.6
4	0.16	0.372	0.55	0.2	0.408	0.65	0.15	0.501
5	0.19	0.42	0.58	0.24	0.432	0.67	0.19	0.668
6	0.23	0.468	0.6	0.29	0.504	0.69	0.2	0.6
7	0.28	0.504	0.63	0.33	0.528	0.71	0.23	0.7
8	0.31	0.528	0.69	0.37	0.564	0.73	0.26	0.8
9	0.32	0.588	0.73	0.41	0.588	0.75	0.31	0.9
10	0.36	0.636	0.75	0.46	0.648	0.77	0.46	1
11	0.4	0.672	0.77	0.47	0.696	0.79	0.55	1.05
12	0.44	0.732	0.78	0.55	0.756	0.81	0.59	1.08
13	0.51	0.78	0.79	0.59	0.816	0.83	0.65	1.1
14	0.55	0.84	0.8	0.65	0.888	0.85	0.74	1.12
15	0.6	0.924	0.81	0.7	0.948	0.88	0.82	1.14
16	0.65	0.996	0.82	0.75	1.02	0.92	0.92	1.16
17	0.71	1.032	0.83	0.82		0.95	0.99	1.2
18	0.76		0.84	0.89		0.98		
19	0.81		0.85	0.96		1		
20	0.86		0.86					
21	0.95		0.89					
22								
23								

Separation = 35cm

time	Test 1			Test 2			Test 3	
	Xp	Xf	Vp	Xp	Xf	Vp	Xp	Vp
0	0.04	0.156	0.668	0.01	0.156	0.1667	0.02	0.3334
1	0.08	0.228	0.668	0.04	0.264	0.5001	0.03	0.4
2	0.11	0.276	0.501	0.07	0.324	0.5001	0.09	0.5
3	0.15	0.324	0.668	0.12	0.36	0.6	0.13	0.6668
4	0.17	0.372	0.334	0.14	0.384	0.5	0.16	0.7
5	0.2	0.42	0.501	0.17	0.42	0.5001	0.21	0.7
6	0.25	0.468	0.5	0.22	0.468	0.7	0.27	0.8
7	0.27	0.492	0.4	0.24	0.492	0.49	0.3	0.8
8	0.28	0.54	0.4	0.27	0.54	0.5001	0.36	0.8
9	0.31	0.576	0.501	0.3	0.588	0.5001	0.41	0.8335
10	0.35	0.6	0.668	0.31	0.624	0.6	0.45	0.84
11	0.4	0.636	0.7	0.38	0.648	0.6	0.49	0.84
12	0.43	0.696	0.6	0.41	0.696	0.7	0.54	0.8335
13	0.47	0.732	0.668	0.47	0.744	0.8	0.58	0.9
14	0.51	0.756	0.668	0.52	0.816	0.8335	0.66	1
15	0.57	0.804	0.9	0.58	0.888	1.0002	0.74	1.1
16	0.57	0.864	0.9	0.63	0.948	0.8335	0.81	1.2
17	0.62	0.924	0.835	0.64	0.972	0.6	0.88	1.1669
18	0.65	0.972	0.7	0.71	1.032	0.6	0.93	1.2
19	0.71	1.032	0.8	0.75		0.6668	0.98	1.1
20	0.77		1.002	0.8		0.8335		
21	0.82		0.835	0.9		1		
22	0.84		1	0.96		1.2		
23	0.92		1					
24	0.97		0.835					

Appendix B

Publications Arising from this Work

1. **Using Cone Calorimeter data for the prediction of fire hazard**
   Accepted for publication in Fire Safety Journal

2. **The early stages of the development of wall fires**
   Presented in the Second Joint Meeting of the US Sections of the Combustion Institute, Oakland, California, US, March 25-28, 2001

3. **The role of the Cone Calorimeter in upward flame spread modelling**
   Presented in the 3rd Asia-Pacific Conference on Combustion, Seoul, Korea, June 24-27, 2001

4. **Modelling the early stages of upward flame spread**
   Proceedings of the 9th International Fire Science and Engineering Conference (Interflam'2001), Edinburgh, Scotland, 17-19 September, pp. 707-718, 2001

5. **Upward flame spread : heat transfer to the unburned surface**
   Submitted for the 7th International Symposium on Fire Safety Science

Accepted to be published in *Fire Safety Journal*

Using Cone Calorimeter data for the prediction of fire hazard

Tsai Kuang-Chung and Dougal Drysdale

Fire Safety Engineering Group, School of Civil and Environmental Engineering
University of Edinburgh, Edinburgh, Scotland

ABSTRACT

The Cone Calorimeter is an apparatus capable of providing quantitative data which are relevant to the response of combustible materials to fire conditions. Several fire models have been developed to use such data to predict various aspects of fire behaviour. This paper considers how these data are used to model upward spread of flame on flat vertical surfaces and proposes that a modified test procedure may be more appropriate.

Keywords: upward flame spread modelling, Cone Calorimeter

Nomenclature

ΔHc	heat of combustion (kW/m^2)
K	constant
$\dot{m}''$	mass loss rate (g/m^2· s)
n	constant
$\dot{Q}'$	rate of heat release per unit width (kW/m^2)
$\dot{Q}''(t)$	rate of heat release (kW/m^2)
$\dot{Q}''_{\max}$	maximum value of the RHR from the Cone Calorimeter (kW/m^2)
t	time (s)
t_p	dummy variable of integral
$V(t)$	flame spread rate (mm/s)
X_b	burnout front height (m)
X_f	flame height (m)
X_p	pyrolysis front height (m)
λ	delay coefficient
τ	ignition delay time (s)
τ_b	burnout time (s)

1.INTRODUCTION

Fire Safety Engineers are responsible for ensuring that buildings will be "safe" in the event of fire. In this context, "safe" implies primarily that the occupants will be able

escape unaided and unharmed. To achieve this, it is necessary to be able to select materials which will not contribute to rapid fire spread. Combustible wall linings are particularly important as their configuration is ideal for rapid spread of fire. Conventionally, wall lining materials are selected using existing standard test methods, but not only are these inflexible but they do not provide engineering data which the Fire Safety Engineer can use to satisfy himself that the material will be "safe" in a particular end-use scenario.

The Cone Calorimeter [1] can provide such data, but there is still considerable debate on how it can best be used. Data have been used to model the response of wall lining materials in the Nordtest Apparatus [2], and to predict the rate of upward flame spread on vertical surfaces. However, insufficient attention seems to have been paid to the relevance of the test scenario of these models. The Cone Calorimeter allows the time to ignition and the rate of heat release to be measured under a range of heat fluxes. Several suggestions have been made about how such data may be used for materials selection, but none has yet been accepted. One school of thought is that the data cannot be used simply to provide arbitrary ranking orders, but should be used in conjunction with flame spread models to assess the likely fire growth rate that could occur in the end-use scenario. The existing upward flame spread models provide a starting point for the development of a proper "engineering tool".

2.MODELLING UPWARD FLAME SPREAD

2.1 The Upward Flame Spread Phenomenon

Vertical flame spread on a combustible wall is rapid because buoyancy-induced boundary layer flow is created by the burning gases: the process is illustrated in Fig. 1. The wall is undergoing pyrolysis (burning) in the region $(X_p\text{-}X_b)$, while the surface ahead of (above) the burning zone is exposed directly to heat transfer from the flame in the region $(X_f\text{-}X_p)$. X_b, X_p and X_f represent the distances of the burnout front, the pyrolysis front and the flame tip from the foot of the "wall". The surface in the region $(X_f\text{-}X_p)$ is heated progressively and when the surface achieves its ignition temperature [3] the leading edge of the pyrolysis zone will advance (i.e. the flame propagates). This is the mechanism of flame spread. Clearly, heat transfer in the region $(X_f\text{-}X_p)$ plays a crucial role [4].

Two upward flame spread models [5, 6] which use data from the Cone Calorimeter to predict full-scale fire behaviour are reviewed and discussed here.

2.2 Karlsson's Model

Karlsson [5] combined the thermal theory of concurrent flame spread developed by Saito, Quintiere and Williams (SQW) [7] with empirical flame height correlations and test data from the Cone Calorimeter to produce an approximate method for predicting fire growth in a corner configuration. Full details can be found in [5], but the assumptions are as follows:

(1) The material is thermally thick, homogeneous and its thermal properties are constant with temperature.
(2) Chemical kinetics is excluded.
(3) The flame length, X_f, depends on a power of $\dot{Q}'$, the rate of convective heat release per unit width of flame front.
(4) Within the region $X_p < X < X_f$, the heat flux from the flame is constant.

He obtained the following expression for the upward flame velocity (an integral equation of the Volterra type (second kind)):

$$V(t)=\frac{1}{\tau}\left[K\left\{X_{po}\dot{Q}''(t)+\int_0^t \dot{Q}''(t-t_p)V(t_p)dt_p\right\}^n-\left(X_{po}+\int_0^t V(t_p)dt_p\right)\right] \quad (1)$$

where $V(t)$ is the flame spread rate, τ is the ignition delay time, X_{po} is the height of the initial burning region, K and n are constants, t is time, t_p is the dummy variable of integration and $\dot{Q}''(t)$ is the rate of heat release (RHR) from the burning material expressed mathematically as

$$\dot{Q}''=\dot{Q}''_{\max}\exp(-\lambda t) \quad (2)$$

where $\dot{Q}''_{\max}$ is the maximum value of the RHR from the Cone Calorimeter test at a heat flux at 20kW/m^2, and λ is the decay coefficient determined empirically from the RHR data. Karlsson used Equation (1) as the basis for calculating the rate of heat release in the room-corner test. There was very satisfactory agreement between predicted and measured values.

2.3 Grant and Drysdale's Model

In Karlsson's model, burnout at the rear of the pyrolysis region is not considered. Grant and Drysdale [6] developed the model further not only to include burnout but also to allow the heat release rate data from the Cone Calorimeter to be used directly as input, without using the approximate form as given in Equation (2). This resolves the problem which arises if the RHR can not be approximated by the equation which assumed that the RHR reaches its maximum value as soon as the sample is ignited, then decreases with a decay coefficient λ.

Before burnout occurs, the expression for the flame spread rate is given in Equation (1), but after burnout occurs, the velocity becomes,

$$V(t)=\frac{1}{\tau}\left[K\left\{\int_{t-\tau_b}^t \dot{Q}''(t-t_p)V(t_p)dt_p\right\}^n-\left(\int_{t-\tau_b}^t V(t_p)dt_p\right)\right] \quad (3)$$

where τ_b is the burnout time. The constants n and K of Equation (1) and (3) are taken as 2/3 and 0.0666, following the flame height correlation of Tu and Quintiere [8]. In the

original application of Grant and Drysdale's model [8], the standard Cone Calorimeter test procedure was used was used with a heat flux of 20 kW/m^2. Very satisfactory results were obtained for the rate of upward flame spread on vertical samples of cardboard.

However, when the model was applied to samples of PMMA, the rate of flame spread was greatly overpredicted [9]. A possible reason for this is that the RHR data from the Cone Calorimeter are obtained under a constant imposed heat flux, selected to model the heat flux to the surface *ahead* of the burning zone. Once burning, the process is self-sustaining and the rate of burning (hence the RHR) is controlled by heat transfer from the flames at the burning surface. No additional heat input is present. The flame spread model still requires data on the time to ignition under an imposed heat flux which models that from the flame in the region (X_f - X_p), but after ignition occurs the RHR in the absence of an imposed heat flux should be used. The schematic of the roles of heat feedback from the flame and the cone heater is presented in Fig.2.

To test this hypothesis, appropriate data have been obtained using the Cone Calorimeter in an unconventional manner. The ignition delay is first determined, but then the cone heater is moved immediately after ignition has occurred, leaving the sample to burn without any supplementary heating. The heater is required only to simulate the heat flux from the flame to the surface in the region (X_f - X_p).

3. EXPERIMENTAL WORK

3.1 Standard Cone Calorimeter Tests

Details of the apparatus, the instrumentation and the standard test procedure for the Cone Calorimeter are given in [1]. A 10 cm square specimen is exposed to a selected radiant flux and the vapours ignited by means of a spark ignition source. The time to ignition is determined and the heat release rate measured by utilising the oxygen consumption principle. This is normalised to unit surface area, giving $\dot{Q}''$ kW/m^2, the main parameter used in the model. For this upward flame spread study, specimens are tested in the vertical orientation. The only other variation from the standard procedure was the backing material used. The sample was held against a 3 mm thick mild steel plate: steel plate of this thickness supported the tall vertical samples on which the rate of upward flame spread was determined.

The heat feedback from the flame to the unburned area in the region (X_f - X_p) is assumed to be constant. In a complementary study [9], this was determined in a series of experiments in which a heat flux meter was mounted flush with the surface of a vertical sample of PMMA, close to the upper edge. This allowed the heat flux from the flame to the unburned zone to be measured as the flame spread upwards. It was found to increase from 6 kW/m^2 near the flame tip to 29 kW/m^2 at the leading edge of the burning zone (Fig.3). This is consistent with measurements made by others [10,11]. A value of 15 kW/m^2 was chosen to represent the average flux for flame spread in the region (X_f - X_p) for vertical samples of PMMA [9]. This is significantly lower than the values taken by

Grant & Drysdale [6], Hasemi [12], Mowrer and Williamson [13] and Kokkala *et al.*[14].

3.2 The Modified Procedure using the Cone Calorimeter

The relevant data were obtained by moving the cone heater away from the sample immediately after ignition. Ideally, it should be removed completely, but this is not possible within the standard equipment. Instead, it was moved upwards into a position in which the lowest edge of the heater was 2.5 cm above the top edge of the sample. In separate experiments the residual radiant flux to the surface was found to be 0.3~0.6 kW/m^2 when the power of the heater was set to give 30 kW/m^2. To a first approximation, it is assumed that the "residual" radiation can be neglected, particularly when the heater is operating at a lower power (15 kW/m^2 at the sample surface).

3.3 Experimental Measurement of the Rate of Upward Flame Spread

A schematic of the experimental set-up is shown in Fig.4. Vertical samples of PMMA (115 cm × 7.5 cm × 6mm thick) were held against a 3 mm thick plate. To obtain one-dimensional flame spread, the vertical edges of the PMMA were protected by strips of mild steel. A 1 cm high strip was ignited at the foot of the sample means of a hand-held blowtorch and the rate of upward flame spread was determined by analysing infra-red videorecordings of each experiment. The accompanying software allowed the pyrolysis front to be tracked as the 300°C contour as it advanced upwards.

4. RESULTS AND DISCUSSION

Typical data on the transient rate of heat release of PMMA samples exposed to 15 kW/m^2 in the standard and "modified" tests are shown in Fig.5. The time to ignition was almost identical in the two tests (480 and 475 s). As expected, the peak rate of heat release observed with the modified procedure is significantly lower than that obtained with the standard procedure. The difference in the duration of burning should also be noted.

The comparison between the experimental results and the flame spread rates predicted from Equations (1) and (3) are shown in Fig 6. It is clear that the result obtained from the model with the RHR data from the modified procedure is in much better agreement with experiment. The early rate of spread appears to be underpredicted, but it is likely that the additional heat provided by the ignition source would affect the early stages of flame spread. This would give a higher initial RHR at the beginning of each experiment.

Given this result, it is surprising that Grant and Drysdale [6] obtained such good agreement for upward flame spread on cardboard when the standard procedure was used to obtain RHR data in the Cone Calorimeter. Using the same model, Anderson and McKeever [15] found good agreement for hardboard, plywood and wallpaper-covered wood surfaces, albeit with a much higher irradiance from the cone heater (35 kW/m^2) [15]. The reason may lie in the sensitivity of the rate of heat release to external radiation.

Brehob and Kulkarni observed that mass loss rates from different materials in the vertical orientation exhibit different sensitivities to external radiation when burning [16]. Assuming that the heat of combustion remains constant during the burning process, mass loss rate is directly proportional to the rate of heat release (Equation (4)) and similar sensitivities would be expected from measurements made in the Cone Calorimeter.

$$RHR = \dot{m}'' \Delta H_c \tag{4}$$

For 6mm thick PMMA (see Fig. 5), the rates of heat release differ markedly in the presence and absence of supporting radiation. Similar results for 2.5mm thick cardboard are shown in Fig.7: there is no significant difference in the RHR curves with and without an imposed heat flux of 15 kW/m^2. Consequently, there is no difference in the predicted rates of upward flame spread on cardboard (Fig. 8).

Clearly it is necessary to use relevant RHR data to be able to apply the model for upward flame spread. For this reason it may be possible to model upward flame spread in alternate scenarios where there is an imposed heat flux. The corner wall configuration falls into the category, in which cross radiation from the adjacent surface enhances the rate of fire development. Karlsson [5] developed his model to predict the development of the rate of heat release in the Nordtest apparatus, using cone data at 20 kW/m^2. This appears to have compensated for the cross radiation effect.

5. CONCLUSION

This paper describes how a modification to the standard procedure for the Cone Calorimeter can provide quantitative data which can be used to model upward flame spread on single vertical sheets of PMMA. The result provides a greater insight into the way in which the test may be used as the basis for the selection of materials for use as wall linings.

REFERENCE

[1] Babrauskas V, The Cone Calorimeter, SFPE Handbook of Fire Protection Engineering, Second Edition, pp. 3-37~3-52, 1995

[2] Nordtest, Surface products: Room fire tests in full scale, Nordtest method NT Fire 025, 1986

[3] Drysdale D, An Introduction to Fire Dynamics, 2nd edition, Wiley-Interscience, New York, 1998

[4] Delichatsios MA, Flame height in turbulent wall fires with significant flame radiation, Combustion Science and Technology, Vol. 39, 00. 195-214, 1984

[5] Karlsson B, A Mathematical model for calculating heat release rate in the room corner test, Fire Safety Journal, Vol. 20, pp. 93-113, 1993

[6] Grant G and Drysdale D, Numerical modelling of early flame spread in warehouse fires, Fire Safety Journal, Vol. 24, pp. 247-278, 1995
[7] Saito K, Quintiere JG and Williams FA, Upward turbulent flame spread, Fire Safety Science, Proceedings of the 1st International Symposium, pp. 75-86, 1985
[8] Tu KM and Quintiere JG, Wall flame heights with external radiation, Fire Technology, Vol.27, pp. 195-203,
[9] Turnbull J and Will G, 4th Year Honours Thesis, Spread of flame on wall lining materials, School of Civil and Environmental Engineering, the University of Edinburgh, 1999.
[10] Quintiere J, Harkleroad M and Hasemi Y, Wall flames and implications for upward flame spread, Combustion Science and Technology, Vol.48, pp. 191-222, 1986
[11] Brehob EG, Kim CI and Kulkarni AK, Numerical model of upward flame spread on practical wall materials, Fire Safety Journal, Vol.36, pp.225-240, 2001
[12] Hasemi Y, Yoshida M, Nohara A and Nakabayashi T, Unsteady-state upward flame spreading velocity along vertical combustible solid and influence of external radiation on the flame spread, Fire Safety Science, Proceedings of the 3rd International Symposium, pp. 197-205, 1991
[13] Mowrer FW and Williamson RB, Flame spread evaluation for thin interior finish materials, Proceedings of the 3rd International Symposium, pp. 689-698, 1991
[14] Kokkala M, Baroudi D and Parker W, Upward flame spread on wooden surface products: Experiments and numerical modelling, Proceedings of the 5th International Symposium, pp. 309-320, 1997
[15] Anderson M and McKeever C, An Experimental study of upward flame spread on cellulosic materials, Proceedings of the Seventh International Fire Safety and Engineering Conference INTERFLAM'96, pp. 169-178, 1996
[16] Brehob EG and Kulkarni AK, Time dependent mass loss rate behavior of wall materials under external radiation, Fire and Materials, Vol. 17, 249-254, 1993

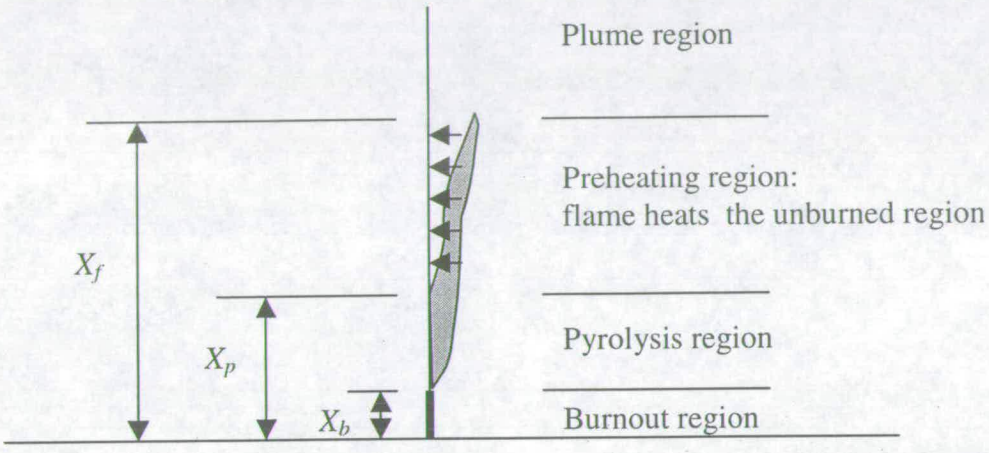

Fig.1 Upward flame spreading

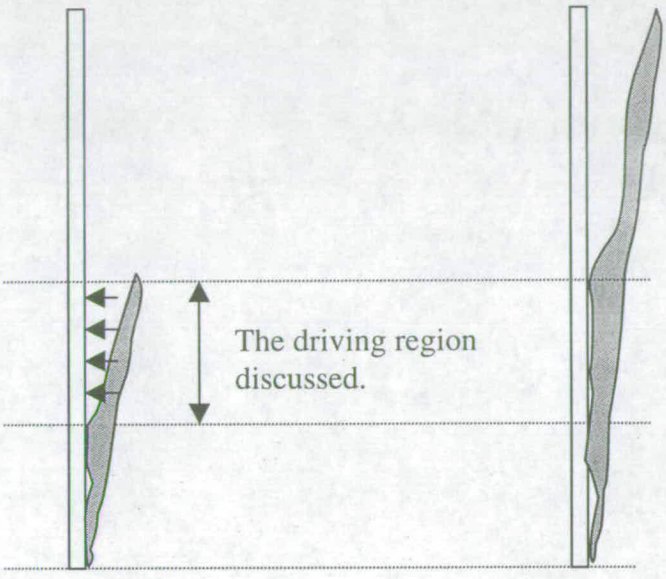

(a) the unburned region before ignition (b) the unburned region after ignition

(a') the sample before ignition (b') the sample after ignition

Fig.2 The schematic of the roles of heat feedback from the flame and the cone heater.

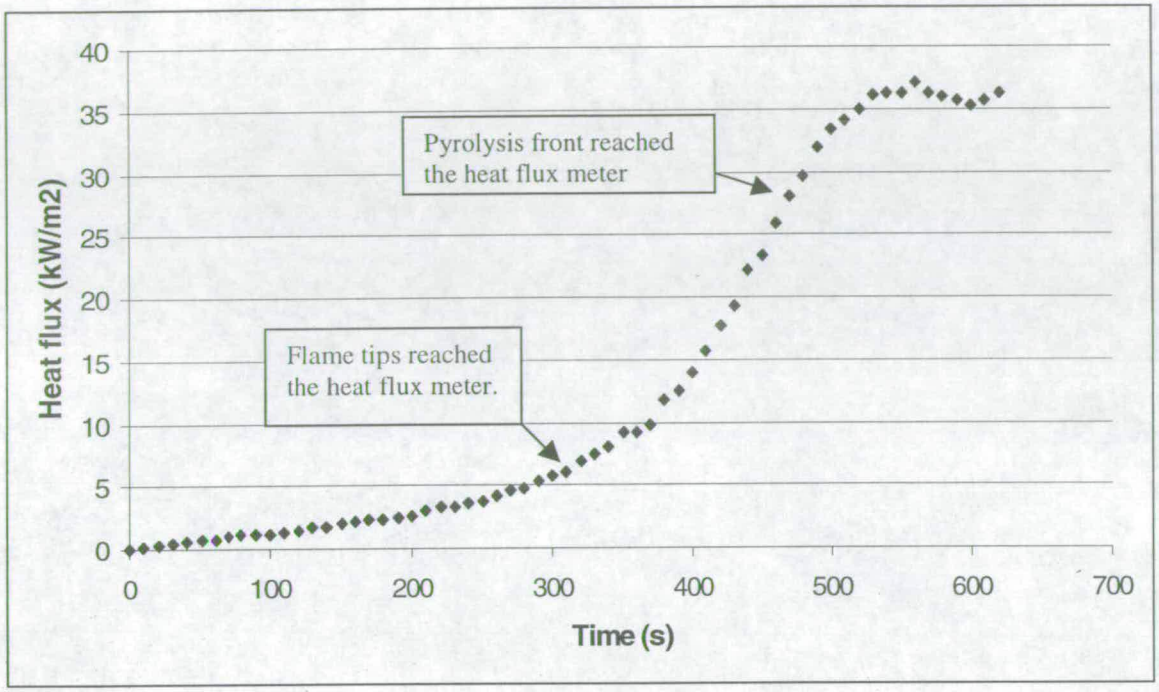

Fig.3 Heat flux measured at the top of a 50cm high PMMA slabs.

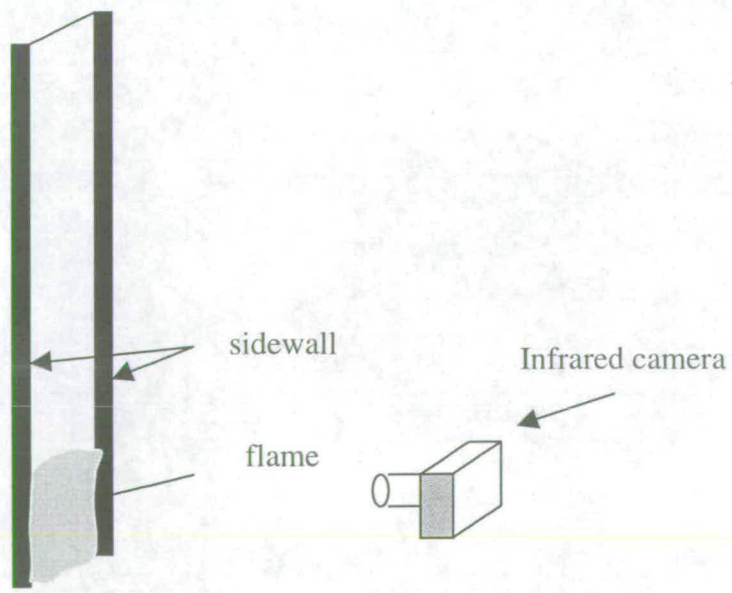

Fig.4 The experimental rig of measuring positions of pyrolysis fronts.

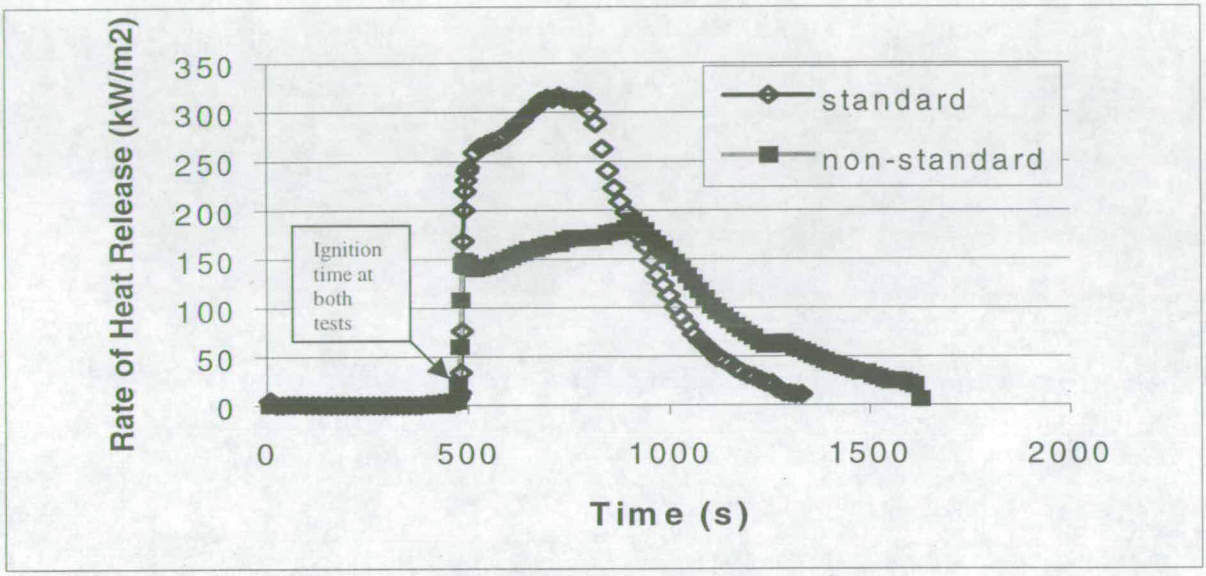

Fig. 5 The rate of heat release of PMMA samples from Cone Calorimeter under irradiance of 15kW/m^2 in the standard and non-standard test procedures.

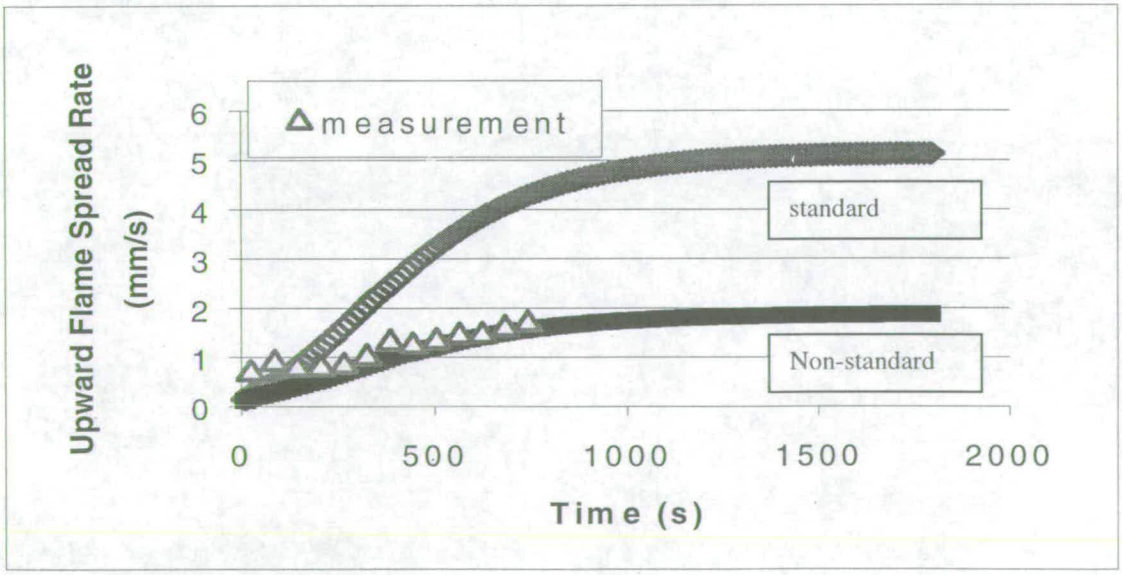

Fig. 6 The comparison of the experimental measurement of the flame spread rate of 6mm thick PMMA slabs and the prediction from Grant and Drysdale's model with the standard and non-standard test procedures.

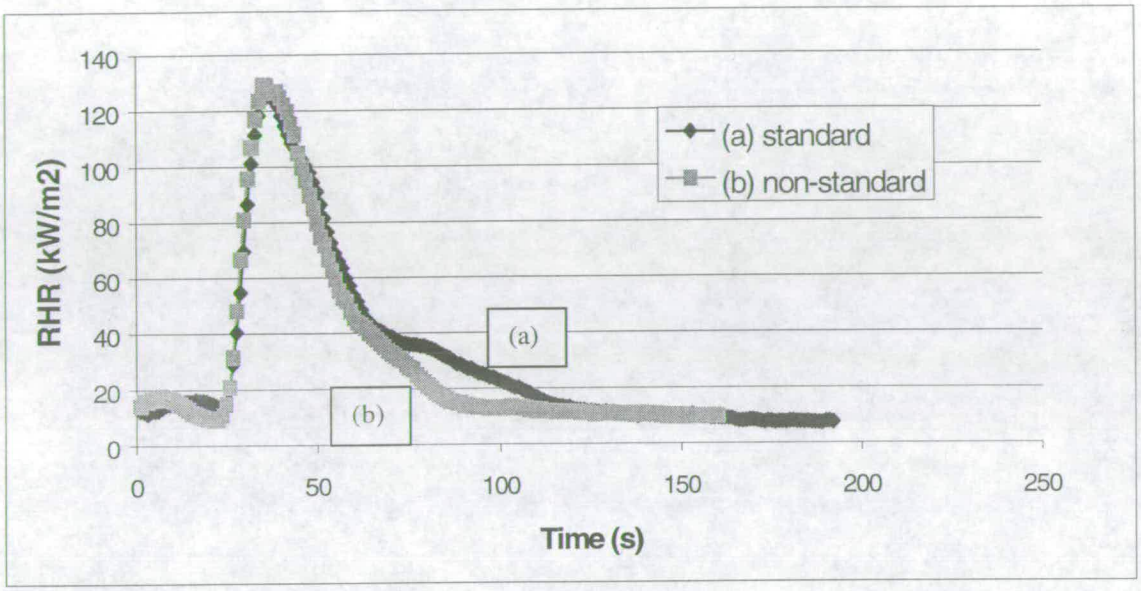

Fig.7 The rate of heat release of 2.5mm thick cardboard from the Cone Calorimeter with the standard and non-standard test procedures. (The irradiance of the cone heater: 20kW/m^2)

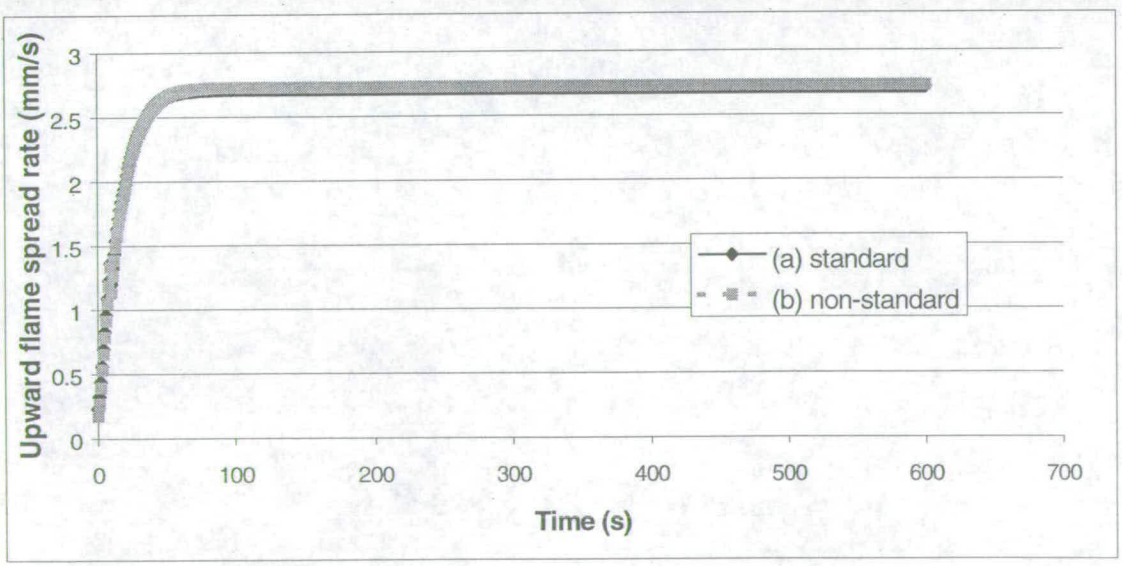

Fig.8 Upward flame spread rate of 2.5mm thick cardboard predicted by Grant and Drysdale's model with the standard and non-standard Cone Calorimeter test procedures. (The two predictions using the standard and non-standard procedures overlap.)

Second Joint Meeting of the US Sections of the Combustion Institute, Oakland, CA, March 25-28, 2001

Paper No. 155

The Early Stages of the Development of Wall Fires

Kuang-Chung Tsai and Dougal Drysdale

Fire Safety Engineering Group, School of Civil and Environmental Engineering

University of Edinburgh, Edinburgh, Scotland, UK

ABSTRACT

Previous work has demonstrated that the flame height of a wall fire is one of the two most important parameters which determine the rate of vertical spread. Models of vertical flame spread rely on empirical flame height correlations which have the form $X_f = K\dot{Q}'^n$, but these are based on simulations of wall fires using line burners, and estimates of the rate of heat release from fires on vertical surfaces. There have been no carefully controlled experiments designed to establish the validity of these correlations and data do not exist for values of $\dot{Q}' <$ c.25 kW/m

This paper describes the first part of an experimental programme designed to examine the flame height correlation by direct, systematic and simultaneous measurement of $\dot{Q}'$ and X_f from real wall fires. The focus here is on the earliest stages of a wall fire in which $\dot{Q}' < 30$ kW/m. PMMA slabs, 6 mm thick, with heights ranging from 2.5 to 25 cm and widths from 5 to 15 cm were used to study the effect of the aspect ratio (width/height) of the burning area as well as the lower edge boundary configuration. Four configurations were examined.

The experimental data suggest that the flame height correlates with $\dot{Q}'$, but there are differences between the four lower edge boundary configurations. There does not appear to be any significant dependence on the aspect ratio of the burning surface, but at these low values of $\dot{Q}'$, the flame height is more sensitive to $\dot{Q}'$ than observed for the larger heat release rates.

NOMENCLATURE

Cp	specific heat of ambient air
D	characteristic length
g	gravity acceleration
K	empirical constant
L_f	flame height (of line fires)
$\dot{m}'$	the rate of supply of fuel (per unit width of burner) (kg/m.s)
$\dot{m}''$	the rate of supply of fuel (kg/m^2.s)
n	constant

$\dot{Q}'$ rate of heat release per unit width (kW/m)
$\dot{Q}''$ rate of heat release per unit area (kW/m^2)
$\dot{Q}_l^*$ dimensionless parameter $\dot{Q}_l^* \equiv \dot{Q}/\rho_\infty C_p T_o g^{1/2} D^{3/2}$
To temperature of ambient air
w width of solid fuel (m)
X_b burnout height (m)
X_f flame height (m)
X_p pyrolysis height (m)
ρ_∞ density of ambient air
γ constant
ΔH_c heat of combustion (kJ/kg)

INTRODUCTION

Flame is the luminous portion of the volume within which combustion is occurring. Thus flame height could be inferred as the vertical visible extent of the gas phase burning process. For a wall fire (flame spreading upwards), flame height has been shown to be one of the two most important parameters driving the rate of upward spread [1], the other being the heat transfer to the unburned surface ahead of the burning zone. Several models [2-9] have combined these parameters to assess the risk of fire growth on vertical surfaces. However, the reliability of these models depends on the accuracy of the flame height correlation.

PREVIOUS THEORETICAL AND EXPERIMENTAL INVESTIGATIONS

Figure 1 is a schematic diagram of a developing wall fire. The solid fuel is pyrolyzing in the region $\left(X_p - X_b\right)$ and the flame tips reach X_f. The region X_b corresponds to the burnt out zone. Where burning is established, fuel vapours are released from the surface and enter the flame which is confined to the buoyancy-induced boundary layer. Heat is transferred to the surface above the pyrolysis region, progressively raising its temperature to the firepoint, allowing the flame to advance upwards.

Based on these observations, several theoretical analyses [1,10,11] have led to a correlation of the flame height for wall fires. Quintiere et al. [10] assumed that a flame extends until the fuel is completely consumed. Delichatsios [1] postulated that flame heights in buoyant diffusion flames (laminar or turbulent) are essentially independent of the stoichiometry and depend only on total heat release rate. This hypothesis was later supported by the derivation of flame height expressions from experimental results and physical arguments of buoyancy, heat transfer, mass flow rate, etc. [1]. Aeklund [11] established a two-dimensional vortex model by demonstrating flame as a region of intense vorticity generation, which is capable of predicting the flame height. All of these studies concluded that the flame height is proportional to the rate of heat release per unit width in a two-thirds power law (n=2/3 in Equation 1).

$$X_f = K\dot{Q}'^n \qquad (1)$$

where X_f is the height of flame, K and n are constants and $\dot{Q}'$ is the rate of heat release (RHR) per unit width from vertical burning solids.

Several experimental investigations [2,10,12-15] using different experimental rigs have also been carried out to analyse the flame height phenomenon. A comparison of these experiments is given in Table 1, showing the type of fire (linear burner or wall fire; whether steady or spreading fires, laminar or turbulent), the geometric configuration and whether or not sidewalls were present. These experiments can be classified into two types: (1) linear fires produced by line burners against a wall, and (2) vertical burning fuels in which the rate of mass loss was measured and the heat of combustion assumed to be constant.

(1) Linear fires produced by line burners against a wall

Porous line burners against isothermal and thermally thin walls were used in studies by Hasemi [12] and Sugawa *et al.* [13] to simulate the wall fires. In Hasemi's study [12], sidewalls were present to help maintain two-dimensional flow. Sidewalls are not mentioned in Sugawa's study [13]. By changing the rate of supply of gaseous fuel, different rates of heat release were simulated. The corresponding heights of the flame tips were recorded by video camera. The rate of heat release (RHR) per unit width was calculated from Equation 2.

$$\dot{Q}' = \dot{m}' \Delta H_c \tag{2}$$

where $\dot{m}'$ is the rate of supply of fuel (per unit width of burner) (kg/m.s) and ΔH_c is its heat of combustion (kJ/kg).

A dimensionless parameter $\dot{Q}_l^* \equiv \dot{Q}/\rho_\infty C_p T_o g^{1/2} D^{3/2}$ was found to determine the flame height as follows:

$$L_f / D = \gamma \dot{Q}_l^{*n} \tag{3}$$

where L_f is the flame height, D is a characteristic length and γ is a constant. In Hasemi's study [12], for $\dot{Q}_l^* \geq 1$, n = 2/3 and γ =6.0. For $\dot{Q}_l^* < 1$, n=0.8. In Sugawa's study [13], n was confirmed experimentally to be 2/3 in the range $5 < \dot{Q}_l^* < 20$.

Hasemi's data [12] with natural gas and other gaseous fuels were interpreted by Tu and Quintiere [14]: the results are plotted in Figure 2 and show the following correlation:

$$X_f = 0.032 \dot{Q}'^{0.76} \tag{4}$$

The r^2 value is 0.89. The value of n is appreciably greater than the expected value of 2/3 derived from theoretical analyses.

(2) Vertical burning fuels, assuming a constant heat of combustion

Flame height measurements on 28.4 cm square samples of burning materials in a vertical orientation were made by Quintiere *et al.* [10]. A pilot ignition flame was placed at the base and sidewalls were provided to prevent lateral air entrainment. By exposing the samples to different levels of external radiation, various solid fuel burning rates could be simulated. Once steady burning had been achieved, the flame height was measured. Assuming a constant heat of combustion, RHR per unit width was calculated by following Equation (5).

$$\dot{Q}' = \dot{Q}'' X_p \tag{5}$$

where $\dot{Q}''$ is the RHR per unit surface area. Their data followed the 2/3 power law (see Equation 1) although there was considerable scatter. Tu and Quintiere [14] modified the experimental rig to allow the measurement of transient mass loss rate and the corresponding flame height for both charring and non-charring materials (PMMA and wood; 28.5 cm wide and 29.5 cm high). Using Equation 6,and then Equation 5,

$$\dot{Q}'' = \dot{m}'' \Delta H_c \tag{6}$$

the flame height correlation was found to obey the 2/3 power law, but the value of K was higher than for the results obtained from line fires against a wall [14]. Figure 3 compares the data from references [10] and [14]. The best fit still follows Equation 1 with a correlation coefficient of 0.79, but with $n = 0.58$.

$$X_f = 0.09 \dot{Q}'^{0.58} \tag{7}$$

Orloff *et al.* [15] and Saito *et al.* (SQW) [2] also measured flame heights but used PMMA sheets up to 150 cm. In both of these studies, line burners were adopted to ignite the lowest edge of samples, but sidewalls were only used by Orloff *et al.* [15]. One significant difference from the earlier work was the presence of a floor which would have altered the mode of air entrainment at the base of the "wall". The flame height of the spreading flame was correlated in SQW's study [2] by calculating the RHR per unit width from the estimated fuel supply rate and heat of combustion (Equation 6 and then 5). The flame height correlation obeyed Equation 1, but with a higher value of n than that obtained from steady burning experiments [10]. This can been seen in Figure 4 which compares all of the above correlations [2, 10, 15] and Delichatsios' analysis [1]. The higher power may be a result of the higher pyrolysis rates achieved in the upper part of the pyrolysing fuel during the spreading process [2,15]. It was also noted that the presence of sidewalls increased the length of the flames because two-dimensional flow patterns were maintained [2].

Although the flame height correlations of the line fires [12,13] and the wall fires [2,10,14,15] seem to be similar and agree with Equation 1, the behaviour of the flames is different. The linear flame experiments cannot simulate real wall fires. Even when "real wall fires" are involved [2, 10, 14], the assumption that the heat of combustion remains constant may not be realistic. There is a need to measure the RHR directly during the experiments.

Consequently, there is still uncertainty in the validity of the correlation. Equation 1 suggests that the flame height is related only to $\dot{Q}'$, and no other factors are considered. In particular, there is no information on the effect of the aspect ratio (height/width) of the burning area. It is known that the rate of upward spread increases with the width of the burning material. This may be explained in terms of increased radiative heat transfer [16], but equally the flame height may be increased. The effect of different geometric configurations at the base of the "wall" (for example, with and without a contiguous floor) has not been considered either. As this will influence the air entrainment pattern at the base of the wall, it may also have an effect of flame height. An experimental rig was designed to provide data which would help resolve the effects of the aspect ratio (height/width) and air entrainment at the early stages of the development of wall fires.

EXPERIMENTAL WORK

The experimental rig is shown in Figure 5 in schematic form. It was designed to hold vertical samples of combustible material at the lower edge of (and in the same plane as) a 60 cm high inert board. The sample was mounted on a 3 mm thick steel plate: in addition to preventing flame spreading up the back of the sample, it kept the rear face relatively cool and prevented distortion and slumping which would otherwise have occurred. The vertical edges of the sample were protected by 3 mm thick mild steel strips designed to hold the sample against the backing plate and help prevent lateral air entrainment along the burning sample. The rig was located below the hood of a Cone Calorimeter, thus allowing the rate of heat release from the burning sample to be measured directly. A hand-held butane-fuelled torch was used to ignite the surface of each sample uniformly. The inert wall was marked with a scale and a Video Camcorder was used to record each experiment. The flame height was determined subsequently by visual examination of the videorecordings which were then matched to the corresponding heat release rates.

The combustible material used was PMMA, as 6 mm thick slabs with heights ranging from 2.5 to 25 cm and widths of 4, 8 and 12 cm to simulate the early stages of vertical burning and to allow the effects of different aspect ratios to be studied. By using sample heights up to 25 cm, the laminar, transition and turbulent burning regimes could be observed, as noted by Orloff *et al.* in their PMMA experiments [15].

Modifications could be made to allow four different geometric configurations to be studied (see Fig.6 (A)-(D)). In three cases, the burning area was at the foot of the "wall". With Case A, there was a contiguous floor, but this was absent in Cases B and C. In Case B, the bottom edge was unprotected while in Case C the bottom edge was protected by a steel strip. In the fourth configuration (Case D), the sample represented a central burning area on an extended wall.

RESULTS AND DISCUSSION

Figure 7 shows the RHR history for a burning PMMA sample, 8cm wide, 10cm high and 6mm thick in the configuration corresponding to Case A (with a contiguous floor). The ignition process took approximately 100 s and was followed by a period of unsteady burning (from 100s to 350s) during which the RHR increased to a steady peak

value (corresponding to 150 kW/m^2 in this case) before burnout started (after 500s). The height of the flame during steady burning was determined (100-350s in Figure 7). The heights of the continuous flame and the flame tip were observed, but the flame height was recorded as the average of the visible flame height.

The effect of aspect ratio (R = height/width) on the correlation is shown in Figure 8 for Cases A and D. These represent the very different geometries and indicate that the effect of R is negligible for $\dot{Q}' < 30$ kW/m^2 within the range of values of R used (0.3125 to 2.5). The same result is found for Cases B and C.

In Figures 9a and 9b, the dependence of X_f on $\dot{Q}'$ for all four geometries is shown as normal and logarithmic plots. When $\dot{Q}'$ is less than c.10 kW/m, the data for all four configurations fall on the same line, but above c.10 kW/m, the data become scattered and systematic differences in the four series of flame height correlations can be observed.

For Case A (a burning wall with a contiguous floor),

$$X_f = 0.016\dot{Q}'^{1.07} \tag{8}$$

For Case B (a burning wall with no floor and no protection of the bottom edge),

$$X_f = 0.018\dot{Q}'^{1.00} \tag{9}$$

For Case C (a burning wall with no floor but with the bottom edged protected)

$$X_f = 0.023\dot{Q}'^{0.98} \tag{10}$$

For Case D (a burning wall with an extended plate),

$$X_f = 0.011\dot{Q}'^{1.25} \tag{11}$$

The r^2 values for these four cases (Equations 8 - 11) are 0.931, 0.968, 0.987 and 0.963 respectively, and the values of n are close to unity. In addition, it can be seen that the burning walls set in an extended plate (Case D) produce the tallest flames. While further work would be required to explain this observation, it seems likely that it is a consequence of the fact that the burning area is part of a larger flat surface. The Case D flames may be less turbulent than those observed for Cases A, B and C. In general, turbulence tends to reduce the height of a diffusion flame, but the Case A flames are of similar height to the Case D flames, both being higher than Cases B and C (Figure 9a). Clearly, the effect of the lower edge boundary conditions needs to be studied in greater detail. The best fit line encompassing the data from all four Cases is included in Figure 4. This shows that the flame height is more sensitive to $\dot{Q}'$ than predicted by Equation 6 in this range of values of $\dot{Q}'$, but that Equation 6 will overpredict the height of the flames when $\dot{Q}' < 25$ kW/m. .

The steady values of $\dot{Q}'$ obtained for the different geometric configurations are listed in Table 2a and plotted in Fig. 10. Samples with a lower-edge protection (Case C) produced the lowest values of $\dot{Q}'$ while Case B samples produced the highest. It seems likely that the increased burning area due to the involvement of the lower edge would account for this observation. When PMMA samples burned with a contiguous floor (Case A), the lowest 10 mm of the flame was blue in colour, suggestive of a well-mixed region producing "premixed-like" burning. This may have caused higher local heat transfer and thus a higher local rate of burning, consequently producing a higher value of $\dot{Q}'$. This is consistent with observations made by Foley and Drysdale [16] on the effect of a "floor" on the rate of heat transfer to a vertical wall exposed to a line burner.

In Table 2b, the steady-state rate of burning (expressed as a mass flux, $\dot{m}''$ g/m^2.s) of PMMA slabs of different heights are compared for these four configurations. The mass fluxes were calculated from the steady state values $\dot{Q}'$, assuming the heat of combustion of PMMA to be constant at 24.89 kJ/g [16]. The burning rate is found to decrease as the height of the burning sample increases. This is consistent with the study carried out by Orloff *et al.* [18] on the burning of thick vertical slabs of PMMA, 0.91 m wide and $\geq$ 1.5 m high. Their configuration corresponded to Case A. They also found that the rate of burning decreased with height over the first 20 cm from the bottom edge although the decrease was not so pronounced (about 15%).

Clearly, the lower edge configuration has a significant effect on the flame height correlation. More work is required to obtain a fuller understanding of this behaviour, but it seems likely that the pattern of air entrainment is an important factor.

CONCLUSION

The flame height correlation of wall fires on their early stages of development ($\dot{Q}' <$ 30kW/m) under different geometric configurations has been shown to conform to a correlation of the form of Equation 1 and be independent of the aspect ratio of the burning surface in the range of parameters studied. For the first time, rates of heat release and flame heights were measured directly in the same experiments. The correlation was found to depend on the lower edge configuration. Data for $\dot{Q}' > 30$ kW/m need to be obtained to investigate the correlation for fully developed turbulent wall flames. The limited space within the test section of the Cone Calorimeter prevented such measurements being carried out in this part of the project.

The configurations which have been studied represent four possible scenarios that may exist during the early stage of fire development on a wall. The correlations were derived from steady flames although a flame height correlation for a spreading wall fire would be closer to the real situation. It is hoped that this study will lead to a better understanding and provide more robust correlations for modelling upward flame spread.

REFERENCE

[1] Delichatsios MA, Flame Heights in Turbulent Wall Fires with Significant Flame Radiation, Combustion Science and Technology, Vol. 39, pp. 195-214, 1984
[2] Saito K, Quintiere JG and Williams FA, Upward Turbulent Flame Spread, Fire Safety Science- Proceedings of the First International Symposium, pp. 75-86, 1985
[3] Hasemi Y, Thermal Modeling of Upward Wall Flame Spread, Fire Safety Science-Proceedings of the First International Symposium, pp. 87-96, 1985
[4] Delichatsios MM, Mathews MK and Delichatsios MA, An Upward Fire Spread and Growth Simulation, Fire Safety Science- Proceedings of the Third International Symposium, pp. 207-216, 1991
[5] Karlsson B, A Mathematical Model for Calculating Heat Release Rate in the Room Corner Test, Fire Safety Journal, Vol.20, pp. 93-113, 1993
[6] Grant G and Drysdale D, Numerical Modelling of Early Flame Spread in Warehouse Fires, Fire Safety Journal, Vol.24, pp. 247-278, 1995
[7] Kokkala M, Baroudi D and Parker WJ, Upward Flame Spread on Wooden Surface Products: Experiments and Numerical Modelling, Fire Safety Science- Proceedings of the Fifth International Symposium, pp. 309-320, 1997
[8] Brehob E and Kulkarni AK, Experimental Measurements of Upward Flame Spread on a Vertical Wall with External Radiation, Fire Safety Journal, Vol.31, pp.181-200, 1998
[9] Ohlemiller TJ and Cleary TG, Upward Flame spread on Composite Materials, Fire Safety Journal, Vol.32, pp.159-172, 1999
[10] Quintiere J, Harkleroad M and Hasemi Y, Wall Flames and Implications for Upward Flame spread, Combustion Science and Technology, Vol. 48, pp. 191-222, 1986
[11] Aeklund TI, A Vortex Model for Wall Flame Height, Journal of Fire Sciences, Vol.4-January/February, pp.4-14, 1986
[12] Hasemi Y, Experimental Wall Flame Heat Transfer Correlations for the Analysis of Upward Wall Flame Spread, Fire Science and Technology, Vol.4, No.2, pp. 75-90, 1984
[13] Sugawa O, Satoh H and Oka Y, Flame Height from Rectangular Fire Sources Considering Mixing Factor, Fire Safety Science- Proceedings of the Third International Symposium, pp. 435-444, 1991
[14] Tu KM and Quintiere JG, Wall Flame Heights with External Radiation, Fire Technology, pp.195-203, 1991
[15] Orloff L, De Ris J and Markstein GH, Upward Turbulent Fire Spread and Burning of Fuel Surface, The Fifteenth Symposium (International) on Combustion, pp. 183-192, 1974
[16] Drysdale DD, Introduction to Fire Dynamics, 2nd edition, John Wiley&Sons, 1998
[17] Foley M and Drysdale DD, Heat Transfer from Flames between Vertical Parallel Walls, Fire Safety Journal, Vol.24, pp. 53-73, 1995
[18] Orloff L, Modak AT and Alpert RL, Burning of Large-Scale Vertical Surfaces, The Sixteenth Symposium (International) on Combustion, pp. 1345-1354, 1976

Investigator(s)	Line or wall fire	Geometric configuration	Laminar or turbulent	Spreading or steady flame	Sidewall	Method used to obtain $\dot{Q}'$ (**)
Hasemi [12]	line fires	without floor but with a line burner below burning slabs	-	steady	yes	ΔHc(E) $\dot{m}'$ (C) (Eqn.2)
Sugawa et al [13]	line fires	with floor	-	steady	no	ΔHc(E) $\dot{m}'$ (C) (Eqn.2)
Quintiere et al [10]	wall fires	without floor but with a line burner below burning slabs	turbulent	Spreading (*)	yes	$\dot{Q}''$ (E) (Eqn.5)
Tu and Quintiere [14]	wall fires	without floor but with a line burner below burning slabs	turbulent	spreading	yes	ΔHc(E) $\dot{m}''$ (M) (Eqn.6)
SQW [2]	wall fires	with floor	turbulent	spreading	no	ΔHc(E) $\dot{m}''$ (E) (Eqn.6)
Orloff et al [15]	wall fires	with floor	from laminar to turbulent	spreading	yes	–

Table 1 Flame situations (line or wall fires; steady or spreading flames; laminar or turbulent), geometric configuration and sidewall effects of previous experimental set-ups on flame height correlations.

(*) The flame produced was spreading but measurements were carried out as it became steady.

(**) (E): estimated, (C): controlled (gas flow), (M) measured

(a) RHR per unit width (kW/m)

Height, Xf (cm)	(Case A) with a floor 	(Case B) without a floor and an extended plate 	(Case C) with lower edged protection 	(Case D) with an extended plate 
2.5	4.59 ± 0.31	5.81 ± 0.71		4.57 ± 0.42
5	8.41 ± 0.44	10.30 ± 0.26	7.58 ± 0.62	9.28 ± 0.08
10	16.92 ± 2.14	18.52 ± 1.27	11.00 ± 0.68	13.78 ± 1.48
15	14.38 ± 0.28	16.08 ± 1.07	14.66 ± 1.27	14.68 ± 1.60
20	19.19		17.40 ± 0.32	18.13
25	21.43 ± 1.43	24.92	21.44 ± 0.86	

(b) Mass loss rate m″ (g/m² s)

(with assumption of the Hc of PMMA: 24.89 kJ/g)

2.5	7.38	9.34		7.34
5	6.76	8.28	6.09	7.46
10	6.80	7.44	4.42	5.54
15	3.85	4.31	3.93	3.93
20	3.85		3.50	3.64
25	3.44	4.01	3.45	

Table 2 (a) and (b) The steady RHR per unit width and mass loss rate of 6mm thick, 8cm wide PMMA samples with different geometric configurations.

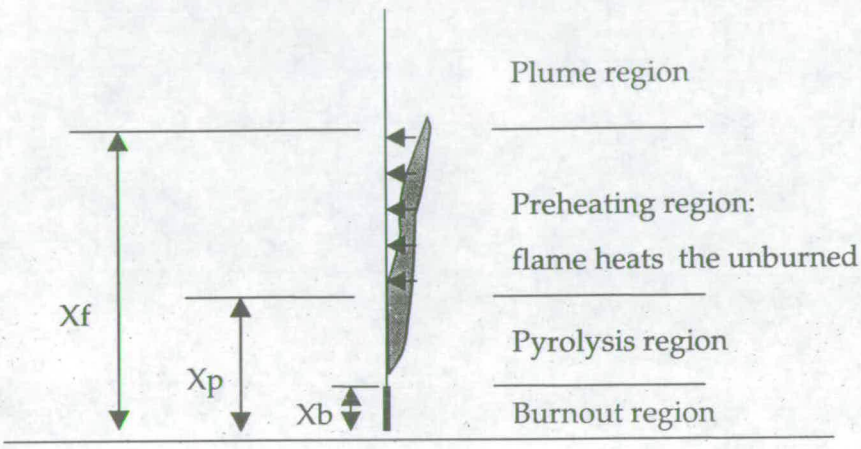

Fig.1 Upward flame spreading

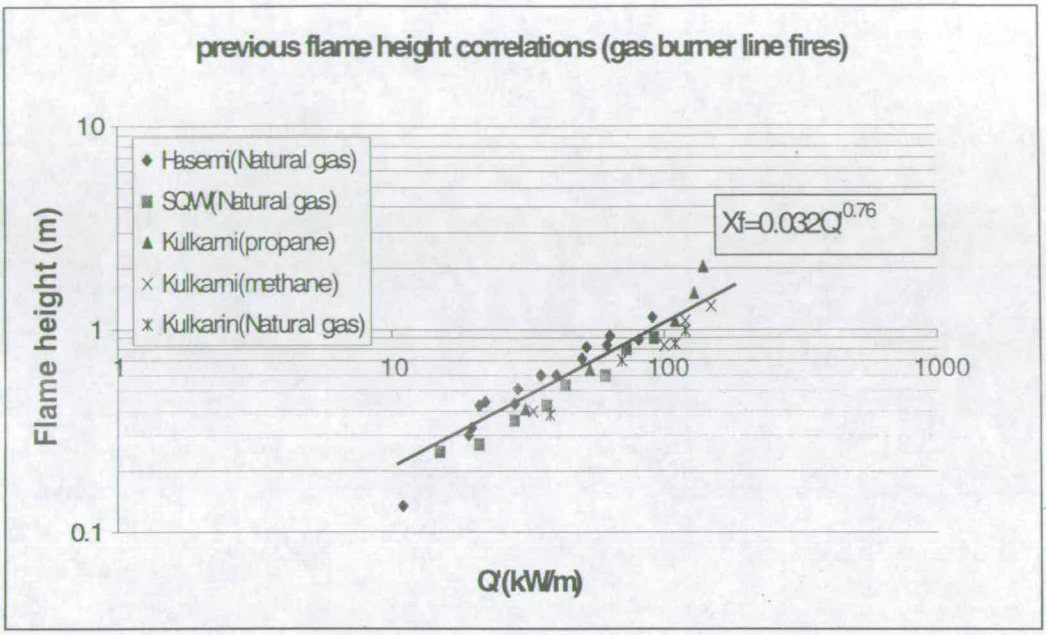

Fig.2 Previous flame height correlations carried out with gas burner line fires by Hasemi [3], SQW [2] and Kulkarni (SQW and Kulkarni's data were interpreted from Tu and Quintiere's study [14]).

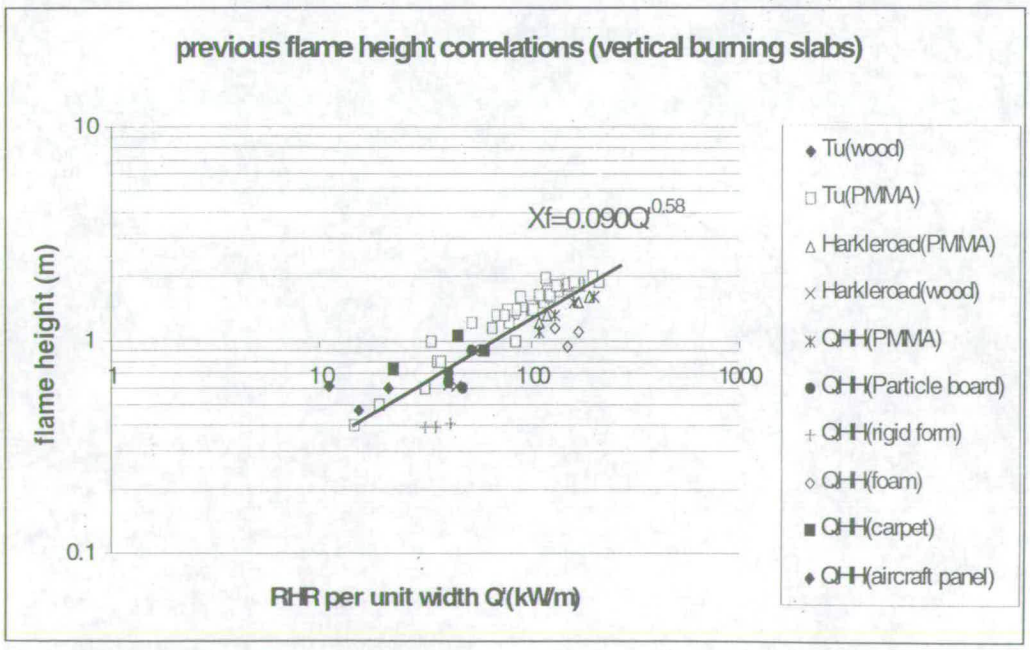

Fig.3 Previous flame height correlations carried out with burning solid fuels by Tu and Quintiere [14], Quintiere et al (QHH) [10] and Harkleroad (interpreted from [14])

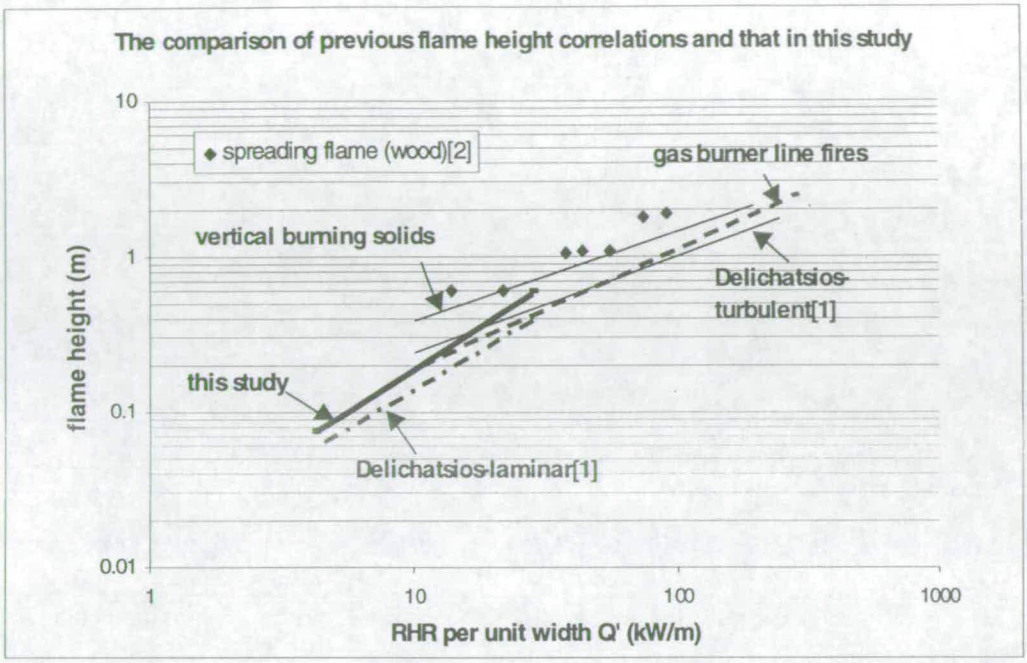

Fig.4 The comparison of previous flame height correlations of spreading fire (wood, [2]), gas burner line fires, vertical burning slabs, Delichatsios analysis (laminar and turbulent) [1] and measurement of this study (details see Fig.9).

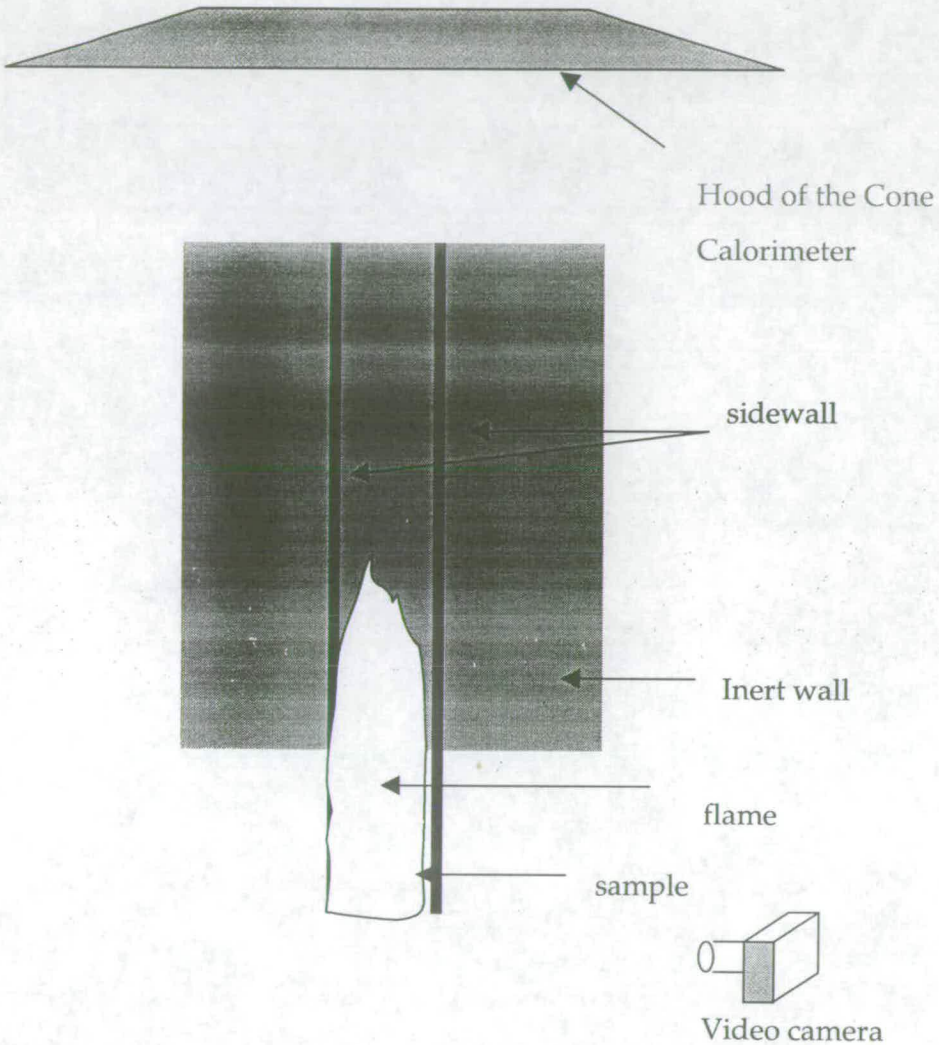

Fig.5 The experimental rig inside the test chamber of the Cone Calorimeter

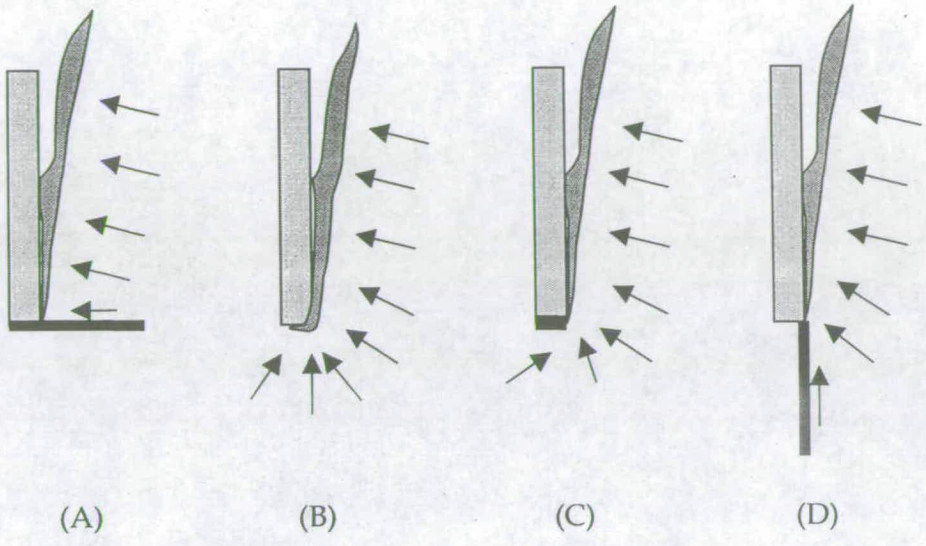

Fig.6 Four geometric configurations which influence the air entrainment patterns of wall fires: Case A: a burning wall with a contiguous floor, Case B: with no floor and no protection of the bottom edge, Case C: with no floor, but with the bottom edge protected and Case D: with an extended wall with a central burning area. (▲ : the direction of air entrainment)

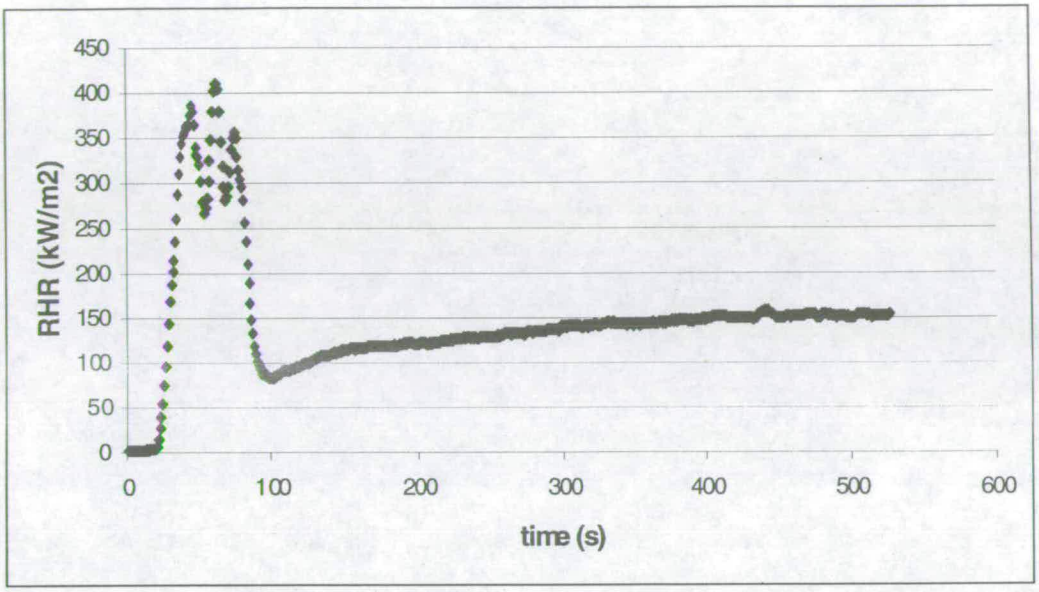

Fig.7 The RHR history of a 6mm thick, 8cm wide and 10cm high burning PMMA sample with a contiguous floor. After the sample was ignited by a torch (after 100s), a period of unsteady burning (from 100s to 350s) was observed before a peak burning period (after 350s) and burnout started (around 500s).

Fig. 8(a) (Case A)

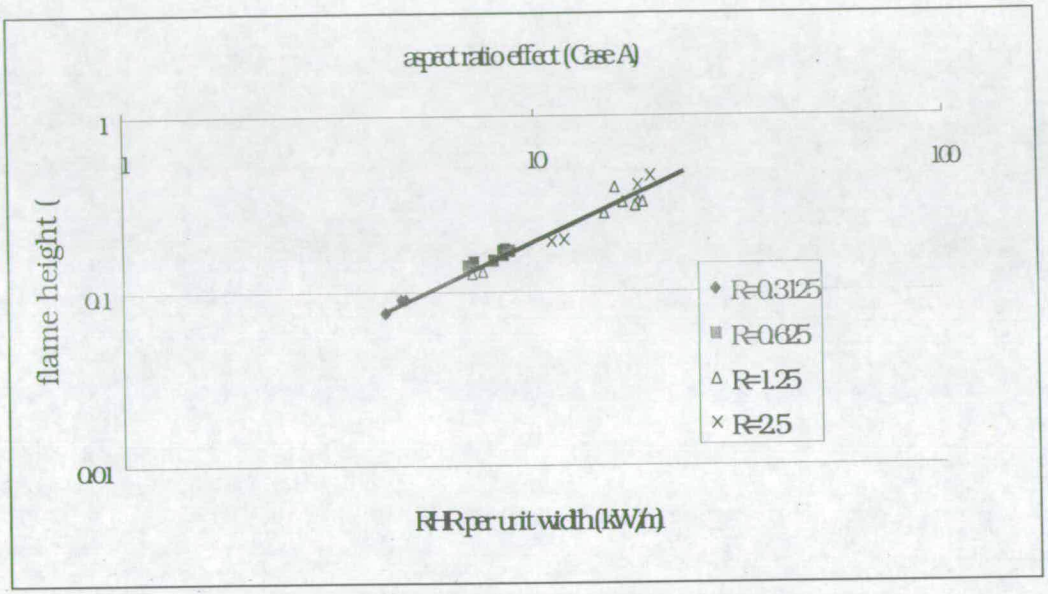

Fig.8(b) (Case D)

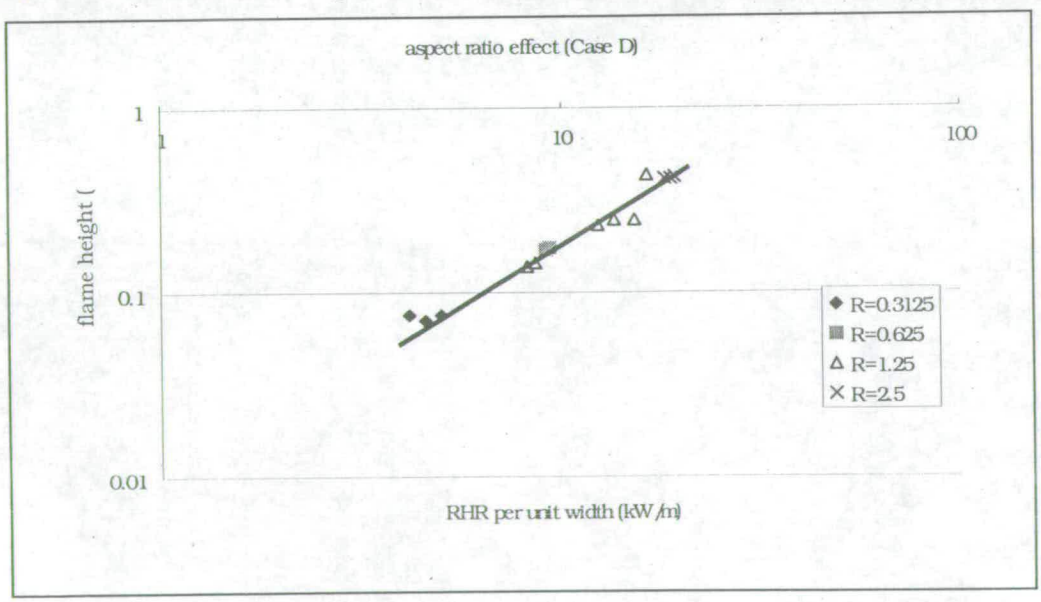

Fig.8 The effect of aspect ratio (height/width) of 6mm thick PMMA samples on the flame height correlation under geometric configurations of Case A and D (in Fig. 6).

Fig. 9(a)

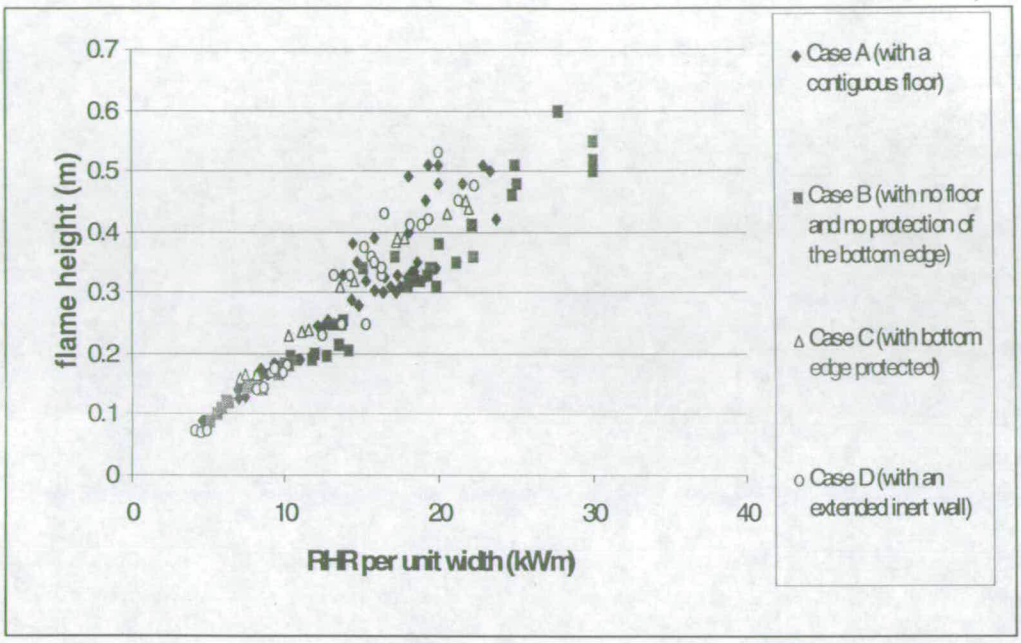

Fig. 9(b)

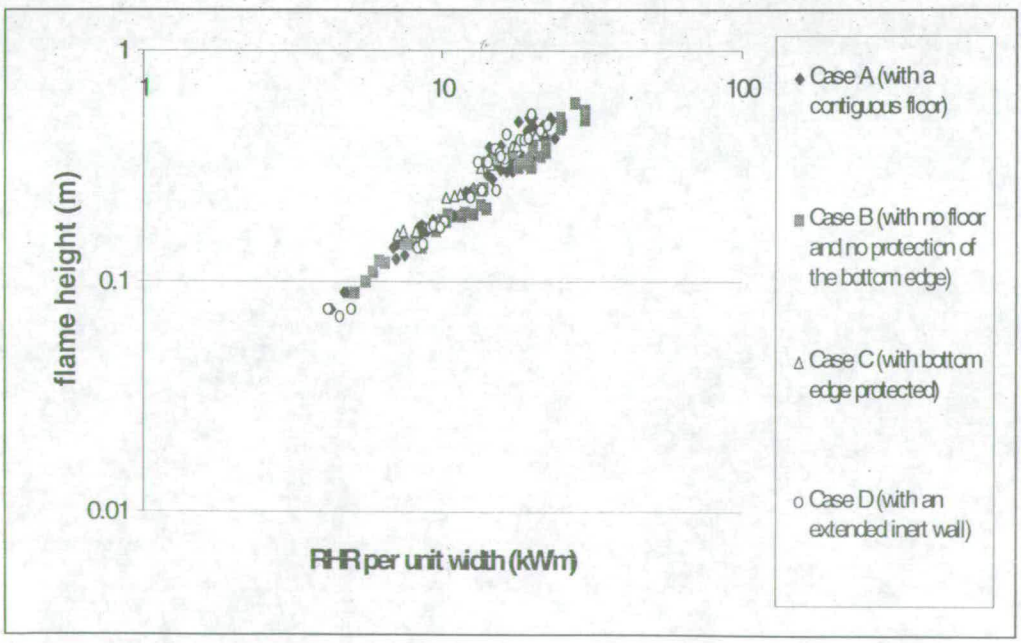

Fig 9(a) and 9(b) The dependence of flame height on RHR per unit width in normal and logarithmic scale.

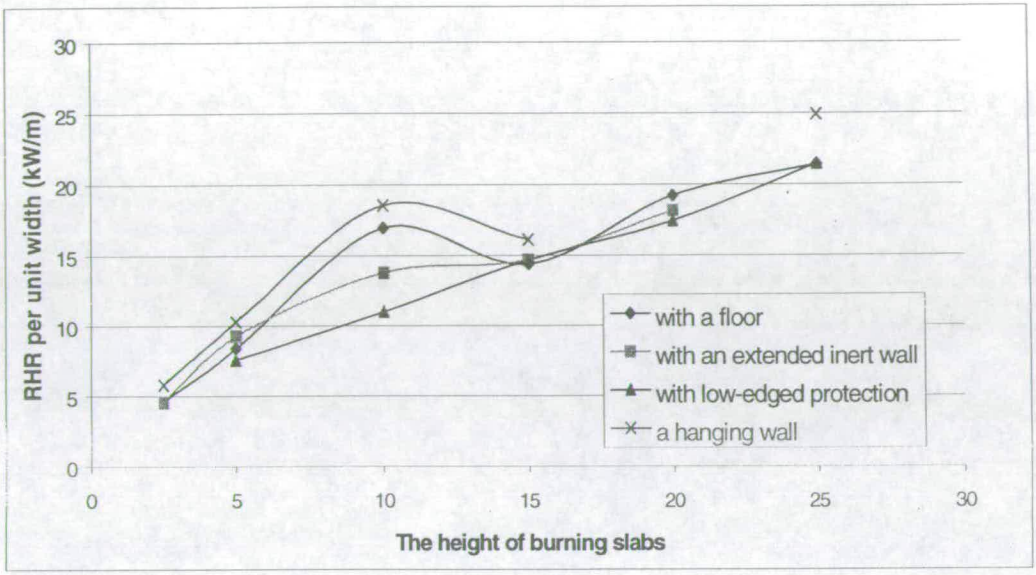

Fig. 10 The steady-state RHR per unit width of 8cm wide PMMA slabs with different heights under the four geometric configurations.

THE ROLE OF THE CONE CALORIMETER IN UPWARD FLAME SPREAD MODELLING

Kuang-Chung Tsai and Dougal Drysdale
Fire Safety Engineering Group, School of Civil and Environmental Engineering
University of Edinburgh
Edinburgh, Scotland

ABSTRACT

The Cone Calorimeter is a standard apparatus capable of providing quantitative data which are relevant to the response of combustible materials to fire conditions. Several fire models have been developed to use such data to predict various aspects of fire behaviour. In this paper, a new, non-standard Cone Calorimeter test procedure capable of providing data for modelling upward spread of flame on vertical flat surfaces is described. In the standard test procedure, samples are exposed to a continuous (constant) radiant heat flux. In the non-standard procedure, the cone heater is removed immediately after the sample has ignited and the rate of heat release is then measured without any external radiant heating. For some materials - particularly polymethylmethacrylate (PMMA) - these conditions more closely resemble the conditions that develop during upward flame spread on flat surfaces in which the material above the burning area is exposed to convective and radiative heating from the flame, yet once ignited burning is self-sustaining. Experimental data on the rate of upward flame spread on samples of 6mm thick PMMA (1m high, and 0.075 m wide, with inert sidewalls) can be modelled more accurately using data obtained in this way.

Keywords: fire safety engineering, upward flame spread, computer modelling, Cone Calorimeter

INTRODUCTION

Fire Safety Engineers are responsible for ensuring that buildings will be "safe" in the event of fire. In this context, "safe" implies primarily that the occupants will be able to escape unaided and unharmed, but to achieve this it may not be possible to rely on the existing regulations, simply because they are too inflexible and cannot be applied to buildings of modern design and construction. A performance-based approach must be used which requires the application of current knowledge of fire behaviour using tried and tested "engineering" models. A number of these are used by Fire Safety Engineers for the design of fire safety systems (e.g. sprinklers, smoke control *etc.*), but complementary methods are required for the selection of materials.

Standard tests are still used which can only rank materials on an arbitrary scale [1-3]. They cannot give the type of quantitative data that are necessary for performance based design. New tests have been developed relatively recently which are capable of providing quantitative data, the most promising being the Cone Calorimeter [4]. It allows the time to ignition and the rate of heat release to be measured under a range of heat fluxes. Several suggestions have been made about how such data may be used for materials selection (e.g. [5]), but none has yet been accepted. However, there is now good evidence that the data can be used in conjunction with upward flame spread models to predict the rate of spread on combustible wall linings, commonly recognised as one of the most hazardous fire scenarios. Such models may prove to be a suitable basis by which data from the Cone Calorimeter could be used for the purpose of material selection and for carrying out risk assessments. This paper will examine this hypothesis further.

UPWARD FLAME SPREAD AND ITS MODELLING

Upward Flame Spread Phenomenon

Vertical flame spread on a wall is rapid because a buoyancy-induced boundary layer flow is created by the burning gases. The process is illustrated in Fig. 1: the "wall" is undergoing pyrolysis (burning) in the region (X_p-X_b) and the surface ahead of the burning zone is exposed to flame over the height (X_f-X_p). X_b, X_p and X_f represent the heights of the burnout front, the pyrolysis front and the flame tip from the bottom edge of the "wall". Heat transfer from the flame to the surface in the region (X_f-X_p) raises the temperature of the surface to its ignition point [6] allowing the burning region to advance. This is the mechanism of flame spread. Clearly, heat transfer in the region (X_f-X_p) plays a crucial role [7]. In upward flame spread, the direction of flame spread and the flow of the hot, burning gases are concurrent, producing one of the most hazardous fire scenarios [6].

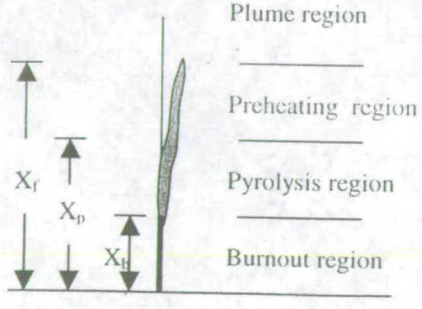

Fig.1 Upward flame spreading

Karlsson's Model

Karlsson [8] combined the thermal theory of concurrent flame spread developed by Saito, Quintiere and Williams (SQW) [9] with empirical flame height correlations and test data from the Cone Calorimeter to produce an approximate method for predicting fire growth in a corner configuration. Full details can be found in [8], but the assumptions were as follows:

(1) The material is thermally thick, homogeneous and its thermal properties are constant with temperature.
(2) Chemical kinetics is excluded.
(3) The flame length, X_f, depends on a power of $\dot{Q}'$, the total heat release rate per unit width.
(4) Heat flux from the flame occurs at constant flux only within the region $X_p < X < X_f$.

He obtained the following expression for the upward flame velocity (an integral equation of the Volterra type (second kind)):

$$V(t) = \frac{1}{\tau}\left[K\left\{ X_{po} \dot{Q}''(t) + \int_0^t \dot{Q}''(t - t_p) V(t_p) dt_p \right\}^n - \left(X_{po} + \int_0^t V(t_p) dt_p \right) \right] \quad (1)$$

where V(t) is the flame spread rate, τ is the ignition delay time, X_{po} is the initial burning region, K and n are constant, t is time, t_p is the dummy variable of integration and $\dot{Q}''(t)$ is the rate of heat release (RHR) from the burning material expressed mathematically as

$$\dot{Q}''(t) = \dot{Q}''_{max} e^{-\lambda t} \quad (2)$$

where $\dot{Q}''_{max}$ is the maximum value of the RHR from the Cone Calorimeter test at a heat flux of 20 kW/m^2, and λ is the decay coefficient, determined empirically from the RHR data. By solving Equation (1) analytically, the rate of flame spread can be predicted.

Grant and Drysdale's Model

In the Karlsson model, burnout is not considered. Grant and Drysdale [10] developed the model further not only to include burnout, but also to allow the heat release rate data from the Cone Calorimeter to be used directly as input, without using the approximate form as given in Equation (2). This resolves the problem which arises if the RHR data cannot be approximated by this equation which assumed that the RHR reaches its maximum value as soon as the sample is ignited, then decreases with a decay coefficient λ.

Before burnout occurs, the expression for the flame spread rate is given by Equation (1), but after burnout occurs, the velocity becomes,

$$V(t) = \frac{1}{\tau}\left[K\left\{ \int_{t-\tau_b}^{t} \dot{Q}''(t - t_p) V(t_p) dt_p \right\}^n - \left(\int_{t-\tau_b}^{t} V(t_p) dt_p \right) \right] \quad (3)$$

τ_b is the burnout time. The constants n and K of Equation (1) and (3) are chosen to be 2/3 and 0.0666, which follow the flame height correlation of Tu and Quintiere [11]. In the original application of Grant and Drysdale's model [10], the standard Cone Calorimeter test procedure was used, and gave very satisfactory results for samples of cardboard.

However, when the model was applied to samples of PMMA, the rate of flame spread was greatly overpredicted [12]. A possible reason for this that the RHR data from the Cone Calorimeter are obtained under a constant imposed heat flux, selected to model the heat flux to the surface *ahead* of the burning zone. Once burning, the process is self-sustaining and the rate of burning (hence the RHR) is controlled by heat transfer from the flames at the burning surface. No additional heat input is present, or necessary. The flame spread model still requires data on the time to ignition under an imposed heat flux which models that from the flame in the region (X_f - X_p), but after ignition occurs the RHR in the absence of an imposed heat flux should be used.

To test this hypothesis, a modified procedure has been used with the Cone Calorimeter, moving the cone heater as far away as possible immediately after ignition. The heater thus simulates the heat flux from the flame (X_f - X_p) for only the required period of time but does not "force" the subsequent rate of burning to any significant extent.

EXPERIMENTAL WORK

Cone Calorimeter Tests

Details of the apparatus, the instrumentation and the standard test procedure for the Cone Calorimeter are given in [4]. A 10 cm square specimen is exposed to a selected radiant flux and the vapours ignited by means of a spark ignition source. The time to ignition is determined and the heat release rate measured by utilising the oxygen consumption principle. This is normalised to unit surface area, giving $\dot{Q}''$ kW/m^2, the main parameter used in the model. For this upward flame spread study, specimens are tested in the vertical orientation.

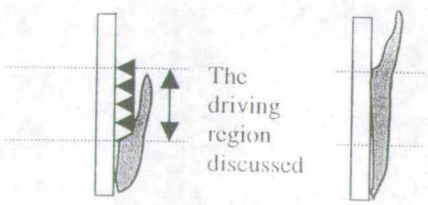

(a)The unburnt region before ignition (b) after ignition

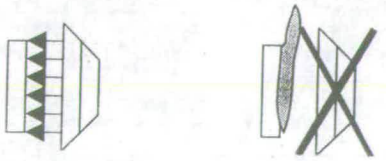

(a') sample before ignition (b') after ignition

Fig. 2 The schematic of the roles of the heat feedback and cone heater

The heat feedback from the flame to the unburned area in the region (X_f - X_p) is assumed to be constant. In these studies, a heat flux meter was mounted near the top of the sample, flush with the surface, to measure the heat flux to the unburned zone. It increased from 5 kW/m^2 near the flame tip to 30 kW/m^2 at the leading edge of the burning zone. A constant value of 15 kW/m^2 was chosen to represent the average flux for flame spread on vertical samples of PMMA [11]. This is significantly lower than the values taken by Grant & Drysdale [10] and Hasemi [13].

A number of tests were carried out following the standard procedure in the Cone Calorimeter. To obtain data which would test the hypothesis, experiments were carried out in which the cone heater was moved away immediately after ignition to simulate the absence of an external radiant flux.

Ideally, the cone heater should be removed, but due to the limited space within the test chamber of the Cone Calorimeter, it could only be moved into a position in which the lowest edge of the cone heater was 2.5 cm above the level of the top edge of the sample. The residual radiant flux to the surface was measured in separate experiments and found to be only 0.3~0.6 kW/m^2 when the power of the heater was set to give 30 kW/m^2. To a first approximation, it is assumed that the "residual" radiation can be neglected, particularly when the heater is operating at a lower power.

Experimental Measurement of the Rate of Upward Flame Spread

Vertical samples of PMMA (115 cm × 7.5 cm × 6mm thick) were held against a 3 mm thick plate. To model one-dimensional flame spread, the samples formed part of a wider "wall" of inert board (6 mm thick "Supalux") and the vertical edges of the PMMA were protected by strips of mild steel which overlapped inert board. A 1 cm high strip of the sample was ignited at the foot of the sample and the rate of upward flame spread was determined by analysing infra-red videorecordings of each experiment. The accompanying software allowed the pyrolysis front to be tracked as the 300°C contour as it advanced upwards.

RESULT AND DISCUSSION

Data on the transient rate of heat release of PMMA samples exposed to 15 kW/m^2 in the standard and modified tests are shown in Fig. 3. The time to ignition was almost identical in the two tests (480 and 475 s). The peak rate of heat release in the modified, non-standard test is lower than that in the standard test because the heater had been moved in the non-standard test. The difference in the duration of burning should also be noted.

The comparison between the experimental results and the flame spread rates predicted from Equations (1) and (3) are shown in Fig 4. It is clear that the result obtained from the model when the RHR data from the modified "Cone Calorimeter test" is in much better agreement with the experimental result. The early rate of spread appears to be underpredicted, but it is likely that in the experiments the early stages of flame spread are affected by the additional heat provided from the ignition source (a gas torch). This would give a higher initial RHR at the beginning of each experiment.

It is surprising that Grant and Drysdale obtained good agreement for upward flame spread on cardboard when the standard procedure was used in the Cone Calorimeter to obtain RHR data [10]. Using the same model, Anderson and McKeever [15] also found good agreement for hardboard, plywood and wallpaper-covered wood surfaces, albeit with a much higher irradiance from the cone heater (35 kW/m^2) [15]. The reason for this apparent anomaly for cardboard lies in the fact that there is little difference between the RHR data obtained by the standard and the modified Cone Calorimeter tests. This is shown for cardboard in Figure 5. The corresponding rates of upward spread according to Equations (1) and (3) are shown in Figure 6.

Brehob and Kulkarni [16] found that mass loss rates from different materials in the vertical orientation exhibited different sensitivities to external radiation when burning. (To a first approximation, it is reasonable to assume that the rate of heat release is closely linked to the mass loss rate through the heat of combustion, which is assumed to be independent of the imposed heat flux, and constant during the period of burning.) The reasons for this have still to be investigated, particularly if a vertical spread model is to be used to predict rates of vertical spread in different scenarios where there is likely to be an imposed heat flux affecting the rate of burning behind the pyrolysis front, e.g. in corner-wall locations or when inward facing surfaces must be considered as a possible scenario.

CONCLUSION

This study provides a good example of how fire models may be developed to characterise the behaviour of materials from small-scale test data. This type of approach - even if modifications to standard test procedures are required – may provide the basis for more robust methods for material classification and selection. However, the prerequisite is to use small-scale tests in a rational manner, based on a fundamental understanding of the relevant fire dynamics.

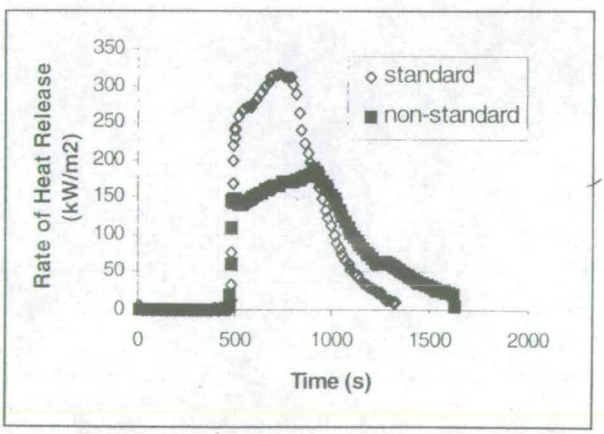

Fig. 3 The rate of heat release of PMMA samples from Cone Calorimeter under irradiance of 15kW/m^2 in the standard and non-standard test procedures.

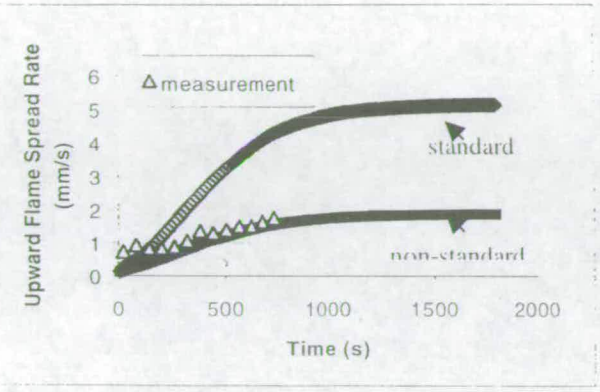

Fig. 4 The comparison of the experimental measurement and the prediction from Grant and Drysdale's model with the standard and non-standard test procedures.

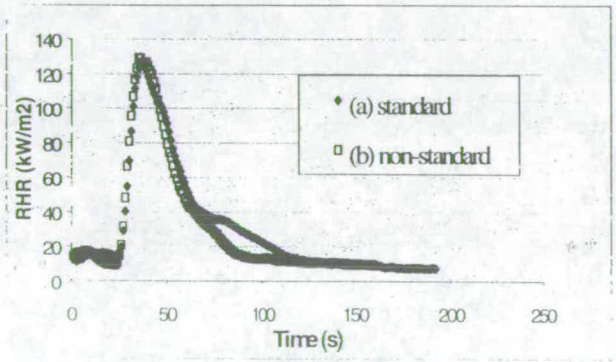

Fig.5 The rate of heat release of 2.5mm thick cardboard from the Cone Calorimeter with the standard and non-standard test procedures. (The irradiance of the cone heater: 20kW/m^2)

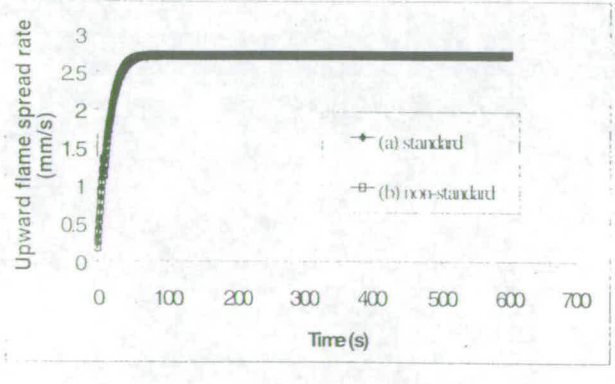

Fig.6 Upward flame spread rate predicted by Grant and Drysdale's model with the standard and non-standard Cone Calorimeter test procedures.

REFERENCES

1. ISO 5660, "Fire Tests, Reaction to Fire. Rate of Heat Release from Building Products", International Organisation for Standardisation, Geneva (1993).
2. ISO 5657, 'Fire Tests, Reaction to Fire. Ignitability of building products'. International Organisation for Standardisation, Geneva (1997)
3. ISO 5658, "Fire Tests, Reaction to Fire. Lateral Ignition and Flame Spread of Building Products", International Organisation for Standardisation, Geneva (1993).
4. Babrauskas V, The Cone Calorimeter, SFPE Handbook of Fire Protection Engineering, Second Edition, pp. 3-37~3-52 (1995)
5. Ostman BAL and Nussbaum PM, Correlation between Small-Scale Rate of Heat Release and Full-Scale Room Flashover for Surface Linings, Fire Safety Science-Proceedings of the Second International Symposium, pp. 823-832, 1988
6. Drysdale, D., "An Introduction to Fire Dynamics", 2nd edition, Wiley-Interscience, New York (1998).
7. Delichatsios, M. A., "Flame Height in Turbulent Wall Fires with Significant Flame Radiation", Combustion Science and Technology, Vol. 39, pp. 195-214 (1984).
8. Karlsson, B., "A Mathematical Model for Calculating Heat Release Rate in the Room Corner Test", Fire Safety Journal, Vol. 20, pp. 93-113 (1993).
9. Saito, K., Quintiere, J. G. and Williams, F. A., "Upward Turbulent Flame Spread, Fire Safety Science", Proceedings of the 1st International Symposium, pp. 75-86 (1985).
10. Grant, G. and Drysdale, D., "Numerical modelling of early flame spread in warehouse fires", Fire Safety Journal, Vol. 24, pp. 247-278 (1995).
11. Tu, K. M. and Quintiere, J. G., "Wall Flame Heights with External Radiation", Fire Technology, Vol.27, pp. 195-203
12. Turnbull, J. and Will, G., 4th Year Honours Thesis, "Spread of Flame on Wall Lining Materials", School of Civil and Environmental Engineering, the University of Edinburgh (1999).
13. Hasemi, Y., Yoshida, M., Nohara, A. and Nakabayashi, T., "Unsteady-State Upward Flame Spreading Velocity along Vertical Combustible Solid and Influence of External Radiation on the Flame Spread", Fire Safety Science, Proceedings of the 3rd International Symposium, pp. 197-205 (1991).
14. Kulkarni, A. K. and Kim, C. I., "Heat Loss to the Interior of a Free Burning Vertical Wall and Its Influence on estimation of effective heat of gasification", Combustion Science and Technology, Vol.73, pp. 493-504 (1990).
15. Anderson, M. and McKeever, C., "An Experimental Study of Upward Flame Spread on Cellulosic Materials", Proceedings of the Seventh International Fire Safety and Engineering Conference INTERFLAM'96, pp. 169-178 (1996).
16. Brehob, E. G. and Kulkarni, A. K., "Time Dependent Mass Loss Rate Behavior of Wall Materials under External Radiation", Fire and Materials, Vol. 17, 249-254 (1993).

MODELLING THE EARLY STAGES OF UPWARD FLAME SPREAD

Kuang-Chung Tsai & Dougal Drysdale
Fire Safety Engineering Group, School of Civil and Environmental Engineering
University of Edinburgh, Edinburgh, Scotland, UK

ABSTRACT

Previous work has demonstrated the flame height of a wall fire is one of the two most important parameters determining the rate of vertical spread. Models of vertical flame spread rely on empirical flame height correlations which have the form $X_f = K\dot{Q}'^n$, *but these are based on simulations of wall fires using line burners, and estimates of the rate of heat release from fires on vertical surfaces. There have been no carefully controlled experiments designed to establish the validity of these correlations and data do not exist for values of* $\dot{Q}' < c.25$ *kW/m.*

Two experimental approaches are described here. In one, burning slabs of PMMA slabs (6 mm thick, with heights between 25 mm and 250 mm and widths between 50 mm and 150 mm) were used as the fire source and measurements of $\dot{Q}'$ *and* X_f *were made simultaneously. These relate to the earliest stages of a wall fire (*$\dot{Q}' < 30$ *kW/m). Various configurations were examined. In the other set of experiments, a gas-fired vertical panel was used. This consisted of an array of 14 independent burners which could be assembled to investigate the effect of the aspect ratio of the burning area on the correlation. The data confirm that the flame height correlates with* $\dot{Q}'$, *but the bottom edge boundary configuration and the width of the burning area have an effect.*

1. INTRODUCTION

Flame height is taken as the average visible extent of the fire plume. For a developing wall fire, flame height has been shown to be one of the two most important parameters driving the rate of upward spread [1], the other being the heat transfer to the unburned surface ahead of the burning zone. Several models [2-9] have combined these parameters to assess the risk of fire growth on vertical surfaces. However, the reliability of these models depends on the accuracy of the flame height correlation.

2. PREVIOUS THEORETICAL AND EXPERIMENTAL INVESTIGATIONS

Figure 1 is a schematic diagram of a developing wall fire. The solid fuel is pyrolyzing in the region $\left(X_p - X_b\right)$ and the flame height reaches X_f. The region $0 < X < X_b$ corresponds to the

burnt out zone. Where burning is established, fuel vapours are released from the surface and enter the flame which is confined to the buoyancy-induced boundary layer. Heat is transferred to the surface above the pyrolysis region, progressively raising its temperature to the firepoint, allowing the flame to advance upwards.

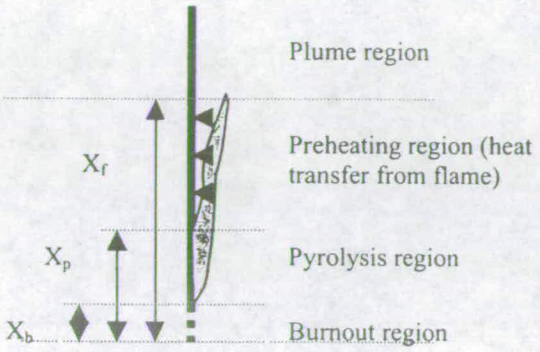

Fig.1: Upward flame spread model

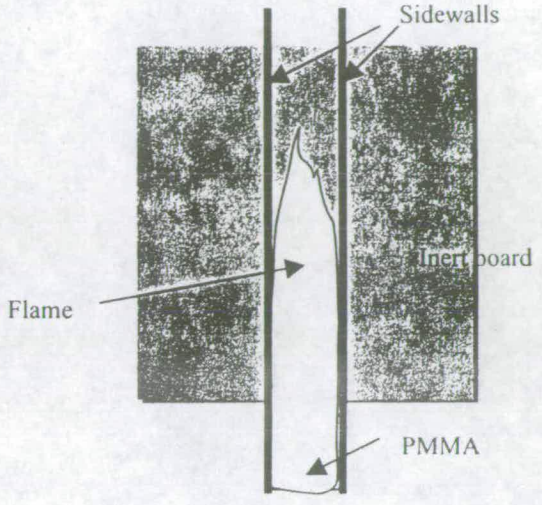

Fig. 2: The schematic diagram of the experimental rig used for PMMA test. The rig was located under the extract hood of a Cone Calorimeter.

Based on these observations, several theoretical analyses [1,10,11] have led to a correlation of the flame height for wall fires. Quintiere *et al.* [10] assumed that a flame extends until the fuel is completely consumed. Delichatsios [1] postulated that flame heights in buoyant diffusion flames (laminar or turbulent) are essentially independent of the stoichiometry and depend only on total heat release rate. This hypothesis was later supported by the derivation of flame height expressions from experimental results and physical arguments of buoyancy, heat transfer, mass flow rate, etc. [1]. Aeklund [11] established a two-dimensional vortex model by demonstrating flame as a region of intense vorticity generation, which is capable of predicting the flame height. All of these studies concluded that the flame height is proportional to the rate of heat release per unit width in a two-thirds power law (n=2/3 in Equation 1).

$$X_f = K\dot{Q}'^n \qquad (1)$$

where X_f is the height of flame, K and n are constants and $\dot{Q}'$ is the rate of heat release (RHR) per unit width of burning material.

Several investigations [2,10,12-16] using different experimental rigs have been carried out to analyse the flame height phenomenon. A comparison of these experiments is given in Table 1, showing the type of fire (linear burner or wall fire; whether steady or spreading fires, laminar or turbulent), the geometric configuration and whether or not sidewalls were present. These experiments can be classified into three types: (1) linear fires produced by line burners against a wall, (2) wall fires produced by vertical gas burners, and (3) vertical burning fuels in which the rate of mass loss was measured or estimated and the heat of combustion assumed to be constant.

Source	Line or wall fire?	Geometric config^n	Laminar or turbulent	Spreading or steady?	Sidewall?	Method used**
Hasemi [12]	LB + burning slabs	no floor	-	steady	yes	ΔHc(E) $\dot{m}'$ (C) (Eqn.2)
Sugawa *et al.* [13]	Line fire	with floor	-	steady	no	ΔHc(E) $\dot{m}'$ (C) (Eqn.2)
Coutin *et al.* [14]	wall fires	no floor	turbulent	steady	Many variations	ΔHc(E) $\dot{m}'$ (C)
Quintiere *et al.* [10]	LB + burning slabs	no floor	turbulent	spreading*	yes	$\dot{Q}''$ (E) (Eqn.5)
Tu and Quintiere [15]	LB + burning slabs	no floor	turbulent	spreading	yes	ΔHc(E) $\dot{m}''$(M) (Eqn.6)
SQW [2]	wall fires	with floor	turbulent	spreading	no	ΔHc(E) $\dot{m}''$(E) (Eqn.6)
Orloff *et al.* [16]	wall fires	with floor	laminar & turbulent	Spreading	yes	–

Table 1: A summary of previous experimental rigs used for flame height correlations.
* The flame produced was spreading but measurements were carried out as it became steady.
** E: estimated; C: controlled (gas flow); M: measured; LB: line burner.

(1) Linear fires produced by line burners against a wall

Porous line burners were used by Hasemi [12] and Sugawa *et al.* [13] to simulate wall fires. In Hasemi's study [12], three burners were used, with sidewalls to help maintain two-dimensional flow. The burner dimensions (width (D) × length (L)) were 0.0375m × 0.27m, 0.82m × 0.27m, and 0.0075m × 0.92m, where D was taken as the characteristic dimension. Sidewalls are not mentioned in Sugawa's study [13]. By changing the rate of supply of gaseous fuel, different rates of heat release were simulated. The corresponding heights of the flame tips were recorded by video camera and the rate of heat release (RHR) per unit width was calculated from Equation 2.

$$\dot{Q}' = \dot{m}' \Delta H_c \qquad (2)$$

where $\dot{m}'$ is the rate of supply of fuel per unit width of burner (kg/m.s) and ΔH_c is the heat of combustion (kJ/kg).

The flame height was found to correlate with the dimensionless group $\dot{Q}_l^* \equiv \dot{Q}' / \rho_\infty C_p T_o g^{1/2} D^{3/2}$ as follows:

$$L_f / D = \gamma \dot{Q}_l^{*n} \qquad (3)$$

where L_f is the flame height, D is the characteristic length and γ is a constant. In Hasemi's study [12], for $\dot{Q}_l^* \geq 1$, n = 2/3 and γ =6.0. For $\dot{Q}_l^* < 1$, n=0.8. In Sugawa's experimental study [13], n was confirmed to be 2/3 in the range $5 < \dot{Q}_l^* < 20$.

(2) Wall fires produced by vertical gas burners

Wall fires were simulated via vertical gas burners by Coutin *et al.* [14]. The burner width was fixed at 0.4 m and the burner height was set at 0.25, 0.5 and 1 m. Three configurations were studied: (a) the burning wall was entirely confined by two sidewalls; (b) the burner was partially confined over its lower part; and (c) there was no confinement. The value of $\dot{Q}'$ was calculated from Equation 2. A new and objective methodology using a CCD camera was applied to map flame luminosity.

They observed that the flame height is sensitive to the geometric configuration. Pyrolysis height and burner width seemed to influence the flame height correlation. However, no systematic measurements were made and there was no clear conclusion.

(3) Vertical burning fuels, assuming a constant heat of combustion

Flame height measurements on 284 mm square samples of burning materials in a vertical orientation were made by Quintiere *et al.* [10]. A pilot ignition flame was placed at the base and sidewalls were provided to prevent lateral air entrainment. By exposing the samples to different levels of external radiation, various solid fuel burning rates could be simulated. Once steady burning had been achieved, the flame height was measured. Assuming a constant heat of combustion, RHR per unit width was calculated by following Equation 4.

$$\dot{Q}' = \dot{Q}'' X_p \tag{4}$$

where $\dot{Q}''$ is the RHR per unit surface area. Their data followed the 2/3 power law (see Equation 1) although there was considerable scatter. Tu and Quintiere [14] modified the experimental rig to allow the measurement of transient mass loss rate and the corresponding flame height for both charring and non-charring materials (PMMA and wood; 285 mm wide and 295 mm high). Using Equation 5,and then Equation 4,

$$\dot{Q}'' = \dot{m}'' \Delta H_c \tag{5}$$

the flame height correlation was found to obey the 2/3 power law, but the value of K was higher than for the results obtained from line fires against a wall [15].

Orloff *et al.* [16] and Saito *et al.* (SQW) [2] also measured flame heights but used PMMA sheets up to 1.5 m. In both of these studies, line burners were adopted to ignite the lowest edge of samples, but sidewalls were only used by Orloff *et al.* [16]. One significant difference from the earlier work was the presence of a floor which would have altered the mode of air entrainment at the base of the "wall". The flame height of the spreading flame was correlated in SQW's study [2] by calculating the RHR per unit width from the estimated fuel supply rate and heat of combustion (Equation 5 and then 4). The flame height correlation obeyed Equation 1, but with a higher value of n than that obtained from steady burning experiments [10]. The higher power may be a result of the higher pyrolysis rates achieved in the upper part of the pyrolysing fuel during the spreading

process [2,16]. It was also noted that the presence of sidewalls increased the length of the flames because two-dimensional flow patterns were maintained [2].

Although the flame height correlations of the line fires [12,13] and the wall fires [2,10,14,15,16] seem to be similar and agree with Equation 1, the behaviour of the flames is different. The linear flame experiments cannot simulate real wall fires. Even when "real wall fires" are involved [2,10,14,15], the assumption that the heat of combustion remains constant may not be realistic. There is a need to measure the RHR directly during the experiments.

Consequently, there is still uncertainty in the validity of the correlation. Equation 1 suggests that the flame height is related only to $\dot{Q}'$, and no other factors are considered. In particular, there is almost no information on the effect of the aspect ratio (height/width) of the burning area. It is known that the rate of upward spread increases with the width of the burning material. This may be explained in terms of increased radiative heat transfer [17], but equally the flame height may be increased. The effect of different geometric configurations at the base of the "wall" (for example, with and without a contiguous floor) has also not been considered. As this will influence the air entrainment pattern at the base of the wall, it may also have an effect on flame height. Two experimental rigs have been used to provide data which would help resolve the effects of the aspect ratio (height/width) and air entrainment at the early stages of the development of wall fires.

3. EXPERIMENTAL WORK AND RESULTS

3.1 PMMA tests

3.1.1 Experimental design

The experimental rig applying combustible solids is shown in Figure 2 in schematic form. It was designed to hold vertical samples of combustible material at the lower edge of (and in the same plane as) a 600 mm high inert board. The sample was mounted on a 3 mm thick steel plate: in addition to preventing flame spreading up the back of the sample, it kept the rear face relatively cool and prevented distortion and slumping which would otherwise have occurred. The vertical edges of the sample were protected by 3 mm thick mild steel strips designed to hold the sample against the backing plate. The rig was located below the hood of a Cone Calorimeter, thus allowing the rate of heat release from the burning sample to be measured directly. A hand-held butane-fuelled blowtorch was used to ignite the surface of each sample uniformly. The inert wall was marked with a scale and a Video Camcorder was used to record each experiment. The flame height was determined subsequently by visual examination of the videorecordings which were then matched to the corresponding heat release rates.

The combustible material used was PMMA, as 6 mm thick slabs with heights ranging from 25 to 250 mm and widths of 40, 80 and 120 mm to simulate the early stages of vertical burning and to allow the effects of different aspect ratios to be studied. By using sample heights up to 250 mm, the laminar, transition and turbulent burning regimes could be observed, as noted by Orloff *et al.* in their PMMA experiments [15].

Modifications could be made to allow four different geometric configurations to be studied (see Table 2, (A)-(D)). In three cases, the burning area was at the foot of the "wall". With Case A, there was a contiguous floor, but this was absent in Cases B and C. In Case B, the bottom edge was unprotected while in Case C the bottom edge was protected by a steel strip. In the fourth configuration (Case D), the sample represented a central burning area on an extended wall.

Table 2 (a) and (b): The steady RHR per unit width and mass loss rate of 6mm thick, 80mm wide PMMA samples with different geometric configurations.

(a) RHR per unit width (kW/m)

Height, Xf (mm)	(Case A) with a floor 	(Case B) without a floor or an extended plate 	(Case C) with lower edged protection 	(Case D) with an extended plate 
25	4.59 ± 0.31	5.81 ± 0.71	---	4.57 ± 0.42
50	8.41 ± 0.44	10.30 ± 0.26	7.58 ± 0.62	9.28 ± 0.08
100	16.92 ± 2.14	18.52 ± 1.27	11.00 ± 0.68	13.78 ± 1.48
150	14.38 ± 0.28	16.08 ± 1.07	14.66 ± 1.27	14.68 ± 1.60
200	19.19	---	17.40 ± 0.32	18.13
250	21.43 ± 1.43	24.92	21.44 ± 0.86	---

(b) Mass loss rate $\dot{m}''$ (g/m^2 s) (assuming ΔH_c (PMMA) = 24.89 kJ/g)

25	7.38	9.34	---	7.34
50	6.76	8.28	6.09	7.46
100	6.80	7.44	4.42	5.54
150	3.85	4.31	3.93	3.93
200	3.85	---	3.50	3.64
250	3.44	4.01	3.45	---

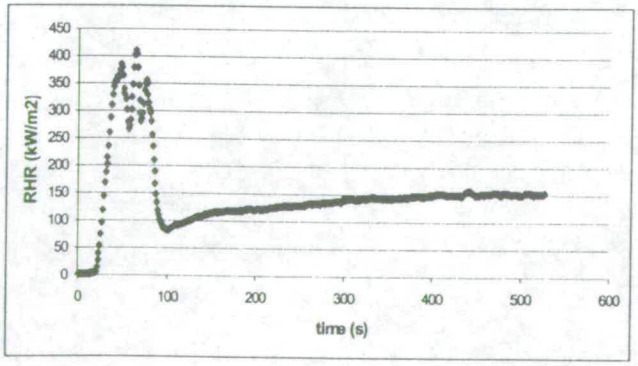

Fig. 3: The RHR history of a 6mm thick, 80mm wide and 100mm high burning PMMA sample with a contiguous floor. After ignition by the torch (at 100s) rate of burning increased to a steady value (after 350s). Burnout started at around 500s.

3.1.2 PMMA test results

Figure 3 shows the typical RHR history for a burning PMMA sample, 80 mm wide, 100 mm high and 6mm thick in the configuration corresponding to Case A (with a contiguous floor). The ignition process took approximately 100 s and was followed by a period of unsteady burning (from 100s to 350s) during which the RHR increased to a steady value (corresponding to 150 kW/m^2 in this case) before burnout started (after 500s). The height of the flame during steady burning was determined (350 – 500 s in Figure 3). The heights of the continuous flame and the flame tip were observed, but the flame height was recorded as the average of the visible flame height.

The effect of aspect ratio (R = height/width) on the correlation is shown in Figure 3 for Cases A and D. These represent the very different geometries and indicate that the effect of R is negligible for $\dot{Q}'$ < 30 kW/m^2 within the range of values of R used (0.3125 to 2.5). The same result is found for Cases B and C.

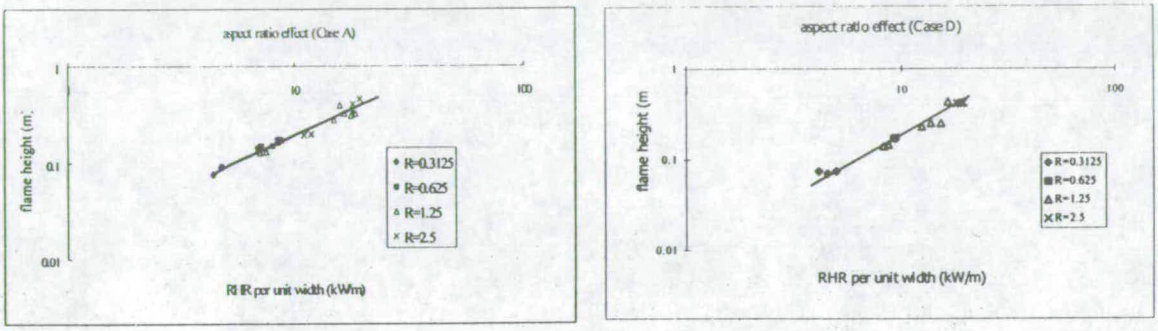

Fig. 4: The effect of aspect ratio (height/width) on the flame height correlation under geometric configurations of Case A (left) and D (right) (see Fig. 3).

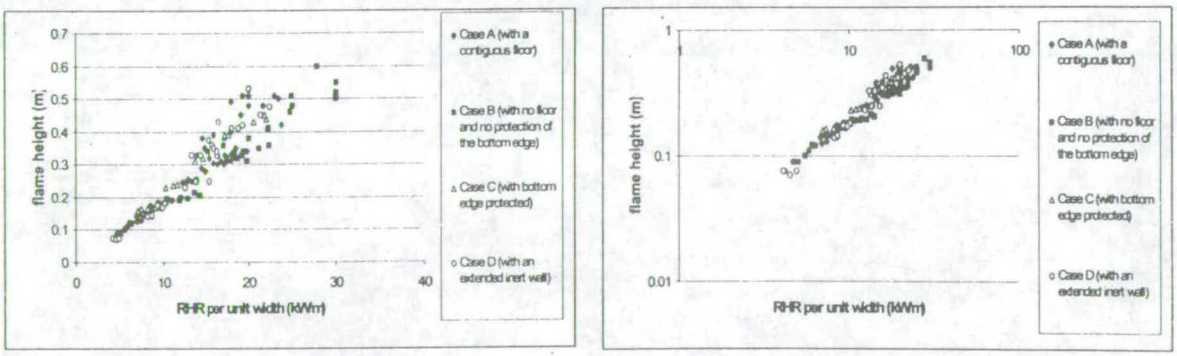

Fig. 5: The dependence of flame height on RHR per unit width plotted on normal and double logarithmic scale (all data).

In Figure 5, the dependence of X_f on $\dot{Q}'$ for all four geometries is shown on normal and double logarithmic plots. When $\dot{Q}'$ is less than c.10 kW/m, the data for all four configurations fall on the same line, but above c.10 kW/m, the data diverge and systematic differences in the four series of flame height correlations are apparent.

For Case A (a burning wall with a contiguous floor),

$$X_f = 0.016\dot{Q}'^{1.07} \tag{6}$$

For Case B (a burning wall with no floor and no protection of the bottom edge),

$$X_f = 0.018\dot{Q}'^{1.00} \tag{7}$$

For Case C (a burning wall with no floor but with the bottom edged protected)

$$X_f = 0.023\dot{Q}'^{0.98} \tag{8}$$

For Case D (a burning wall with an extended plate),

$$X_f = 0.011\dot{Q}'^{1.25} \tag{9}$$

The r^2 values for these four cases (Equations 6–9) are 0.931, 0.968, 0.987 and 0.963 respectively, and the values of n are close to unity. In addition, it can be seen that the burning walls set in an extended plate (Case D) produce the tallest flames. While further work would be required to explain this observation, it seems likely that it is a consequence of the fact that the burning area is part of a larger flat surface. The Case D flames may be less turbulent than those observed for Cases A, B and C. In general, turbulence tends to reduce the height of a diffusion flame, but the Case A flames are of similar height to the Case D flames, both being higher than Cases B and C (Figure 9a). Clearly, the effect of the lower edge boundary conditions needs to be studied in greater detail. The best fit line encompassing the data from all four cases is included in Figure 7 which compares all of the previous correlations [2,10,16] and Delichatsios' analysis [1] discussed in Section 2. This shows that the flame height is more sensitive to $\dot{Q}'$ than predicted by other correlations [1,2,10,16] in this range of values of $\dot{Q}'$, but that these correlations will overpredict the height of the flames when $\dot{Q}' < 25$ kW/m. .

The steady values of $\dot{Q}'$ obtained for the different geometric configurations are listed in Table 2a. Samples with a lower-edge protection (Case C) produced the lowest values of $\dot{Q}'$ while Case B samples produced the highest. It seems likely that the increased burning area due to the involvement of the lower edge would account for this result. When PMMA samples burned with a contiguous floor (Case A), the lowest 10 mm of the flame was blue in colour, suggestive of a well-mixed region producing "premixed-like" burning. This may have caused higher local heat transfer and thus a higher local rate of burning, consequently producing a higher value of $\dot{Q}'$. This is consistent with observations made by Foley and Drysdale [18] on the effect of a "floor" on the rate of heat transfer to a vertical wall exposed to a line burner.

In Table 2b, the steady-state rate of burning (expressed as a mass flux, $\dot{m}''$ g/m^2.s) of PMMA slabs of different heights are compared for these four configurations. The mass fluxes were calculated from the steady state values $\dot{Q}'$, assuming the heat of combustion of PMMA to be constant at 24.89 kJ/g [17]. The burning rate is found to decrease as the height of the burning sample increases. This is consistent with the study carried out by Orloff *et al.* [19] on the burning of thick vertical slabs of PMMA, 0.91 m wide and ≥ 1.5 m high. Their configuration corresponded

to Case A. They also found that the rate of burning decreased with height over the first 200 mm from the bottom edge although the decrease was not so pronounced (about 15%).

Clearly, the lower edge configuration has a significant effect on the flame height correlation. More work is required to obtain a fuller understanding of this behaviour, but it seems likely that the pattern of air entrainment is an important factor.

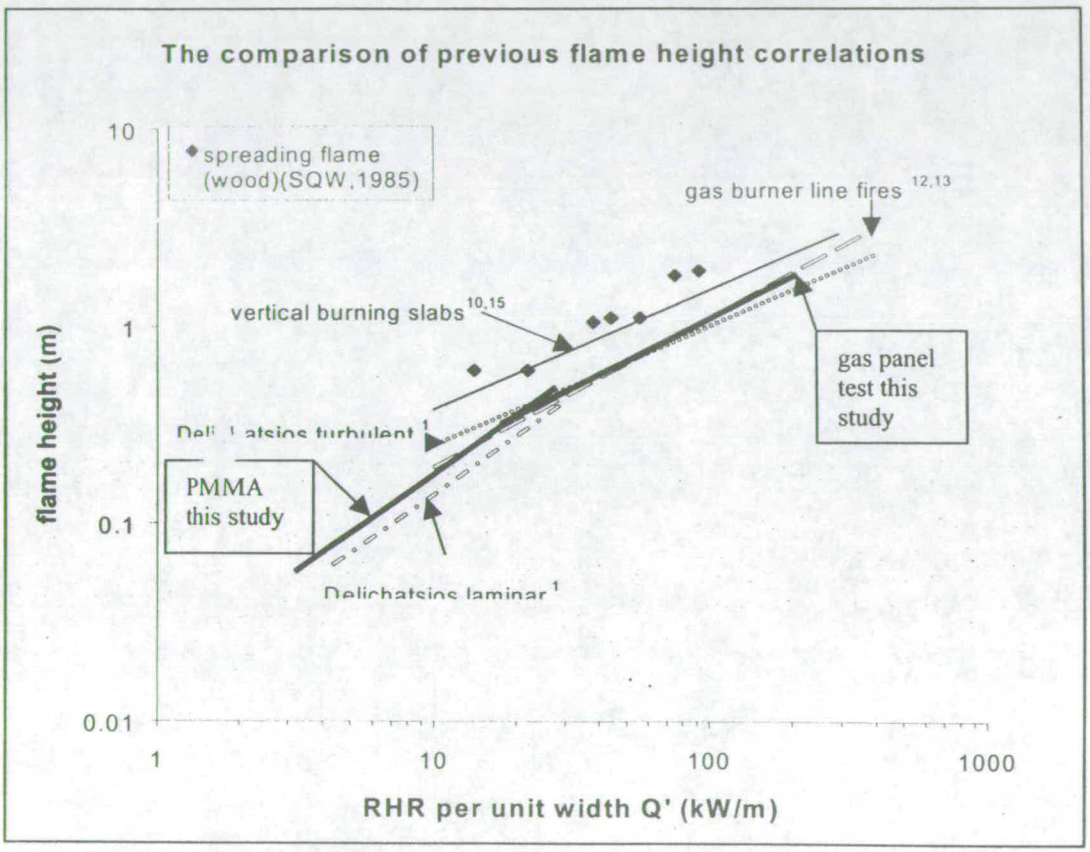

Fig. 6: A comparison of the correlations obtained in this study with earlier ones [1,2, 10,12, 13, 15]

3.2 Gas panel tests

3.2.1 The experimental rig

The experimental rig is in Fig. 7. A propane fuelled vertical panel (600 mm high and 840 mm wide) was constructed from 14 burners. An inert board was located as a vertical extension, against which the flame heights were determined. The 14 burners were controlled separately by individual valves so that burning areas of different aspect ratio could be selected. The mass flow rate was controlled by a mass flow controller. The resultant $\dot{Q}'$ was calculated using Equation 2, assuming complete combustion with the heat of combustion of propane is 46.45 kJ/g. The inert board was marked with a scale for visual determination of flame height.

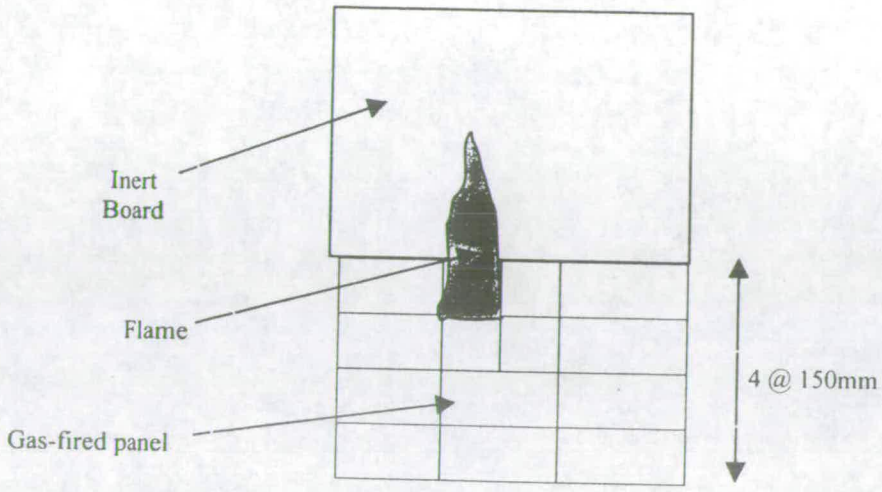

Fig. 7: The gas panel apparatus. Each rectangle of the panel represents an independent burner with an individual gas supply which can be controlled independently.

3.2.2 Experimental Results

Fig.8 shows the dependence of X_f on $\dot{Q}'$ for different burning areas in normal scale. It can be seen that the flame height correlates with $\dot{Q}'$ but divergence exists following the width of the burning areas.

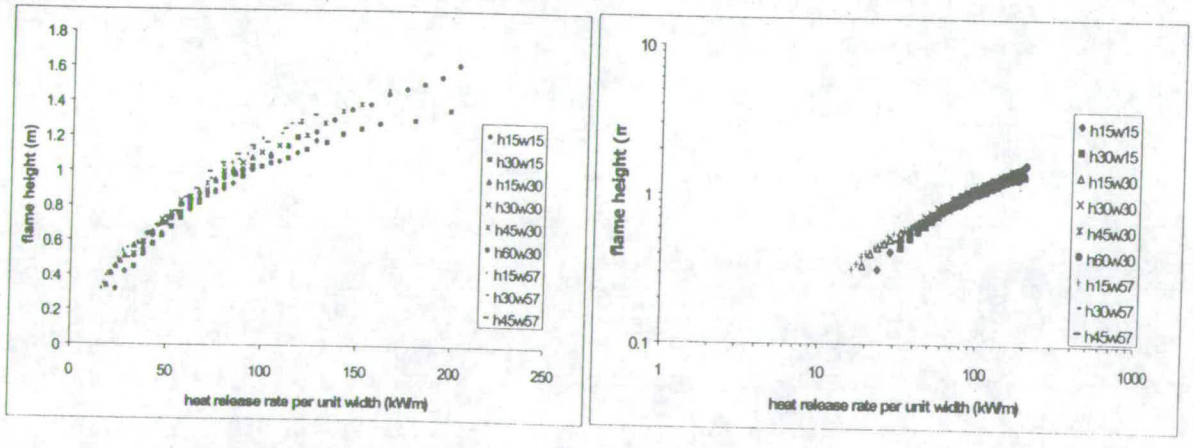

Fig. 8: The relation between X_f and $\dot{Q}'$ from the vertical propane burner (Fig. 7) with fires of different burning areas (normal and double-logarithmic plots). In the legend, **h15w15** indicates that the burner is 150 mm high and 150 mm wide.

For fires produced by 150 mm wide burners,

$$X_f = 0.058\dot{Q}'^{0.646} \tag{10}$$

For fires produced by 300 mm wide burners,

$$X_f = 0.07\dot{Q}'^{0.616} \tag{11}$$

For fires produced by 570 mm wide burners,

$$X_f = 0.061\dot{Q}'^{0.655} \tag{12}$$

The r^2 for these three correlations are 0.965, 0.989 and 0.991 respectively and the values of n are close to 0.66 which was determined by theories discussed in Section 2 [1,10,11]. The comparison of the best fit line encompassing the data of Equations 10, 11 and 12 with other correlations is shown in Fig.6. A very consistent result was obtained. The fires from wider burning areas produced higher flames. The same observation can be seen in Hasemi's work (Fig. 3 in [3]) using line burners with different widths although the effect was not discussed. It may contribute to the increase in the rate of upward flame spread as the width of the burning material is increased. However, more detailed research into air entrainment behaviour is required.

4. CONCLUSION

The flame height correlation of wall fires on their early stages of development ($\dot{Q}' < 30$ kW/m) under different geometric configurations has been shown to conform to a correlation of the form of Equation 1, with no significant influence from the aspect ratio of the burning surface. For the first time, rates of heat release and flame heights were measured directly in the same experiments. The correlation was found to depend on the lower edge boundary condition. Data for $\dot{Q}' > 30$ kW/m should be obtained by the same technique to investigate the correlation for fully developed turbulent wall flames, but the limited space within the test section of the Cone Calorimeter prevented such measurements being made in this part of the project.

The flame heights from a gas-fired panel were measured and were shown to correlate according to Equation 1, with a value of n very close to 2/3, as determined by others. The rate of heat release was calculated from the mass flowrate and the data suggest that flame height is influenced by the width of the burning area, i.e. the aspect ratio has some effect.

The correlations in this study were derived from steady flames from a combustible material and a gas panel, although the correlation between flame height for a spreading wall fire in which the corresponding rate of heat release was measured simultaneously should be examined. However, it is hoped that this study will lead to a better understanding and more robust correlations for modelling upward flame spread.

REFERENCES

1 Delichatsios MA, Flame Heights in Turbulent Wall Fires with Significant Flame Radiation, Combustion Science and Technology, Vol. 39, pp. 195-214, 1984

2 Saito K, Quintiere JG and Williams FA, Upward Turbulent Flame Spread, Fire Safety Science- Proceedings of the First International Symposium, pp. 75-86, 1985

3 Hasemi Y, Thermal Modeling of Upward Wall Flame Spread, Fire Safety Science- Proceedings of the First International Symposium, pp. 87-96, 1985

4 Delichatsios MM, Mathews MK and Delichatsios MA, An Upward Fire Spread and Growth Simulation, Fire Safety Science- Proceedings of the Third International Symposium, pp. 207-216, 1991

5 Karlsson B, A Mathematical Model for Calculating Heat Release Rate in the Room Corner Test, Fire Safety Journal, Vol.20, pp. 93-113, 1993

6 Grant G and Drysdale D, Numerical Modelling of Early Flame Spread in Warehouse Fires, Fire Safety Journal, Vol.24, pp. 247-278, 1995

7 Kokkala M, Baroudi D and Parker WJ, Upward Flame Spread on Wooden Surface Products: Experiments and Numerical Modelling, Fire Safety Science- Proceedings of the Fifth International Symposium, pp. 309-320, 1997

8 Brehob E and Kulkarni AK, Experimental Measurements of Upward Flame Spread on a Vertical Wall with External Radiation, Fire Safety Journal, Vol.31, pp.181-200, 1998

9 Ohlemiller TJ and Cleary TG, Upward Flame spread on Composite Materials, Fire Safety Journal, Vol.32, pp.159-172, 1999

10 Quintiere J, Harkleroad M and Hasemi Y, Wall Flames and Implications for Upward Flame spread, Combustion Science and Technology, Vol. 48, pp. 191-222, 1986

11 Aeklund TI, A Vortex Model for Wall Flame Height, Journal of Fire Sciences, Vol.4-January/February, pp.4-14, 1986

12 Hasemi Y, Experimental Wall Flame Heat Transfer Correlations for the Analysis of Upward Wall Flame Spread, Fire Science and Technology, Vol.4, No.2, pp. 75-90, 1984

13 Sugawa O, Satoh H and Okà Y, Flame Height from Rectangular Fire Sources Considering Mixing Factor, Fire Safety Science- Proceedings of the Third International Symposium, pp. 435-444, 1991

14 Coutin M, Most JM, Delichatsios MA and Delichatsios MM, Flame heights in wall fires: effects of width, confinement and pyrolysis length, Fire Safety Science- Proceedings of the Sixth International Symposium, pp. 729-740, 1999

15 Tu KM and Quintiere JG, Wall Flame Heights with External Radiation, Fire Technology, pp.195-203, 1991

16 Orloff L, De Ris J and Markstein GH, Upward Turbulent Fire Spread and Burning of Fuel Surface, The Fifteenth Symposium (International) on Combustion, pp. 183-192, 1974

17 Drysdale DD, Introduction to Fire Dynamics, 2nd edition, John Wiley&Sons, 1998

18 Foley M and Drysdale DD, Heat Transfer from Flames between Vertical Parallel Walls, Fire Safety Journal, Vol.24, pp. 53-73, 1995

19 Orloff L, Modak AT and Alpert RL, Burning of Large-Scale Vertical Surfaces, The Sixteenth Symposium (International) on Combustion, pp. 1345-1354, 1976

Submitted for the 7th International Symposium on fire Safety Science

Upward flame spread: heat transfer to the unburned surface

Tsai Kuang-Chung and Dougal Drysdale

Fire Safety Engineering Group, School of Civil and Environmental Engineering
University of Edinburgh, Edinburgh, Scotland

ABSTRACT

An experimental programme was intended to analyse the heat feedback from a spreading wall fire to its unburned surface, one of the two important parameters determining its spread rate. The heat flux from PMMA fires was observed to be higher than those from previous investigations as plotted with normalised flame height (X/X_f). However, very good consistency was performed with another study as a parameter $\dot{q}_{wo}$" is introduced with heat flux plotted in another normalisation. The averaged heat flux, an important parameter used in upward flame spread modelling, was discussed and suggested to be around 15–20 kW/m^2. This is much lower than the commonly accepted 25-30 kW/m^2.

Keywords: heat feedback, upward flame spread

Nomenclature

C_o	a constant (-)
C_p	specific heat (J/kgK)
D	dimension of burner (m)
g	gravitational acceleration constant (m/s^2)
Q_l	heat release rate of the line burners (kW/m)
Q_l*	dimensionless variable of rate of heat release (-)
$\dot{q}_w$"	heat flux from flame to unburned surface (kW/m^2)
$\dot{q}_{wo}$"	maximum heat flux from flame to unburned surface (kW/m^2)
$\dot{q}_{wp}$"	heat flux from flame to unburned surface as the pyrolysis front reached the heat flux meter (kW/m^2)
T	temperature (^{0}C or K)
t_f	the time as flame tip reaches heat flux meters (s)
t_p	the time as pyrolysis front reaches heat flux meters (s)
X	vertical distance from the bottom of wall (m)
X_b	burnout front height (m)
X_f	flame height (m)
X_p	pyrolysis front height (m)
ρ_o	density (g/m^3)

1. INTRODUCTION

Upward flame spread on vertical surfaces has attracted the attention of fire safety scientists and engineers for more than 30 years because it represents a particularly hazardous scenario which can produce very rapid fire development. Research has provided an understanding of the phenomenon by identifying the controlling mechanisms through mathematical formulations which are capable of simulation fire spread behaviour. Figure 1 is a schematic diagram of a flame spreading upwards on a vertical surface. The wall is undergoing pyrolysis (burning) in the region $(X_p\text{-}X_b)$, the flame tip reaches X_f and below X_b is the region of burnout. Fernandez-Pello and Hirano [1] pointed out that the heat transfer from the flame to the unburned fuel is the primary controlling mechanism. Delichatsios [2] further noted that the heat flux to the surface above the end of the pyrolysis region up to the flame tip (the preheating region $(X_f\text{-}X_p)$ in Fig.1) and the extent of burning, i.e. the flame height in wall fires, are the two important parameters determining its flame spread rate.

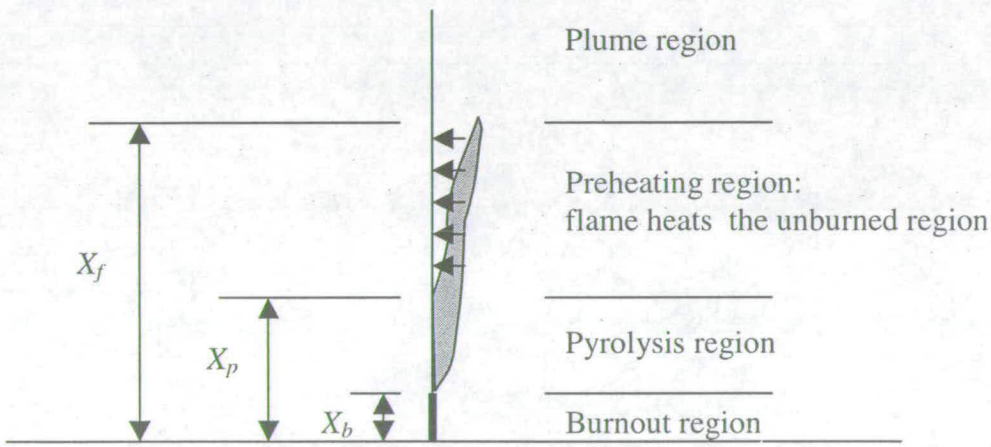

Figure 1. Upward flame spread.

In this paper, the heat flux from the flame to unburned surface in the region $X_f - X_p$ is considered in detail. Measurements have been made from spreading PMMA wall fires and compared with previous investigations in which a similarity has been observed for a wide range of materials. In addition, the average heat flux in the preheating region is discussed as this is used in many upward flame spread models.

2. PREVIOUS EXPERIMENTAL INVESTIGATIONS

One of the earliest sets of measurements of the wall flame heat flux distribution was made by Hasemi [3,4] who used porous, methane line burners (30cm long and 3.7 or 8.2cm wide) against the foot of a water-cooled isothermal wall, and a methane line burner

(92 cm long and 7.5cm wide) against a thermally thin wall. The isothermal wall had sidewalls, but no contiguous floor, while the thin wall had a contiguous floor but no sidewalls. Total heat fluxes were determined by means of Gardon gauges. Hasemi noted that the behaviour of flames near the line burners appeared to be different from the behaviour of flames from vertical fuels. However, his data appeared to be consistent with earlier work of others [5,6]. The heat flux data were found to lie in four distinct regions defined by the parameter $\dot{Q}_l^{*2/3} D = \left(\dot{Q}_l / \rho_o C_p T_o g^{1/2}\right)^{2/3}$. (This parameter is also used to correlate the visible flame heights of gas burner line fires.) The regions are:

(1) The lower part of the solid flame ($X / \dot{Q}_l^{*2/3} D \leq 1$) in which $\dot{q}_w''$ tends to increase with height.

(2) The upper part of the solid flame ($1 \leq X / \dot{Q}_l^{*2/3} D \leq 2.8$) in which $\dot{q}_w''$ is apparently constant and appears to be a weakly increasing function of $\dot{Q}_l^*$. The flame thickness is almost constant with height.

(3) The transition region ($2.8 \leq X / \dot{Q}_l^{*2/3} D \leq 10$) in which the slope is the steepest among the four regions with all the data falling onto

$$\dot{q}_w'' \approx 45\left(X / \dot{Q}_l^{*2/3} D\right)^{-5/2} \tag{1}$$

(4) The plume region ($10 \leq X / \dot{Q}_l^{*2/3} D$) in which the heat flux can be correlated by

$$\dot{q}_w'' \approx 2.5\left(X / \dot{Q}_l^{*2/3} D\right)^{-1.3} \tag{2}$$

Quintiere *et al.* [7] also took heat flux measurements during their work on flame heights with 28.5× 28.5cm burning surfaces (PMMA, rigid foam, carpet, flexible foam, aircraft panel and particle board). Heat flux meters were flush mounted on a contiguous water-cooled plate which was located above the samples. Cooled side-plates were used to form a channel to preserve two-dimensionality of the boundary layer flow over the plate by preventing air entering the flame from the sides. They plotted their heat flux data in terms of X/X_f and found them to be very consistent with Hasemi's data plotted in the same format [3,4].

Brehob *et al.* [8] suggested another form for the correlation of $\dot{q}_w''$ with height based on the data reported by Quintiere *et al.* [7] and Kim [9], *viz.*

$$\frac{\dot{q}_w''}{\dot{q}_{wo}''} = \exp\left[-C_o\left(\frac{X - X_p}{X_f - X_p}\right)\right] \tag{3}$$

where $\dot{q}_{wo}''$ is the maximum heat feedback from flames to surface and the decay factor C_o was determined to be 1.37. The correlation allows $\dot{q}_w''$ to be determined from a single value of $\dot{q}_{wo}''$ which Brehob suggests may be regarded as a "fire property" of the wall lining material.

3. AVERAGED HEAT FLUX USED IN UPWARD FLAME SPREAD MODELLING

A number of upward flame spread models have been developed in which the heat flux correlations of Hasemi [3, 4] and Quintiere *et al.* [7] have been used. However, to simplify the problem, most of these models [9-18] assume that $\dot{q}_w''$ is constant over the preheating region, becoming zero at heights above X_f. Saito *et al.* [9] took 25 kW/m^2 as the constant heat flux exposed to which mass loss rate was obtained for their steady-state model. Good consistency has been shown with their PMMA flame spread rate measurement. Mowrer and Williamson [10] chose 30 Kw/m^2 as the irradiance of the Cone Calorimeter under which material flammability properties were carried out. In addition, they chose 50 kW/m^2 to obtain the data of burning duration time. Delichatsios and co-workers [11] also adopted 30 kW/m^2 to be the fixed total flame heat flux of burning walls with flame heights shorter than 1.5 m in their Upward Fire Spread and Growth (UFSG) code, and considered radiative and convective heat transfer separately for flames higher than 1.5 m. However, 25 kW/m^2 was used in their projects concerning PE/PVC cables [12] and charring materials [13]. In addition, Grant and Drysdale [14] took the average of the heat flux measured with their cardboard tests, and suggested 20 kW/m^2 to represent the heating scenario. Applying the Grant and Drysdale's model, Anderson *et al.* [15] used 35 kW/m^2 as the constant heat flux for hardboard, plywood and wallpaper covered wood surfaces. But 25 kW/m^2 was chosen again in the modelling work of Kokkala *et al.* [16] focusing on wood surface produces, Qian and Saito [17] analysing the difference of the heat feedback over vertical flat and corner walls and Quintiere and Lee [18] assessing ignitor and thickness effects on upward flame spread. Table 1 lists the representative heat flux chosen for these models.

Table 1: Heat fluxes selected for the preheating region

Modelling work	Heat flux chosen (kW/m^2)	Comments
Saito *et al.* [9]	25	
Mowrer and Williamson [10]	30	50 for obtaining burning duration time data
Delichatsios *et al.*[11]	30	
Delichatsios and Delichatsios [12]	25	
Delichatsios and Chen [13]	25	
Grant and Drysdale [14]	20	averaged value during the whole burning process
Anderson *et al.* [15]	35	
Kokkala *et al.* [16]	25	
Qian and Saito [17]	25	
Quintiere and Lee [18]	25	

4. EXPERIMENTAL WORK

Figure 2 shows in schematic form the experimental rig designed to allow samples to be ignited along the lower edge while in a horizontal position before being rotated into the vertical position at the start of the test. The samples were 6mm thick, 70 mm wide PMMA slabs of heights 200, 300, 400 and 500 mm. They were held against a 2 mm thick steel plate which not only prevented flame spreading up the back of the sample but also kept the rear face sufficiently cool to prevent distortion and slumping. The vertical edges of the samples were secured against the backing plate by two 3 mm thick mild steel strips which overlapped the samples by 5 mm on each long side: these also protected the vertical edges of the samples. A 5 mm wide slot was cut along the centreline of the backing plate to allow the pyrolysis front to be observed through the back of the sample, using the leading edge of the sub-surface bubbles as the marker. A heat flux meter was mounted flush with the sample surface, with its centre 20 mm from the top end of the sample. This was used to monitor the heat flux from the flame to the unburned surface during upward flame spread.

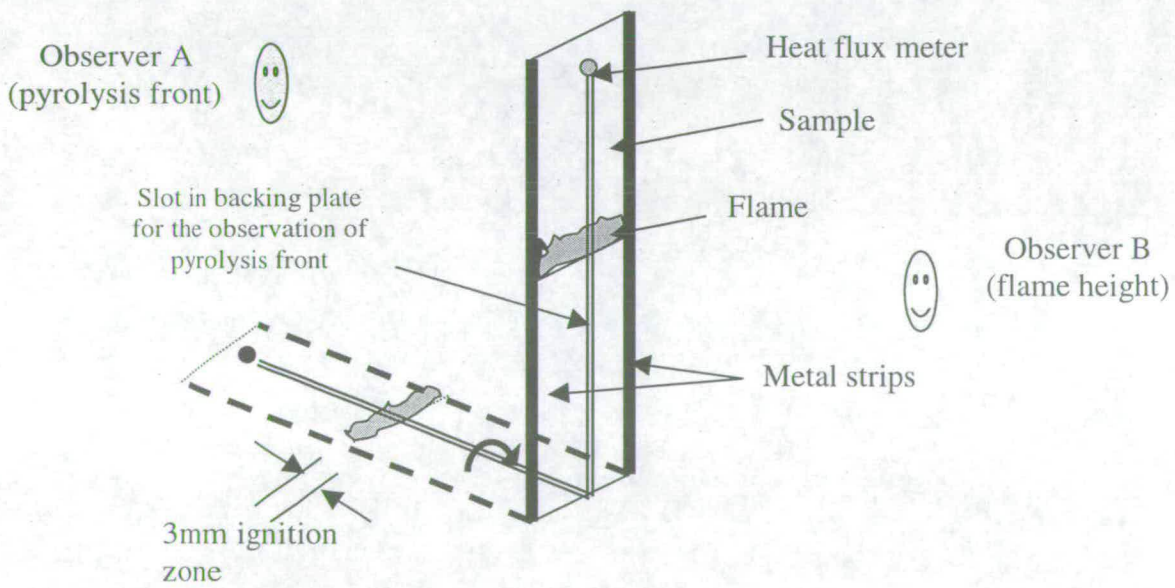

Figure 2: Experimental rig used in this study. The dashed lines represent the horizontal position of the rig during ignition. It is then rotated into the vertical position (solid lines). The flame and pyrolysis heights were observed by eye from the front and rear of the rig.

A mild steel plate, 3 mm thick, was held against lower end of the sample, leaving an unprotected 3 mm strip of PMMA which could be ignited by a hand-held butane-fuelled torch. The steel plate prevented extensive heating of the region ahead of the 3 mm ignition zone and was removed after ignition had been effected and immediately before the sample was raised into the vertical position. Measurements were taken by two people: observer A at the rear of the sample recorded the pyrolysis front as it advanced

by 10 mm steps while observer B recorded the flame height visually at each corresponding time.

5. RESULTS AND DISCUSSION

The experiments were designed to provide data on the early stages of fire growth on a vertical surface. The results are relevant to combustible surfaces exposed to localised ignition sources and not for combustible linings exposed to large diffuse sources. This would require work on a larger scale.

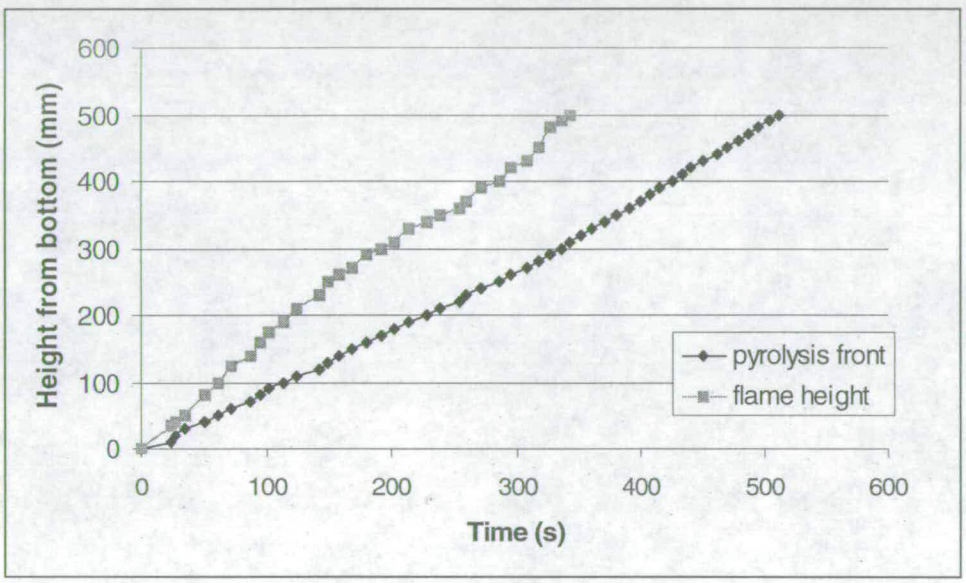

Figure 3: A typical flame height and pyrolysis front measurement on a 500 mm height PMMA sample as a function of time. The gradient of the pyrolysis front line gives the rate of spread.

Figure 3 shows typical measurements of the pyrolysis front and flame height on a 500 mm high PMMA sample. Figure 4 shows heat flux measurements (average of three tests each) 20 mm from the top edge for 200, 300, 400 and 500 mm high samples. The quantities t_f and t_p can be identified as the times when the flame tip and pyrolysis front reach the heat flux meter, respectively. The difference (t_p - t_f) then represents the time during which the preheating region is exposed to a direct heat flux from the flame (Figure 1). The heat fluxes at t_f and t_p for different heights of sample are identified on Figure 4 and are listed in Table 2. Figure 4 also shows that the maximum heat flux occurs just behind the pyrolysis fronts, i.e. at the onset of steady burning. The average maximum heat flux was approximately 38 kW/m^2.

Figure 5 shows the heat flux distribution of the spreading PMMA wall fires plotted as a function of height (X) normalised against the flame height. The data from Quintiere *et al.* [7] are included for comparison. It can be seen that these are lower then the measurements from this study. However, there is a significant difference between the

two sets of experiments: in this study the data were obtained by measuring the heat fluxes during upward flame spread on vertical PMMA samples up to 500 mm high, while Quintiere *et al.* [7] made their measurements during the steady state burning of 285 mm square samples with the heat flux meters flush mounted on a water-cooled copper plate above the burning area. This will have a cooling effect on the boundary layer flow and consequently reduce the heat flux measured at the heat flux meters.

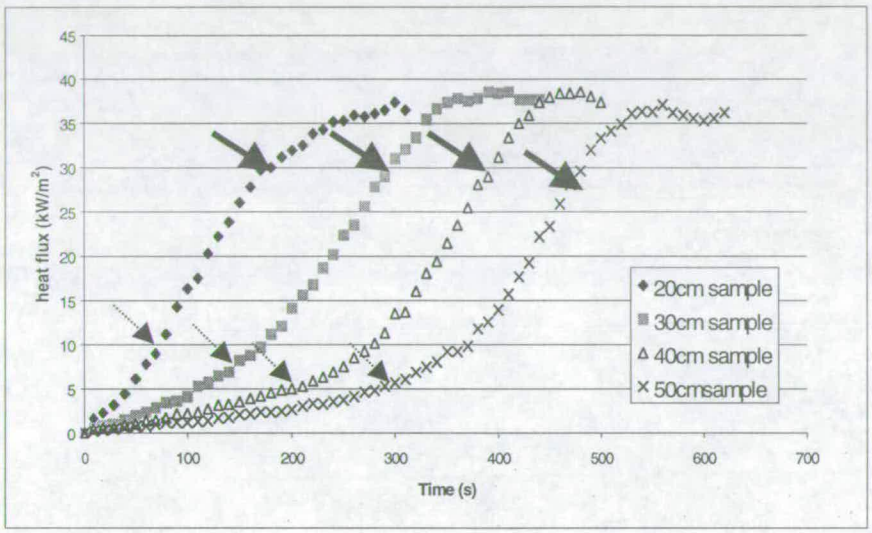

Figure 4: Variation of heat flux 20 mm from the top of the 200, 300, 400 and 500 mm samples (no sidewalls). (⇢ marks the time when the flame tips reach the heat flux meter; → indicates when the pyrolysis fronts reached the heat flux meters.)

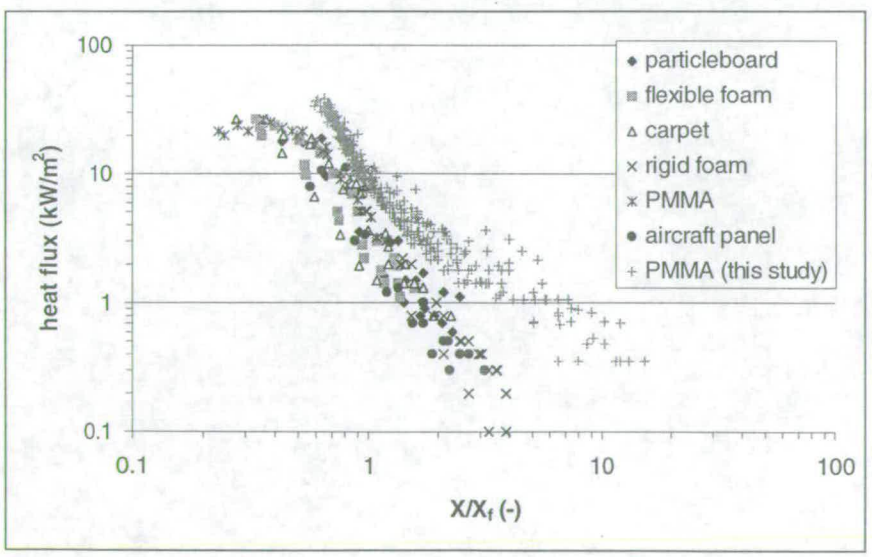

Figure 5: The heat flux distribution of measurements from Quintiere *et al.* [7] and from the spreading PMMA flames plotted against (X/X_f).

Sample height (mm)	Heat flux at flame tip (kW/m^2)	Heat flux at pyrolysis front (kW/m^2)
200	9.6	31
300	8.8	30
400	6.5	29
500	6.4	29

Table 2: Heat fluxes at the flame tip and the leading edge of the pyrolysis front

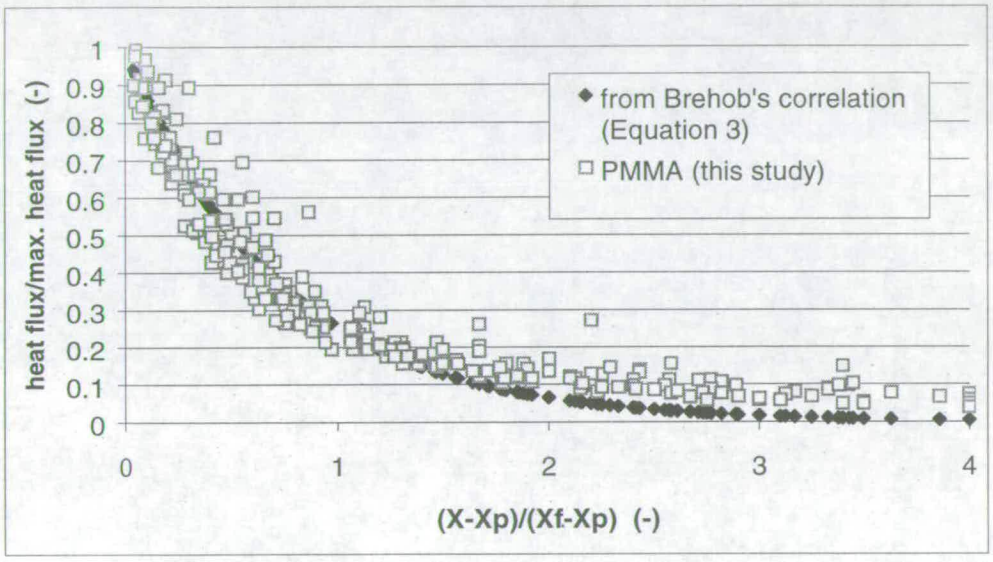

Figure 6: The comparison of heat flux distributions following Brehob *et al.* [8] (Equation 3) and in this study. (Brehob *et al.* [8] used the final heat flux $\dot{q}_{wo}$" to be the maximum one , but in this study the heat flux as the pyrolysis front reached the heat flux meter $\dot{q}_{wp}$" was used.)

In Figure 6, the heat flux distributions shown in Figure 5 are plotted in a form suggested by Brehob *et al.* [8], namely, as $\dot{q}''_w/\dot{q}''_{wp}$ vs $(X - X_p)/(X_f - X_p)$, where the heat flux $\dot{q}''_{wp}$ corresponds to t_p rather than the final (maximum) value $\dot{q}''_{wo}$ in the pyrolysis regions (Figure 1) as in Equation 3. The best-fit function is:

$$\frac{\dot{q}_w''}{\dot{q}_{wp}''} = 0.21\left[\frac{X - X_p}{X_f - X_p}\right]^{-0.81} \qquad (4)$$

The correlation (r^2 equal to 0.927) is in a different format from that of Brehob *et al.* [8] (Equation 3), however, good agreement can be seen for $[(X-X_p)/(X_f-X_p)]<1$.

In upward flame spread models, it is important to use as input data the best available representation of heat transfer to the preheating region. Ideally, a function such as Equation 4 should be used, but a simpler approach has been generally adopted. This has been dictated partly by the availability of data from the Cone Calorimeter which apply to a single (constant) heat flux for both the time to ignition and rate of heat release measurements. Table 1 shows the range of heat fluxes used by different investigators to obtain t_{ig} and RHR data (and apply to their models). With the exception of Grant and Drysdale [14], all are 25 kW/m^2 or above. However, the current data show that the heat flux varies from c. 7.8 kW/m^2 at the flame tip to c. 29.8 kW/m^2 at the leading edge of the pyrolysis zone. It would seem appropriate to use t_{ig} and RHR data obtained in the Cone Calorimeter at an average value less than 20 kW/m^2. The heat flux distributions derived by Hasemi [5,6], Quintiere *et al.* [7], Brehob *et al.* [8] and in this study are similar enough to suggest that they may be material-independent. This offers the possibility that a single representative heat flux could be used for a range of materials, taking the average of the highest and lowest heat fluxes measured in the preheating region (Figure 1). This would provide a value of c. 18.8 kW/m^2, which is much lower than the values chosen by others (Table 1).

Further support for this conclusion is to be found in a recent paper by Tsai and Drysdale [19]. They point out that it is unreasonable to use the RHR data obtained from the Cone Calorimeter at the same heat flux at which t_{ig} was determined. After a vertical surface has been ignited (and the source of ignition removed), the process is self-sustaining. The rate of burning of the area below the pyrolysis front is determined by heat feedback from the established flame. In reference [19] it is shown that excellent agreement is obtained between experimental data and prediction by Grant and Drysdale's model [14] when t_{ig} at 15 kW/m^2 and the RHR with no imposed heat flux were used as input data. These data were obtained by using a non-standard procedure with the Cone Calorimeter in which the cone heater was removed immediately after ignition [19].

6. CONCLUSION

Measurements of the heat feedback from upward spreading PMMA fires were carried out and compared with previous experimental correlations. Fairly good agreement was observed. An important parameter, representative heat flux within the preheating region of upward flame spread used in many wall fire models, was discussed. A lower value than commonly accepted ones was suggested.

7. ACKNOWLEDGEMENTS

The authors wish to thank John Turnbull and Gavin Will, final year undergraduate students in Edinburgh University, for their assistance to carry out experimental data.

8. REFERENCES

1. Fernandez-Pello AC and Hirano T, Controlling mechanisms of flame spread, Combustion Science and Technology, Vol. 32, pp.1-31, 1983
2. Delichatsios MA, Flame heights in turbulent wall fires with significant flame radiation, Combustion Science and Technology, Vol. 39, pp. 195-214, 1984
3. Hasemi Y, Thermal modeling of upward wall flame spread, Fire Safety Science-Proceedings of the First International Symposium, pp. 87-96, 1985
4. Hasemi Y, Experimental wall flame heat transfer correlations for the analysis of upward flame spread, Fire Science and Technology, Vol.4, No.2, pp. 75-90, 1984
5. Ahmad T. and Faeth GM, Turbulent wall fires, 17th Symposium (International) on combustion, pp. 1149~1160, 1978
6. Liburdy JA and Faeth GM, Heat transfer and mean structure of a turbulent thermal plume along a vertical isothermal wall, Journal of Heat Transfer, Vol.100, pp. 177-183, 1978
7. Quintiere J, Harkleroad M and Hasemi Y, Wall flames and implications for upward flame spread, Combustion Science and Technology, Vol. 48, pp. 191-222, 1986
8. Brehob EG, Kim CI and Kulkarni AK, Numerical model of upward flame spread on practical wall materials, Fire safety Journal, Vol. 36, pp.225-240, 2001
9. Saito K, Quintiere JG and Williams FA, Upward turbulent flame spread, Fire Safety Science- Proceedings of the First International Symposium, pp. 75-86, 1985
10. Mowrer FW and Williamson RB, Flame spread evaluation for thin interior finish materials, Fire Safety Science- Proceedings of the Third International Symposium, pp. 689-698, 1991
11. Delichatsios MM, Mathews MK and Delichatsios MA, An upward fire spread and growth simulation, Fire Safety Science- Proceedings of the Third International Symposium, pp. 207-216, 1991
12. Delichatsios MA, and Delichatsios MM, Upward flame spread and critical conditions for PE/PVC cables in a tray configuration, Fire Safety Science- Proceedings of the Fourth International Symposium, pp. 433-444, 1995
13. Delichatsios MA and Chen Y, Flame spread on charring materials: numerical predictions and critical conditions, Fire Safety Science- Proceedings of the Fourth International Symposium, pp. 457-468, 1995
14. Grant G and Drysdale D, Numerical modelling of early flame spread in warehouse fires, Fire Safety Journal, Vol.24, pp. 247-278, 1995
15. Anderson M, McKeever C, Pehrson R and Barnett J, An experimental study of upward flame spread on cellulosic materials, InterFlam'96, pp.169-178, 1996
16. Kokkala M, Baroudi D and Parker WJ, Upward flame spread on wooden surface products: experiments and numerical modelling, Fire Safety Science- Proceedings of the Fifth International Symposium, pp. 309-320, 1997
17. Qian C and Saito K, An empirical model for upward flame spread over vertical flat and corner walls, Fire Safety Science- Proceedings of the Fifth International Symposium, pp. 285-296, 1997
18. Quintiere JQ and Lee CH, Ignitor and thickness effects on upward flame spread, Fire Technology, Vol.34, No.1, pp.18-38, 1998
19. Tsai K-C and Drysdalé D, Using Cone Calorimeter data for the prediction of fire hazard, Fire Safety Journal, accepted for publication.